Doctoral Thesis

Chemical, magnetic and electronic properties of NaxCoO2 and related compounds.

Manuel Bañobre López

NaxCoO2 has been extensively studied for decades. However, the discovery of novel properties (i.e. high thermoelectric power or the occurrence of superconductivity below 5K) and their possible relationship with similar phenomena found in other materials boosted a renewed interest in this highly electronic correlated system. In this thesis, the structural, magnetic and electronic properties of NaxCoO2 have been studied in detail in order to understand deeply some of the most fundamental aspects which drive the chemical and physical behaviour of this system: presence of oxygen vacants, the role of water played in the occurrence of superconductivity, the proximity of the system to a quantum phase transition or the nature of the unconventional thermoelectric and magnetic properties with x, specifically at the half-doped x=0.5. All of them are kept under strong scientific discussions that, far from solving them, contribute to generate an even higher controversy. On other hand, the efficiency of topotactic reactions in order to exchange Na+ ions by other mono- or di-valent ions, such as Li+, Ag+, Ca2+ or Sr2+, has been studied. The physical properties of the resulting compounds are shown and compared to those ones from the analogous NaxCoO2 precursor.Therefore, in the pages inside, the reader will can find our main results and conclusions achieved in each one of these subjects, in a modest attempt to explain the chemistry and physics involved in NaxCoO2 and related compounds.

Manuel Bañobre López
Chemical, magnetic and electronic properties of NaxCoO2 and related compounds.

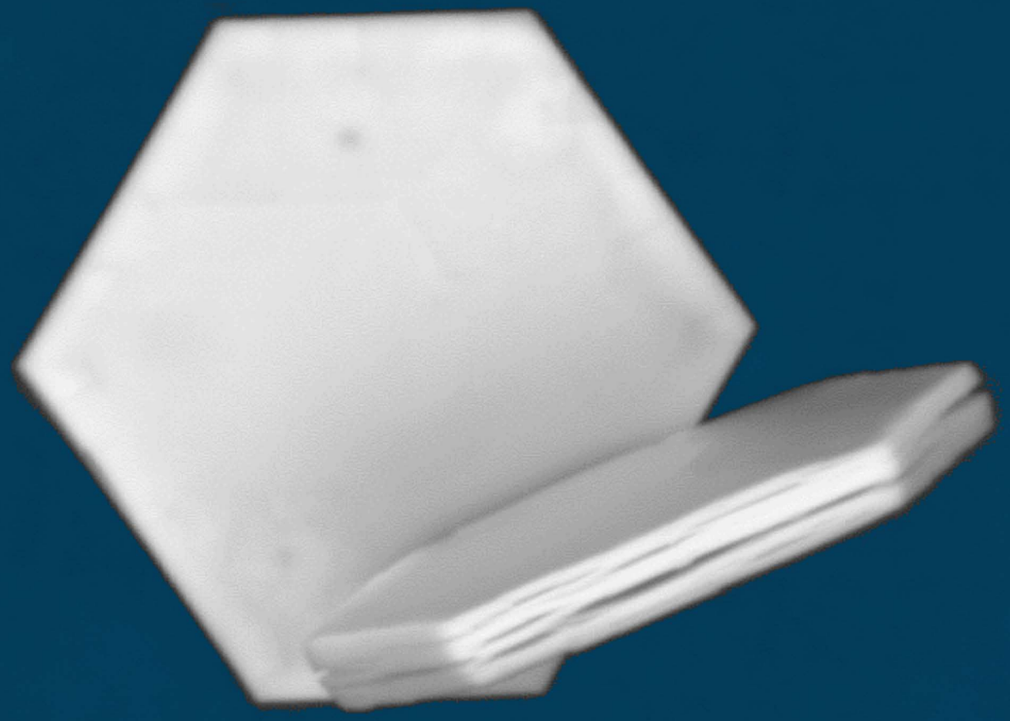

USC UNIVERSIDADE DE SANTIAGO DE COMPOSTELA
FACULTADE DE QUÍMICA
Departamento de Química-Física

Universidad de Santiago de Compostela
Departamento de Química Física

Chemical, magnetic and electronic properties of Na_xCoO_2 and related compounds.

Memoria presentada por D. Manuel Bañobre López
Para optar al grado de Doctor en Química
Universidad de Santiago de Compostela
Abril, 2011

ISBN 978-84-9887-753-3 (Edición Digital PDF)

USC UNIVERSIDADE DE SANTIAGO DE COMPOSTELA

DEPARTAMENTO DE QUÍMICA FÍSICA

D. Manuel Arturo López Quintela, catedrático del departamento de Química Física de la Universidad de Santiago de Compostela; D. José Francisco Rivadulla Fernández, profesor titular del departamento de Química Física de la Universidad de Santiago de Compostela y D. Carlos Vázquez Vázquez, contratado doctor del departamento de Química Física de la Universidad de Santiago de Compostela,

Certifican:

Que el trabajo descrito en la memoria titulada **"Chemical, magnetic and electronic properties of Na_xCoO_2 and related compounds"** ha sido realizado bajo nuestra dirección por D. Manuel Bañobre López y reúne todos los requisitos necesarios para ser presentado como Tesis Doctoral.

Santiago de Compostela, 8 de Abril de 2011.

Fdo.:Prof. D. M. Arturo López Quintela	Fdo.:Prof. D. J. Francisco Rivadulla Fernández	Fdo.:Prof. D. Carlos Vázquez Vázquez

Fdo.: Manuel Bañobre López
El doctorando

Agradecimientos (Spanish readers)

En primer lugar me gustaría agradecer a mi director, el Prof. M. Arturo López Quintela, por darme la oportunidad de trabajar en su grupo y confiar en mí durante todo este tiempo. De su parte siempre he recibido buenas ideas, consejos, libertad y toda la dirección que he necesitado.

Mi más sincero agradecimiento también para mi co-director el Prof. Francisco Rivadulla. Lo que a continuación podréis leer es el resultado de un reto que ambos nos propusimos hace ya unos años, y que él tenía en su cabeza. De él destaco y agradezco su profesionalidad, su metodología, su dedicación, y esas charlas de café en las que consigue renovar tu motivación e ilusión, tantas veces decaídas. Con él comencé a familiarizarme con el mundo del estado sólido, y sin duda que el futuro confirmará que habrá sido el mejor maestro posible. Mis disculpas si no he estado a la altura y no he aprendido más. Pero además de un buen jefe es un mejor amigo, siempre accesible y dispuesto a ayudar cuando se le necesita, tanto en lo profesional como en lo personal; se me ocurren muchas cosas que agradecerte, pero bueno…mejor es que siga con esto. Gracias Fran.

Gracias también a mi co-director el Prof. Carlos Vázquez, con el que empecé a trabajar en un laboratorio sintetizando nanopartículas de óxidos de cromo, y más tarde, lo que se puso por delante. Con él aprendí a fijarme en los detalles y no dar nada por perdido en el lab. Gracias Carlos por estar siempre disponible para echar esa mano que tantas veces hizo falta. Un gran amigo.

Gracias también al Prof. José Rivas, que siempre que lo he necesitado me ha dado su tiempo y nunca me ha escatimado medios para avanzar y seguir adelante. Y por permitirme el pluriempleo!, e ir terminando esta escritura al tiempo que trabajamos en la hipertermia magnética de materiales híbridos y multifuncionales.

Mi más sincero agradecimiento para el Prof. J. B. Goodenough, por aceptarme en su grupo para una estancia realizada en el Texas Materials Institute de la Universidad de Texas en Austin. Una ejemplar combinación de lucidez, responsabilidad y respeto. Su

puerta siempre estuvo abierta para recibirme y responder mis preguntas, seguramente absurdas. Aunque ha sido poco tiempo, la experiencia de trabajar en su grupo y haberlo conocido ha sido inolvidable, y un honor. Gracias también a Román Caudillo, por su recibimiento y su colaboración en el estudio del Na_xCoO_2. Y al Dr. Huang, por enseñarme a fabricar baterías!

Aquí de nuevo…Gracias a los *X-men* (y a la *X-woman*) de la unidad de difracción de rayos-X de la USC, especialmente al Dr. Bruno Dacuña, a quién recurría cuando algún ajuste se podía mejorar o cuando quería echarme unas risas.

Y llega el turno del FEDER…hay una larga lista de amigos ahí dentro, ellos son los responsables de ese gran ambiente que consigue que uno trabaje agusto. Sois muchos, así que gracias a todos. Pero permitidme que destaque a los componentes del laboratorio de estado sólido, que han sido los verdaderos compañeros de batalla: a los que están, Bea (de inestimable ayuda en su etapa en Física, ¿cuántos transfers habremos hecho?), Camilo (el principal responsable del diseño de esta portada y de la síntesis industrial del CrN en el lab); y a los que ya no están, Marta, Santi, Pablito Botta…con quiénes solucionaba los problemas que surgían en el día a día. Y a Suelih, mi contrabandista de papers en Brasil! Gracias también a Alfonso Fondado, que tantas veces tuvo que arreglar el aparato de poder termoeléctrico por mi culpa. Pero, sobre todo, gracias a mis compis de despacho: Yolanda (la Mamma, los galones, cuantos consejos me habrá dado!), Ana (la mejor gestora del tiempo que conozco, la que siempre está para una caña (ejem…), la que poco a poco está descubriendo el perfeccionismo, jeje…ánimo!), Camilo otra vez (un erudito de las ciencias y las artes, respetuoso del orden y las proporciones y fiel seguidor de Diógenes, jeje), Cristina Hoppe (la bohemia marplatense que nos visita en cuanto puede)…Ellos son los que han sufrido más de cerca aquellos días en que uno se levantaba con mejor o peor pie, los que escuchaban las aventuras y desventuras cotididanas, las risas, los problemas, el silencio a veces, y los más dispuestos a arrimar el hombro cuando hacía falta. Sois ya amigos de una época, gracias!.

Gracias también a todos los co-autores que han participado de una u otra forma en las publicaciones en las que aparece mi nombre, por su trabajo.

Gracias ahora a los amigos que hacen que el tiempo de ocio sea, precisamente, eso, especialmente a los de la “aldea Gala”, a Jenaro en particular por esa capacidad de sacar GB libres de un disco duro repleto, cuántas veces me habrá salvado la vida...Mención especial para Myriam, que ha seguido de cerca esta tesis y a la que tengo mucho que agradecer, entre otras cosas su confianza y sus palabras de ánimo.

A Arnold, el filósofo-psicólogo de la vida defensor de la agricultura orgánica y ahora también de las cervezas de triple fermentación, jeje. Y a Matt, por esas cañas con acento inglés!

Y a los colegas emigrados, que a pesar de los kilómetros de distancia siempre hacen lo que sea por reunirse, Juan Carlos (un llanero solitario en el Sahara que convierte la arena en cemento; como te echo de menos, tío), David de Lires (un percebeiro da Costa da Morte reconvertido a “Texan driller engineer” en el Golfo de México) y Julito (un “bilingual teacher” que tiene la “tecnología para hacerlo”).

Y a David Abeal, un amigo de siempre que lo relativiza todo, y eso ayuda.

Gracias también a la financiación, parte crucial en estas labores. A la Xunta de Galicia y al Ministerio de Educación y Ciencia (en aquella época), por la estabilidad que me proporcionaron en mis inicios y en esos cuatro años de FPU, respectivamente.

Claro, GRACIAS a Cristiana, por su sosiego, por decir siempre lo que uno necesita oír en los momentos difíciles y por ayudarme a encontrar un final feliz para esta historia.

Y el último lugar lo reservo para quién más se lo merece, mi familia. GRACIAS. Especialmente a mis padres, a mi madrina (también abuela) y a mi padrino (también abuelo, también Manolo), de quiénes nunca se deja de aprender. Vuestra comprensión y vuestro sacrificio ha sido fundamental para llegar hasta aquí, de otra forma no habría sido posible. Gracias por compartir vuestra ilusión y por no cansaros nunca de preguntar “¿como va esa tesis?” Ahora os respondo: “Aquí está”. Es también vuestra.

Acknowledgments (English readers)

First I would like to thank my director, Prof. M. Arturo López Quintela, for giving me the opportunity to work in his group and trust me all this time. For his part I have always received good ideas, tips, freedom and all the direction I needed.

My sincere thanks also to my co-director Prof. Francisco Rivadulla. The following work is the result of a challenge that both we proposed some years ago, and that he had in his head. Of him, I emphasize and appreciate his professionalism, his methodology, his dedication, and the talks we had over a coffe that renewed my motivation and enthusiasm, as often decayed. With him I began to familiarize myself with the world of solid state, and the future will confirm that he will have been the best teacher possible. My apologies if I have not learned more. But besides a good boss is a better friend, always available and willing to help when needed, both professionally and personally, I can think of many things to thank you, but...better to continue with this. Thanks Fran.

Thanks also to my co-director Prof. Carlos Vázquez, with whom I started working in a lab synthesizing chromium oxide nanoparticles and, later, clusters of Cu. I share research with him on everything that is put forward, and also friendly relationship. Thank you for being available to take that hand that I needed so many times.

Thanks a lot to Prof. José Rivas, who gave me his valuable time whenever I needed and who have never spared resources in order to advance and move forward. And also for allowing me moonlighting!, and let me to finish this dissertation while working on magnetic hyperthermia of hybrid and multifunctional materials.

My sincere thanks to Prof. J. B. Goodenough, for accepting me in his group for a stay made in the Texas Materials Institute, University of Texas at Austin. An exemplary combination of insight, responsibility and respect. His door was always open to receive me and answer my questions, surely absurd. Although there has been little time, the experience of working in his group and have known him personally have been unforgettable, and an honor. Also thanks to Roman Caudillo, part of their group at that time, for his warm

welcome and cooperation in the study of Na_xCoO_2. And to Dr. Huang, for teaching me to make some batteries!

Here again…thanks to the X-Men (and X-woman) of the unit X-ray diffraction of the USC, especially Dr. Bruno DaCunha, who resorted when some refinament could be improved or needed to share a laugh.

And it is the turn of the FEDER ... there is a long list of friends there, they are responsible for the great atmosphere in which you get a comfortable work. You are many, so thank you to everyone. But let me highlight the components of solid-state laboratory, which have been the true sparring partners: those who are, Bea (of invaluable help during his time in Physics, how many transfers we will have done?), Camilo (primarily responsible for the design of the cover and industrial synthesis of CrN in the lab), and no longer, Marta, Santi, Pablito Botta...who I solved the problems found in day to day with. And to Suelih, my papers smuggler in Brazil!. Thanks also to Alfonso Fondado which so often had to fix the thermoelectric power apparatus because of me. But above all, thanks to my office compis: Yolanda (the Mamma, the gallons, how many good tips during this time!), Ana (the best time manager I know, who never says not to a beer (...), who is slowly discovering the perfectionism, hehe...courage), Camilo again (an erudite of science and arts, respectful with the order and proportions and faithful follower of Diogenes), Cristina Hoppe (bohemian marplatense who visit us as possible)...they are the ones who have closely suffered those days when you wake up with a good or bad spirit, those who listen the daily adventures and misadventures, laughs, problems, silence sometimes, and anyway they are willing to help when needed. You are already friends of a time, thank you.

Thanks also to all co-authors who have participated in one way or another in the publications in which my name appears, for their work.

Now, thanks to friends who make leisure time is precisely that, especially to the "Gala village", to Jenaro in particular for his ability to take GB free from a full hard disk, how many times you saved my life... Special mention for Myriam, who has closely followed this work and to who I have a lot to be thankful for, among other things their confidence and encouragement.

To Arnold, the philosopher-psychologist of the life defender of organic farming and now also of the triple fermentation beer, hehe. And also to Matt, for those beers with an English accent! What a patience you all have!

And the friends emigrants who, despite the miles of distance always do whatever they can to meet, Juan Carlos (a lone ranger in Sahara who turns sand into cement; I miss you, man), David de Lires (a barnacle hunter in Costa da Morte converted to "Texan driller engineer" in the Gulf of Mexico) and Julio (a "bilingual teacher who "has the technology to do it").

I do not forget David Abeal, with whom I have a friendship forged in Santiago, for its ability to relativize everything, which helps a lot sometimes.

Thanks also to the financial support, a crucial part in this work. The Xunta de Galicia and Ministry of Education and Science, for the stability provided to me at the beginning and later with four years of FPU, respectively.

Of course, thanks to Cristiana, for her calm, for saying always what one needed to hear in the difficult moments and for helping me to find a happy end to this story.

And I kept the last place for those who most deserve it, my family. THANKS. Especially my parents, my godmother (also grandmother) and my godfather (also grandfather, also named Manolo), from whom one never stops learning. Your understanding and your sacrifice has been the key in getting here, otherwise it would not have been possible. Thank you for your enthusiasm and for never getting tired of asking "how that thesis is going on?" Now I can answer: "Here it is". It is also yours.

Abbreviations

AFM: Antiferromagnetic
BLH: Bilayer-hydrate
CO: Charge ordering
CW: Curie-Weiss
DSC: Differential Scanning Calorimetry Analysis
EDAX: Energy Dispersive X-ray Spectroscopy
E_F: Fermi Energy
FC: Field Cooling
FL: Fermi Liquid
FM: Ferromagnetic
FZ: Floating Zone
HS: High Spin
ICP-OES: Inductively Coupled Plasma Optical Emission Spectroscopy
ICSD: Inorganic Crystallographic Sample Database
IS: Intermediate Spin
LDA: Local Density Approximation
LS: Low Spin
MLH: Monolayer-hydrate
NMR: Nuclear Magnetic Resonance
NQR: Nuclear Quadropolar Resonance
O: Octahedric Na^+ coordination
P: Trigonal Prismatic Na^+ coordination
PM: Paramagnetic
QCP: Quantum Critical Point
QPT: Quantum Phase Transition
SC: Superconductivity
SDW: Spin Density Wave
SEM: Scanning Electron Microscopy
SFT: Spin Fluctuation Theory
SG: Spin-glass

T_c: Superconducting Critical Temperature
TEP: Thermoelectric Power
TGA: Thermogravimetric Analisys
WIFM: Weak Itinerant Ferromagnet
XRD: X-ray Diffraction
ZFC: Zero Field Cooling

Table of Contents

Chemical, magnetic and electronic properties of Na_xCoO_2 and related compounds.

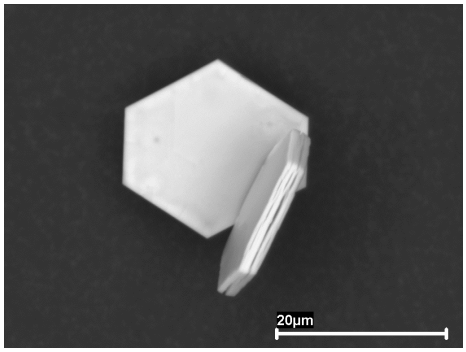

Prologue (Spanish readers)

En el momento de escribir esta tesis acerca de las propiedades químicas y físicas del Na_xCoO_2, mi ambición principal fue la de presentársela al lector de una forma sencilla y amena. Con el objetivo de ofrecer una lectura comprensible, ligera y dinámica, esta tesis fue confeccionada como un ensamblaje de historias individuales en las que, a menudo, resultados, interpretaciones y referencias se intercalan casi sin pausa, más al estilo de un libro especializado en un sistema en particular que al de una tesis.

Teniendo esto en cuenta, esta presentación se divide en seis capítulos, conclusiones y un apéndice. La común introducción teórica general utilizada normalmente en las disertaciones doctorales, ha sido sustituida aquí por una breve introducción específica al principio de cada capítulo. Por lo tanto, el lector dispondrá de una visión general del estado del arte de la materia que se desarrolla en cada capítulo en particular y apreciará mucho mejor la contribución de este trabajo a la comprensión de las propiedades químicas y físicas del sistema.

Sin embargo, una introducción general a la fenomenología básica del sistema, así como la descripción de la motivación que nos ha llevado a la realización de esta tesis, sigue siendo necesaria, y será, por tanto, brevemente proporcionada en las páginas siguientes.

El Na_xCoO_2 no es un material nuevo; fue primeramente sintetizado en la década de 1970[1] y ha sido estudiado ampliamente desde entonces[2,3,4]. Sin embargo, el descubrimiento de nuevas propiedades y su posible relación con fenómenos similares en otros materiales, ha impulsado un renovado interés en este sistema. Si se hace una búsqueda bibliográfica en un explorador científico (Scifinder, por ejemplo) por la palabra clave "Na_xCoO_2", y se representan los resultados siguiendo un orden cronológico, podemos observar el gran número de artículos publicados en la última década acerca de este sistema (Figura P.1).

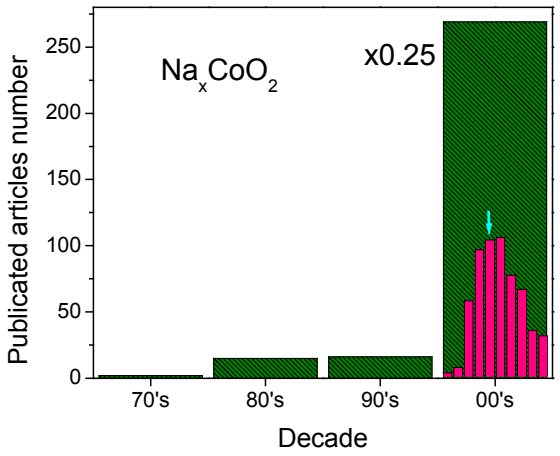

***Figure P.1**: Evolución del número de artículos científicos publicados cada año durante la última década en el sistema Na_xCoO_2, de acuerdo con el buscador Scifinder. La flecha en cian indica cronológicamente el punto inicial de esta tesis.*

---

[1] C. Fouassier, G. Matejka, J.-M. Reau and P. Hagenmuller. *J. Solid State Chem*. **6**, 532 (**1973**).

[2] R. Berthelot, D. Carlier and C. Delmas. *Nature Materials* **10**, 74 (**2011**).

[3] S. Hébert and A. Maignan. Thermoelectric Oxides, in *Functional Oxides* (eds D. W. Bruce, D. O'Hare and R. I. Walton), John Wiley & Sons, Ltd, Chichester, UK. ISBN: 9780470997505 (**2010**).

[4] Y. Ihara, K. Ishida, H. Sakurai and E. Takayama-Muromachi. Phase diagram for $Na_x(H_3O)_zCoO_2 \bullet yH_2O$, in New research on Superconductivity (ed. B. P. Martins), Nova Science Publishers, Inc, New York, USA. ISBN: 978-1-59454-197-1 (**2007**).

El Na_xCoO_2 es excepcional en este sentido, ya que ha conseguido el interés de la comunidad científica durante las últimas tres décadas por diferentes razones. Así, en los años 80 se investigó debido a sus propiedades electroquímicas (alta movilidad iónica, alta conductividad eléctrica) [5,6,7,8,9] y su potencial aplicación como cátodo en baterías alcalinas reversibles, al igual que su análogo Li_xCoO_2.[10] En los 90, sus propiedades termoeléctricas fueron las que despertaron el interés de este material para la captación de energía a alta temperatura y la refrigeración[11]. El rendimiento termoeléctrico de un sistema particular se cuantifica a partir del valor proporcionado por la figura de mérito termoeléctrica (ecuación [P.1]),

$$Z = \frac{S.\rho}{k} \qquad \text{eq. [P.1]}$$

donde S, ρ and κ son el poder termoeléctrico, la resistividad eléctrica y la conductividad térmica, respectivamente. El poder termoeléctrico representa el voltaje creado por un gradiente térmico entre dos puntos de la muestra.

La tabla P.1 muestra los valores del poder termoeléctrico expresados a partir de la figura de mérito de la ecuación [P.1] a diferentes temperaturas para monocristales y policristales de Na_xCoO_2, en comparación con un material termoeléctrico convencional tipo-*p*.

Pero la verdadera revolución científica originada por este material llegaría en 2005, después de que *Takada et al*[12] reportaran superconductividad (SC) a temperaturas por debajo de 5 K en una fase de bajo contenido de Na^+ después de que moléculas de agua se intercalasen en su estructura, $Na_{0.3}CoO_2 \bullet 1.3H_2O$ (Figura P.2). Después de esta

[5] C. Delmas, J. J. Braconnier, C. Fouassier and P. Hagenmuller. *Solid State Ionics* **3-4**, 165 (**1981**).
[6] J. Molenda, C. Delmas and P. Hagenmuller. *Solid State Ionics* **9-10**, 431 (**1983**).
[7] S. Kikkawa, S. Miyazaki and M. Koizumi. *J. of Power Sources*, **14**, 231 (**1985**).
[8] S. Kikkawa, S. Miyazaki and M. Koizumi. *J. Solid State Chem.* **62**, 35 (**1986**).
[9] J. Molenda, C. Delmas, P. Dordor. *Solid State Ionics* **12**, 473 (**1989**).
[10] K. Mizushima, P.C. Jones, P.J. Wiseman and J.B. Goodenough. *Mater. Res. Bull.* **15**, 6, 783 (**1980**).
[11] I. Terasaki, Y.Sasago, K.Uchinokura. *Phys. Rev. B* **56**, 12685 (**1997**).
[12] K. Takada, H. Sakurai, E. Takayama-Muromachi, F. Izumi, R. A. Dilanian and T. Sasaki. *Nature* **422**, 53 (**2003**).

publicación, las similitudes entre el Na_xCoO_2 y los cupratos superconductores surgieron de forma inminente. Particularmente, la proximidad a una fase aislante de Mott en x=0.5 incrementó las especulaciones de que la superconductividad en los óxidos de cobalto y de cobre podría estar gobernada por mecanismos similares.

Table P.1: *Valores de la figura de mérito adimensional, ZT, para monocristales y policristales de Na_xCoO_2 en comparación con un material termoeléctrico convencional.*

	$Na_xCoO_{2-\delta}$ single crystal		**$Na_xCoO_{2-\delta}$ polycrystal**		**$Si_{0.95}Ge_{0.05}$ typical p-type**	
	300K	**800K**	**300K**	**800K**	**300K**	**800K**
ZT	**0.03**	**1.2**	**0.08**	**0.31**	**0.16**	**0.57**

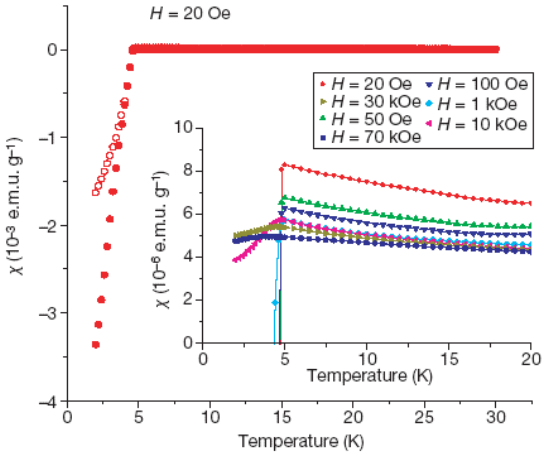

Figure P.2: *Susceptibilidad magnética en función de la temperatura en $Na_xCoO_2 \bullet H_2O$ reportada por Takada et al (Ref. 12) mostrando el estado SC por debajo de 5 K.*

Sin embargo, muchos puntos fundamentales en la química y física de este sistema permanecen sin ser clarificados para el entendimiento de la superconductividad en Na_xCoO_2. El más importante es el cuál es el papel que ejerce el agua en la aparición de la superconductividad en el sistema. Pero también la relación existente entre el contenido de Na^+ y la concentración de portadores en los planos de CoO_2, o el efecto de la dimensionalidad estructural y electrónica son aspectos clave que no han sido explicados todavía.

Con el objetivo de comprender un poco mejor las propiedades químicas y físicas de este sistema, es esencial describir brevemente los aspectos estructurales y electrónicos del Na_xCoO_2.

La estructura cristalina de este óxido consiste en capas bidimensionales de octaedros CoO_6 que comparaten aristas y que se encuentran separadas entre sí por capas de iones Na^+ (see Figure P.3). En esta estrucutura, los átomos de Co forman una red hexagonal con enlaces triangulares M-M.

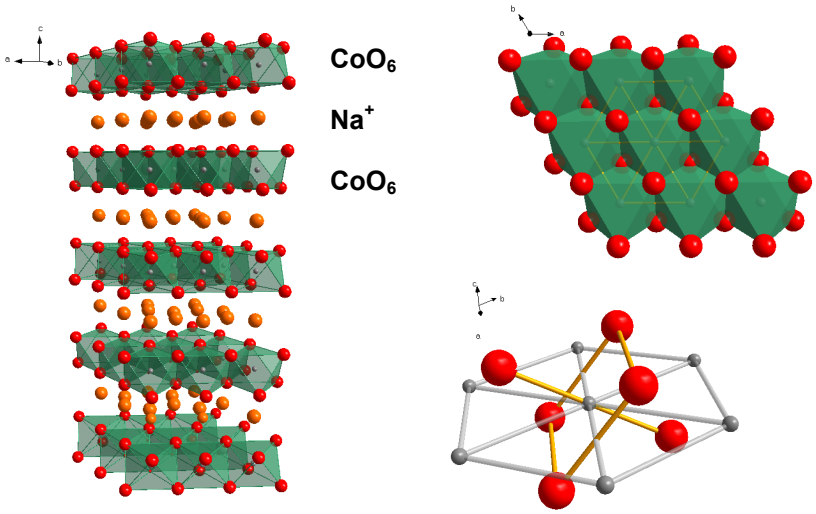

Figure P.3: *Izquierda: Representación 3D de la estructura bidimensional de Na_xCoO_2. Las bolas grises (rojas) [naranjas] representan los átomos de cobalto (oxígeno) [sodium]. Derecha: (arriba) Disposición de los octaedros CoO_6 a lo largo de las capas de CoO_2 perpendiculares al eje c (abajo) Detalle de la coordinación alrededor de un átomo de Co.*

Los iones Na^+ ocupan dos posiciones cristalográficas diferentes en la estructura del Na_xCoO_2: octaédrica (O) o trigonal prismática (P), ambas situadas en el mismo plano y a la mitad de la distancia que separa las capas de CoO_2. La celda unidad de Na_xCoO_2 está determinada por la orientación relativa de los planos de CoO_2 y la geometría de los sitios de Na^+ (Figure P.4). [13]

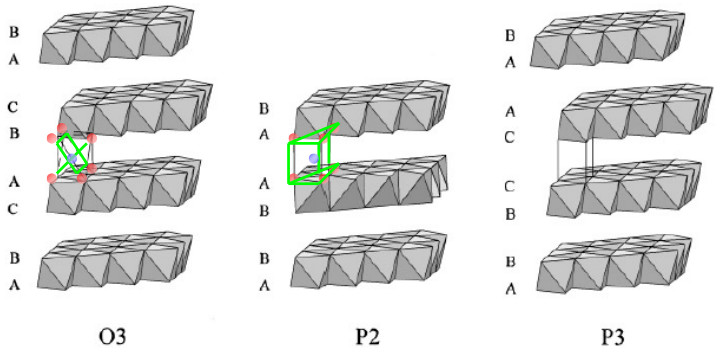

Figure P.4: *Representación de las diferentes celdas unidad para Na_xCoO_2: O3, P2 and P3. La letra indica la geometría del sitio de Na^+, octaédrica (O) o trigonal prismática (P). El número 2 o 3 indica el número de capas de CoO_2 presentes en la celda unidad (Ref. 13).*

De esta forma, fases y estructuras diferentes pueden aparecer en función del contenido de Na^+ (Table P.2) [1432]:

[13] B. L. Cushing and J. B. Wiley. *J. Solid State Chem.* **141**, 385 (**1998**).

[14] L. Viciu, J. W. G. Bos, H. W. Zandbergen, Q. Huang, M. L. Foo, S. Ishiwata, A. P. Ramirez, M. Lee, N. P. Ong and R. J. Cava. *Phys. Rev. B* **73**, 174104 (**2006**).

Table P.2: *Simetría de la celda unidad observada en compuestos de estequiometría Na_xCoO_2 (0.3<x<1) en función de la coordinación de los iones Na^+ y el número de capas por celda unidad (Ref. 14).*

Refined composition	Space group	Sodium coordination	Structure type
	Two-layer structures		
$Na_{0.34}CoO_2$[a]	$P6_3/mmc$	Trigonal prism	$P2$
$Na_{0.5}CoO_2$[b]	$Pnmm$	Trigonal prism	$P2$
$Na_{0.63}CoO_2$[a]	$P6_3/mmc$	Trigonal prism	$P2$
$Na_{0.71}CoO_2$[a]	$P6_3/mmc$	Trigonal prism	$P2$
$Na_{0.76}CoO_2$[a]	$P6_3/mmc$	Trigonal prism	$P2$
$Na_{0.80}CoO_2$[a]	$P6_3/mmc$	Trigonal prism	$P2$
Na_1CoO_2[a]	$P6_3/mmc$	Trigonal prism	$P2$
	Three-layer derived structures		
$Na_{0.32}CoO_2$[c]	$R\bar{3}m$	Octahedral	$O3$
$Na_{0.5}CoO_2$[c]	$C2/m$	Trigonal prism	$P1$
$Na_{0.6}CoO_2$[c]	$C2/m$	Trigonal prism	$P1$
$Na_{0.67}CoO_2$[d]	$C2/m$	Trigonal prism	$P1$
$Na_{0.75}CoO_2$[c]	$C2/m$	Octahedral	$O1$
$Na_{0.92}CoO_2$[c]	$R\bar{3}m$	Octahedral	$O3$

En el caso de la fase superconductora, $Na_{0.3}CoO_2 \bullet 1.3H_2O$, el agua se intercala entre las capas de iones Na^+ y CoO_2 incrementando dramáticamente el parámetro de red *c* desde ~11.1 Å a ~19.5 Å, Figure P.5. Se ha sugerido que el efecto del agua en la reducción de la dimensionalidad de la estructura es esencial para la obtención de la superconductividad en el sistema[10], lo cual está soportado por la no observación de SC en la fase parcialmente hidratada $Na_{0.3}CoO_2 \bullet 0.6H_2O$, que presenta el mismo estado de oxidación del Co pero substancialmente menor separación entre las capas de CoO_2 en comparación con las muestras superconductoras[15].

[15] M. L. Foo, R. E. Schaak, V. L. Miller, T. Klimczuk, N. S. Rogado, Y. Wang, G. C. Lau, C. Craley, H. W. Zandbergen, N. P. Ong and R. J. Cava. *Solid State Comm.* **127**, 33 (**2003**).

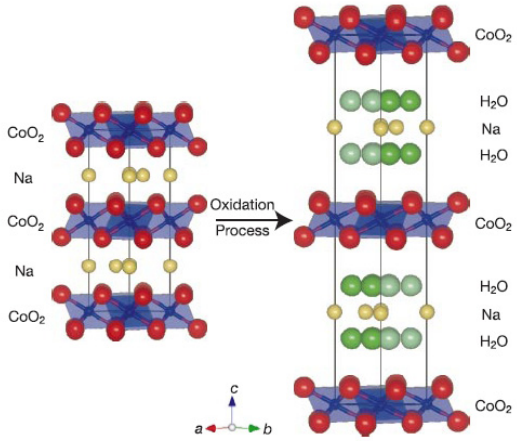

Figure P.5: *Representación esquemática que muestra el incremento de la celda unidad del Na_xCoO_2 in la dirección c una vez que el agua es intercalada en la estructura (from Ref. 9).*

La intercalación de agua en la red origina nuevos detalles estructurales que deben ser analizados. La resolución de la estructura cristalina de la fase superconductora ha sido una de las tareas más importantes de los últimos años, ya que constituye un punto crucial para la comprensión del mecanismo de apareamiento de los spines que origina la superconductividad en este sistema. Sin embargo, aunque diferentes modelos estructurales de sistemas agua-intercalados $Na_xCoO_2 \bullet yH_2O$ han sido propuestos, no ha sido todavía alcanzado un acuerdo entre ellos. En lo que sí se coincide en este momento es que muchas composiciones con diferentes cantidades de H_2O intercalada coexisten en las muestras hidratadas, complicando aún más su análisis.

Echemos ahora un vistazo más de cerca de la estructura electrónica de los átomos de Co en el Na_xCoO_2. Para x=0, por tanto simplemente CoO_2, cada átomo de Co se encuentra en el estado de oxidación Co^{4+}, con sus 5 electrones de valencia ocupando los orbitales 3d (si asumimos un cuadro puramente iónico). En una configuración de bajo spin el Co^{4+} presenta un solo electron desapareado, y por tanto con spin ½. Cuando se introducen iones Na^+ en la estructura, cada uno contribuye con un electrón adicional, transformando así los iones Co^{4+} en iones Co^{3+}, que en una configuración de bajo spin presentan comportamiento diamagnético. Por tanto, para x=1, $NaCoO_2$, todos los átomos de Co estarían en el estado Co^{3+} y conducirían a

un sistema íntegramente diamagnético. Los niveles de energía de estas dos configuraciones de spin límites están representados en el diagrama de la figura P.6.

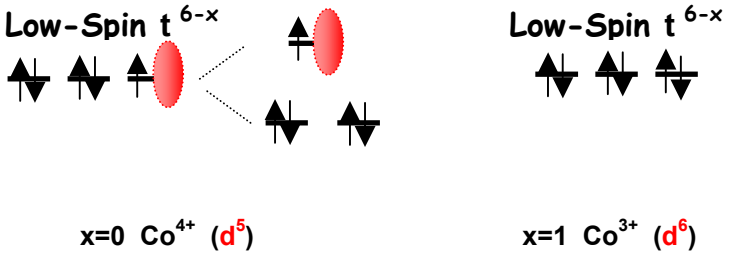

***Figure P.6**: Representación esquemática de los niveles de energía y configuraciones de spin para Na_xCoO_2 x=1 and x=0.*

La posibilidad de valencia mixta, junto con las diferentes configuraciones de spin posibles y la fuerte hibridación entre los orbitales 3d del cobalto y los orbitales 2p del oxígeno, son los responsables de la riqueza del diagrama de fases del Na_xCoO_2.

Al comienzo de esta tesis, el diagrama de fases aceptado para este sistema era el reportado por *Shaak et al*[16], que mostraba una gran variedad de fases magnéticas y eléctrónicas en función del dopaje y la temperatura (Figura P.7): paramagnetismo de Pauli (PM), comportamiento Curie-Weiss (CW) dependiente de la temperatura, orden antiferromagnético (AFM) o densidad de ondas de spin (SDW). Todas estas fases magnéticas coinciden con un comportamiento eléctrico tipo metálico, excepto para x=0.5, composición en la que el sistema pasa a través de una transición "metal-aislante" como consecuencia de un cierto tipo de ordenamiento de carga (CO)[17]. Además, es importante resaltar el estado superconductor que aparece por debajo de 5 K cuando se intercala agua en la estructura para composiciones de Na^+ $1/4 \leq x \leq 1/3$.

[16] R. E. Schaak, T. Klimczuk, M. L. Foo and R. J. Cava. *Nature*, **424**, 527 (**2003**).
[17] M. L. Foo, Y. Wang, S. Watauchi, H. W. Zandbergen, T. He, R. J. Cava and N. P. Ong. *Phys. Rev. Lett.* **92**, 247001 (**2004**).

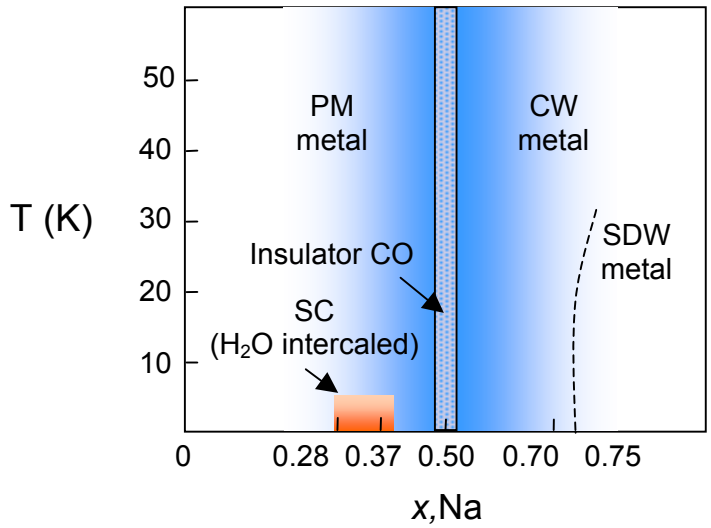

Figure P.7: *Magnetic/electric phase diagram of Na_xCoO_2 propposed by Schaak et al in Ref. 16.*

En este estrecho rango de composiciones de Na^+ entre las que se logra superconductividad, la dependencia de la temperatura de transición superconductora (T_c) con el dopaje de Na^+ sigue siendo confusa. En un principio, se estableció una fuerte correlación entre la T_c y el contenido de Na^+ de las muestras y se reportó un dopaje químico óptimo que originaba superconductividad con una $T_c \approx 4.5$ K para una composición de Na^+ $x \approx 0.3$[35]. Esta dependencia de T_c con el dopaje muestra el mismo tipo de tendencia encontrada también en los cupratos. Por esta razón, se consideró que este material sería un buen candidato para aportar respuestas al mecanismo que rige la superconductividad en estos óxidos. Sin embargo, posteriormente, se generó una gran controversia cuando valores de T_c casi independientes de x fueron reportados[18,19].

Como consecuencia de todas estas controversias, al principio de este trabajo existía un número de preguntas abiertas que permanecían sin

[18] D. P. Chen, H. C. Chen, A. Maljuk, A. Kulakov, H. Zhang, P. Lemmens, and C. T. Lin. *Phys. Rev. B* **70**, 024506 (**2004**).
[19] C. J. Milne, D. N. Argyriou, A. Chemseddine, N. Aliouane, J. Veira, S. Landsgesell and D. Alber. *Phys. Rev. Lett.* **93**, 247007 (**2004**).

respuesta y que, al mismo tiempo, eran de crucial importancia para el entendimiento de este fenómeno:

1) ¿Cuál es el papel de la covalencia del enlace Co-O?

2) Relacionado con esto, ¿existe una relación directa entre el contenido de Na^+ y el estado de oxidación real del Co?

3) ¿Actúa el H_2O solamente como un espaciador químico o juega algún otro papel?

4) ¿Cuál es el papel de la fase aislante x=0.5 en el diagrama de fases?

Con el objetivo de contribuir a responder estas preguntas, hemos llevado a cabo un análisis exhaustivo y sistemático de las propiedades magnéticas y de transporte del Na_xCoO_2, particularmente centrado en las nuevas fases magnéticas que aparecen alrededor de $x\approx0.5$ y su relación con la superconductividad descubierta en el sistema.

Esperamos que esto ayude a explicar algunas de las muchas cuestiones acerca de la química y la física de este material que todavía continúan sin respuesta.

Prologue (English readers)

At the time of writting this thesis, my main concern was to present the chemical and physical properties of Na_xCoO_2 in an amenable way to the reader. In order to offer an understable, lighter and dynamic reading of this thesis, the whole dissertation can be considered as an assembly of individual “stories”, where results, interpretations and references are intercalated continuously in an almost “non-stop” way, more in the style of a book or a scientific paper about a particular system, than in a thesis.

Taking this into account, this presentation is divided into seven chapters and two appendixes. The common general theoretical introduction normally used in the PhD dissertations, has been replaced by a brief specific introduction at the beginning of each chapter. Therefore, the reader will have a specific overview of the state of the art in the topic developed in each particular chapter and will appreciate much better the contribution of this work to the understanding of the chemical and physical properties of the system.

However, some general introduction to the basic phenomenology of the system, as well as to the motivation of the thesis is still needed, and provided in the following pages.

Na_xCoO_2 is not a novel material; it was first synthetized in the 1970's[20] and it has been extensively studied since then[21,22,23]. However, the discovery of novel properties and their possible relationship with similar phenomena found in other materials, boosted a renewed interest in this system. If we make a bibliographic search in a scientific browser (*i. e. Scifinder*) by the key_word "Na_xCoO_2", and plot the results following a cronological order, we can observe the large number of articles published in the last decade (Figure P.1).

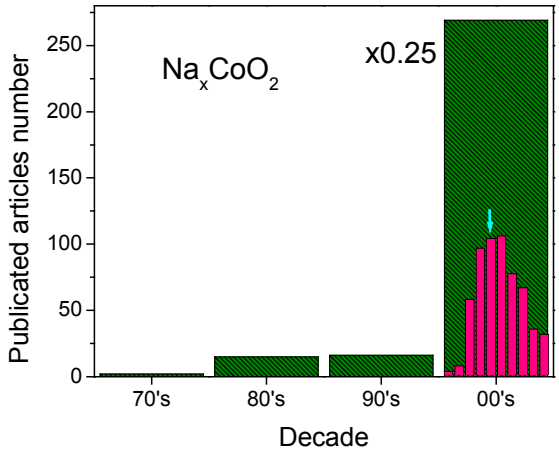

Figure P.1: *Evolution of the number of scientific articles published each year in the system Na_xCoO_2, according to the Scifinder. The cian arrow marks the starting point of this thesis.*

[20] C. Fouassier, G. Matejka, J.-M. Reau and P. Hagenmuller. *J. Solid State Chem*. **6**, 532 (**1973**).
[21] R. Berthelot, D. Carlier and C. Delmas. *Nature Materials* **10**, 74 (**2011**).
[22] S. Hébert and A. Maignan. Thermoelectric Oxides, in *Functional Oxides* (eds D. W. Bruce, D. O'Hare and R. I. Walton), John Wiley & Sons, Ltd, Chichester, UK. ISBN: 9780470997505 (**2010**).
[23] Y. Ihara, K. Ishida, H. Sakurai and E. Takayama-Muromachi. Phase diagram for $Na_x(H_3O)_zCoO_2 \bullet yH_2O$, in New research on Superconductivity (ed. B. P. Martins), Nova Science Publishers, Inc, New York, USA. ISBN: 978-1-59454-197-1 (**2007**).

Na_xCoO_2 is excepcional in this sense, as it raised the interest of the community by different reasons during the last three decades. In the 80´s, it was investigated due to its electrochemical properties (high ionic mobility, high electrical conduction)[24,25,26,27,28] and tested as a cathod in reversible alkaline cells, as its analogous Li_xCoO_2[29]. In the 90's, its thermoelectric properties raised the interest of this material for energy harvesting at high temperature and refrigeration[30]. The thermoelectric performance of a particular system is quantified by the thermoelectric figure of merit (equation [P.1]),

$$Z = \frac{S.\rho}{k} \qquad \textbf{eq. [P.1]}$$

where S, ρ and κ are the thermoelectric power, electrical resistivity and thermal conductivity, respectively. The thermoelectric power represents the voltage created by a thermal gradient between two points of the sample.

Table P.1 shows the values of the thermoelectric performance expreseed by the figure of merit (equation [P.1]) at different temperatures for Na_xCoO_2 single- and polycrystals in comparison with a conventional *p*-type thermoelectric material.

But the breakthrough come in 2005, after Takada *et al*[31] reported superconductivity (SC) below 5 K after water intercalation in a phase with low Na^+ content, $Na_{0.3}CoO_2 \bullet 1.3H_2O$ (Figure P.2). Inmediately after this report the similarities of Na_xCoO_2 with the superconducting cuprates were raised. Particulary, the proximity to a Mott insulating phase at x=0.5 fuelled

[24] C. Delmas, J. J. Braconnier, C. Fouassier and P. Hagenmuller. *Solid State Ionics* **3-4**, 165 (**1981**).
[25] J. Molenda, C. Delmas and P. Hagenmuller. *Solid State Ionics* **9-10**, 431 (**1983**).
[26] S. Kikkawa, S. Miyazaki and M. Koizumi. *J. of Power Sources*, **14**, 231 (**1985**).
[27] S. Kikkawa, S. Miyazaki and M. Koizumi. *J. Solid State Chem*. **62**, 35 (**1986**).
[28] J. Molenda, C. Delmas, P. Dordor. *Solid State Ionics* **12**, 473 (**1989**).
[29] K. Mizushima, P.C. Jones, P.J. Wiseman and J.B. Goodenough. *Mater. Res. Bull.* **15**, 6, 783 (**1980**).
[30] I. Terasaki, Y.Sasago, K.Uchinokura. *Phys. Rev. B* **56**, 12685 (**1997**).
[31] K. Takada, H. Sakurai, E. Takayama-Muromachi, F. Izumi, R. A. Dilanian and T. Sasaki. *Nature* **422**, 53 (**2003**).

speculation that superconductivity in the cobalt and copper oxides could be governed by similar mechanisms.

Table P.1: *Values of the dimensionless figure of merit, ZT, for Na_xCoO_2 single- and polycrystals in comparison with a conventional thermoelectric material.*

	$Na_xCoO_{2-\delta}$ single crystal		$Na_xCoO_{2-\delta}$ polycrystal		$Si_{0.95}Ge_{0.05}$ typical p-type	
	300K	800K	300K	800K	300K	800K
ZT	0.03	1.2	0.08	0.31	0.16	0.57

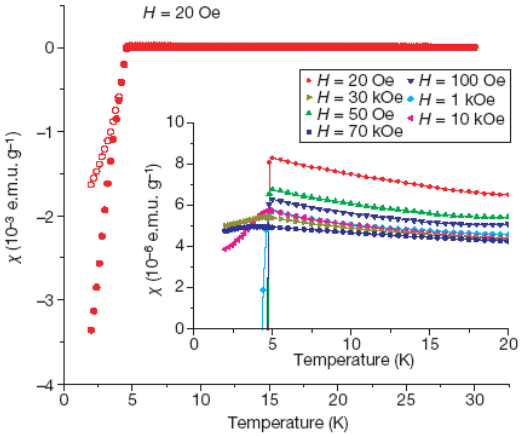

Figure P.2: *Temperature dependence of the magnetic susceptibility in $Na_xCoO_2 \bullet H_2O$ by Takada et al (Ref. 12) showing the SC state below 5K.*

However, many fundamental issues remain to be clarified for the understanding of SC in Na_xCoO_2. The more important is the role that water plays in the occurrence of superconductivity. Also the direct relationship between the Na^+ content and the concentration of charge carriers in the

CoO_2 planes, or the effect of structural/electronic dimensionality are key aspects that have not been explained yet.

In order to understand a little better the chemical and physical properties of this system, it is essential to describe shortly the basic structural and electronic aspects of Na_xCoO_2.

The crystal structure of this oxide consists of two dimensional layers of edge-sharing CoO_6 octahedra separated by Na^+ layers (see Figure P.3). Co-atoms form an hexagonal lattice with triangular M-M bonding.

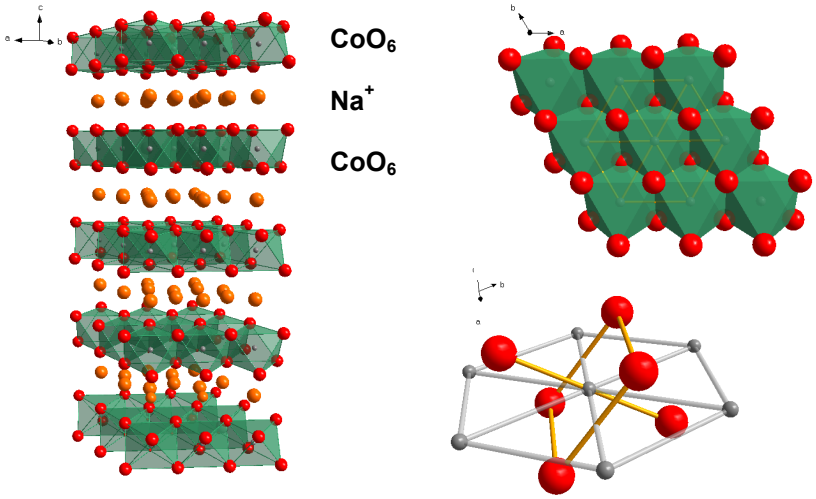

Figure P.3: *Left: 3D-representation of the layered structure of Na_xCoO_2. The grey (red) [orange] balls represent the cobalt (oxygen) [sodium] atoms. Right: (upper) Arrangement of the CoO_6 octahedra in the CoO_2 layers perpendicular to the c-axis. (lower) Detail of the coordination around a Co atom.*

In Na_xCoO_2, Na^+ ions can occupy two different crystallographic positions in the structure, octahedric (O) or trigonal prismatic (P), both of them in the same plane and a halfway between the CoO_2 layers. The unit cell of Na_xCoO_2 is determined by the relative orientation of the CoO_2 planes and the geometry of the Na^+ sites (Figure P.4).[32]

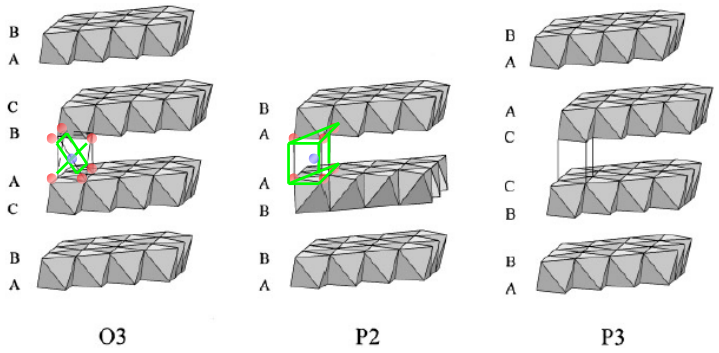

Figure P.4: *Representation of different unit cells for Na_xCoO_2: O3, P2 and P3. The letter indicates the geometry of the Na site, octahedral (O) or trigonal prismatic (P). The number 2 or 3 indicates the number of CoO_2 layers in the unit cell (Ref. 13).*

In this way, different phases and structures can be distinguished depending on the Na^+ content (Table P.2)[3332]:

[32] B. L. Cushing and J. B. Wiley. *J. Solid State Chem.* **141**, 385 (**1998**).
[33] L. Viciu, J. W. G. Bos, H. W. Zandbergen, Q. Huang, M. L. Foo, S. Ishiwata, A. P. Ramirez, M. Lee, N. P. Ong and R. J. Cava. *Phys. Rev. B* **73**, 174104 (**2006**).

Table P.2: *Symmetry of the unit cell for Na_xCoO_2 compounds (0.3<x<1) depending on the Na^+ coordination and the number of layers per unit cell (Ref. 14).*

Refined composition	Space group	Sodium coordination	Structure type
	Two-layer structures		
$Na_{0.34}CoO_2$[a]	$P6_3/mmc$	Trigonal prism	$P2$
$Na_{0.5}CoO_2$[b]	$Pnmm$	Trigonal prism	$P2$
$Na_{0.63}CoO_2$[a]	$P6_3/mmc$	Trigonal prism	$P2$
$Na_{0.71}CoO_2$[a]	$P6_3/mmc$	Trigonal prism	$P2$
$Na_{0.76}CoO_2$[a]	$P6_3/mmc$	Trigonal prism	$P2$
$Na_{0.80}CoO_2$[a]	$P6_3/mmc$	Trigonal prism	$P2$
Na_1CoO_2[a]	$P6_3/mmc$	Trigonal prism	$P2$
	Three-layer derived structures		
$Na_{0.32}CoO_2$[c]	$R\bar{3}m$	Octahedral	$O3$
$Na_{0.5}CoO_2$[c]	$C2/m$	Trigonal prism	$P1$
$Na_{0.6}CoO_2$[c]	$C2/m$	Trigonal prism	$P1$
$Na_{0.67}CoO_2$[d]	$C2/m$	Trigonal prism	$P1$
$Na_{0.75}CoO_2$[c]	$C2/m$	Octahedral	$O1$
$Na_{0.92}CoO_2$[c]	$R\bar{3}m$	Octahedral	$O3$

In the case of the superconducting phase, water intercalates between the Na^+ and CoO_2 layers to $Na_{0.3}CoO_2 \bullet 1.3H_2O$, increasing dramatically the *c*-axis lattice parameter from ~11.1 Å to ~19.5 Å, Figure P.5. It has been suggested that the influence of water in reducing dimensionality of the structure is essential to superconductivity (Ref. 10). This is supported by the observation of the absence of SC in $Na_{0.3}CoO_2 \bullet 0.6H_2O$ with the same

oxidation state but substantially less separation between the CoO_2 layers than the SC samples.[34]

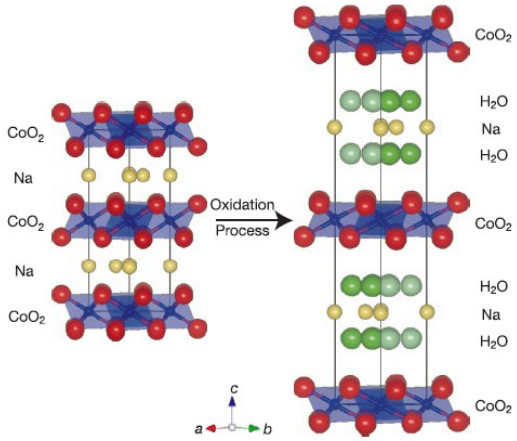

Figure P.5: *Schematic representation of the increase of the unit cell of Na_xCoO_2 in the c-direction as water is intercalated into the structure (from Ref. 9).*

Once water intercalates into the lattice, new structural details arise that should be analyzed. Solving the crystal structure of the superconducting phase has been one of the most important tasks for the last years. It constitutes a crucial point for the understanding of the pairing mechanism that originates superconductivity in this system. However, different structural models of water-intercalated $Na_xCoO_2 \bullet yH_2O$ have been proposed and no agreement has been reached between them to date. What is clear is that many compositions with different amounts of intercalated H_2O coexist in hydrated samples, complicating the analysis even further.

Now, let´s look closer at the electronic structure of the Co atoms in Na_xCoO_2. For x=0, simply CoO_2, each Co atom is in the Co^{4+} valence state and 5 electrons occupy the 3*d* orbitals (assuming a purely ionic picture). In a low-spin configuration, only one electron is unpaired and Co^{4+} has a spin ½. As Na^+ ions are added to the structure, each contributes one electron, thereby changing Co^{4+} to a diamagnetic Co^{3+} state. At x=1, $NaCoO_2$, all the

[34] M. L. Foo, R. E. Schaak, V. L. Miller, T. Klimczuk, N. S. Rogado, Y. Wang, G. C. Lau, C. Craley, H. W. Zandbergen, N. P. Ong and R. J. Cava. *Solid State Comm.* **127**, 33 (**2003**).

Co atoms would be in the Co^{3+} valence state, rendering a diamagnetic system. The energy levels of these two limiting spin configurations are represented in the diagram of Figure P.6.

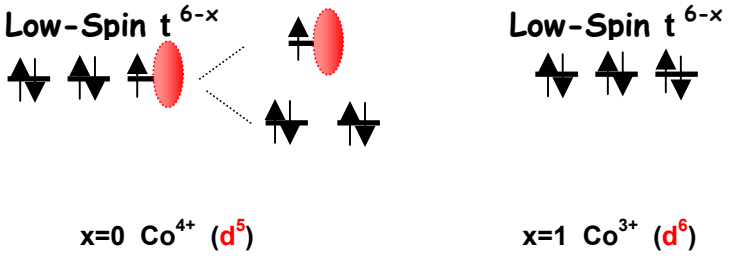

Figure P.6: *Schematic representation of the energy levels and spin configurations for Na_xCoO_2 x=1 and x=0.*

The possibility of mixed valence, along with the resulting spin configurations and the strong Co-*3d*:O-*2p* hybridization, are responsible for the richness of the phase diagram of Na_xCoO_2.

At the beggining of this thesis, the accepted phase diagram for this system was that one reported by Shaak *et al*[35], which shows a wide variety of magnetic and electric phases with doping and temperature (Figure P.7). A number of different magnetic phases like Pauli paramagnetism (PM), Curie-Weiss temperature dependence (CW), antiferromagnetic order (AFM), spin density waves (SDW) are found as a function of Na^+. All of these have a metal-like behaviour, except at x=0.5, where the system goes through a "metal-insulator" transition due to a certain type of charge order[36]. At $1/4 \leq x \leq 1/3$ superconducting state appears below 5 K as water is intercalated into the structure.

[35] R. E. Schaak, T. Klimczuk, M. L. Foo and R. J. Cava. *Nature*, **424**, 527 (**2003**).
[36] M. L. Foo, Y. Wang, S. Watauchi, H. W. Zandbergen, T. He, R. J. Cava and N. P. Ong. *Phys. Rev. Lett.* **92**, 247001 (**2004**).

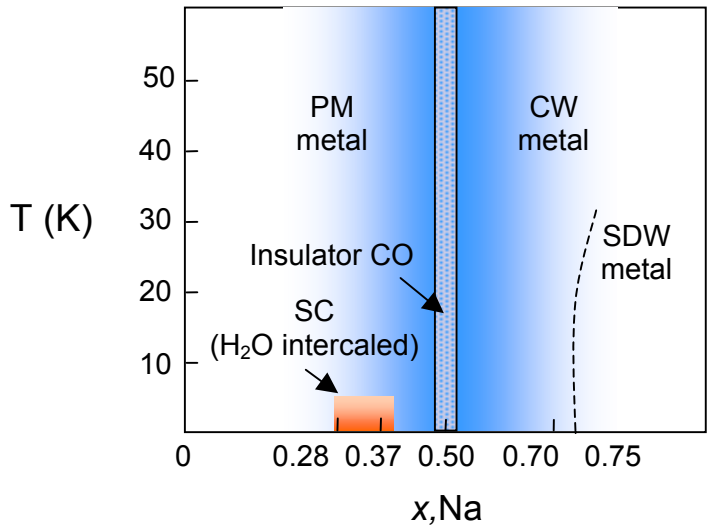

Figure P.7: *Magnetic/electric phase diagram of Na_xCoO_2 propposed by Schaak et al in Ref. 16.*

In this narrow range of Na^+ compositions in which superconductivity is achieved, the dependence of superconducting temperature transition (T_c) as a function of Na^+ doping remains still unclear. Initially, a strongly correlation between T_c and the Na^+ content of the samples was established, and an optimal chemical doping level for superconductivity with $T_c \approx 4.5$ K at $x \approx 0.3$ was reported[35]. This "dome-like" dependence of T_c with doping shows the same kind of trend that cuprates. For this reason, it has been thought that this material would be a good candidate to shed a light on the superconductivity mechanism in these compounds. However, a great controversy was generated when subsequent reports observed an almost independent value of T_c with *x*.[37,38]

[37] D. P. Chen, H. C. Chen, A. Maljuk, A. Kulakov, H. Zhang, P. Lemmens, and C. T. Lin. *Phys. Rev. B* **70**, 024506 (**2004**).

So, at the beginning of this work there were a number of open questions that were important to understand these phenomena:

1) What is the role of Co-O covalency?

2) Related to this, is there a direct relationship between the Na^+ content and the actual Co oxidation state?

3) Is H_2O just a chemical apacer or does it play another role?

4) What is the role of the insulating x=0.5 phase in the phase diagram?

With the aim of contributing to answer these questions, we have carried out an exhaustive and systematic analysis of the magnetic and transport properties of Na_xCoO_2, particulary focusing on the new magnetic phases found close to $x\approx0.5$ and its relation with superconductivity.

We hope this will help to explain some of the many questions about the chemistry and physics of this material that remain unanswered still.

[38] C. J. Milne, D. N. Argyriou, A. Chemseddine, N. Aliouane, J. Veira, S. Landsgesell and D. Alber. *Phys. Rev. Lett.* **93**, 247007 (**2004**).

1. Synthesis, chemical and structural characterization of Na_xCoO_2

1.1. Polycrystalline samples

1.1.1. Parent compound: $Na_{0.7}CoO_2$

Polycrystalline samples of $Na_xCoO_2$with a sodium content x~0.7 have been synthesized by conventional solid state reaction. The reactants used in the synthesis and their chemical purity grade are shown in Table 1.1.

Table 1.1: *Chemical specifications of the reactants used in the synthesis of $Na_{0.7}CoO_2$.*

Reactant	Molecular Weight	Purity
Na_2CO_3	105.99	99.5 %
Co_3O_4	240.80	70 (in Co) %

Before starting the synthesis, the reactants were dried in air in a oven at 80 ºC for approximately 12 hours. Once perfectly dried, Na_2CO_3 and Co_3O_4 were thoroughly mixed in a molar ratio Na/Co=0.7, using a hand mortar for 15-20 minutes, and then an automatic agate mortar for 15-20 minutes more. A 10% molar excess of Na_2CO_3 was added to compensate the loss due to Na-evaporation at high temperatures. The synthesis procedure performed was basically the "rapid heat-up" technique proposed by *Motohasi et al*[39]. It took place in two heating treatments:

In the first one, the mixed powder was hand pressed in an Al_2O_3 crucible and directly placed in a furnace preheated at 750 ºC to reduce Na-evaporation to the minimum extent. The temperature of the furnace was subsequently raised at 3 ºC/min up to 850 ºC. This temperature was kept for 12 h. Then, a similar second heat treatment was carried out at 900 ºC for 12 h. Both heat treatments took place in air, with the heating up and cooling down ramps set to 3 ºC/min. Before the second treatment the powder was reground to ensure homogeneity and pelletized in a 13 mm diameter tungsten carbide die. The final product was grinded, washed with generous amounts of water and acetone, and dried at 120 ºC for approximately one hour before storing it in a vacuum desicator.

Motohasi et al[1] observed that if the reaction powder is introduced in a preheated furnace at 700 ºC, Na-evaporation is considerably reduced and the sodium content determined experimentally agrees very well with the nominal value. A scheme of this synthesis procedure is shown in Figure 1.1.

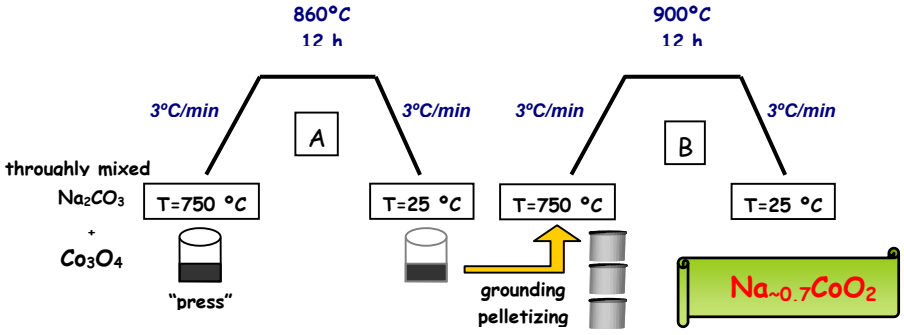

Figure 1.1: *Scheme of synthetic path followed to synthesize the parent phase* $Na_{0.7}CoO_2$.

[39] T. Motohasi, E. Naujalis, R. Ueda, K. Isawa, M. Karppinen and H. Yamauchi. *Appl. Phys. Lett.* **79**, 1480 (**2001**).

Alternative routes based in solid-state reactions have been developed by other authors to obtain polycrystalline, non-hydrated Na_xCoO_2 compounds. The experimental details of the most representative preparation paths found in the literature are mentioned below:

a) Co metal and anhydrous NaOH, fired at 700 ºC under flowing oxygen for 5 days[40].

b) Na_2CO_3 and Co_3O_4 heated at 850 ºC under O_2 gas[41].

c) Na_2O and Co_3O_4 heated in air at a temperature of 970 ºC[42].

d) Na_2O_2 and Co_3O_4 heated at 530 ºC under O_2 gas[43].

Polycrystalline Na_xCoO_2 compounds obtained directly from the synthesis can be slightly different to each other in their Na^+ content. In this way, the first two paths were reported to lead to Na_xCoO_2 with $x\approx1$ and $x\approx0.85$, respectively. In the other cases, the reaction leads to Na^+ content of $x\approx0.7$. This phase seems to represent a particurally stable composition, the reason for this is still not well understood, although it could be related to a change from octahedral ($x>0.7$) to trigonal prismatic ($x\leq0.7$) coordination of the Na^+ ion at this particular composition. Surprisingly, the reactions which take place under O_2 atmosphere led to a final product with a higher Co^{3+} ion concentration (higher Na^+ content) than the corresponding ones in air or Ar, with a higher concentration of the Co^{4+} ion. In the last years, the most popular route of synthesis to get polycrystalline Na_xCoO_2 was that one developed by *Motohasi et al*[39] in any of its modified versions. In this work, we have chosen this synthesis procedure due to its simplicity and reproducibility in the final Na^+ stochiometry of the phases obtained.

Figure 1.2 shows the X-ray diffraction pattern obtained for Na_xCoO_2, $x\approx0.7$, synthesized by direct solid-state reaction. A single phase corresponding to $x\approx0.7$ was identified by comparison of all the reflections with one of the patterns included in the Inorganic Crystallographic Sample Database for $Na_{0.74}CoO_2$ (*ICSD-50301*). Inductively coupled plasm (ICP) analysis indeed confirmed that Na^+ stochiometry for this phase is $x=0.67$.

---

[40] B. L. Cushing and J. B. Wiley. *Synth. React. Inorg. Met.-Org. Chem.* **29(7)**, 1199 (**1999**).
[41] P.W. Barnes, M. Avdeev, J. D. Jorgensen, D. G. Hinks, H. Claus and S. Short. *Phys. Rev. B* **72**, 134515 (**2005**).
[42] A. Stoklosa, J. Molenda and Do Than. *Solid State Ionics* **15**, 211 (**1985**).
[43] Y. Ono, R. Ishikawa, Y. Miyazaki, Y. Ishii, Y. Morii and T. Kajitani. *J. Solid State Chem.* **166**, 177 (**2002**).

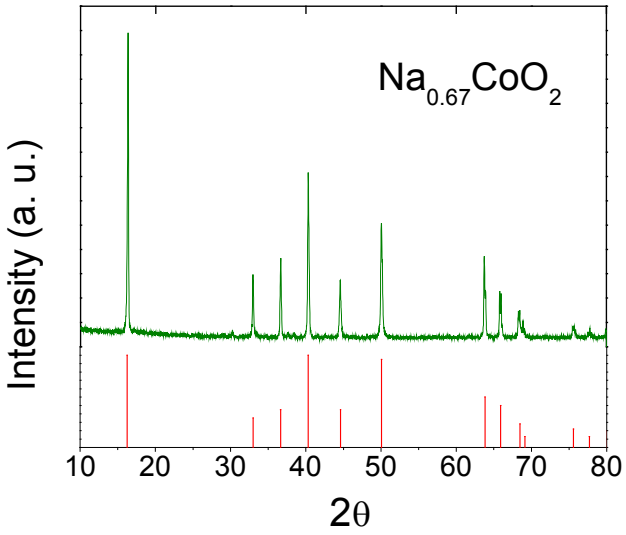

Figure 1.2: *(top) Experimental X-ray diffraction pattern for powder $Na_{0.67}CoO_2$. (bottom) Reflections lines expected for the $Na_{0.74}CoO_2$ diffraction pattern (ICSD-50301).*

Due to the difficulty to control precisely the stoichiometry of the Na_xCoO_2 compounds from the molar ratio of the reactants, an extensive variety of crystallographic phases were reported for Na^+ contents close to x~0.7 [44,45]: although the unit cell for the most stable phase, $x \approx 0.7$, is considered hexagonal with space group *P63/mmc* (nº 184), the monoclinic *C2/m* (nº 12) phase has been also reported for nearly the same composition. Moreover, different arrangements of Na^+ ions in the structure may change the symmetry. In the case of superconducting samples the complexity and controversy are even bigger because of a mixture of fully and partially hydrated phases normally coexist in the same specimen[46], and also different unit cell simmetries. We confirmed that the best fits of our X-ray diffraction patterns of powder samples with x~0.7 were achieved on the basis of a single phase with space group *P63/mmc* (Figure 1.3). The lattice parameters

[44] B. L. Cushing, J. B. J. Wiley. *Solid State Chem.* **141**, 385 (**1998**).
[45] L. Viciu, J. W. G. Bos, H. W. Zandbergen, Q. Huang, M. L. Foo, S. Ishiwata, A. P. Ramirez, M. Lee, N. P. Ong and R. J. Cava. *Phys. Rev. B* **73**, 174104 (**2006**).
[46] D. P. Chen, H. C. Chen, A. Maljuk, A. Kulakov, H. Zhang, P. Lemmens, C. T. Lin. *Phys. Rev. B* **70**, 24506 (**2004**).

calculated from Rietveld analysis for this phase, *a*=2.8355(1) Å and *c*=10.8987(4) Å are close to the values reported by *Fouassier et al*,[47] *a*=2.833 Å and *c*=10.88 Å.

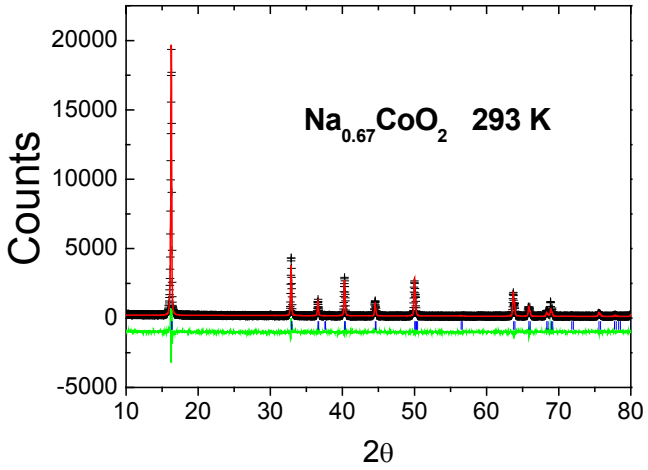

Figure 1.3: *X-ray diffraction pattern (+) and Rietveld refinment (red line) of $Na_{0.67}CoO_2$ at room temperature. Vertical blue lines mark the expected position for the reflexions of the space group P63/mmc. The green line is the difference between the experimental and calculated intensities. R_{wp}=9.92%.*

We also tried to synthesize other samples with a different Na^+ content, in the range 0.5<*x*<1, from the direct solid state reaction of the corresponding stochiometric mixture of reactants. However, in all the cases, the product obtained finally presented a similar Na^+ content of $x\approx0.7$. Therefore, it is important to remark that the Na^+ content of the final cobalt oxides obtained directly from this conventional solid-state reaction does not depend on the initial Na/Co ratio. The most stable phase for Na_xCoO_2 system obtained directly from the synthesis corresponds to $x\approx0.7$. So, this observation should be considered in the case of the older papers where Na_xCoO_2 samples with $x\neq0.7$ were reported from direct, solid state reactions[48,49].

[47] C. Fouassier, G. Matejka, J. M. Reau and Hagenmuller. *J. Solid State Chem*. **6**, 532 (**1973**).
[48] V. M. Jansen and R. Hoppe. *Z. anorg. Allg. Chem*. **408**, 104 (**1974**).

Scanning electron microscopy (SEM) images from polycrystalline samples were taken for some representative Na^+ compositions in the Na_xCoO_2 system to study the morphology of this compound. Micrographs were taken in a LEO-435VP scanning electronic microscope working at 20 kV with a maximum resolution of 6 nm (under P~10 Pa).

Figure 1.4 shows SEM and optical photographs for polycrystalline samples of Na_xCoO_2 with x=0.67. Pictures were taken over the surface of cold-pressed pellets of ∅~5 mm, which were pressed mechanically at 12-13 Ton/cm^2. In the case of the non-hydrated sample (a), as it would be deduced by Energy Dispersive X-ray (EDAX) analyses later, we can visually verify by SEM that the surface of the pellet is actually homogeneous in composition. It can also be observed the presence of several porous along the whole surface. This fact is a general characteristic of the Na_xCoO_2 system in a wide range of x. This porosity complicates intrinsic resistivity and thermal conductivity measurements in polycrystalline samples of these compunds. In picture (b), an optical photograph of exactly the same pellet after being exposed to ambient conditions for one week is shown. These compounds are highly hygroscopic. Their ageing under ambient conditions leads to the formation of small white crystals appreciable over the whole surface of the pellet. They resulted to be NaOH crystals as determined by EDAX analyses and X-ray diffraction. They are formed because of the reaction of Na^+ ions at the surface and the water present in the atmosphere at normal conditions of pressure and temperature.

It is important to realize that this spontaneous reaction of formation of NaOH will leave behind a surface of the sample with a Na^+ content lower than inside the pellet, so the Co^{4+} concentration will be higher in the surface than in the inner regions. It is indicative of an inhomogeneous composition, resulting in a different distribution of charge carriers through the sample. This is something not normally considered in the literature, although it could determine the behaviour of the system to a large extent, even in single crystals.

[49] T. Valla, P. D. Johnson, Z. Yusof, B. Wells, Q. Li, S. M. Loureiro, R. J. Cava, M. Mikami, Y. Mori, M. Yoshimura and T. Sasaki. *Nature* **417**, 627 (**2002**).

$Na_{0.67}CoO_2$

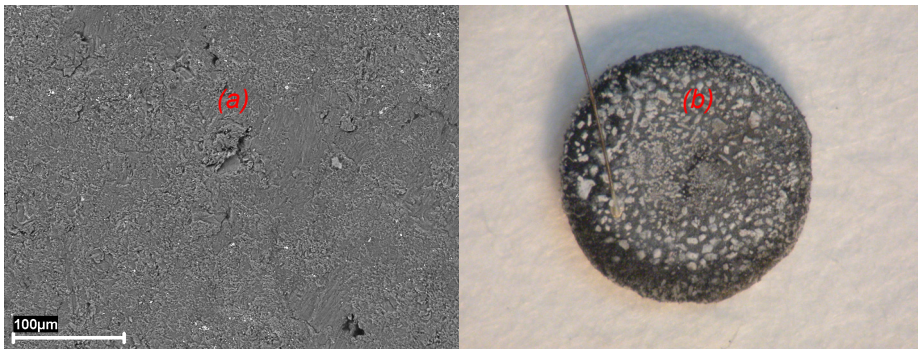

Figure 1.4: *(a) SEM and (b) optical photographs from the surface of a (a) fresh sample of $Na_{0.67}CoO_2$ and (b) the same sample after being exposed to ambient for one week. There is a Cu wire (20 μm) attached with silver epoxy resin to the surface of the sample in (b).*

1.1.2. Na_xCoO_2 series, 0.3<x<0.7

In order to obtain samples with different values of Na^+, intercalation/deintercalation processes were done by using chemical methods of oxidation/reduction of the Co^{4+}/Co^{3+} redox pair.

1.1.2.1. Na^+ deintercalation

There are different methods in the literature that can achieve an efficient Na^+ deintercalation from $Na_{\approx 0.7}CoO_2$. They can be grouped in two types: *chemical* and *electrochemical* methods. In the first group are included those procedures involving a chemical oxidation of the transition metal redox pair. Among them, Br_2/CH_3CN[4], I_2/CH_3CN[3,50],

[50] X. Z. Chen, Z. A. Xu, G. H. Cao, J. Q. Shen, L. M. Qiu and Z. H. Gan. *arXiv:cond-mat/0412299* (**unpublished**).

$KMnO_4/H_2O$[51], $Na_2S_2O_8/H_2O$[52] or $NaClO_3/H_2O$[53] oxidizing solutions are employed. On the other hand, using $KMnO_4$ as oxidizing agent can result in substitutions at the Na and Co sites, being replaced by K and Mn, respectively, even at room temperature. However, the oxidizing deintercalation with Br_2 in non-aqueous medium[4] is the method more extensively used to reduce the sodium content between the CoO_6 sheets in layer cobalt oxides. Its simplicity and speed make it a very useful method for Na^+ deintercalation. Furthermore, it is possible to reach low Na^+ contents x~0.3. Using I_2 instead of Br_2 allows a more accurate control over the experimental Na/Co ratio due to the softer oxidation strenght. The use of a non-aqueous medium is also strongly recommended to avoid the water intercalation between the CoO_2 layers[54].

The dependence of the redox potential of the Co^{4+}/Co^{3+} pair in Na_xCoO_2 upon x reported in the literature suggests that the minimum x value which can be obtained using Br_2 as the oxidizing agent is x=0.4-0.5 (the potential of the Co^{3+}/Co^{4+} redox pair increases as Na^+ content decreases). However, it is usual to find x values lower than x=0.40 in the bibliography, and also our results show a minimum Na^+ content of x=0.31.

Chou et al[55] used an electrochemical technique for deintercalating Na^+ from $Na_{0.7}CoO_2$ as an alternative to chemical deintercalation. They highlighted the precise control over the final Na^+ content and the reduction of the environmental hazards derivated of the use of high concentrations of Br_2 as the main advantages of their procedure.

In this thesis, samples of Na_xCoO_2 with sodium contents between $0.25<x<0.67$ were obtained by Na^+ deintercalation from polycrystalline $Na_{0.67}CoO_2$ by stirring the powder in a Br_2/CH_3CN oxidizing solution for 5 days at room temperature[56]. Bromine oxidizes the Co^{3+} to Co^{4+}, favoring the motion of the Na^+ ions out from the interlayer space to keep the charge electroneutrality in the compound.

---

[51] (a) C.-J. Liu, C.-Y Liao, L.-C. Huang, C.-H. Su, S. Neeleshwar and Y.-Y. Chen. Chin. *J. Phys.* **43**, 547 (**2005**) (b) C.-J. Liu, W.-C. Hung, J.-S. Wang and C.-J. C. Liu. *J. Amer. Chem. Soc.* **127**, 830 (**2005**). (c) C.-J. Liu, C.-Y Liao, L.-C. Huang, C.-H. Su, S. Neeleshwar, Y.-Y. Chen and C.-J.C. Liu. *Physica C* **416**, 43 (**2003**).

[52] S. Park, Y. Lee, A. Moodenbaugh and T. Vogt. *Phys. Rev. B* **68**, 180505(R) (**2003**).

[53] M. L. Foo, Y. Wang, S. Watauchi, H. W. Zandbergen, T. He, R. J. Cava and N. P. Ong. *Phys. Rev. Lett.* **92**, 247001 (**2004**).

[54] K.Takada, K. Fakuda, M. Osada, I. Nakai, F. Izumi, A. R. Dilanian, K. Kato, M. Takata, H. Sakurai, E. Takayama-Muromachi, E. J. Sasaki. *J. Mater. Chem*. 14, 1448 (**2004)**.

[55] F. C. Chou, E. T. Abel, J. H. Cho and Y. S. Lee. *J. Phys. Chem. Solid* **66**, 155 (**2005**).

[56] K. Takada, H. Sakurai, E. Takayama-Muromachi, F. Izumi, R. A. Dilanian and T. Sasaki. *Nature* **422**, 53 (2003).

By adjusting the Br_2 concentration of the solution, various phases with different *x* can be obtained.[53,57] Bromine concentrations representing substoichiometric (×0.5), stochiometric (×1) and molar excess (×5, ×10, ×50, ×100) relative to the amount that would be needed to remove all of the Na^+ from $Na_{0.67}CoO_2$ were employed, according to the following reaction:

$$Na_xCoO_2\,(s) + \left(\frac{y}{2}\right) Br_2\,(l) \leftrightarrow Na_{x-y}CoO_2\,(s) + y\,Na^+ + y\,Br^-$$

After this time, the samples were filtered, washed with generous amounts of CH_3CN and acetone, dried in an oven at low temperature (60-70 ºC) and stored in a desicator under vacuum. In this way, samples with a wide range of sodium compositions were obtained. All the samples, independently of their sodium content, are highly hygroscopic. For this reason, their manipulation was carried out minizing as much as possible any exposure to ambient moisture.

The Na and Co contents were determined in the Na_xCoO_2 phases by inductively coupled plasma optical emission spectroscopy (ICP-OES). To dissolve the samples, an exactly weighted amount of the dried powder was added to a water diluted HCl solution (1:1) under stirring and heated in an autoclave at low temperature for 12 hours. Na and Co volumetric standars provided by Aldrich were used in the determination of these ions in the samples. The Na/Co ratios obtained are shown in Table 1.2 for each concentration of Br_2.

[57] R. E. Shaak, T. Klimczuk, M. L. Foo and R. J. Cava. *Nature* 2003, **424**, *527*.

Table 1.2: *Results of the ICP-OES of Na_xCoO_2*

Br_2 excess	Na/Co Ratio
Precursor	0.673(7)
×1	0.450(4)
×5	0.429(6)
×10	0.402(5)
×20	0.381(6)
×30	0.369(5)
×40	0.362(4)
×50	0.322(4)
×100	0.310(3)

The analysis confirms that the amount of Na^+ decreases systematically as the excess of Br_2 increases. The Na^+ content drops very fast to x~0.45, even for the lowest amount of Br_2. Then, increasing the amount of the oxidant reduces *x* down to ~0.30.

The structural data of Na_xCoO_2 samples have been determined from a lebail refinment of the X-ray powder diffraction patterns (XRD) using the program Rietica[58]. The Na^+ deintercalated sample using a stochiometric amount of Br_2 (×1) was single phase, and can be indexed within the space group *P63/mmc*, like the original $Na_{0.7}CoO_2$. For the sodium deintercalated samples with Br_2 excesses above the stochiometric amount (×5, ×10, ×20…×100) new additional reflections were found. These new reflections were indexed after considering two minority phases with hexagonal symmetry, *P63/m* and *P6/m*, with lattice parameters *a=5.3443(4)*, *c=19.525(3)* and *a=5.4027(7)*, *c=20.466(2)*, respectively. Figure 1.5 shows all the X-ray patterns for the Na_xCoO_2 series. So a mixture of 3 phases is present from *x*~0.43 down to *x*~0.3.

[58] Rietica: B. A. Hunter and C. J. Howard. Australian Nuclear Science and Technology Organization. Lucas Heights Research Laboratories, **1998**.

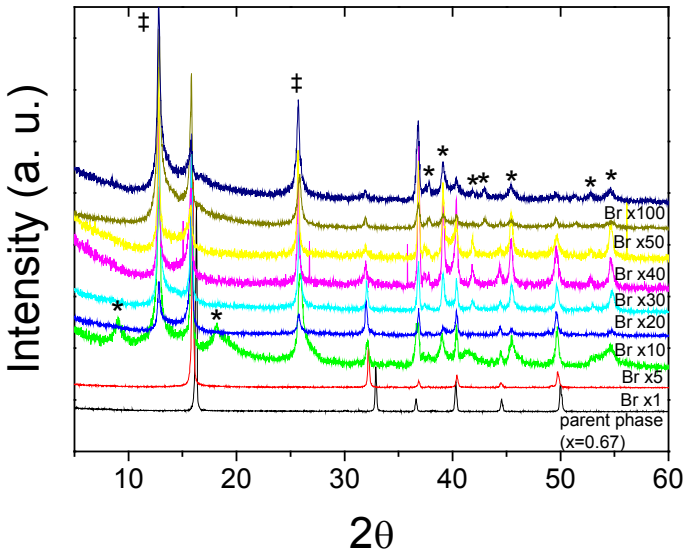

Figure 1.5: *X-ray diffraction patterns for Na_xCoO_2 deintercalated samples. Reflections belonging to hexagonal space groups P63/mmc, P63/m (*) and P6/m (‡) are shown.*

As indicated before, there is no precise control over the stochiometry of the parent compounds that are obtained directly from solid state reaction, although most of them correspond to sodium content about $x \approx 0.7$. In addition, the Na^+ deintercalation with Br_2 is a process controlled by the diffusion of the Na^+ ions through the material, from bulk to surface. As a consequence, the presence of inhomogeneities in several zones of the material is expected and several crystallographic phases can result in the same sample due to slight variation of Na^+ content. For this reason, the appearance of several phases with different symmetry is expected, although the ratio among them unpredictable. There are several reports in the literature of samples with an equal Na^+ content that belong to different space groups[44,45,47,48]. In my oppinion, this is most probably a consequence of an inhomogeneous distribution of Na^+ along the sample and/or possible Na^+ ordering[53]. So, discrepancies between results obtained by different groups could result from small variations in the temperature of synthesis, number of heat treatments, Br_2 concentration used in the Na^+ deintercalation process or the time employed in each one of these experimental steps.

Another important factor to take into account is the time that the samples are kept in an open atmosphere before being measured, due to their high hygroscopic character. Moreover, this hygroscopic character increases as Na^+ content decreases; so deintercalated samples with higher Br_2 excess will be more easily hydrated. The water absorption in between the CoO_6 layers provokes important structural changes characterized by the appearance of new reflections, especially at low angles[59] (to be discussed later).These can be erronously indexed as a new phase of the "dry" sample.

A significant displacement of the (002) reflection to lower (*2θ*) angles is clearly observed after Na^+ deintercalation at the *P63/mmc* phase (Figure 1.6). This reflection is indicative of the separation between adjacent CoO_6 planes, indicating an appreciable expansion of the lattice in the direction perpendicular to them after Na^+ removal.

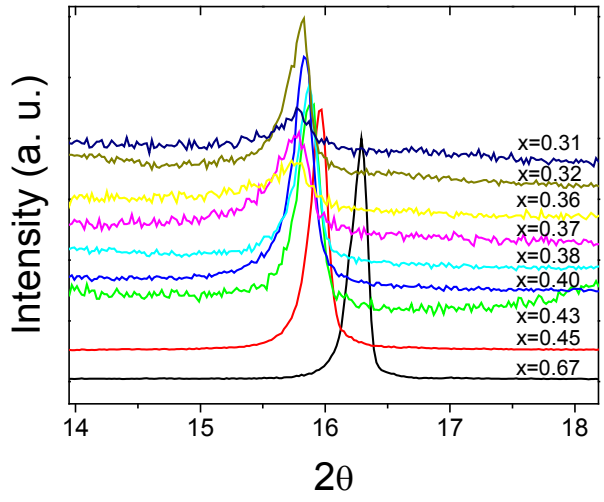

Figure 1.6: *Displacement of the (002) reflection of the majority phase P63/mmc after Na^+ deintercalation in Na_xCoO_2.*

The lattice parameters calculated for the majority P63/mmc phase were obteained for each sample, by fitting all the reflections of the X-ray

[59] J. D. Jorgensen, M. Avdeev, D. G. Hinks, J. C. Burley and S. Short. *Phys Rev. B* **68**, 214517 (**2003**).

pattern with Rietica. The results are shown in the Table 1.3. A significant increase of the *c*-axis lattice parameter is observed with decreasing Na^+ content while the *a*-axis parameter decreases slightly, but continuously over all the sodium content range. This appreciable expansion of the unit cell along the *c*-axis is signaling a decrease in bonding strength between the CoO_2 layers as Na^+ is removed. This has been typically associated to the increase of the Coulomb repulsion between the CoO_6 sheets as the Co^{4+}/Co^{3+} ratio increases. Surprisingly, the expansion of the *c*-axis parameter is less marked below x=0.40, leading to an approximately constant c/a ratio down to x=0.30. If the explanation of the Coulomb repulsion is correct, this fact could be signaling the impossibility of further charging the CoO_2 planes upon doping beyond $x \leq 0.4$.

Figures 1.7 and 1.8 show different plots of the lattice parameters as a function of the Na^+ content in the Na_xCoO_2 samples.

Table 1.3: *Lattice parameters for Na_xCoO_2 (for the majority phase P63/mmc). The hexagonal symmetry of the space group P63/mmc implies that a=b.*

x	*a=b*	*c*
0.673(7)	2.8355(1)	10.8987(4)
0.642(6)	2.8295(1)	10.9287(6)
0.450(4)	2.8145(1)	11.1207(2)
0.429(6)	2.8132(5)	11.114(2)
0.420(6)	2.8152(1)	11.1324(2)
0.402(5)	2.8125(7)	11.169(2)
0.381(6)	2.8129(6)	11.128(3)
0.380(6)	2.8149(1)	11.1761(2)
0.369(5)	2.8097(1)	11.162(1)
0.362(4)	2.8108(1)	11.177(2)
0.322(4)	2.8113(4)	11.163(1)
0.310(3)	2.8074(3)	11.146(2)

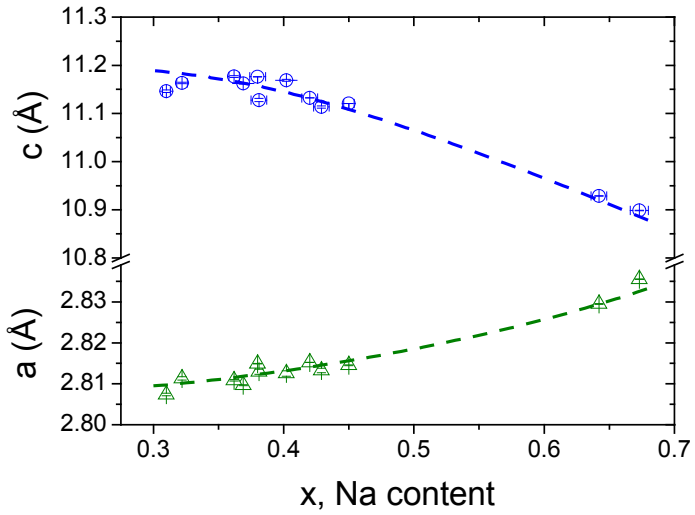

Figure 1.7: *Lattice parameters for Na_xCoO_2 as a function of the Na^+ content. Line is a guide to the eye.*

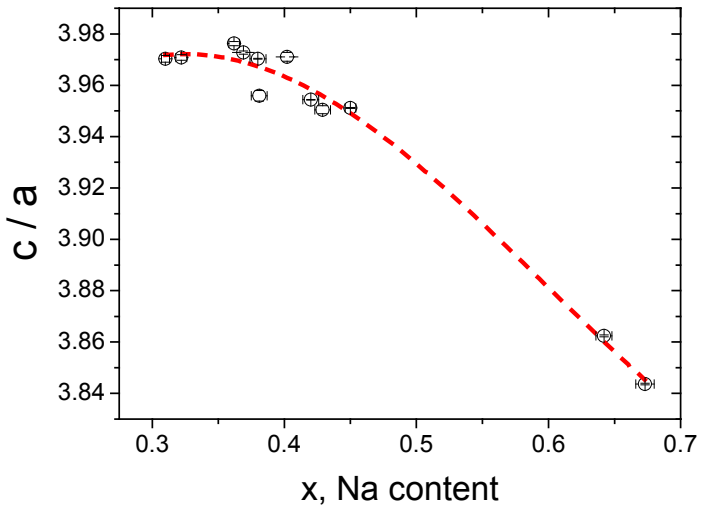

Figure 1.8: *Evolution of the c/a ratio in Na_xCoO_2 for the majority phase P63/mmc. Line is a guide to the eye.*

The decreasing of the *a*-lattice parameter as Na^+ content (*x*) decreases can be explained if we take into account that the removal of Na^+ from the structure introduces Na^+ site vacancies in the Na^+ layers and oxidizes partially the Co ions, with the subsequently decrease in the effective ionic radius ($r_{Co3+}>r_{Co4+}$). Moreover, Na^+ deintercalation process takes σ^* electrons away, so the bonding strength of the Co-O bonds becomes stronger. As a consequence, a shortening of the d_{Co-O} in the CoO_6 octahedra and a reduction of the unit cell in the *ab* direction are appreciable. Looking at Figure 1.8 we can conclude that the structural anysotropy of the system increases as the Na^+ content decreases.

A similar effect was reported in the related material Li_xCoO_2.[60] The constant *c/a* ratio at low *x* was ascribed to the growing amount of oxygen vacancies that accompanies Li^+ deintercalation beyond $x<0.5$. It is of fundamental relevance for the understanding of the magnetic/transport properties of Na_xCoO_2 to know whether a significant amount of vacancies are also present in this case.

We determined the oxidation state of the Co for all Na_xCoO_2 compositions from iodimetric titration, establishing a relationship between the sodium content and the formal charge of Co.

Some groups reported the presence of an oxygen content lower than the stoichiometric in both hydrated[61,54] and nonhydrated[9,62] samples of Na_xCoO_2. However, just a few, very specific compositions were studied in these works, and in the case of the hydrated samples the amount of water present which is not inserted between the layers is difficult to determine, and this introduces an important source of error. So, to determine the presence and extent of oxygen vacancies in this material, we carried out the first meticulous and sistematic determination of the Co oxidation state in the non-hydrated samples in a wide compositional range ($0.3<x<0.7$)[63].

Titration methods are based on the dissolution of the sample in acid and subsequent reduction of the high valent cobalt species, Co^{3+} and Co^{4+}, with an appropriate reductant. Among the redox titrations, that one using iodide I^- as reducting agent is probably the most widely used to determine the oxidation states of transition metal ions in oxides, like perovskite-cobalt

[60] S. Venkatraman and A. Manthiram. *Chem. Mater.*, **14**, 3807 (**2002**).
[61] M. Karppinen, I. Asako, T. Motohasi and H. Yamauchi. *Chem. Mater.* **16**, 1693 (**2004)**.
[62] H. Sakurai, S. Takenouchi, N. Tsujii, E. J. Takayama-Muromachi. *Phys. Soc. Jpn* **73**, 2081 (**2004**).
[63] M. Bañobre-López, F. Rivadulla, R. Caudillo, M. A. López-Quintela, J. Rivas and J. B. Goodenough. *Chem. Mater.* **17(8)**, 1965 (**2005**).

oxides[64,65,66,67]. After this analysis, the oxygen content of the oxides[68,69,70] can be obtained if the metal content can be measured by an independent analytical method. However, although the volumetric iodimetric titration is the most standard redox method used to determine both the Co^{3+}/Co^{4+} ratio and the oxygen content, *Karppinen et al*[71] have successfully applied the cerimetric and coulometric titration to the analysis of cobalt oxides (based on the use of Fe^{2+} and Cu^{+} as reductant agents, respectively).

We describe below the process followed in this work. In a typical analysis, a known amount (between 35 and 75 mg) of a perfectly dried powder of Na_xCoO_2 was dissolved in an acid mixture composed by 3M HCl solution containing an excess of KI (~1g). In this process, the Cl_2 generated in the reduction of tri- and tetra-valent cobalt species to Co^{2+} ions reacts with the free I^- ion present in solution to form a stochiometric amount of I_2, according to:

$$2Co^{3+} + 2Cl^- \rightarrow Cl_2 + 2Co^{2+}$$

$$Co^{4+} + 2Cl^- \rightarrow Cl_2 + Co^{2+}$$

$$2I^- + Cl_2 \rightarrow 2Cl^- + I_2$$

[64] C. Martin, A. Maignan, D. Pelloquin, N. Nguyen and B. Raveau. *Appl. Phys. Lett*. **71**, 1421 **(1997).**
[65] A. Maignan, C. Martin, D. Pelloquin, N. Nguyen and B. Raveau. *J. Solid State Chem.* **142**, 247 **(1999).**
[66] J. E. Sundstrom IV, K. V. Ramanujachary and M. Greenblatt. *J. Solid State Chem.* **139**, 388 (**1998**).
[67] H. W. Brinks, H. Fjellvag, A. Kjekshus and B. C. Hauback. *J. Solid State Chem.* **147**, 464 **(1999).**
[68] M. Karppinen and H. Yamauchi, in International Book series: *Studies of High Temperature Superconductors*, Vol.37, A. V. Narlikar (Ed.), Nova Science Publishers, New York, **2001**.
[69] M. Karppinen and H. Yamauchi. *Mater. Sci. Eng. R* **26**, 51 (**1999**).
[70] M. Karppinen, A. Fukuoka, L. Niinistö and H. Yamauchi. *Supercond. Sci. Technol*. **9**, 121 (**1996**).
[71] M. Karppinen, M. Matvejeff, K. Salomäki and H. Yamauchi. *J. Mater. Chem.* **12**, 1761 (**2002**).

Iodine was then titrated with $Na_2S_2O_3$ solution (0.010 M, previously standarized by volumetric titration) using starch as indicator:

$$2S_2O_3^{2-} + I_2 \rightarrow 2I^- + S_4O_6^{2-}$$

Starch (0.5 mL, 1% in weight) was added just before the neutralization point to determine the end-point. The end-point was detected visually as the blue colour of the starch complex disappeared and the solution turned into a very soft pink. To prevent any ambient oxidation of I^-, the acidic solution used as a solvent was free from dissolved oxygen before each experiment by boiling the water and subsequent Ar bubbling. Also, it is important to perform the titrations quickly and in absence of air, under flowing Ar. It is very important to remark that, for each analysis, the experiments were repeated at least three times.

In general, the stochiometry of the cobalt oxides that will be studied in this work can be formulated as:

$$Na_xCo^{III}_{x+y}Co^{IV}_{(1-x)-y}O_{2-\delta}$$

Therefore, the Co^{3+} and Co^{4+} content can be calculated from the following equation:

$$y = \frac{P_M MV + mx - 2m}{8MV - m}$$

where *x* is the Na^+ content determined independently by ICP-OES for each specific cobalt oxide sample, *m* is the mass of the sample, *M* is the molar concentration of the $S_2O_3^{2-}$ solution, *V* is the volume of this solution needed in the titration and P_M is the molecular weight of the cobalt oxide analyzed, that depends of the Na^+ content (x).

This analysis assumes a perfect stoichiometry of Co in the system. This has been verified by ICP-OES analysis of our samples, and the results confirm previous reports from other authors.[61,62]

Then, the oxygen content is deduced from the following expression; assuming the electric neutrality of the structure:

$$2-\delta = 2-\frac{y}{2}$$

The amount of Co^{3+}/Co^{4+} ions and oxygen content were determined with a reproducibility of about ±0.007. This procedure was carried out for each composition in Na_xCoO_2 and the results are summarized in Table 1.4.

Table 1.4: *Results of %Co^{3+} and oxygen content (2-δ) from the iodimetric analysis for the Na_xCoO_2 samples. Two different precursors were synthesized in order to confirm the initial state of the series.*

Na/Co ratio	%Co^{3+}	2-δ	Br_2 excess
0.690(1)	89.0(1)	1.90(1)	Precursor (1)
0.673(7)	77.3(7)	1.95(4)	Precursor (2)
0.450(4)	61.0(4)	1.92(2)	×1
0.429(6)	58.9(6)	1.92(4)	×5
0.402(5)	56.6(5)	1.91(3)	×10
0.381(6)	58.1(6)	1.90(4)	×20
0.369(5)	53.8(5)	1.92(3)	×30
0.362(4)	54.2(4)	1.91(2)	×40
0.322(4)	52.2(4)	1.90(2)	×50
0.310(3)	57.0(3)	1.87(2)	×100

Reproducible iodometric titrations were consistent with an oxidation state of $Co^{3+/4+}$ that is considerably lower (a larger amount of Co^{3+} and a smaller amount of Co^{4+}) than expected from the Na^+ content determined by ICP-OES. This is especially evident for low Na^+ content.

The percentage of Co^{3+} and the oxygen content determined experimentally from the iodimetric analyses are plotted in Figure 1.9, versus the Na^+ content determined by ICP-OES. The compound is always oxygen deficient, even at the largest doping probed in this work (x=0.69). The amount of oxygen vacancies increases very much below $x\approx0.5$. In fact, deintercalation of Na^+ below $x\approx0.4$ has almost no effect in the final oxidation state of Co, which remains close to ~3.45+, down to at least x=0.3, the lowest Na^+ content probed in this work. The creation of an important number of oxygen vacancies below $x\approx0.4$ and the consequent reduction of the expected charge of the metallic layers could be the reason of the almost constant *c/a* ratio reported earlier (see Figure 1.8).

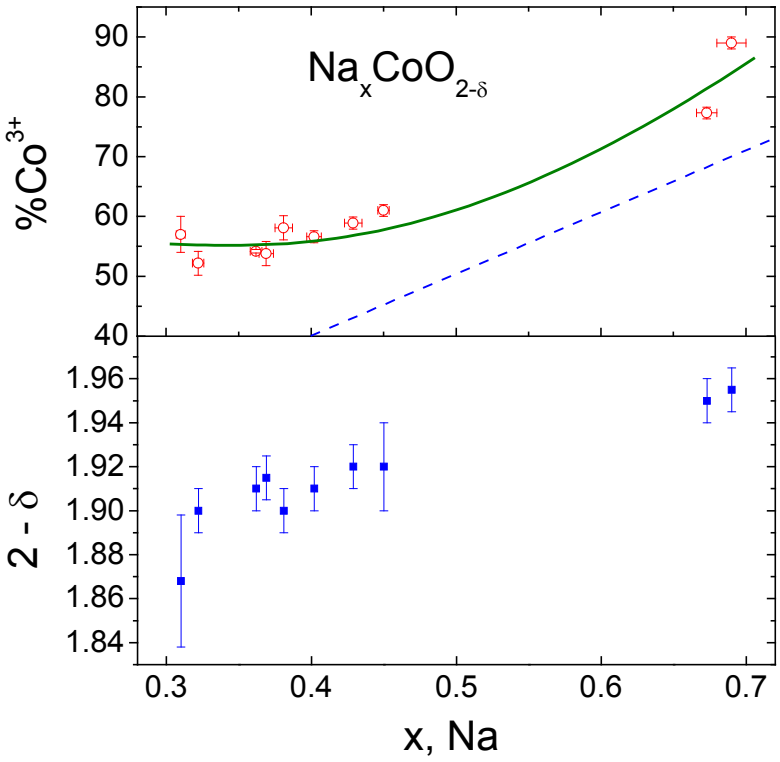

Figure 1.9: *Actual Co^{3+} percentage (top) and oxygen content (bottom) as a function of the Na^+ measured by ICP-OES. The solid line in thet top panel is a guide to the eye and the dotted line is the %Co^{3+} expected on the basis of the Na^+ content, for an oxygen stoichiometry of (2-δ)=2.00.*

The loss of oxygen is made possible by a pinning of the $Co^{3+/4+}$:t_{2g} band at the top of the O^{2-}:$2p^6$ band. The initial energy difference between them at x>0.4 is completely saved as x decreases due to the stabilization of the Co^{3+}/Co^{4+} (t_{2g}) band. In this case, a redox process between the pairs $Co^{3+/4+}$ and O^{2-}/O_2,

$$Co^{4+} + e^- \rightarrow Co^{3+}$$

$$O^{2-} \rightarrow ½\ O_2 + 2e^-$$

can occur when holes are actually introduced into the oxygen band. *Marianetti et al*[72] proposed an alternative mechanism in which hole-doping at the t_{2g} band rehybridizates the e_g and O:2p orbitals, which produces an effective hole transfer to the oxygen band and hence the same global redox process described above.

This redox process $Co^{3+/4+} \leftrightarrow O^{2-}/O^2$ makes it extremely difficult to reach a good control over doping of the CoO_2 layers through variation of the Na^+ content.

This is a result of fundamental importance: we can conclude that there is not a direct correlation between the Na^+ content and the amount of charge introduced into the CoO_2 planes. This is an important difference with cuprates.

1.1.2.2. Na^+ intercalation

At this point we have discussed in detail the synthesis and chemical properties of the Na_xCoO_2 samples obtained by Na^+ deintercalation with Br_2. However, if we look at the Na^+ content of the different samples studied in the literature we can observe that there are just a few Na^+ compositions covering the compositional range $0.5<x<0.7$. For this reason, and inspired by previous works about the chemical insertion of Li^+ ions in Li_xCoO_2[¡Error! Marcador no definido.], we decided to check whether the insertion of Na^+ ions in Na_xCoO_2 is possible, in order to cover the range $0.5<x<0.7$.

A completely new serie was synthetized by Na^+ intercalation with Na^+/I^- acetonitrile from a low Na^+ sample, $Na_{0.32}CoO_2$, previously obtained by Na^+ deintercalation from $Na_{0.67}CoO_2$. The experimental procedure consists in mixing a certain amount of $Na_{0.32}CoO_2$ in a solution formed by NaI and acetonitrile (as a non-aqueous solvent) in Ar atmosphere. A large amount of

[72] C. A. Marianetti, G. Kotliar and G. Ceder. *Phys. Rev. Lett.* **92**, 196405 (**2004**).

$Na_{0.32}CoO_2$ was splitted in several parts (0.200 g each one) and added into NaI/acetonitrile mixtures (25 mL) presenting different amounts of NaI (0.0075-1.5 g). The time of the reaction was also a parameter of control, varying from 23 h to 140 h for a given NaI concentration. At the end of the reaction all the samples were filtered and washed several times with acetonitrile in order to avoid possible rests of NaI.

All the samples were characterized structurally by X-ray diffraction. All the diffraction patterns resulted to be single phase and they were indexed to the hexagonal *P63/mmc* space group. Figure 1.10 shows the evolution of the (002) reflexion peak for some representative Na^+ intercalated samples. Large amounts of NaI, and longer times led to phases with the highest Na^+ content. The continuous displacement of the (002) reflexion to higher angles indicates that the Na^+ content in the samples is increasing, reducing the interlayer distance. On the other hand, the width of the peaks remains constant after the intercalation process, which supports an homogeneous distribution of Na^+ through the sample.

It is important to remark that with this technique the highest Na^+ content achieved was x~0.63, only slightly lower than the Na^+ composition of the initial precursor obtained directly through solid state reaction, x=0.67. However, we were able to obtain a wide range of compositions in the range of $0.5<x<0.7$.

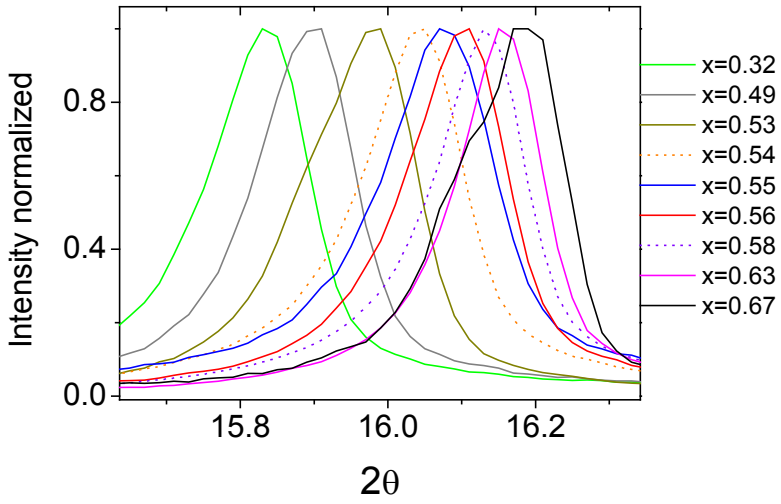

Figure 1.10: *Evolution of the (002) reflexion peak as Na^+ is intercalated into $Na_{0.32}CoO_2$.*

All the diffraction patterns were fitted with Rietica in order to calculate the cell parameters of the different phases. Figure 1.11 shows the evolution of the the cell parameters of the Na^+ intercalated/deintercalated series.

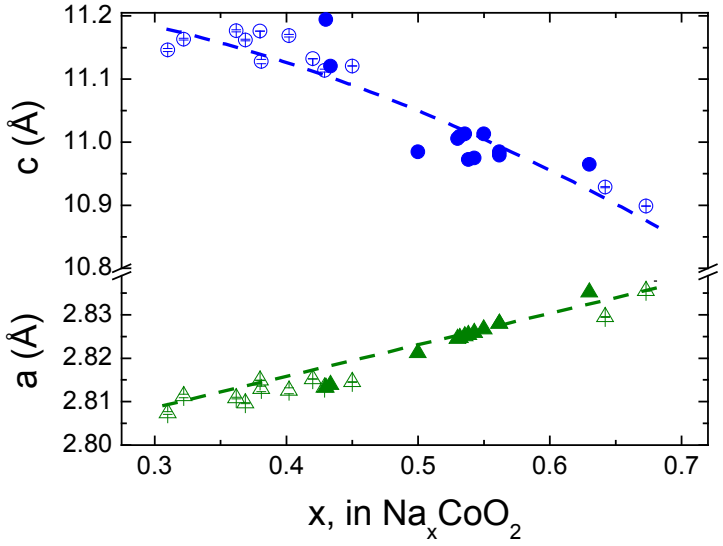

Figure 1.11: *Lattice parameters for Na^+ deintercalated (open symbols) and Na^+ intercalated (closed symbols) Na_xCoO_2 series, as a function of the Na^+ content. Lines are guides to the eye.*

The magnetic and transport properties of these samples will be discussed in the following chapters, paying special attention to the comparison of samples with the same *x* but obtained after deintercalation/intercalation from a higher/lower *x*.

Combining the deintercalation and intercalation approaches, it is possible to cover a broad range of compositions between $0.3 \leq x \leq 0.7$.

It is important to mention here that Na^+ deintercalation/intercalation processes can be also performed electrochemically, in which a Na_xCoO_2 host would act as a cathode. Moreover, phase transitions in intercalation materials can be identified electrochemically by studying the open circuit voltage (o.c.v.) of a battery as a function of the amount of intercalated ion present in the host structure. In a battery configuration the anode potential is constant, the net concentration of Li^+ ions in the electrolyte is also constant and the variations in the o.c.v. with deintercalation/intercalation are the relative to the electrochemical potential of electrons in the cathode material. Therefore, the shape of the o.c.v.-composition curve depends on the electronic structure of the cathod material and the related variation of their Fermi level. The o.c.v.-composition curve[73] for Na_xCoO_2 shows a discontinuous potential change with several characteristic plateaus that are associated to different phase transitions along *x*. These structural phase transitions are related to the alteration of sodium coordination from octahedral to trigonal prismatic. In fact, the coexistence of two different structural phases (O3 and P3) has been observed for Na^+ compositions $0.65 \leq x \leq 0.8$.

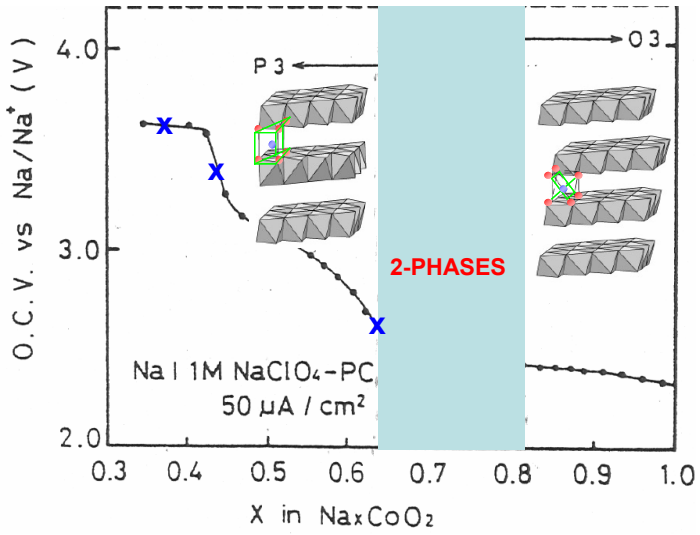

Figure 1.12: *Open circuit voltage data for a Na_xCoO_2 cell. (Plot taken from Ref. 35). Blue crosses correspond to the o.c.v. measured for three different Na_xCoO_2 cells.*

[73] S. Kikkawa, S. Miyazaki and M. Koizumi. *J. Power Sources* **14**, 231 (**1985**).

Three Na_xCoO_2 batteries with different x were performed in order to measure their o.c.v. and compare it with that one obtained in Ref. 35. The Na^+ composition estimated from the o.c.v. curve is similar to that determined by ICP-OES.

On the other hand, sodium cobaltates are highly higroscopic. However, the amount of water absorbed and the chemical stability depends strongly on the sodium content of the samples. As a general rule, as sodium content decreases, the hygroscopic character increases notably. Figure 1.13 shows the thermogravimetric analysis (TGA) up to 360 ºC for the parent compound (x≈0.7) and for a Na^+ deintercalated sample (x≈0.4) after being synthetized and kept for one day in a desicator with a 40% of humidity. The *x*=0.4 sample shows a drastic weight loss of about 3% below 100 ºC, while the mass of the *x*≈0.7 sample remains almost invariant in the whole range of temperature. This weight loss is related to the humidity present in the powder. Above 100 ºC, the *x*≈0.4 sample shows a continuous weight loss with temperature up to the highest temperature measured, which must be due to intercalated water.

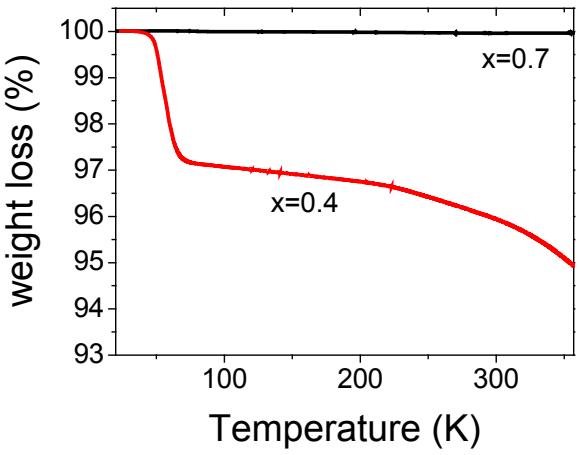

Figure 1.13: *TGA analysis of the x≈0.7 and x≈0.4 samples with temperature up to 360 ºC at 10 ºC/min under N_2 flowing.*

Figure 1.14 shows SEM images for a Na^+ deintercalated sample with x≈0.5, before and after hydration. Their layered strcture is clearly evidenced in both of them by the stacking of the CoO_2 sheets. The micrograph at the

right corresponds to the hydrated sample and a larger exfoliation between the stacked layers can be observed.

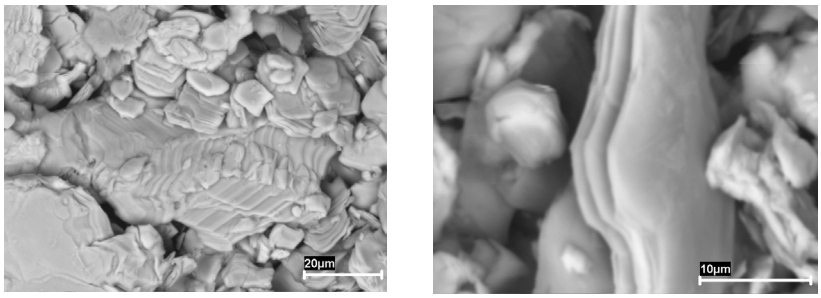

Figure 1.13: *SEM micrographs of the non-hydrated (left) and hydrated (right) x≈0.5 sample.*

1.1.3. Na_xCoO_2, x>0.70

The achievement of Na_xCoO_2 phases with $x>0.7$ is not trivial. The direct synthesis by solid state reaction from the most common starting materials, Na_2CO_3 and Co_3O_4, leads always to the more stable phase, $Na_{\sim 0.7}CoO_2$. The preparation of phases with a low Na^+ content ($x<0.7$), is relatively easy through Na^+ deintercalation. Taking this into account, other methods of synthesis involving different experimental procedures were carried out in order to obtain different Na_xCoO_2 compositions with $x>0.7$. Among the most popular, we can distinguish those based on the direct synthesis between Na_2O_2 and Co_3O_4[74,75], Co metal and NaOH to obtain the $NaCoO_2$ (*O3*) phase[76] or Na_2CO_3 and Co_3O_4 to give, after several annealings at high temperature, $x>0.8$ samples[77]. Also an original chemical method where the parent compound $Na_{0.7}CoO_2$ reacts with Na metal was

[74] G. Lang, J. Bobroff, H. Alloul, P. Mendels, N. Blanchard and G. Collin. *Phys. Rev. B*, **74**, 094404 (**2005**).
[75] Q. Huang, M. L. Foo, R. A. Pascal, Jr., J. W. Lynn, B. H. Toby, Tao He, H. W. Zandbergen and R. J. Cava. *Phys. Rev. B*, **70**, 184110 (**2004**).
[76] B. L. Cushing and J. B. Wiley. *Synth. React. Inorg. Met.-Org. Chem*, **29(7)**, 1199 (**1999**).
[77] H. Sakurai, S. Takenouchi, N. Tsujii and E. Takayama-Muromachi. *J. Phys. Soc. Jpn.* **73**, *2081* (**2004**).

used to obtain x>0.8 samples[78]. However, in spite of the existence of several methods of synthesis, in many cases the sodium composition of the resultant products reported in the literature is very ambiguous and uncertain, and actually not well intercalated between the CoO_2 layers.

In order to obtain a sample of Na_xCoO_2 with x>0.7 sample, we have checked the efficence of some of these methods. After an exhaustive analysis of the final product to determine unambiguously the actual sodium composition of the sample, we obtained the best results with the methods reported in the references *39* and *40.* Below, we will describe the experimental procedures carried out following these methods for our specific case of Na_xCoO_2 (x>0.7) synthesis:

1) Solid state reaction[77].

In order to obtain a final product with x=0.82, stochiometric amounts of Na_2CO_3 and Co_3O_4 (previously dried at 300ºC overnight) were well mixing and pestle under mechanical cold pressure at ~15 tons/cm^2. The reaction that takes place is exactly the same that one previously described in the synthesis of the parent compound $Na_{0.7}CoO_2$. All the pellets were placed in a tubular furnace under O_2 flow gas and three heat treatments were performed at different temperatures: 800ºC, 850ºC and 900ºC respectively. Each thermal annealing took 6h and the samples were regrinding and pressed before each new annealing. A more detailed description about the experimental conditions of the annealings performed in the samples is found in reference *38*.

2) Chemical synthesis[78].

For the synthesis of samples with x>0.75, sodium metal (0.3g) and tetrahydrofuran (40 ml) were placed in a 25mm x 150mm Pyrex screw-capped tube, and were heated by placing the lower 25mm in an silicon bath maintained at 95 °C. After 1 h, benzophenone (2g) was added. After heating another hour, powdered $Na_{0.7}CoO_2$ precursor (1.5g) was added, and the mixture was heated, with agitation by a magnetic stirring bar, for 48 h. As the mixture was cooled down to room temperature, ethanol (20 ml) was added to destroy the benzophenone ketyl radical anion and any unreacted sodium metal. After 20 min, the mixture was centrifuged for 3 min at 2000 rpm in a

[78] Q. Huang, M. L. Foo, R. A. Pascal, Jr., J. W. Lynn, B. H. Toby, Tao He, H. W. Zandbergen and R. J. Cava. *Phys. Rev. B*, **70**, 184110 (**2004**).

stainless-steel centrifuge tube. The organic supernatant was decanted, the solid was resuspended in dichloromethane (20ml), the mixture was centrifuged, and the organic supernatant was again decanted. Two more dichloromethane washes were performed in the same way, and then the final black pellet was broken up and air dried overnight. This process led in different syntheses to sodium-enriched materials with $0.80<x<0.90$. This difference may be associated to the presence of a two-phase region in the phase diagram at these compositions, or possibly due to uncertainties in the temperature or any other variable of the reaction.

The sodium content of the samples was determined by the ICP-OES method. The stochiometry of the resultant samples was $Na_{0.82}CoO_2$. Also the increase in the Na^+ content of the samples was confirmed through structural refinements of the XRD patterns. Figure 1.14 shows the X-ray diffraction pattern for $Na_{0.69}CoO_2$ as well as for the samples with a high Na^+ content obtained by solid state reaction and chemical synthesis, respectively. Both of them are single phase and were indexed with the hexagonal space group P63/mmc, maintaining the *P3* symmetry. This is opposite to other works where a change from *P3* to *O3* structure was reported for samples with stochiometry x=0.75 and 0.92[79]. Only the pattern of the sample obtained by chemical synthesis present a couple of small reflexions marked with stars which have not been identified, probably due to partially hydrated phases. The displacement observed of the (002) reflexion peak to higher angles indicates that the interlayer distance is shorter than in the case of the parent compound $Na_{0.69}CoO_2$. This is consistent with a higher number of sites being ocupped by Na^+ ions.

[79] L. Viciu, J. W. G. Bos, H. W. Zandbergen, Q. Huang, M. L. Foo, S. Ishiwata, A. P. Ramirez, M. Lee and N. P. Ong. *Phys. Rev. B*, **73**, 174104 (**2006**).

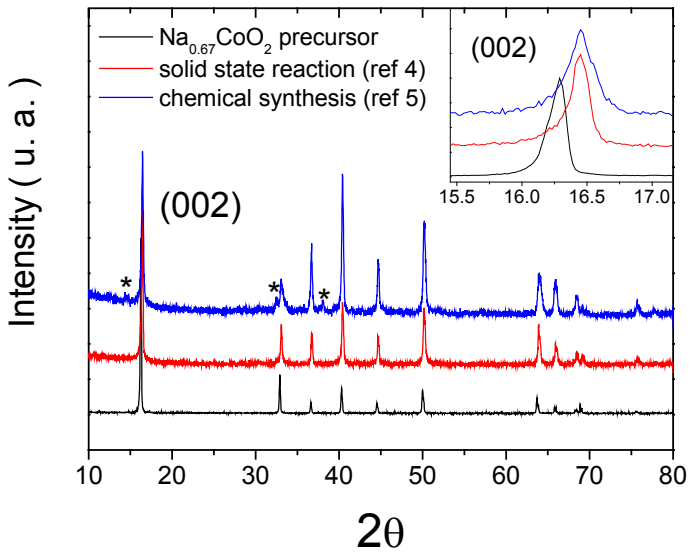

Figure 1.14: *XRD patterns for the parent compound $Na_{0.67}CoO_2$ and the samples with a higher Na^+ content obtained by solid state reaction and chemical synthesis, respectively. The inset shows the position of the (002) reflexion for all these samples, indicating a shift to higher angles in the case of the samples presenting a higher Na^+ content. The stars (*) indicate reflections belonging to impurities which have not been identified.*

1.2. Synthesis of $Na_{0.7}CoO_2$ single-crystal.

There are basically two synthetic routes in the literature to obtain single crystals of Na_xCoO_2: the *flux* method and growth by the *optical floating-zone (FZ)* technique. Single crystals obtained from the latter can be several centimetres long and width, so they are easily orientable and their transport and magnetic properties can be measured as a function of a particular crystallographic direction.

In this work, due to the lack of a FZ furnace, single crystals of $Na_{0.7}CoO_2$ have been synthesized by the flux method from $Co(NO_3)_3.5H_2O$ and NaOH following a slight modification of the method by *Shivakumara et*

al[80]. The reactants were weighted in the ratio 1:10 ($Co(NO_3)_3.5H_2O$:NaOH), grounded and mixed under Ar atmosphere in a dry box to avoid water absorption. Then, they were placed in an Al_2O_3 crucible and heated at 400 ºC in air for 12 hours. The heating rate was 3 ºC/min while the cooling rate was 0.5 ºC/h from 400 ºC to 200 ºC, and 3 ºC/min from 200 ºC to room temperature.

The size of the crystals obtained using the flux method is of the order of a few tens of μm. Some of the micrographs obtained for $Na_{\approx 0.7}CoO_2$ single crystals are shown in Figure 1.15. In all of them, the hexagonal structure can be clearly appreciated. It is also distinguishable the stacking of layers along the *c*-axis, slightly exfoliated.

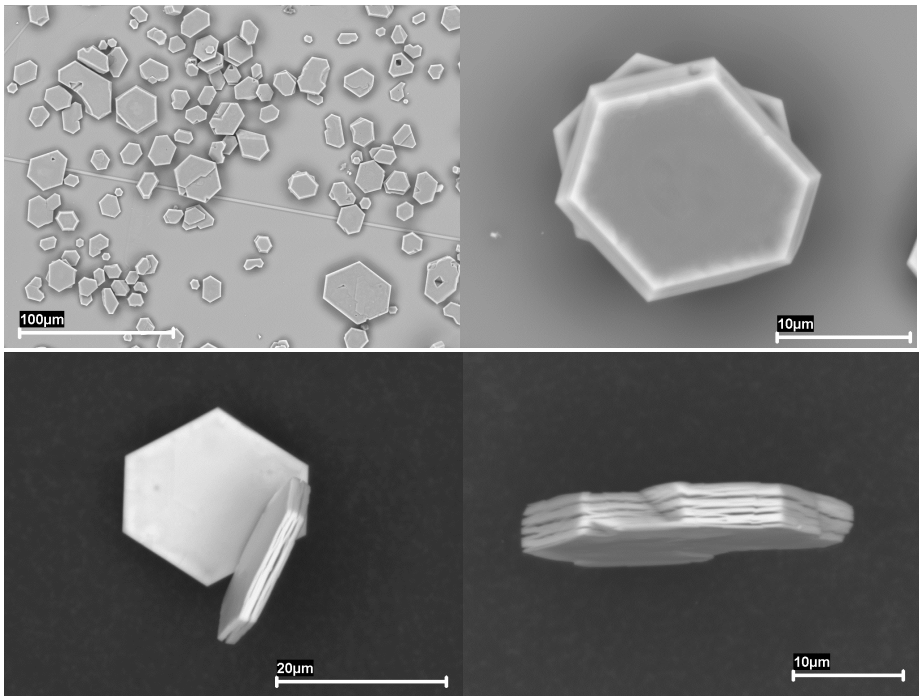

Figure 1.15: *SEM micrographs of $Na_{\approx 0.7}CoO_2$ single crystals.*

[80] C. Shivakumara and M. S. Hegde. *Proc. Indian Acad. Sci (Chem. Sci.)* **115**, 447 (**2003**).

Single crystals of K_xCoO_2 were also synthetized by this technique. The techniques described previously to deintercalate sodium from polycrystalline samples, are equally applicable to Na_xCoO_2 single crystals. However, it is important to remark that chemical deintercalation from single crystals results in an inhomogeneous distribution of Na^+ along the sample. This is due to the smaller effective surface area of the single crystal compared to the powder. This makes the results in deintercalated single crystals very much sample-dependent. This, along with the difficulty to obtain large enough crystals to make reliable transport experiments, drove us to focus on the polycrystalline samples.

2. Magnetic and transport properties of Na_xCoO_2

Na_xCoO_2 (x<1) has been studied because of the richness of its magnetic and electric phase diagram, which shows a wide variaty of physical properties with doping and temperature. As a function of x, Na_xCoO_2 goes from AFM behaviour[81] at high x to PM behaviour at low x, showing other interesting phenomena like an unusually large thermoelectric power[82], the appearance of SDW[83], charge ordering (CO)[84] or low temperature superconductivity[85].

---

[81] S. P. Bayrakci, C. Bernhard, D. P. Chen, B. Keimer, R. K. Kremer, P. Lemmens, C. T. Lin, C. Niedermayer and J. Strempfer. *Phys. Rev. B* **69**, 100410 (**2004**).
[82] Y. Wang, N. S. Rogado, R. J. Cava and N. P. Ong. *Nat. Mater*. **423**, 425 (**2003**).
[83] S. P. Bayrakci, I. Mirebeau, P. Bourges, Y. Sidis, M. Enderle, J. Mesot, D. P. Chen, C. T. Lin and B. Keimer. *Phys. Rev. Lett*. **94**, 157205 (**2005**).
[84] M. L. Foo, Y. Wang, S. Watauchi, H. W. Zandbergen, T. He, R. J. Cava and N. P. Ong. *Phys. Rev. Lett*. **92**, 247001 (**2004**).
[85] K. Takada, H. Sakurai, E. Takayama-Muromachi, F. Izumi, R. A. Dilanian and T. Sasaki. *Nature* **422**, 53 (**2003**).

Most of the articles published in the last decade about this material have focused on the origin of the unconventional character of the superconductivity[86,87,88,89]. However, systematic investigations of the evolution of the magnetic and transport properties as a function of *x* are scarce. On the other hand, it is important to remark that samples of Na_xCoO_2 samples are intrinsically inhomogenous and phases with slightly differences in the Na^+ content have been reported at the same nominal composition in the literature. This fact is reflected later in the chemical and physical properties, making very difficult their reproducibility and so their understanding.

For this reason we present here a systematic study of the magnetic and transport properties of the system Na_xCoO_2, particulary focusing on the new magnetic phases emerging close to $x \approx 0.5$. To determine the intrinsic transport properties, we have measured the temperature and *x* dependence of the thermoelectric power, *S(T, x)*. Different to the conductivity, *S* is not so influenced by intergrain bondary scattering, as no current flows to the sample during the experiment.

Na_xCoO_2 $x \sim 0.7$ exhibits an unusual combination of transport properties: it shows a low electrical resistivity of 200 μΩcm in the direction paralell to the CoO_2 planes accompained by a large thermopower ≈100 μV/K at room temperature (in single crystals)[90], which is about ten times larger than in typical metals. In particular, a thermoelectric figure of merit $ZT>1$ above 800 K has been reported. It is important to remark that the good thermoelectric properties were found in between CO and SDW limits (Figure 2.1). In addition, it is well known that Na_xCoO_2 samples are extremely sensitive to temperature and humidity conditions which result in irreversible changes in their chemical and physical properties that would modify its electronic phase diagram.

[86] I. I. Mazin and M. D. Johannes. *Nature Phys.* **1**, 91 (**2005**).
[87] H. Sakurai, K. Takada, S. Yoshii, T. Sasaki, K. Kindo and E. Takayama-Muromachi. *Phys. Rev. B* **68**, 132507 (**2003**).
[88] A. Tanaka and X. Hu. *Phys. Rev. Lett*. **91**, 257006 (**2003**).
[89] K. Kuroki, Y. Tanaka and R. Arita. *Phys. Rev. Lett*. **93**, 077001 (**2004**); *Phys. Rev. B* **71**, 024506 (**2005**).
[90] I. Terasaki, Y. Sasago and K. Uchinokura. *Phys. Rev. B* **56**, 12685 (**1997**).

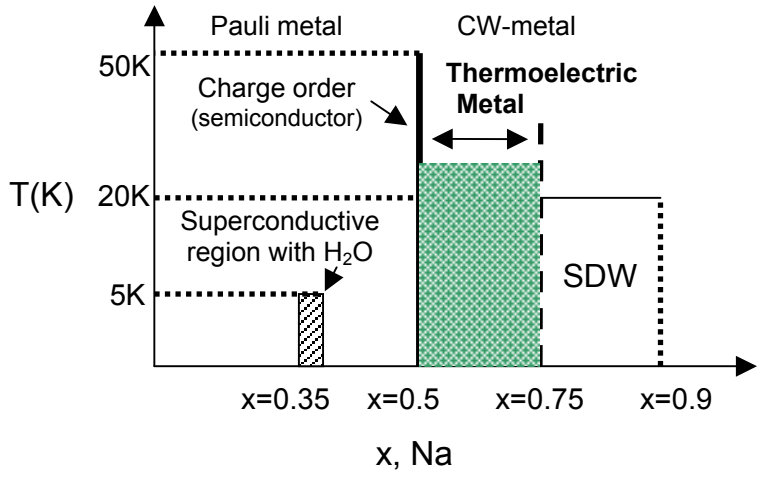

Figure 2.1: *Electronic phase diagram of Na_xCoO_2 as a function of the Na^+ content x.*

2.1 Na_xCoO_2 (0.3<x<0.7)

Polycrystalline Na_xCoO_2 (0.70<*x*<0.30) series have been obtained by Na^+ deintercalation from $Na_{0.7}CoO_2$, as described in Chapter 1. The Na and Co contents of the new phases were determined by ICP-OES.

Figure 2.2 shows the temperature dependence of the absolute electrical resistance for two representative Na^+ compositions: $Na_{0.7}CoO_2$ (upper) and $Na_{0.51}CoO_2$ (lower). In order to keep the intrinsic properties of the material, we have not performed any additional annealing in $Na_{0.51}CoO_2$ after Na^+ extraction and before the electrical resistance experiments. However, the strong intergrain contribution in the case of $Na_{0.7}CoO_2$ forced us to anneal the sample in order to being able to perform the measurement. In any case, the effect of the annealing is not so critical in the case of *x*=0.7 content, since the small amount of Na^+ vacancies allows a lower number of possible Na^+ rearrangements.[91]

[91] T. F. Schulze, P. S. Häfliger, Ch. Niedermayer, K. Mattenberger, S. Bubenhofer and B. Batlogg. *Phys. Rev. Lett.* **100**, 026407 (**2008**).

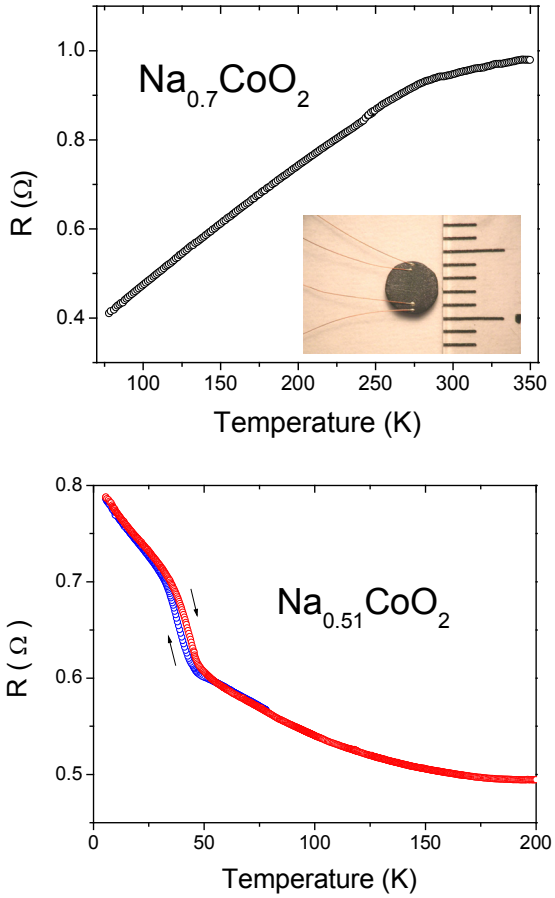

Figure 2.2: *Temperature dependence of the electrical resistance with temperature for $Na_{0.7}CoO_2$ (upper) and $Na_{0.51}CoO_2$ (lower). Inset in the upper figure shows the contacts on the surface of the pellet (four-probe method) to measure the electrical resistance. We could not cut the pellet, due to its extreme softeness and sensivity to ambient conditions. For $Na_{0.51}CoO_2$, heating (red) and cooling (blue) runs are indicated.*

Although the temperature scales are essentially different in both cases, completely different electrical behaviours are observed in $Na_{0.7}CoO_2$ and $Na_{0.51}CoO_2$. Whereas the $Na_{0.7}CoO_2$ shows a typical metallic behaviour

increasing the resistance with temperature, $Na_{0.51}CoO_2$ shows an increase of the resistance below 45 K, which is associated to the formation of a SDW[92] rather than to an effective charge localization, as ocurrs in others systems[93] like manganites or nickelates due to a CO effect. This has been also observed in single crystals.[84]

On the other hand, intrinsic transport properties can be proved through the Seebeck coefficient, a magnitude that is not so sensitive to intergrain scattering as no current flows through the sample. We have carried out TEP measurements with temperature from 90 K to 450 K in both Na^+ deintercalated and intercalated Na_xCoO_2 series. Thermopower is the most sensitive electronic transport property of a metal: it is very susceptible to variations in the number of carriers and gives direct information of the asymmetry of the density of states around the Fermi energy (E_F)[94].

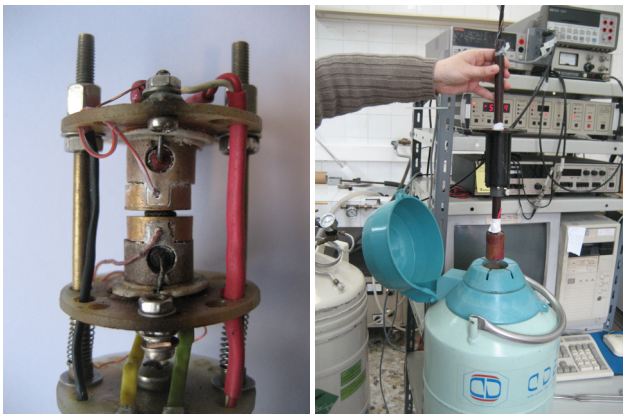

Figure 2.3: *(Left) Detail of the home-made sample holder used in the thermpoelectric power measurements. Cold pressed pellets are placed in between two gold-platted cupper blocks. A thermal gradient of ±1 K is established between the cupper blocks. (Right) The sample holder is protected and introduced in a dewar containing liquid nitrogen that provides a cold bath for temperature control.*

---

[92] J. Bobroff, G. Lang, H. Alloul, N. Blanchard and G. Collin. *Phys. Rev. Lett.* **96**, 107201 (**2006**).

[93] "Colossal Magnetoresistance, Charge Ordering and Related Properties of Manganese Oxides", C. N. R. Rao, B. Raveau, Eds. World Scientific, Singapore (**1998)**

[94] J. M. Ziman. *Electrons and Phonons.* ISBN: 0-19-850779-8. Clarendon Press, Oxford (**2001**).

The results for a Na^+ deintercalated Na_xCoO_2 series are shown in Figure 2.4. The samples with a large Na^+ content show a thermoelectric power similar to that previously reported by several authors[84,95]. The thermopower increases with temperature, but the value and the temperature dependence deviates from what in principle should be expected in a metal with such a low resistivity. An interpretation for this anomalously large thermoelectric power in Na_xCoO_2 has been given, on the basis of a large spin entropy contribution, due to the different magnetic states that could be adopted by $Co^{3+/4+}$ (LS, IS or HS for low, intermediate and high spin state)[82,96,97,98]. As Na^+ is removed the thermopower decreases and becomes less temperature dependent, being practically insensitive to variations of Na^+ doping below x<0.45. These results are fully consistent with the results obtained previously from iodometric titration analysis (see Chapter 1), where no variations in the valence state of cobalt is observed for x<0.45.

Therefore, our TEP results provides also another experimental proof that a direct relationship between the Na^+ content and the number of holes introduced into the CoO_2 planes does not exist in Na_xCoO_2. This effect is particularly dramatic at low Na^+, where superconductivity is found after hydration.

On the other hand, a rapid increase is observed above ~350 K in the TEP. This increase is more noticeable in the low Na^+ regime and agrees with an exothermic peak observed by differential scanning calorimetry analysis (DSC) in a x=0.4 sample (Figure 1.13, dash curve). For x=0.7 nor exothermic or endothermic peaks are observed. To the best of our knoledge, this has not been reported in the literature, and could be indicating some structural rearrangement or order/disorder transition at the Na^+ sites leading to a lower energy configuration. We will discuss this again related to high temperature Seebeck results in the following pages.

Na_xCoO_2 samples with $x\approx0.5$ were very difficult to obtain by Na^+ deintercalation. However, the x=0.5 phase represents a very interesting point in the phase diagram of this material. For this purppose, we have carried out the synthesis of a completely new series by Na^+ deintercalation, adjusting very carefully the amount of Br_2 needed to achieve the desired

[95] K. Takahata, Y. Iguchi, D. Tanaka, T. Itoh and I. Terasaki. *Phys. Rev. B* **61**, 12551 (**2000**).
[96] W. Koshibae, K. Tsutsui and S. Maekawa. *Phys. Rev. B* **62**, 6869 (**2000**).
[97] W. Koshibae and S. Maekawa. *Phys. Rev. Lett.* **87**, 236603 (**2001**).
[98] M. Lee, L. Viciu, L. Li, Y. Wang, M. L. Foo, S. Watauchi, R. A. Pascal Jr, R. J. Cava and N. P. Ong. *Nature Mater*. **5**, 537 (**2006**).

phase. Figure 2.5 shows the TEP of the new Na_xCoO_2 series with three representative samples very close to x=0.5.

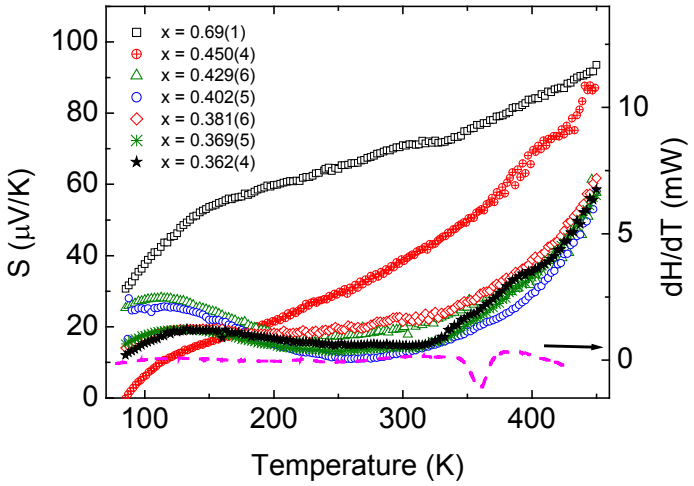

Figure 2.4: *Evolution of the temperature dependence of the thermopower with Na^+ content. Below x~0.42, the thermopower does not show a dependence on the Na/Co ratio due to the invariance of doping at the CoO_2 planes in this range of x. Dash curve shows a DSC analysis with temperature for a x≈0.4 sample performed at 10 ºC/min.*

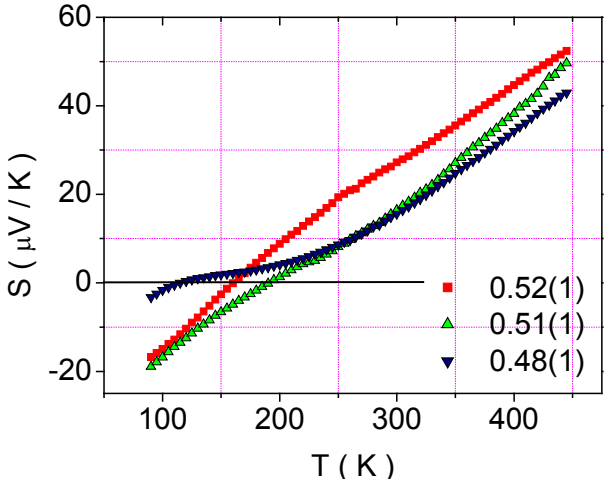

Figure 2.5: *Thermoelectric power of a Na^+ deintercalated Na_xCoO_2 series.*

Now, we are in a position to establish general trends related to the Na^+ content, which can be summarized in:

(a) At large x ($0.5<x<0.7$) the TEP is always large and positive, and increases almost linearly over the whole temperature range.

(b) In the samples very close to $x\approx0.5$ ($0.47<x\leq0.5$) $S(T)$ also increases continuously over the whole temperature range, although a characteristic crossover to negative values is clearly observed below $\approx$150K.

(c) For $x<0.5$ the positive sign of the TEP is recovered in the whole temperature range.

(d) As x decreases below $x<0.5$ the thermopower shows a temperature independent plateau which is practically insensitive to variations in the Na^+ content. The linear T-dependence is recovered above ~375 ºC, in agreement with the exothermic peak observed in DSC calorimetry. It could be presumibly associated to Na^+ ion mobility.

The invariance of the thermopower in the lowest doping region corroborates the inefficiency of Na^+ removal to introduce charge carriers in the CoO_2 layers. The same TEP behaviour with temperature was confirmed for a Na_xCoO_2 series in which Na^+ was progresively intercalated from x=0.47 (Figure 2.6).

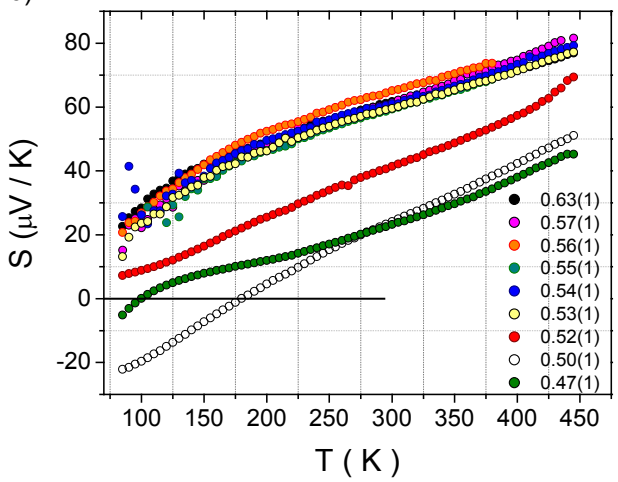

Figure 2.6: *Temperature dependence of the thermopower of a Na^+ intercalated Na_xCoO_2 series from a sample with x=0.47.*

These measurements were extended down to ~10 K for three representative samples of these doping ranges (Figure 2.7).

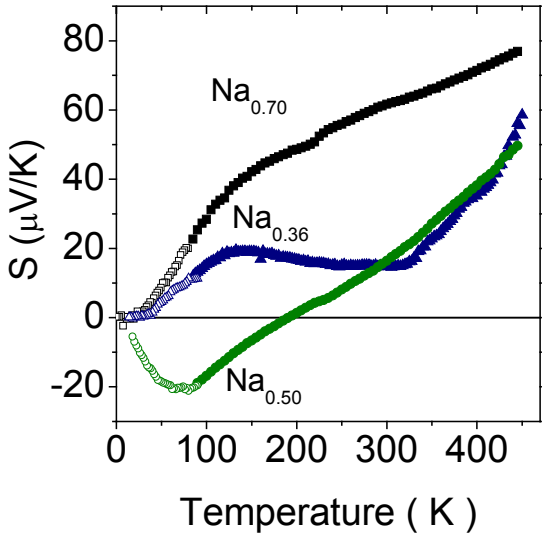

Figure 2.7: *Temperature dependence of the thermoelectric power of representative Na^+ compositions in Na_xCoO_2 (x= 0.70, 0.50 and 0.36).The low-T (open) and high-T (filled) data were measured in different equipments.*

It is highly improbable that exactly the same Na^+ arrangement is reached after chemical removal/insertion of Na^+. So, these results demonstrate that only the $Na^+/Co^{3+/IV}$ ratio is important in determining the *S(T)* of Na_xCoO_2.

An important information about the band structure of Na_xCoO_2 could be obtained from the analysis of these data. Of special interest here are the increase of the slope with increasing Na^+ content at low-T and the crossover to negative values at T~190 K in the $x\approx0.5$ sample. At this specific composition, $x\approx0.5$, the Seebeck coefficient is negative at low temperatures and crosses to positive values between 100-150 K, depending on the exact composition.

Kaurav et al[99] showed similar results although the negative cuadrant and the minimum Seebeck were observed at T~85 K and T~50 K, respectively. Based on previous neutron scattering, susceptibility, magnetic resonance and transport results in $Na_{0.5}CoO_2$[84,100,101], the authors associated this crossover to the charge and antiferromagnetic orders. The difference of these characteristic temperatures with our data for the same Na^+ composition could lie in very small differences in the Na^+ content.

Such a change in the sign of *S(T)* and the broad peak observed at low temperature indicates that the electronic structure of this sample must be fundamentally different to the neighboring compositons. However, for an AFM phase with an associated conventional charge-odering below ~40 K, there should be a substantial increase of the absolute value of hte thermopower and a thermal activated conduction; none of these are observed.

On the other hand, the combination of an electrical resistivity as low as that of a metal, with a thermoelectric power that is typically an order of magnitude larger than expected on the basis of this, is not easily understood within the framework of conventional band theory for metals. So, the question being asked here is…what is the origin of this enhancement of the thermoelectric power?

The magnitude of the linear temperature dependence of the Seebeck coefficient in an itinerant-electron system is determined by the band structure around the Fermi energy, according to Mott's equation[102]:

$$S(T) = \frac{-\pi^2 k_B^2 T}{3e}\left(\frac{d\ln N(\varepsilon)}{dE}\right)_{E_F} \qquad \textbf{eq. [3.1]}$$

which represents the solution of the Boltzman transport equation[94] in the low temperature limit ($K_BT<W$, where W is the bandwidth) and where k_B is the

[99] N. Kaurav, K. K. Wu, Y. K. Kuo, G. J. Shu and F. C. Chou. *Phys. Rev. B* **79**, 075105 (**2009**).
[100] G. Gasparovic, R. A. Ott, J-H. Cho, F. C. Chou, Y. Chu, J. W. Lynn and Y. S. Lee. *Phys. Rev. Lett*. **96**, 046403 (**2006**).
[101] F. L. Ning, S. M. Golin, K. Ahilan, T. Imai, G. J. Shu and F. C. Chou. *Phys. Rev. Lett*. **100**, 086405 (**2008**).
[102] N. F. Mott and H. Jones. "The theory of the properties of metals and alloys". Ed. By Dover, NY **1958**.

Boltzman constant, T is the temperature, e is the charge of the electron and $N(\varepsilon)$ is the density of electronic states at the Fermi level. Rapidly varying $N(\varepsilon)$, characteristic of many strongly correlated systems, result in large values of *S(T)*, through the increse of the derivative part of equation [3.1] The complex band structure derived from the trigonal-field splitting of the Co^{3+}/Co^{IV} t_{2g} manifold, could in principle justify the large slope of *S(T)*. Chemical doping with different cations could help testing this hypothesis, as we will discuss later.

On other hand, Boltzmann transport equation tends to a temperature-independent solution at the high temperature limit ($K_BT>W$), resulting in the so-called Heikes formula

$$S = -\frac{k_b}{e}\ln\left(\frac{x}{1-x}\right) \qquad \textbf{eq. [3.2]}$$

where *x* is the concentration of mobile holes (Co^{IV}) in the Co^{3+} lattice. So, on the basis of conventional Boltzmann transport theory, the general behavior that can be expected for a correlated (not so large W) system is schematically pictured in Figure 2.8.

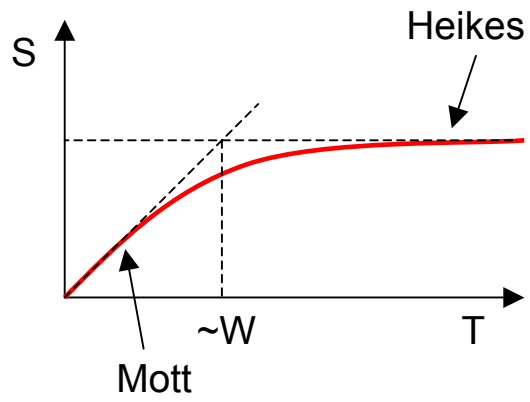

Figure 2.8: *General behaviour of S(T) expected for a correlated system in basis of Boltzman transport theory.*

The transition between the Mott and Heikes limits will be determined by the band width and its structure around E_F for each particular material.

In the last few years some alternative explanations have been given for the temperature dependence of *S(T)* in layered cobaltites.[103] *Terasaki et al*[104] speculated that the high thermoelectric power in Na_xCoO_2 could arise from spin fluctuations, as in the case of heavy fermions and/or valence-fluctuation systems[105]. Particulary, *Koshibae et al*[96,97] proposed a generalization of the Heikes formula[106] to include the spin entropy contribution from Co^{3+} and Co^{IV}. In their theory, the competition between the crystalline field and Hund coupling leads to large degeneracy in the cobalt *3d* states, where the electrons would be rather localized. They took into acount these considerations in a new term that includes the different possible spin configurations (LS, IS and HS) in addition to the Heikes formula,

[103] J. O. Haerter, M. R. Peterson and B. S. Shastry. *Phys. Rev. Lett.* **97**, 226402 (**2006**)
[104] I. Terasaki, Y. Sasago and K. Uchinokura. *Phys. Rev. B* **56**, 685 (**1997**).
[105] C. S. Garde and J. Ray. *Phys. Rev. B* **51**, 2960 (**1995**).
[106] P. M. Chaikin and G. Beni. *Phys. Rev. B* **13**, 647 (**1976**).

$$S = -\frac{k_b}{e}\ln\left(\frac{g_3}{g_4}\frac{x}{1-x}\right) \qquad \textbf{eq. [3.3]}$$

where g_3 and g_4 represent the degeneracy of the spin sate of the Co^{3+} and Co^{IV} ions. Initial support for this interpretation came from the strong suppression of the thermopower under a magnetic field[107,108]. However, it has been demonstrated recently[109] that the suppression of *S(T)* by a magnetic field can be explained by the field-induced spin polarization, in the context of Boltzman transport theory[110]. In fact, the applicability of equation [3.3] to systems like Na_xCoO_2 is doubtful. First of all, it predicts a temperature independent thermoelectric power, not observed in Na_xCoO_2 at large doping (see Figure 2.4). Since this equation is strictly applicable only in the limit where incoherent charge excitations dominate the electronic transport ($k_BT > W$), the temperature dependence of *S(T)* in metallic Na_xCoO_2 ($x\approx0.7$) demonstrate that this limit is still not reached at room temperature.

On the other hand, for x=0.35 and x=0.5 there is a temperature-independent plateau in which the applicability of Heikes formula can be tested.

It is important to remember at this point that in Na_xCoO_2 the amount of holes is not exactly determined by the Na^+ content[111,112,113,114]. For $x\approx0.7$ the average valence is ≈3.2+ instead of 3.3+, and a constant charge of 3.57(3)+ is reached for x<0.45. For a comparison between the results from equation [3.3] and the experiment, a precise determination of the actual concentration of holes in the system is crucial. Using the experimental values for Co^{3+}/Co^{IV}, the values of S(x=0.35, x=0.5) at the plateau are well

[107] Y. Wang, N. S. Rogado, R. J. Cava and N. P. Ong. *Nature* **423**, 425 (**2003**).
[108] P. Limelette, S. Hébert, V. Hardy, R. Frésard, Ch. Simon, and A. Maignan. *Phys. Rev. Lett.* **97**, 046601 (**2006**).
[109] H. J. Xiang and D. J. Singh. *Phys. Rev. B* **76**, 195111 (**2007**).
[110] T. Takeuchi, T. Kondo, T. Takami, H. Takahashi, H. Ikuta, U. Mizutani, K. Soda, R. Funahashi, M. Shikano, M. Mikami, S. Tsuda, T. Yokoya, S. Shin and T. Muro. *Phys Rev. B* **69**, 125410 (**2004**).
[111] M. Karppinen, I. Asako, T. Motohashi and H. Yamauchi. *Chem. Mater.* **16**, 1693 (**2004**).
[112] H. Sakurai, S. Takenouchi, N. Tsujii and E. Takayama-Muromachi. *J. Phys. Soc. Jpn.* **73**, 2081 (**2004**).
[113] M. Bañobre-López, F. Rivadulla, R. Caudillo, M. A. López-Quintela, J. Rivas and J. B. Goodenough. *Chem. Mater.*, **17**, 1965 (**2005**).
[114] C. A. Marianetti, G. Kotliar and G. Ceder. *Phys. Rev. Lett.* **92**, 196405 (**2004**).

reproduced by the Heikes equation without the need to include the spin degeneracy term.

On the other hand, the Heikes limit seems to be reached also at higher doping ($Na_{0.84}CoO_2$) and in misfit $Ca_3Co_4O_9$ (also sharing a triangular Co-lattice), as can be seen in Figure 2.9.

For $Na_{0.84}CoO_2$ using equation [3.3] with a LS configuration (g_3/g_4=1/6) will require an unphysical number of holes to justify the plateau at $S(k_BT > W) \approx 105\ \mu VK^{-1}$. However, the conventional Heikes formula (g_3/g_4=1) predicts the correct experimental value for a concentration of holes of 0.23, roughly consistent with the chemical formula.

The same trend is observed for $Ca_3Co_4O_9$. In this material photoemission spectroscopy experiments measured a concentration of holes $[Co^{4+}] \approx 0.23$, consistent with a LS configuration in the 3+/4+ ionic species. Using equation [3.3] would predict a $S(k_BT > W) \approx 258\ \mu VK^{-1}$, while the conventional Heikes equation results in $S(k_BT > W) \approx 105\ \mu VK^{-1}$. The latter value is very close to the experimental one (see Figure 2.9).

So, the conclusion with respect to x=0.7 is that the Heikes limit is not reached and, therefore, our experimental data only show the progresive S(T) evolution from a dominant Mott to Heikes state.

To reconcile this with the large slope of the thermopower at low temperatures is only possible if a complex band structure with contributions from a narrow a_1 and a broad *e* band at E_F is considered.[115]

An important point that remains to be explained is the rapid increase of the TEP with temperature above 350 K, particularly evident at low *x*. The formation of larger polarons and/or a dynamic spin transition from LS to IS or HS spin configurations with temperature would explain this behavior from the renormalized statistics (number of holes *vs* available sites) that must be considered in the Heikes formula.

[115] F. Rivadulla, J.-S. Zhou and J. B. Goodenough. Phys. Rev. B **68**, 07510 (**2003**).

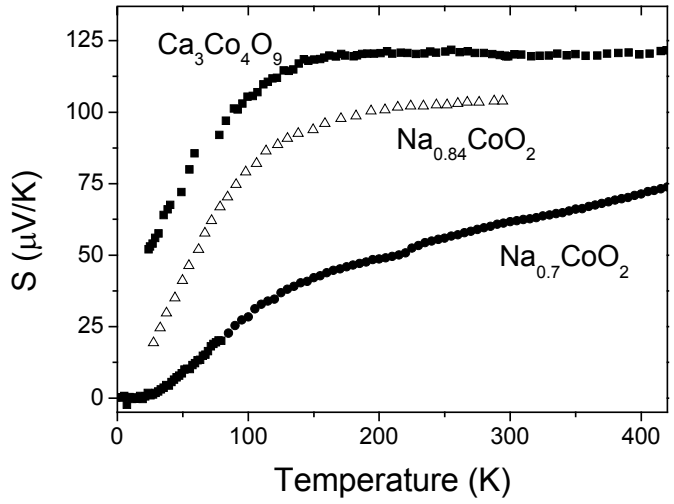

Figure 2.9: *Temperature dependence of the thermoelectric power for two compositions of Na_xCoO_2 (data for x=0.84 taken from Ref.20, and $Ca_3Co_4O_9$. Note that in $Na_{0.70}CoO_2$ the linear behaviour predicted by eq. [4] is not obeyed in the whole temperature range. Instead S(T) shows a change of slope about 150 K, although it does not reach saturation. We have taken the low temperature part to fit the data to equation [3.1].*

So, the agreement between the results of equation [3.3] with the experiment is most probably based on an erroneous estimation of the concentration of holes. Conventional Heikes formula predicts the correct value of the high temperature limit of the thermopower in layered cobaltites, once the correct number of charge carriers is considered.

Magnetic measurements performed in Na_xCoO_2 are presented below. It is important to mention again that no further thermal annealings of the samples were performed after synthesis and special attention has been paid in their storage during the time passed between the electrical, thermoelectric and magnetic measurements in order to preserve their intrinsic chemical and physical properties, and to make these measurements fully comparable among them. The time between the transport and magnetic measurements for each specific Na^+ composition did not exceed more than one day in any case.

Figure 2.10 shows the evolution of the zero field and field cooled (ZFC-FC) magnetization curves with *x* in the Na_xCoO_2 series. In general, an almost temperature independent magnetization region over a large range of

temperature (above ~100 K) is appreciated. However, a careful analysis of the results shows a slight and continuous increase of the magnetization from ~140 K up to 300 K for Na^+ contents between $0.52 \geq x \geq 0.40$ (see inset to Fig. 2.10).

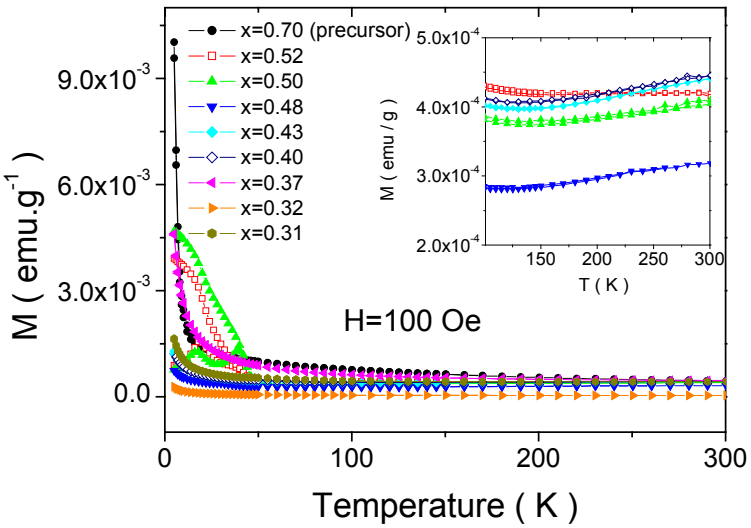

Figure 2.10: *ZFC-FC curves as a function of temperature in Na_xCoO_2 at an applied magnetic field of H=100 Oe. Inset: Zoom in the temperature region T>100 K to show the thermically activated term of the magnetization.*

This observation has been already reported by other authors[84,116] and it could be attributed to a continuous excitation above a spin gap whose origin is unknown.

Below T~140K, $\chi(T)$ increases in all the samples with decreasing temperature. The magnetization is not fitted by a Curie-Weiss law, so it should be separated in two different magnetic behaviours: divergent susceptibility at low temperature and Pauli susceptibility above a certain temperature (it is not as temperature independent as expected because of the spin gap transition, which provokes a slight increase of the magnetization at that temperature range.

[116] G. Lang, J. Bofroff, H. Alloul, G. Collin and N. Blanchard. Phys. Rev. B **78**, 155116 (**2008**).

In principle, fitting the magnetic data to a Curie-Weiss law will imply the assumption of a spin localized picture. However, local moments have not been reported in this itinerant system. Moreover, the results of the fitting of different compositions is not consistent with the local-moment picture as we will see now. Figure 2.11 shows the fitting of the high temperature magnetic data to a modified Curie-Weiss law plus a temperature independent term:

$$\chi = \chi_0 + \left(\frac{C}{T - \theta_{CW}} \right) \qquad \textbf{eq. [3.4]}$$

where χ is the magnetic susceptibility, χ_0 is the temperature independent term, C is the Curie temperature, *T* is the absolute temperature and θ_{CW} is the Curie-Weiss temperature. From the values of C obtained from the fitting we can calculate the effective magnetic moment (μ_{eff}) per Co atom (Table 2.1), and so the estimated Co^{3+}/Co^{IV} ratio in the sample.

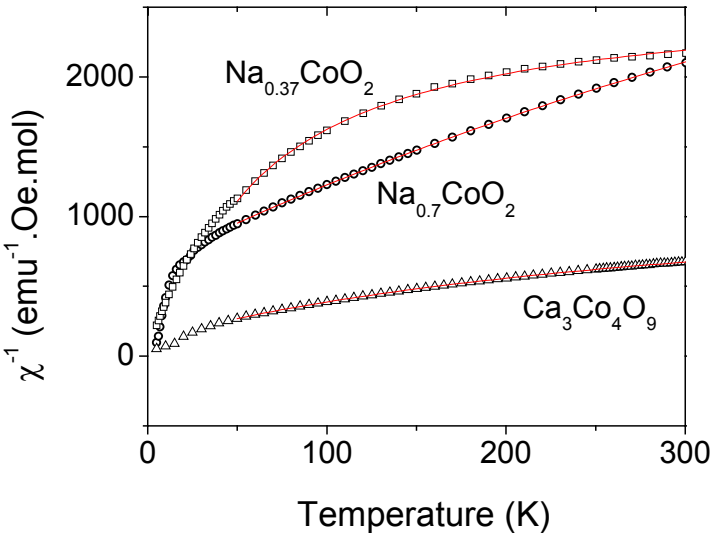

Figure 2.11: *Temperature dependence of the inverse of the susceptibility, χ^{-1}, for two representative Na_xCoO_2 samples (x=0.70 and x=0.37) and $Ca_3Co_4O_9$. Red lines are the fitting of the magnetic data to equation [3.4] from 50 K to 300 K.*

Table 2.1: *Parameters from the fitting of $\chi(T)$ for different samples to equation [3.4], assuming a local-moment picture. The errors are determined from the fitting of different samples with the same compositions.*

x, Na	χ_0 (emu.mol^{-1}.Oe^{-1})	C (emu.K.mol^{-1}.Oe^{-1})	Θ_{CW} (K)	μ_{eff} (μ_B)	T_range (K)
$Na_{0.70}CoO_2$	$1.5(2)\times10^{-4}$	0.12(1)	-91(2)	1.0(5)	50-300
$Na_{0.37}CoO_2$	$4.0(2)\times10^{-4}$	0.02(1)	30(2)	0.35(5)	50-300
$Ca_3Co_4O_9$	$7.8(1)\times10^{-4}$	0.22(2)	-26(3)	1.3(1)	100-300

The fitting gives a μ_{eff} that decreases with x in spite of the increase of Co^{IV}. Also, the Co^{3+}/Co^{IV} ratio estimated from μ_{eff} is not in agreement with our previous results from the iodimetric titrations and seebeck coefficient: for x=0.70 and x=0.37 compositions, the $\%Co^{4+}$ calculated from the iodimetric titrations is equal to ~20% and ~45%, respectively, whereas if we assume a LS configuration for the Co^{4+} ions (as it is mainly accepted in the literature[117, 118, 119] μ_{eff}=1.73 μ_B), the $\%Co^{4+}$ deduced from the fittings would be equal to ~57% and ~27%, respectively, in a strong disagreement with the iodimetric analysis.

In order to show the generic magnetic behaviour of 2D cobaltites in Figure 2.12 we compare the magnetic properties of Na_xCoO_2 and $Ca_3Co_4O_9$. Layered Co(III)/Co(IV) oxides have in common a set of CoO_2 planes of edge-sharing CoO_6 octahedrons that result in a triangular Co-lattice. Given that the magnetic and transport properties are mostly determined by CoO_2 planes, is not surprising that all these systems show a quite similar phenomenology, particularly the puzzling CW-like $\chi(T)$ and a large thermoelectric power combined with a metallic resistivity.

[117] T. Mizokawa, L. H. Tjeng, P. G. Steeneken, N. B. Brookes, I. Tsukada, T. Yamamoto, and K. Uchinokura. *Phys. Rev. B* **64**, 115104 (**2001**).
[118] T. Mizokawa, L. H. Tjeng, H.-J. Lin, C. T. Chen, R. Kitawaki, I. Terasaki, S. Lambert and C. Michel. *Phys. Rev. B* **71**, 193107 (**2005**).
[119] T. Kroll, M. Knupfer, J. Geck, C. Hess, T. Schwieger, G. Krabbes, C. Sekar, D. R. Batchelor, H. Berger and B. Buchner. *Phys. Rev. B* **74**, 115123 (**2006**).

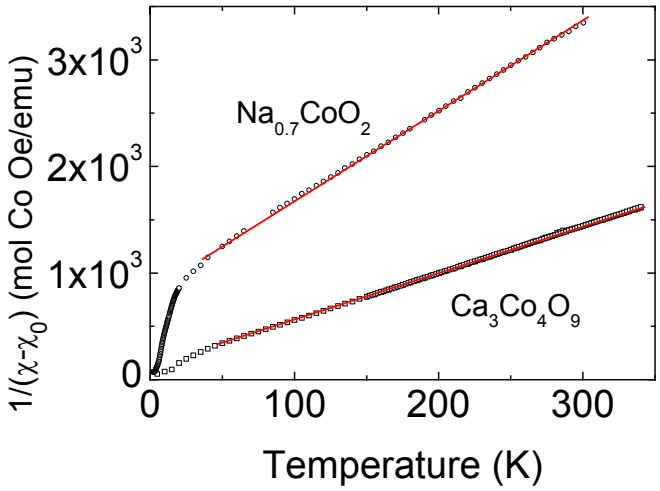

Figure 2.12: *Temperature dependent part of the inverse susceptibility $(\chi-\chi_0)^{-1}$ in $Ca_3Co_4O_9$ and $Na_{0.7}CoO_2$, along with the fitting to eq. [3.4].*

The results of the fittings for $Ca_3Co_4O_9$ are also summarized in Table 2.1. The values are similar to those obtained by other authors[120,121] and this behavior is generic to metallic 2D-cobaltatites with triangular Co lattices in a wide range of dopings.

On the basis of these results, we think that Na_xCoO_2 and in general the itinerant cobaltites with a triangular lattice must be classified as weak itinerant ferromagnet (WIFM),[122,123] according to Moriya's spin fluctuation theory (SFT).[124] In these systems, the thermodynamic and transport properties are governed by the temperature dependence of the amplitude of the local spin density, $\langle SL^2 \rangle$. Basically, the inverse magnetic susceptibility, $\chi^{-1}(T)$, in weak itinerant magnets and nearly ferromagnetic metals is proportional to the mean square of the local amplitude of spin fluctuations, $\langle SL^2 \rangle$. In the paramagnetic regime $\langle SL^2 \rangle \propto T$, resulting in a Curie-Weiss like $\chi(T)$, with a slope determined by the stiffness against a change in the

[120] C. Michel, A A. C. Masset. Maignan, M. Hervieu, O. Toulemonde, F. Studer, B. Raveau, and J. Hejtmanek. *Phys. Rev. B* **62**, 166 (**2000**).
[121] T. Yamamoto, K. Uchinokura and I. Tsukuda. *Phys. Rev. B* **65**, 184434 (**2002**).
[122] K. Adachi, K. Sato, M. Takeda, J. Phys. Soc. Japan **26**, 631 (1969).
[123] K. Sato, K. Adachi, T. Okamoto, E. Tatsumoto, J. Phys. Soc. Japan **26**, 639 (**1969**).
[124] T. Moriya. *Spin Fluctuations in Itinerant Electron Magnetism*. Springer, Berlín, **1985**).

amplitude of the spin fluctuations. This thoery provides a mechanism for the CW dependence of the susceptibility in itinerant electron systems, through the temperature dependece of $<SL^2>$.

On the other hand, a clear irreversivility between ZFC-FC curves shows up below T_{irr}~40 K in the samples closer to *x*=0.5 (*x*=0.52, *x*=0.50, *x*=0.48) pointing to some kind of FM-like ordering, related to the transition observed in the electrical resistivity. Two magnetic transitions are clearly observed in these samples at ≈18 K and ≈40 K respectively (see details in Figure 2.13). The first one is completely absent in the magnetic curves corresponding to *x*>0.52 and *x*<0.48 samples. However, the second one remains in some of the samples lower Na^+ doped (*x*=0.32 and *x*=0.31), although the temperature at which it appears is slightly displaced to higher values, T~44 K, and the splitting of the ZFC-FC is much smaller. These new magnetic phases emerge at a very narrow Na^+ content range around *x*≈0.5 and their appearance is most probably related to the charge ordering reported at half-doping.

In Figure 2.14 it is shown an additional magnetic transition at T~90K has been observed in samples with *x*≈0.5 (*x*=0.52, *x*=0.50 and *x*=0.48). This transition has been attributed to an AFM transition[125].

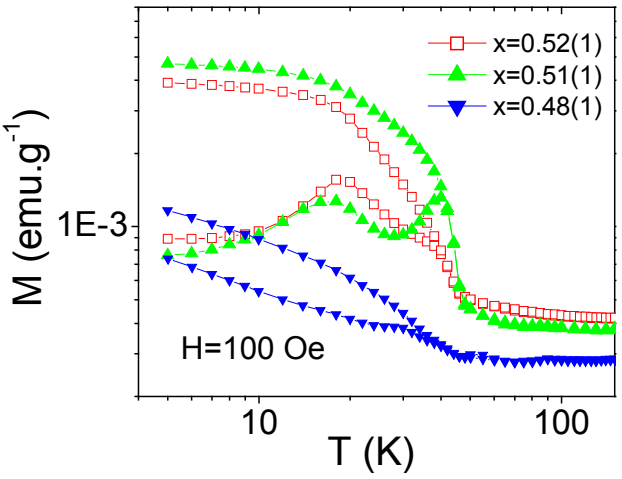

Figure 2.13: *Log-log plot of the magnetic behaviour for x=0.52, x=0.51 and x= 0.48 samples.*

[125] D. N. Argyriou, O. Prokhnenko, K. Kiefer and C. J. Milne. *Phys. Rev. B* **76**, 134506 (**2007**).

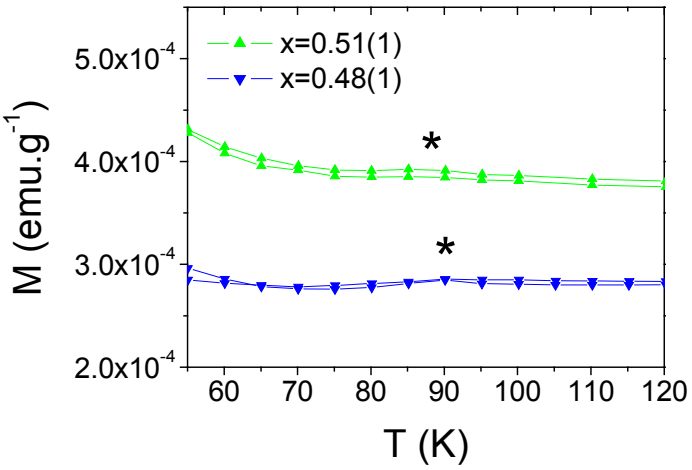

Figure 2.14: *Zoom in the magnetization curves of the samples x=0.51 and x=0.48 showing more clearly the magnetic transition at ~90 K (*), which is attributed to an AFM order.*

2.2. Na_xCoO_2 (x>0.7)

Figure 2.15 shows the ZFC-FC susceptibility curves as a function of the temperature for the $Na_{0.82}CoO_2$ sample. The magnetic behaviour is quite different to the parent compound with $x \approx 0.7$. Three transitions are observed at 45 K, 22 K and 11 K. The magnetic transition at ~45 K was previously observed in $Na_{0.75}CoO_2$[79] and $Na_{0.85}CoO_2$[74], although the magnetic behaviour is qualitatively different. However, the magnetic transition at 11 K has not been reported before (to the best of our knowledge). On other hand, the transition at 22 K, T_m, is that commonly assumed as the PM to AFM phase transition temperature for x>0.7.[126] The inset of Figure A2 shows the inverse of the susceptibility and the fitting of the high temperature magnetic data to a Curie-Weiss law. Opposite to what happens in the x<0.75 samples, the effective moment estimated from the values of the Curie constant is 1.6

[126] C. A. M. dos Santos, J. J. Neumeier, Y.-Kuo Yu, R. K. Bollinger, R. Jin, D. Mandrus and B. C. Sales. *Phys. Rev. B* **74**, 132402 (**2006**).

μ_B, which is much higher than expected if we take into account the amount of Co^{4+} present at that Na^+ composition.

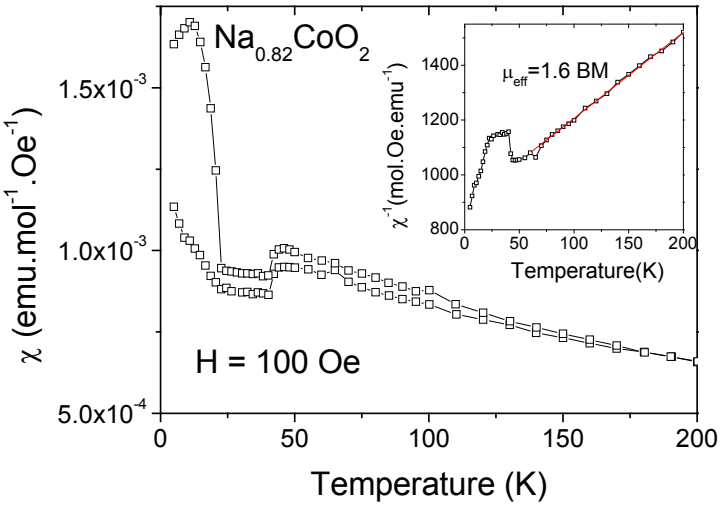

Figure 2.15: *ZFC-FC magnetization curves for $Na_{0.82}CoO_2$ obtained by solid state reaction at an applied magnetic field of 100Oe. Inset shows the inverse of the susceptibility, where the red line indicates the fitting of the data to a Curie-Weiss law.*

In order to determine the compresibility of $Na_{0.82}CoO_2$ along the *ab*- and *c*-directions and relate it to $T_m(P)$ data found in the literature, powder X-ray diffraction measurements under pressure were collected at room temperature at the Daresbury Synchrotron Radiation Source (SRS) (England). A commercial diamond anvil cell from EasyLab was used to reach the desired pressure. The diamonds were of 400μm and the hole of the gasket was 125μm (Figure 2.16).

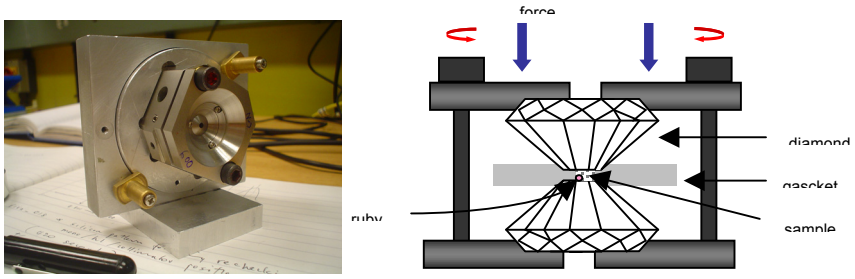

Figure 2.16: *Diamond anvil cell used in the measurements of X-ray with pressure, and scheme of the cell assembly.*

A small ruby mixed with the sample was used to monitor the internal pressure through the pressure dependence of its fluorescence peak. The fluorescence lines exhibit a pronounced red-shift with applied pressure, as shown in Figure 2.17. A 4:1 ethanol-methanol mixture was used as the hydrostatic pressure-transmitting medium. Data for each pattern were collected for 10 minutes.

A standard of Silicon was refined to obtain the instrumental parameters that we need to refine our measurements by the Rietveld method.

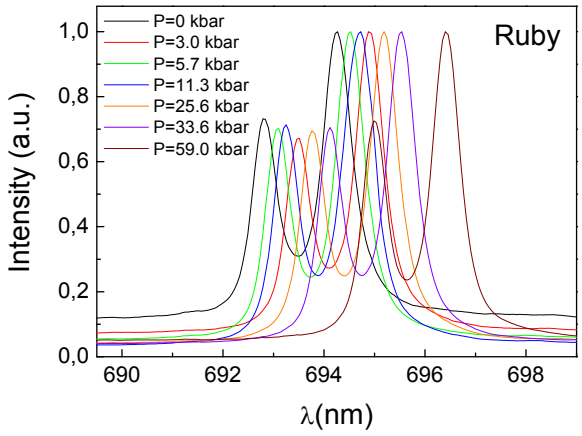

Figure 2.17: *Example of the red-shift of the fluorescence lines of ruby with pressure.*

In Figure 2.18 we show all the x-ray diffraction patterns obtained for polycrystalline $Na_{0.82}CoO_2$ as pressure is increased. The inset shows a detail of the evolution of the main peak of the XRD patterns with pressure.

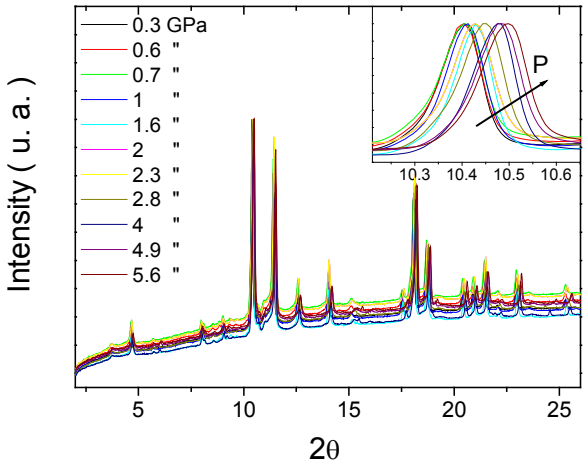

Figure 2.18: *Evolution of the XRD with pressure at room temperature for $Na_{0.82}CoO_2$. The inset shows the evolution of the main peak to higher angles as pressure increases. The wave length of the beam line used was λ=0.44397 Å.*

Through Lebail fittings with Rietica of all the diffraction patterns at different pressures, we have derived the evolution of the volume with the pressure, and fitted the volume-pressure data to the Birch-Murnaghan equation, to obtain the bulk modulus, K_0, of the material[127].

$$P = 3K_0 f_E (1+2f_E)^{5/2}\left(1+\frac{3}{2}(K'-4)f_E\right) \qquad \textbf{(Eq. A1)}$$

[127] R. J. Angel, in "High-Temperature and High-Pressure Crystal Chemistry", Reviews in Mineralogy and Geochemistry, Vol. **41**, Mineralogical Society of America, Virginia (**2000**).

where K_0 is the zero pressure bulk modulus, $K'=\partial K_0/\partial P$, and $f_E = \frac{1}{2}\left[\left(\frac{V_0}{V}\right)^{2/3} - 1\right]$ is the Eulerian strain.

Figure 2.19 shows the results obtained considering the first order of the Birch-Murnagan equation, *k'=4*. The fitting of the $P(V_0/V)$ data to the Birch Murnagham equation, let us to estimate an experimental value of K_0 of the order of 120(3) kbar.

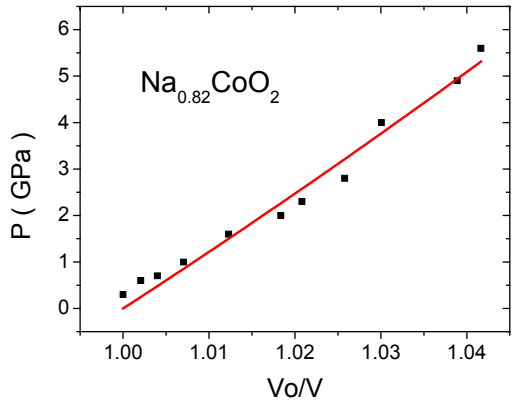

Figure 2.19: *Fitting of the experimental $P(V_0/V)$ data to the Birch-Murnaghan equation, truncated at second order, k'=4.*

In order to analyze the effect of the pressure separately on the *c* and *ab*-directions, we plotted in the Figure 2.20 the evolution of the *c* and *a*-lattice parameters with increasing pressure and fitted the data to the same Birch-Murnaghan equation described above.

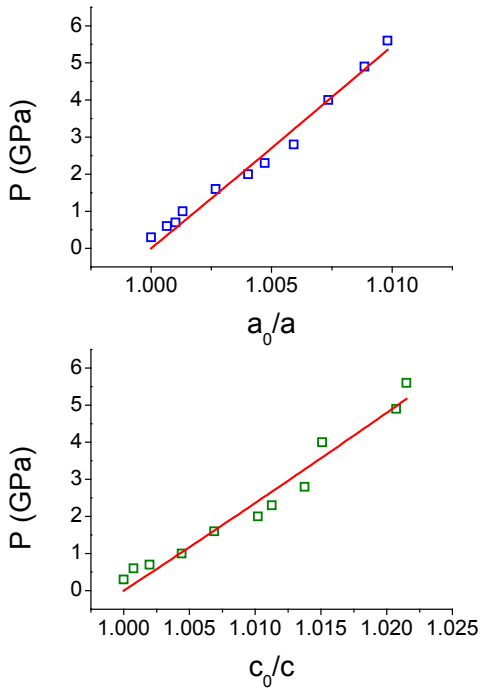

Figure 2.21: *Fitting of the P(a_0/a) (upper) and P(c_0/c) (lower) data to the Birch-Murnaghan equation, truncated at second order, k'=4.*

The *pseudo* Bulk modulus estimated were 537(14) GPa in the *ab*-plane and 232(9) GPa in the *c*-axis. This indicates that the system is more compresible in the *c*-direction, as it is expected from the layered structure.

The compressibility of the unit cell along the *c*-direction with pressure is strongly related to the pressure dependence of the AFM ordering temperature observed by *Wooldridge et al* [128] in x>0.7 single-crystals, increasing from 21.5 K to 25.5 K at 10 Gpa. This pressure dependence of T_m is similar to dT_m/dP = 4.4(3) K/GPa estimated in x=0.8.[126]

These results indicate the existence of a direct effect of the interlayer distance on the AFM exchange interaction, which is stabilized as the CoO_2-

[128] J. Wooldridge, D. M^{c}K. Paul, G. Balakrishnan and M. R. Lees. *Condens. Matter. J. Phys.: Condens. Matter* **18**, 4731 (**2006**).

CoO_2 separation is reduced. Therefore, they suggest that not only the CoO_2 planes dominate the physical properties of the system at x>0.7, the 3D dimensionality plays an active role that should be considered. We will take this into acount and will be discussed in next chapters.

To sumarize, we reported a detailed analysis of the magnetic susceptibility, χ, and thermoelectric power, *S*, of metallic Na_xCoO_2 and $Ca_3Co_4O_9$, as representative examples of layered cobalt oxides with a triangular Co lattice. We have shown that the magnetic and transport properties are mostly determined by CoO_2 planes in the range $0.3<x<0.7$. This fact explains the similar phenomenology found in different 2D cobalt oxides based on hexagonal Co arrangments, particulary the puzzling temperature dependent $\chi(T)$ and large thermoelectric power combined with a metallic resistivity.

We have demonstrated that the temperature dependence of the magnetic susceptibility in triangular lattice Co-oxides cannot be justified assuming a spin localized model. We suggest that the origin of the temperature dependence of the magnetization is due to the temperature dependence of the spin fluctuations of itinerant electrons.

We have also shown that the unusually large thermopower is related to a band-structure effect understandable within the framework of Boltzmann transport theory, withouth the need to consider an extra spin-entropy contribution. In the high temperature limit the Heikes formula predicts correctly the sign and magnitude of the temperature independent thermopower in these systems, when a correct estimation of the charge carrier density is available.

In the special case around $x\approx0.5$, our data evidence the differentiate nature of the electronic properties.

Finally, we have shown that the AFM exchange interaction is strongly influenced by the 3D character of the strucuture for x>0.7, that plays a more than expected active role.

3. Proximity to a quantum phase transition

In this chapter we carry out an exhaustive study of the magnetic properties of metallic Na_xCoO_2, both above and below x=0.5. We will focus on the two representative compounds x≈0.69 and x≈0.36. These experiments provide a good evidence of the proximity of this material to a magnetic phase transition at very low temperature. Our data show that the actual temperature of this transition is well below 1.8 K and probably at zero Kelvin (quantum phase transition, QPT). The possible role of magnetic fluctuations in the superconductivity is discussed to the light of the observed (H, T) scaling of the magnetization. The new electronic phases identified lead us to proposs a new (T, H) phase diagram for these two distinguishable metallic states.

It is commonly believed that the microscopic explanation for high temperature superconductivity can be constrained by determining the interplay between band-filling, magnetic interactions and dimensionality. In this sense, the report[129] of superconductivity in $Na_xCoO_2 \cdot yH_2O$ generated an intense debate about the nature of the pairing interaction in this material, which is becoming a test ground for the theories of superconductivity. Although the layered structure, the mixed valence character, and the proximity of the superconductive compositions to a localized charge-ordered phase[130] makes it very tempting to make a straightforward comparison with the cuprates, the metallic precursor of the superconducting phase shows its own peculiarities: an electronically active triangular cobalt lattice is supposed to be responsible for the strong temperature dependence of the metallic susceptibility (so called "Curie-Weiss metal" behaviour at high x)[131], the anomalous temperature dependence of the resistivity[132], or the surprisingly large thermopower[133]. Moreover, local density approximation (LDA) calculations[134,135] predicted a ferromagnetic (FM) ground state in the metallic precursor, although the material never orders down to the lowest temperature probed. The discrepancy between theory and experiment was tentatively attributed to the proximity to a quantum phase transition (QPT)[135], which would imply the existence of strong FM fluctuations in the metal. This opens the possibility of a magnetically mediated superconducting state due to exchange of FM spin fluctuations, like it was proposed for Sr_2RuO_4 [136] and high-pressure UGe_2[137]. Actually, ^{59}Co NMR and ^{23}Na NQR experiments[138]

[129] K. Takada, H. Sakurai, W. T. Muromachi, F. Izumi, R. A. Dilanian and T. Sasaki. *Nature* **422**, 53 (**2003**).
[130] R. E. Schaak, T. Klimczuk, M. L. Foo and *R. J. Cava*. *Nature*. **424**, 527 (**2003**)
[131] M. L. Foo, Y. Wang, S. Watauchi, H. W. Zandbergen, T. He, R. J. Cava and N. P. Ong. *Phys. Rev. Lett.* **92**, 247001 (**2004**).
[132] F. Rivadulla, J.-S. Zhou and J. B. Goodenough. *Phys. Rev. B* **68**, 75108 (**2003**).
[133] Y. Wang, N. S. Rogado, R. J. Cava and N. P. Ong. *Nature* **423**, 425 (**2003**)
[134] D. J. Singh. *Phys. Rev. B* **61**, 13397 (**2000**).
[135] D. J. Singh. *Phys. Rev. B* **68**, 20503 (**2003**).
[136] I. I. Mazin and D. J. Singh. *Phys. Rev. Lett*. **79**, 733 (**1997**).
[137] S. S. Saxena, P. Agarwal, K. Ahilan, F. M. Grosche, R. K. W. Haselwimmer, M. J. Steiner, E. Pugh, I. R. Walker, S. R. Julian, P. Monthoux, G. G. Lonzarich, A. Huxley, I. Sheikin, D. Braithwaite and J. Flouquet. *Nature* **406**, 587 (**2000**).
[138] K. Ishida, Y. Ihara, Y. Maeno, C. Michioka, M. Kato, K. Yoshimura, K. Takada, T. Sasaki, H. Sakurai and E. Takayama-Muromachi, *J. Phys. Soc. Japan* **72**, 3041 (**2003**); Y. Ihara, K. Ishida, C. Michioka, M. Kato, K. Yoshimura, H. Sakurai and E. Takayama-Muromachi. *J. Phys. Soc. Japan* **73**, 2963 (**2004**).

revealed an unconventional form of a superconducting spin-triplet phase in $Na_xCoO_2 \cdot yH_2O$, as well as the existence of strong FM spin fluctuations in the metallic counterpart, confirmed by inelastic neutron scattering[139,140]. However, a solid evidence for any particular pairing state remains lacking in $Na_xCoO_2 \cdot yH_2O$, although most of the proposals found in the literature have been excluded after testing them against the well established properties of the compound.[141]

Having in mind that understanding superconductivity requires a deep knowledge of the electronic precursor from which it forms, we have performed a detailed magnetic study of the water-free metallic precursors at representative compositions of the Na_xCoO_2 series. For high Na^+ content ($x \approx 0.69$, when superconductivity is never achieved under hydration) we have found that the temperature independent magnetic susceptibility, (T,H), in the Fermi liquid (FL) state is renormalized at low temperature. This behavior is consistent with previous resistivity[142] and specific heat[143,144] results, which support the existence of a strongly correlated state at high Na^+ content, with m^* strongly field dependent. On the other hand, at $x \approx 0.36$, near the optimum value for superconductivity, strong magnetic fluctuations introduce a new phase with non-FL behavior and spin-glass relaxation. A detailed scaling analysis of the low temperature χ(T, H) suggests that these effects are due to the proximity of metallic Na_xCoO_2 to a magnetic QPT.

Samples with compositions Na_xCoO_2, $x \approx 0.69$ and $x \approx 0.36$ were synthesized as described in Chapter 1. All the results discussed here correspond to single-phase materials, where long-time X-ray scans revealed the complete absence of any secondary phase; we paid special attention to avoid any trace of Co_3O_4. The peaks are very narrow, which ensures a good crystallinity, and the lattice parameters are in accordance with the literature[145].

---

[139] A. T. Boothroyd, R. Coldea, D. A. Tennant, D. Prabhakaran, L. M. Helme and C. D. Frost. *Phys. Rev. Lett.* **92**, 197201 **(2004)**.

[140] L. M. Helme, A. T. Boothroyd, R. Coldea, D. Prabhakaran, D. A. Tennant, A. Hiess and J. Kulda. *Phys. Rev. Lett.* **94**, 157206 (**2005**).

[141] I. I. Mazin and M. D. Johannes. *Nature Physics* **1**, 91 (**2005**).

[142] S. Y. Li, L. Taillefer, D. G. Hawthorn, M. A. Tanatar, J. Paglione, M. Sutherland, R. W. Hill, C. H. Wang and X. H. Chen. *Phys. Rev. Lett.* **93**, 56401 (**2004**).

[143] M. Brühwiler, B. Batlogg, S. M. Kazakov and J. Karpinski. Cond-mat/0309311.

[144] F. C. Chou, J. H. Cho, P. A. Lee, E. T. Abel, K. Matan and Y. S. Lee. *Phys. Rev. Lett.* **92**, 157004 (**2004**).

[145] C. Fouassier, G. Matejka, J. M. Reau and P. Hagenmuller. *J. Solid State Chem*. **6**, 532 (**1973**).

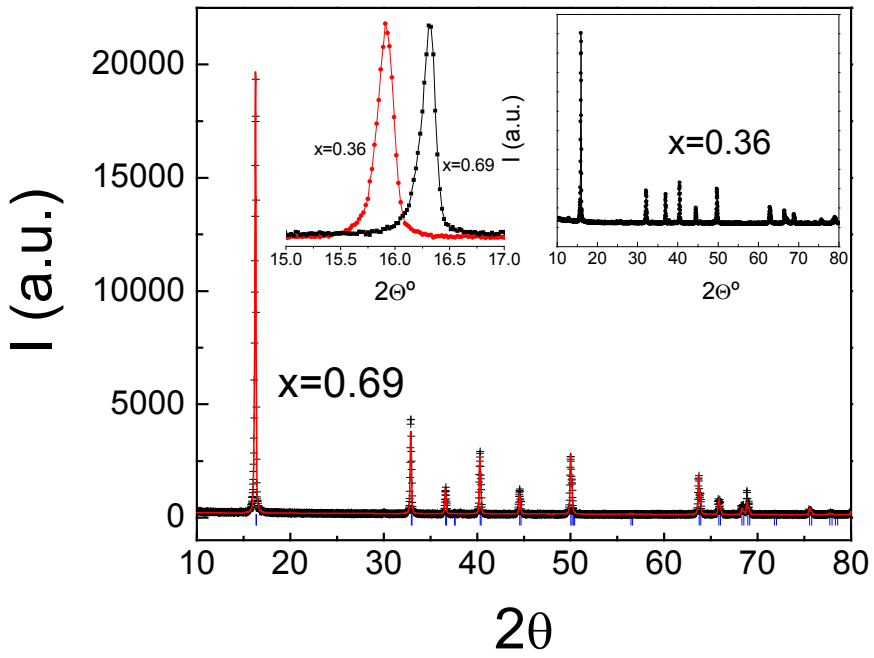

Figure 1: *X-ray diffraction patterns of two samples with x=0.36 and x=0.69. Main panel: Experimental dots are marked by crosses and the red line is a lebail fitting with the program Rietica, using the space group P63/mmc. In both Na^+-compositions, all the peaks belong to this phase. The vertical blue lines mark the positions of the reflections expected on the basis of a P63/mmc space group. The left inset shows the evolution of the (002) reflection after Na^+-deintercalation, which indicates the expected increase in the interlayer distance.*

It is important to remark that the following results presented here for $x \approx 0.36$ correspond to samples that we have verified to become superconductive after water insertion. Superconducting samples were obtained by stirring Na_xCoO_2, $x \approx 0.36$, in water for two days at room temperature. Only those that showed the non-FL phase at low temperature that will be discussed in the following pages became superconductive after water immersion. Here is an example in Figure 2.

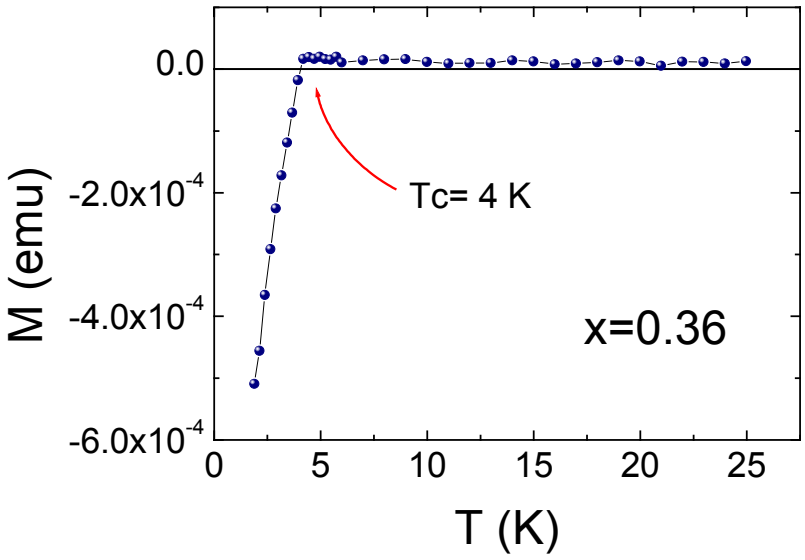

Figure 2: *We have checked every sample of x≈0.36 used in this chapter for superconductivity immersing them in water after the proper characterization of the dry sample.*

It is well know that the magnetic susceptibility of metallic polycrystalline Na_xCoO_2 depends on temperature, essentially at very low temperatures. Although we observed a similar behaviour of the magnetic susceptibility in single crystals and in polycrystalline samples (Figure 3), we decided to use polycrystalline samples for this work due to the better bulk homogeneity after the Na^+ deintercalation process, and the possibility of getting larger magnetic signals that decrease the error of the measurements.

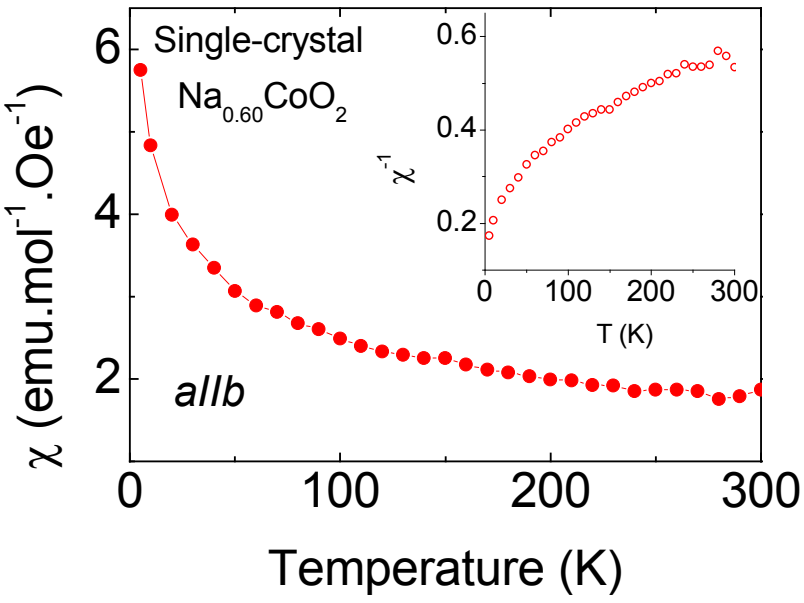

Figure 3: *Temperature dependence for a $Na_{0.6}CoO_2$ single crystal with the applied magnetic field (H=100 Oe) parallel to the ab plane.*

At low temperature, typically below 10 K, both samples (x=0.69 and x=0.36) show a continuous negative departure from the linear *M(H)* behavior expected in a conventional paramagnet (PM) (Figure 4), although no magnetic order was detected in the susceptibility, resistivity, etc. This deviation is even clearer for the metallic precursors of the superconducting phases ($x \approx 0.36$). No metamagnetic transition was induced up to 9 T for any composition.

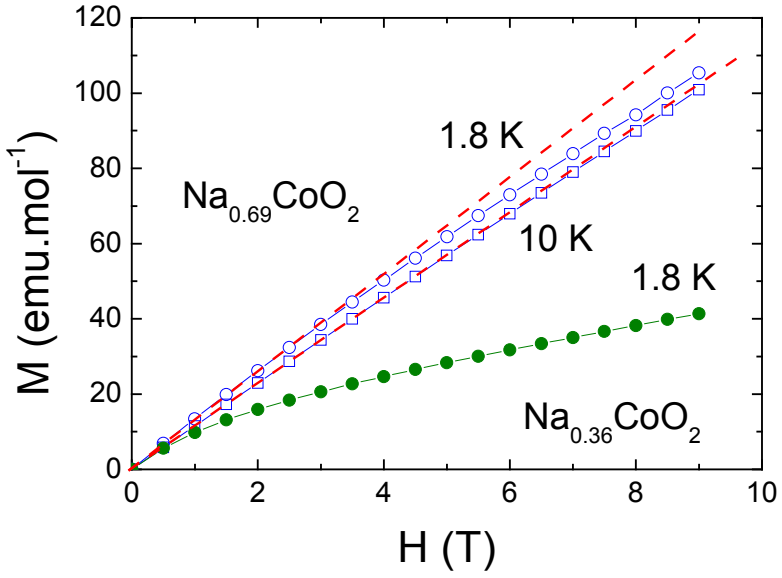

Figure 4: *Magnetization vs. applied magnetic field at two different temperatures in polycrystalline Na_xCoO_2, (x=0.69, open symbols, and x=0.36, closed symbols) up to 9 T and down to 1.8 K. The dashed straight lines were generated from the initial susceptibility.*

The first possibility to explain this behaviour is the presence of a paramagnetic impurity. In a conventional paramagnet or in a metallic system with paramagnetic (non interacting) impurities, the magnetization will show a curvature at low temperatures when the thermal and magnetic energy are comparable. In this case, the magnetization will follow the Brillouin function, which for $(\mu H/kT)\rightarrow\infty$ predicts a collapse of the *M(H)* isotherms in a *H/T* scale. This possibility is examined in Figure 5. However, the strong deviations of the experimental *M(H)* isotherms from the *M* vs. *H/T* scaling expected for the curvature of the Brillouin function at low temperatures and high fields demonstrates that the curvature of *M(H)* at low temperature is not due to the conventional behaviour of localized paramagnetic impurities.

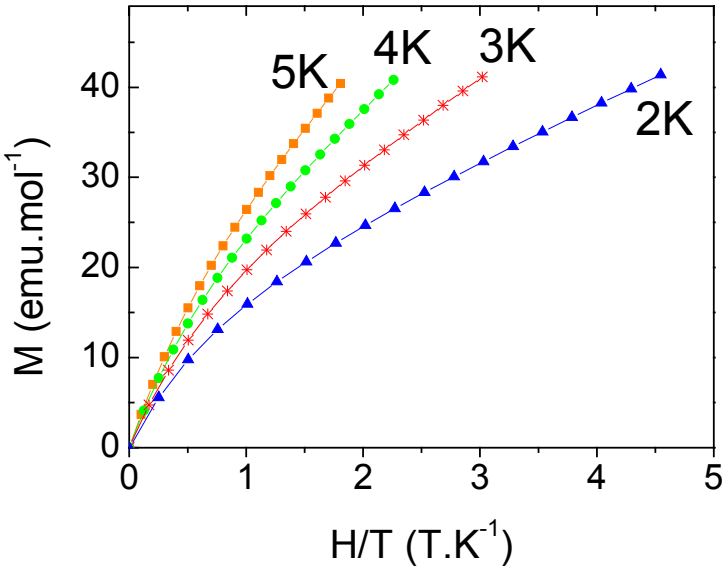

Figure 5: *Checking of the scaling of the magnetization in x=0.36 predicted by the Brillouin function for a simple paramagnet. A similar result was obtained for the sample with x=0.69.*

Also, the temperature dependence of the magnetic susceptibility does not follow an usual temperature dependence: in a paramagnet or an ordered system with a $T_C \rightarrow 0$ K, the magnetic susceptibility is expected to diverge with an exponent equal to 1 (to obey a simple Curie or Curie-Weiss law with $\theta_{CW} \rightarrow 0$ K. This will not change by the contribution of a temperature independent term. However, this is not the behaviour observed, as will be discussed below, and so the origin of the divergent magnetic susceptibility in Na_xCoO_2 must be connected to some other effect, which is intrinsic to this material.

The temperature and field dependence of the magnetic susceptibility is shown in Figure 6 for x=0.69. The low-field $\chi(T)$ shows a large enhancement over the free electron value below ≈10 K. A closer inspection (inset of Figure 6) reveals that $\chi(T)$ flattens and becomes constant below ≈4 K. The almost constant $\chi(T)$ at high temperature in this metal can be reasonably ascribed to the splitting of the spin up/down states by a magnetic

field, *i. e.* the Pauli paramagnetism.[146] This term is proportional to the density of states at the Fermi energy, $N(E_F)$, and hence on the effective mass, m^*. Then, the step increase in the temperature independent χ as $T \rightarrow 0$ must be sensing a renormalization of the effective mass m^* of the charge carriers at the Fermi surface. The situation shows some parallelisms with the heavy-fermions[147], weak itinerant ferromagnets[148,149] or nearly ferromagnetic paramagnets[150], in which the FL theory is still applicable although the interactions strongly renormalize the effective mass. In this case, the dependence observed on the magnetic field ($m^* \propto H^{-0.4}$) shows that the interactions are magnetic in origin; the spin polarization achieved with an applied magnetic field attenuates the amplitude of the magnetic fluctuations and restores progressively the normal FL behavior. The result agrees very well with the report by *Li et al*[142] of an anomalously large Kadowaky-Woods ratio, which is strongly field-dependent. However, these authors suggest that this is due to an enhancement of the quasiparticle scattering rate (a large value of the coefficient in the electrical resistivity, $\rho \approx AT^2$), more than to an increase of m^*.

[146] N.W. Ashcroft and N.D. Mermin. *Solid State Physics*. Holt, Rinehart and Winston, New York (**1976**).
[147] E. D. Bauer, V. S. Zapf, P.-C. Ho, N. P. Butch, E. J. Freeman, C. Sirvent and M. B. Maple. *Phys. Rev. Lett.* **94**, 46401 (**2005**).
[148] N. Doiron-Leyraud, I. R. Walker, L. Taillefer, M. J. Steiner, S. R. Julian and G. G. Lonzarich. *Nature* **425**, 595 (**2003**).
[149] M. Otero-Leal, F. Rivadulla, M. García-Hernández, A. Piñeiro, V. Pardo, D. Baldomir and J. Rivas. *Phys. Rev. B* **78** 180415 (**2008**).
[150] J. R. Stewart, B. D. Rainford, R. S. Eccleston and R. Cywinski. *Phys. Rev. Lett.* **89**, 186403 (**2002**).

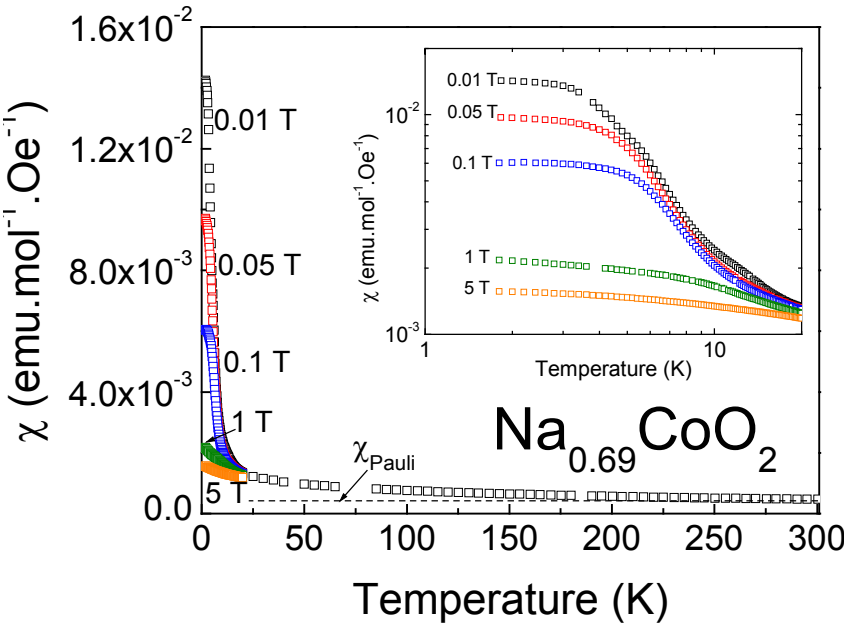

Figure 6: *Temperature and field dependence of the zero-field cooling (ZFC) magnetic susceptibility in x=0.69. The dotted line is the Pauli susceptibility determined from high temperature M(H) isotherms. Inset: Logarithmic plot of the low temperature susceptibility.*

We have also considered a possible role of anisotropy on the flatness of these curves, as a strong magnetic anisotropy was previously reported[151] on single crystals with a large Na^+ content below ≈20 K. However, a suppression of χ(T, H//*ab*) under field along with clear signs of saturation at low temperature, was also observed in single crystals[152], which indicates that the flatness and the field evolution of polycrystalline samples (Figure 6) is not due to a mixed contribution from the magnetization along *ab* and *c* directions.

[151] S. P. Bayrakci, C. Bernhard, D. P. Chen, B. Keimer, R. K. Kremer, P. Lemmens, C. T. Lini, C. Niedermayer and J. Strempfer. *Phys. Rev. B* **69**, 100410 (**2004**).
[152] D. Prabhakaran, A. T. Boothroyd, R. Coldea, L. M. Helme and D. A. Tennant. Cond-mat/0312493 (unpublished).

The most probable scenario is that the spin polarization achieved with an applied magnetic field attenuates the amplitude of the magnetic fluctuations and restores progressively the normal FL behavior. From the minimum in the derivative of $\chi(T)$ we can determine the existence of an inflexion point in the susceptibility curve. This would mark the flattening of the curve and hence would point to the recovery of constant FL behaviour. Figure 7 shows the derivative of the temperature-dependent susceptibility below 20 K at different applied magnetic fields. This result is consistent with the observation of an anomalously large AT^2 coefficient in the electrical resistivity[142] or a sublinear temperature variation of the specific heat[143,144], strongly field dependent.

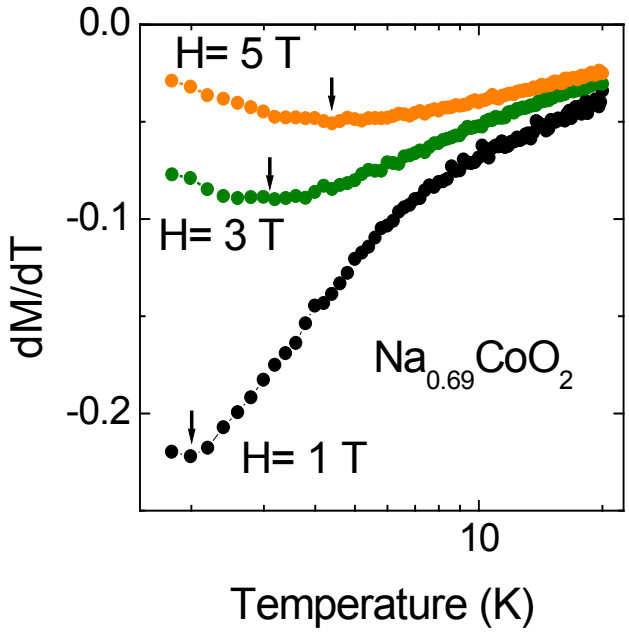

Figure 7: *Derivative of the χ vs. T curves at different applied magnetic fields (H=1, 3 and 5T) in the x=0.69 sample.*

In Figure 8, $\chi(T)$ is shown for x=0.36 at two different fields. The behaviour is completely different to the sample with high Na^+ content. A clear irreversibility between the zero-field and field cooling (ZFC-FC) magnetization curves shows up below $T_{irr}\approx12$ K, which is suppressed at

moderately large fields. Figure 9 shows the disappeareance of this irreversibility in the ZFC magnetization curve as H increases from 0.05 T to 0.1 T. The existence of the irreversibility, its field dependence, and the logarithmic variation of the relaxation rate below T_{irr} (Figure 10) would suggest the emergence of a new phase with spin-glass (SG) like dynamics at low temperatures, and for low values of *x*. This has been observed in other samples and is representative of compositions around *x*~0.3-0.4. In the SG phase, $\chi(T)$ remains strongly temperature-dependent down to the lowest temperature probed (1.8 K), not recovering the constant behavior. The degree of disorder or frustration in the system must be absolutely comparable between samples with different doping levels, so we think that the SG phase at *x*=0.36 is an effect of the underlying mechanism that introduces strong quasiparticle correlations. One possibility for the breakdown of the FL description in itinerant paramagnets is the proximity to a QPT. In some cases, the proximity to the QPT only renormalizes the scattering rate or the effective mass of the quasiparticles, but the description in terms of a FL model is still applicable, as it happens at *x*=0.69.

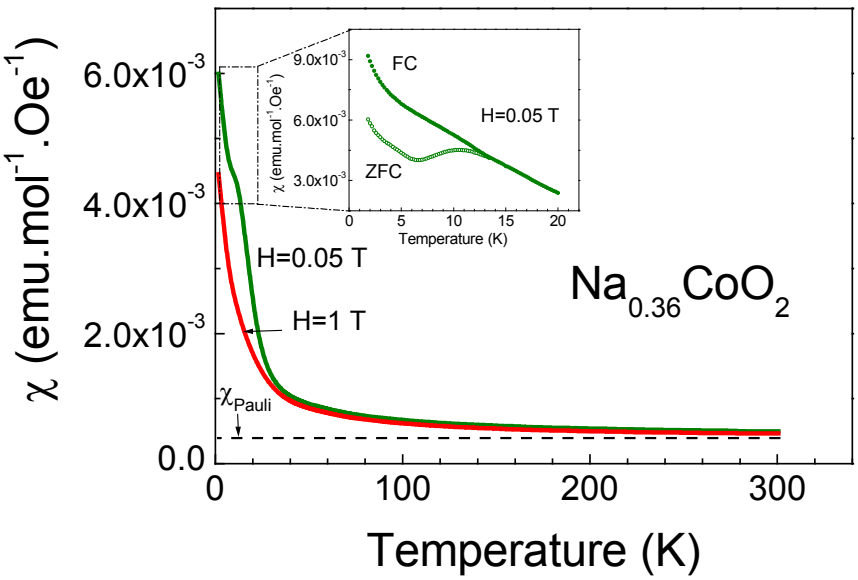

Figure 8: *ZFC magnetic susceptibility of x=0.36 at two different magnetic fields. The dotted line is the Pauli susceptibility calculated from high temperature M(H) isotherms. Upper inset: Detail of the ZFC-FC irreversibility visible at low fields below ≈12 K.*

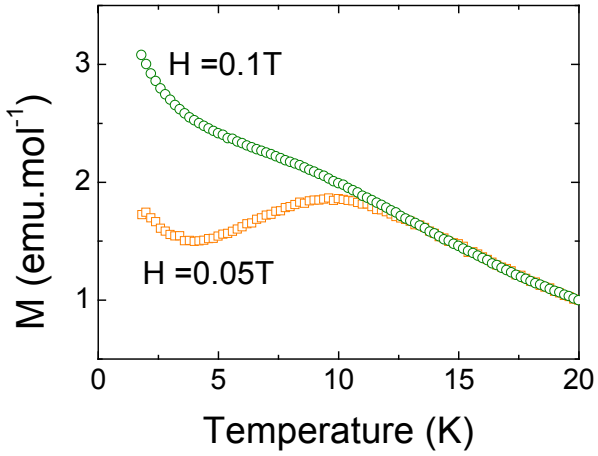

Figure 9: *ZFC magnetization curve of x=0.36 at low temperature at two different magnetic fields, H=0.05 and 0.1 T.*

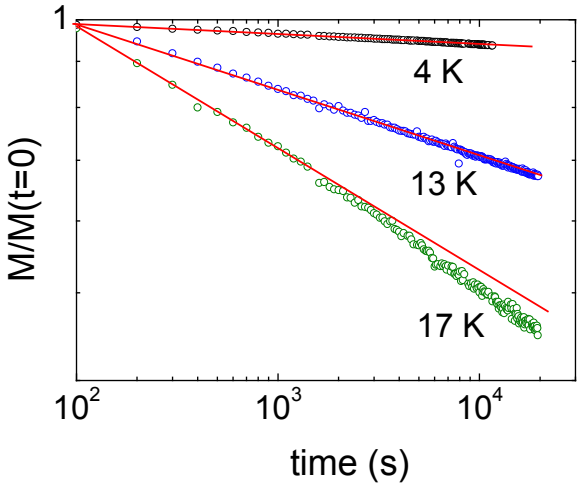

Figure 10: *Relaxation rate of the normalized magnetization for x=0.36. Above T_{irr}, the relaxation departs from the slow logarithmic behavior observed at low temperatures.*

The experimental signatures of the proximity to a second-order phase transition are the divergent character of the susceptibility, and over all, its scaling. In Figure 11 we show the divergence of $\chi(T)$ as T→0 K, and the progressive recovery of the constant behavior as H increases. Below ≈5 K, the low temperature susceptibility shows a power-law temperature dependence of the form

$$\chi = T^{-\eta} \qquad \text{eq. [1]}$$

with η strongly field dependent. The values of η go from ~0.30 at low fields to close to zero at high fields (Figure 12), which indicates the recovery of the FL state at low temperatures, due to the field suppression of spin fluctuations.

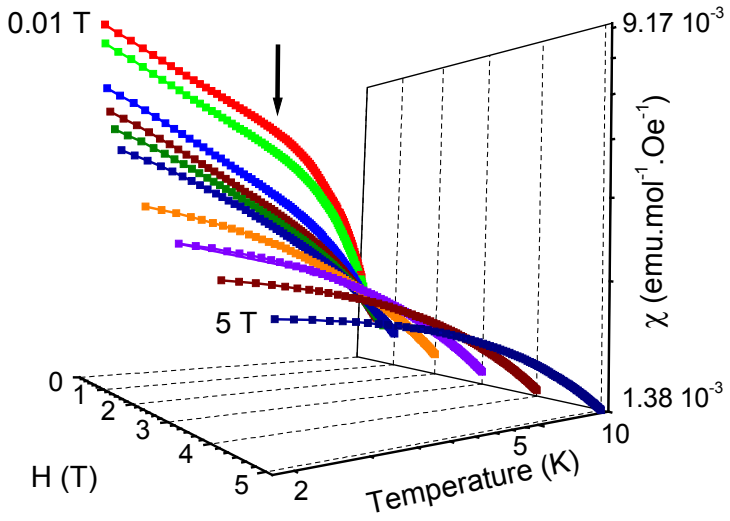

Figure 11: *The divergent character of the low field χ(T→0) fits to equation [1] below ≈5 K (marked by the arrow) for x=0.36. At high fields the susceptibility recovers FL behaviour, with a decreasing constant value of χ(T→0) as H increases.*

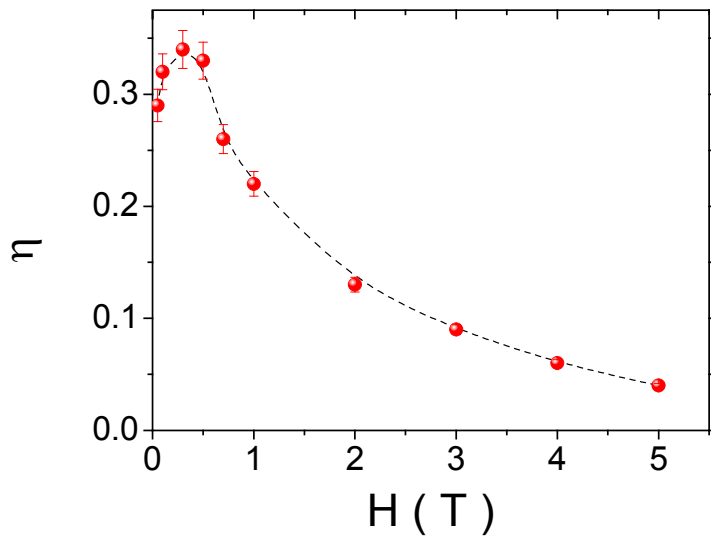

Figure 12: *Values of η obtained from fittings of the M(T) curves to equation [1] below ≈5 K at different applied magnetic fields from 0.01 T to 5 T. (Dashed line is a guide to the eye). The value of η goes asimtotically to zero at high field.*

Another indirect evidence of the proximity of $Na_{0.36}CoO_2$ to a magnetic phase transition comes from the behaviour of the χ_3; at the vicinity of a phase transition non-linear magnetization becomes relevant and the higher order terms of the magnetization must be retained in the equation of state. In the paramagnetic range M is an odd function of H, so

$$M = \chi_1 H + \chi_3 H^3 + \chi_5 H^5 + \ldots \qquad \text{eq. [2]}$$

where the third-order susceptibility, χ_3, is normally quoted as the nonlinear susceptibility. In a mean field approximation we can get some information

about the behavior of the linear and cubic terms of the susceptibility when the critical temperature is approached from above[153]

$$\chi_1 \propto \frac{1}{\left(\frac{T}{T_C}-1\right)}$$
$$\chi_3 \propto \frac{-1}{\left(\frac{T}{T_C}-1\right)^4} \qquad \text{eq. [3]}$$

Equation [3] gives a positive divergence for χ_1 and a negative divergence of χ_3 above the Curie point. A similar treatment gives a positive divergence of χ_3 as $T \rightarrow T_C$ from below. This provides an accurate method to determine the transition temperature of a ferromagnetic-paramagnetic transition. However, and in spite of the critical behavior of χ_3 is commonly used to characterize the spin-glass transition[154], it has been rarely applied for the characterization of conventional second order FM-PM phase transitions.[153]

We have fitted the *M(H)* curves of several compositions of Na_xCoO_2 in the interval $0.33 \leq x \leq 0.69$ every degree below 25 K down to 1.8 K to extract $\chi_3(T)$, and the results are plotted in Figure 13 for two representative compositions. There is a clear departure from the high temperature value ($\chi_3 \rightarrow 0$) and a negative divergence of χ_3 below ≈15 K. The nonlinear susceptibility shows the typical signatures of a system just above the transition temperature from a magnetically ordered state.

We should remind here that the possibility of a saturating paramagnetic impurity as the source of the non-linear susceptibility has been discarded before.

An important point is whether this magnetic transition occurs at zero kelvin or if it takes place at low but finite temperature. Although our experiments cannot reassure the absence of the transition below 1.8 K, χ_3 does not show any sign of rounding still at this temperature, which indicates that we are still far from the critical point.

[153] S. Nair and A. Banerjee. *Phys. Rev. B* **68,** 94408 (**2003**).
[154] Spin Glasses and Random Fields. Ed. by A. P. Young, World Scientific (**1998**).

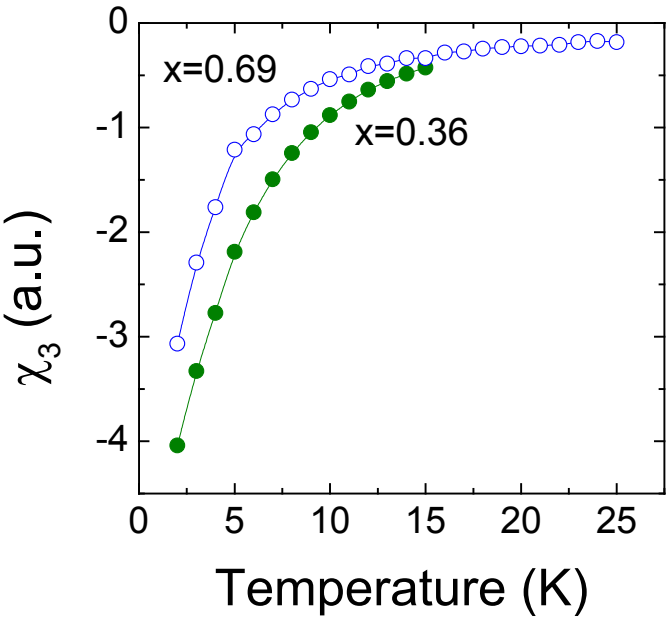

Figure 13: *Temperature dependence of the nonlinear susceptibility as T→0 K for x≈0.69 (open circles) and x≈0.36 (solid circles). Similar behaviour was observed in the whole range of x checked (between 0.3 and 0.69).*

In the conventional theory of metals close to a magnetic QCP, long-wavelength fluctuations (q→0) of the order parameter (paramagnons) are the relevant low-energy magnetic excitations. For 2D magnetic systems close to a QPT *Si et al*[155] predicted the presence of spatially localized magnetic fluctuations (q→∞) coexisting with the spatially extended ones (q→0). In this scenario close to a second order QPT, hyperscaling relationships ensure that the following scaling law must be obeyed by the singular part of the susceptibility, once the reduced temperature has been replaced by T to account for the 0 K transition temperature,[156,157]

[155] Q. Si, S. Rabello, K. Ingersente and J. L. Smith. *Nature* **413**, 804 (**2001**).
[156] N. Goldenfeld in "Lectures on phase transitions and the renormalization group", Frontiers in Physics Vol **85**, Addison-Wesley, NY **1992**.
[157] G. R. Stewart. *Rev. Mod. Phys.* **73**, 797 (**2001**).

$$\frac{M}{H}T^{\eta} = f\left(\frac{H}{T^{\beta}}\right) \qquad \text{eq. [4]}$$

The result of the scaling is shown in Figure 14. The best fittings were obtained with the values η=0.31(1) and β=1.12(3). The value of η is consistent with the fitting of the low-field susceptibility to equation [1], and both η and β are internally consistent ($1+\eta/2=\beta$) within the error. For a true FL, no such scaling behavior should be observable as its mere presence shows that there is an energy scale other than Fermi energy that dominates its thermodynamic properties.

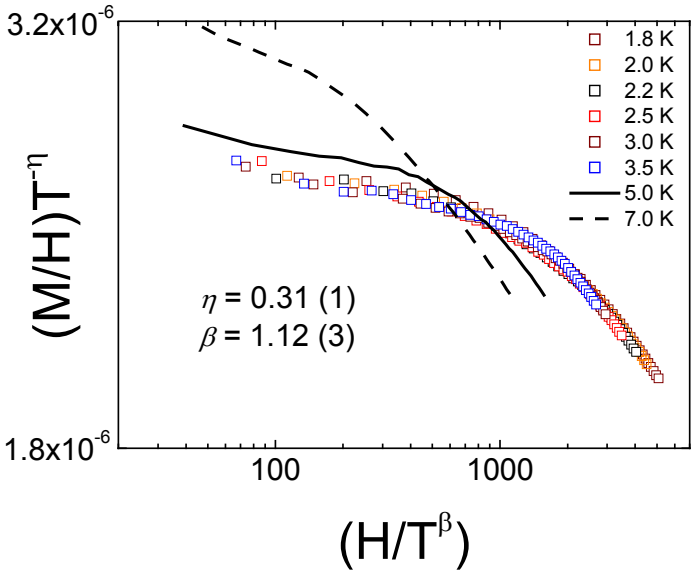

Figure 14: *Scaling of the divergent low temperature susceptibility for x=0.36. The data departs from the low temperature scaling above ≈4 K, i.e. as the limit of the divergent behavior in $\chi(T\rightarrow 0)$ is approached from below (see Fig. 11). The 5 K and 7 K curves are shown as an example of deviation of the scaling at higher temperatures.*

To discard completely the proximity to a magnetic phase transition at very low temperature but above zero, measurements at the milikelvin range are desirable.

As discussed before, *Li et al*.[142] related the anomalously high value of the Kadowaki-Woods ratio in $Na_{0.7}CoO_2$ (and its suppression by a magnetic field)to the proximity to a magnetic QPT. This scenario is now supported by the fitting of the data to equations [1] and [4] shown in Figures 11 and 14.

A fundamental issue that has to be explored is the origin of the SG phase and the nature of the magnetic fluctuations at low temperature, as well as its relationship with the appearance of superconductivity. Na_xCoO_2 is an itinerant paramagnet normally considered as a frustrated antiferromagnet due to the triangular arrangement of the Co atoms in the close-packed CoO_2 planes[158]. However, according to *Goodenough*,[159] a simple extension of the cation-cation superexchange spin correlations for localized electrons to the low-spin octahedral-site Co-t_{2g} itinerant electrons would predict the existence of an itinerant FM ground state for this material. Even partial splitting of the threefold-degenerate t_{2g} orbitals into an a_1^T and twofold-degenerate e^T orbitals by the trigonal field, will keep the same prediction. The O:2p-Co:e_g rehybridization process proposed by *Marianetti et al*,[160] would introduce the possibility of a Zener-like double exchange mechanism, also resulting in a ferromagnetic, metallic ground state like in $SrCoO_3$ or Sr_2CoO_4.[161,162] The contraction of the *a*-axis on Na^+ removal, as well as the almost constant cobalt valence,[163] ensures that rehybridization is indeed playing a role in the material. These arguments are in clear agreement with NMR[138] and neutron scattering[140] experiments which demonstrate the existence of strong FM fluctuations. Fluctuations can be the source of a short-range partial ordering of the conduction electrons, as it was observed in the high-pressure non-FL phase of MnSi.[164] The coexistence of partially ordered regions (super-spins), was proposed to be responsible of the non-FL and SG characteristics of

---

[158] N. P. Ong and R. J. Cava. *Science* **305**, 52, (**2004**).

[159] J. B. Goodenough, in Magnetism and the Chemical Bond, John Willey & Sons, New York (**1963**).

[160] C. A. Marianetti, G. Kotliar and G. Ceder. *Phys. Rev. Lett.* **92**, 196405 (**2004**).

[161] R. H. Potze, G. A. Sawatzky and M. Abbate. *Phys. Rev. B* **51**, 11501 (**1995**).

[162] J. Matsuno, Y. Okimoto, Z. Fang, X. Z. Yu, Y. Matsui, N. Nagaosa, M. Kawasaki and Y. Tokura. *Phys. Rev. Lett*. **93**, 167202 (**2004**).

[163] M. Bañobre-López, F. Rivadulla, R. Caudillo, M. A. López-Quintela, J. Rivas and J. B. Goodenough. *Chem. Mater,* **17**, 1965 (**2005**).

[164] C. Pfleiderer, D. Reznik, L. Pintschovius, H. v. Löhneysen, M. Garst and A. Rosch. *Nature* **427**, 227 (**2004**).

many heavy-fermions,[147] in which a divergence of the type $\chi(T) \propto C(T)/T \propto T^{1+\lambda}$ was predicted.[165] This electronically inhomogeneous state is characterized by an exponent $\lambda<1$, and is equivalent to the Griffiths phase of dilute magnetic systems.[166] Reanalysis of our data following this argument leads to $\lambda\approx0.7$ from the fitting of the divergent low-temperature susceptibility at low applied magnetic fields (Figure 15).

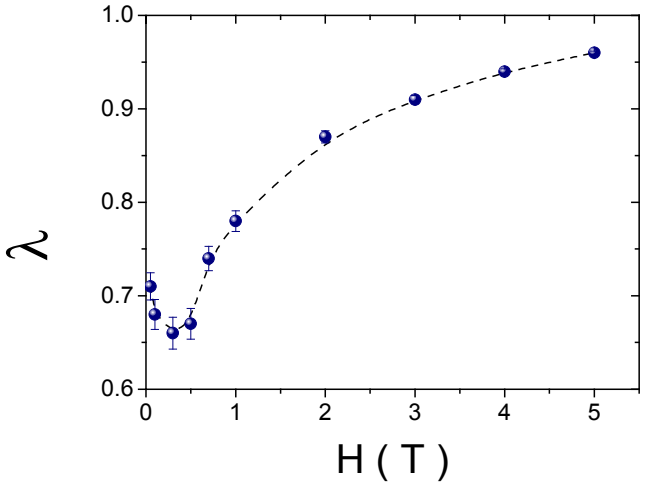

Figure 15: *Values of λ obtained from fittings of the $\chi(T)$curves to the relation $\chi(T) \propto C(T)/T \propto T^{1+\lambda}$ below ≈5 K at different applied magnetic fields from 0.01 T to 5 T. (Dashed line is a guide to the eye).*

The results for the electronic heat capacity, $\Delta C(T)/T$, are shown in Figure 16. To obtain the electronic part, a lattice contribution was fitted to $\beta_3T^3+\beta_5T^5$, and subtracted from the total specific heat. From our specific heat measurements, $\lambda\approx0.4(2)$. This value is very much influenced by the temperature range taken to fit the lattice contribution (β_3 and β_5 change considerably with the range fitted, between 0.15-0.30 $mJ.mol^{-1}.K^{-4}$ and 2×10^{-3}-7×10^{-4} $mJ.mol^{-1}.K^{-6}$, respectively). Very important is that the electronic component is suppressed by a magnetic field below ~5 K, which is approximately the same temperature below which the low field $\chi(T)$ diverges

[165] A. H. Castro Neto, G. Castilla and B. A. Jones. *Phys. Rev. Lett.* **81**, 3531 (**1998**).
[166] R. B. Griffiths. *Phys. Rev. Lett.* **23**, 17 (**1969**).

(see Fig. 11), and the field suppression indicates the presence of magnetic fluctuations at low temperatures. It should be mentioned that *Brüwhiler et al*[143] reported *C(T)/T* in field data for *x*=0.7-0.75. These authors observed a low-temperature divergence, $\lambda<1$, which is suppressed by the magnetic field. Although the field dependence is qualitatively similar to our data, the low-temperature divergence (not observed in our case) and the quantitative effect of the field are different. Differences in the stoichiometry of the samples or problems in the handling due to their extreme moisture sensitivity could be at the origin of this discrepancy. From Ref. 12 $\lambda\approx0.87$, which differs somewhat from the value derived from our susceptibility data.

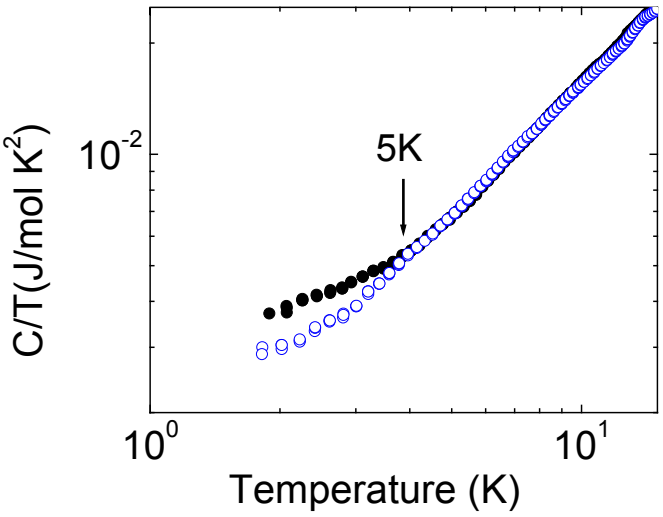

Figure 16: *Electronic specific heat at H=0 T (closed symbols) and at H=5 T (open symbols), after subtraction of the lattice contribution as explained in the text.*

Taken together, these results suggest the presence of a strongly correlated (n-FL) phase at low temperature, which is greatly affected by the field; a recurrent phenomenology to many heavy-fermions close to a QPT.[147] Based on the analysis of different samples, the (T,H) phase diagrams are presented in Figure 17 for the large-Na^+ metallic phase and the low-Na^+ metallic precursor of the superconducting phase. A departure from FL behavior appears in the metallic precursor of the superconducting phase. The characteristic temperature below which FL behavior is recovered

increases with H, which supports the hypothesis of the FM character of the fluctuations. The proximity of this material to a QPT makes many competing states become nearly degenerate at low temperatures (the large m^* introduces a high density of states at E_F) and the systems becomes very susceptible to the formation of new phases, among which superconductivity could be a possibility. This is consistent with the behaviour observed in many materials artificially tuned across or close to a QPT.[137,164]

In the case of Na_xCoO_2, dimensionality, doping, and magnetic field must be playing the role of a control parameter that places the system at a distance from the QCP.

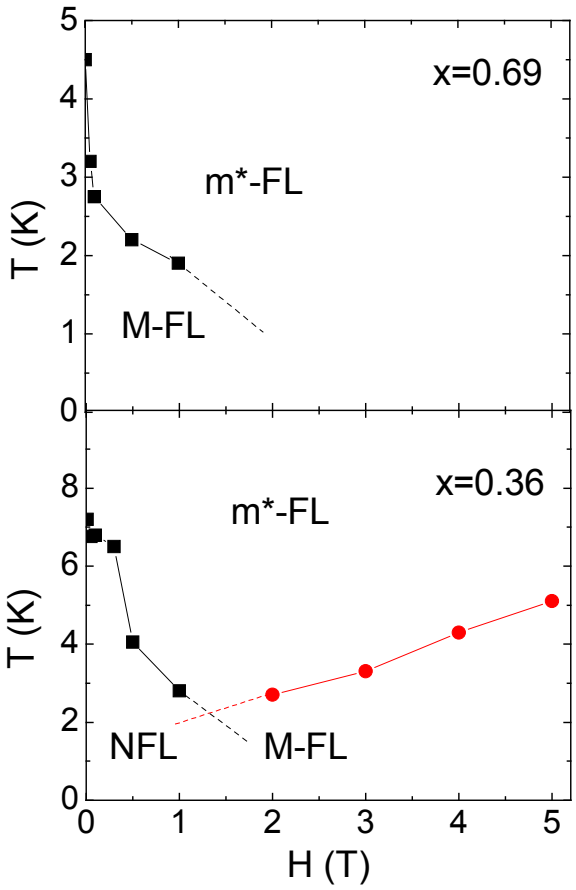

Figure 17: *Temperature vs. magnetic field phase diagram for Na_xCoO_2, for high (top) and low (bottom) Na^+ content.The non-Fermi Liquid (NFL), heavy Fermi Liquid (M-FL), and conventional Fermi Liquid (m*-FL) phases, are indicated.*

In summary, we have shown that metallic Na_xCoO_2 is a FL at high doping levels of Na^+, with the quasiparticle *m** becoming heavily renormalized and field dependent at low temperature. When the Na^+ content is around the optimum values for superconductivity, a new phase with spin-glass and non-FL characteristics develops at low temperature. Our experimental evidence suggests that this behavior is a consequence of the proximity to a second-order magnetic QPT, where the magnetic correlations dominate the phase diagram of the system. At this point, the fundamental assumption of the Fermi-liquid model, i. e. the short-range character of the quasiparticles correlations, is violated and many (or all) of the observable consequences of the model (linear specific heat, weakly-T dependent susceptibility, T^2 dependence of the resistivity at low temperature, etc.) are expected to fail. Another consequence of the $\lambda \rightarrow \infty$ spin fluctuations is the existence of an effective magnetic interaction that can be attractive for fermions with the same spin orientation, favoring the formation of the Cooper pairs in the triplet state, and under certain conditions can lead to a magnetically mediated superconductivity.[167]

Our results make superconducting $Na_{0.36}CoO_2 \cdot yH_2O$ a clear candidate for magnetically mediated pairing.

[167] G. G. Lonzarich. *"Electron"*. Ed. by M. Springford. Cambridge University Press. Cambridge (**1997**).

4. The role of water in the development of superconductivity

In this chapter, I will present some of our results that could help to shed light into the origin of the SC state in hydrated Na_xCoO_2. I will also start with a brief review about the, in my opinion, most interesting results about the issue of superconductivity in hydrated Na_xCoO_2. Particulary, we will discuss in detail about the role played by intercalated H_2O in the achievement of superconductivity.

Superconductivity is one of the most relevant topics in solid state physics. Since the discovery of the high-Tc cuprates in 1986[168], the search for other families of superconductors that might help to understand the origin of SC in layered cooper oxides has been an active area of research.

[168] J. C. Bednorz and K. A. Muller. *Z. Phys. B* **64**, 189 (**1986**).

The discovery of superconductivity below T=5 K in the double layer hydrated cobalt oxide $Na_{0.35}CoO_2 \cdot 1.3H_2O$ by *Takada et al* in 2003[169] has attracted a great interest in the scientific community, and boosted the revision of the physical properties of this system in the last years.

Four are the main characteristics which can be emphasized in the case of the cobalt oxide superconductor that make it very interesting for its study:

1. It is the first time that these physical properties are achieved in an oxide with lattice of Co atoms.

2. SC ocurrs in a lattice of Co atoms with triangular geometry, what means that strongly frustrated magnetic exchange interactions and their corresponding excitations can come into play.

3. The 2D character of its structure seems to play an important factor in the occurrence of superconductivity.

4. It is the first superconductor where the presence of water seems to be critical for superconductivity.

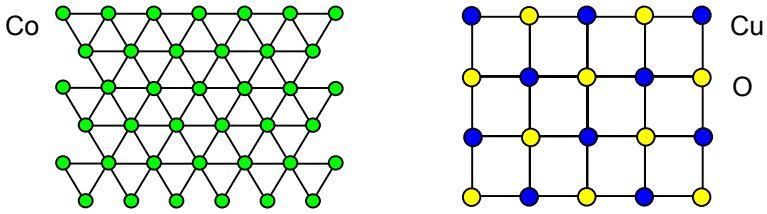

Figure 4.1: *Hexagonal arrangement of Co atoms in the ab-plane in Na_xCoO_2 (left) in opposite to the cuadratic planar geometry of the Cu and O atoms in the cuprate superconductors (right).*

It was thought initially that the effect of intercalated H_2O was solely to increase the distance between CoO_2 planes in the unit cell. However, it is now known that factors like ordering of Na^+ and H_2O play an active role in

[169] K. Takada, H. Sakurai, E. Takayama-Muromachi, F. Izumi, R. A. Dilanian and T. Sasaki. *Nature* **422**, 53 (**2003**).

the configuration of the electronic properties of this system[170]. Also, it is not clear whether H_2O, H_3O^+ or both are playing the decissive role for the appearance of superconductivity in hydrated Na_xCoO_2.

On other hand, strong magnetic fluctuations could be important in such geometry and play a role in the occurrence of superconductivity[171,172] Investigations to clarify if the superconducting state of Na^+ is conventional (BCS) or not, have been carried out from both theoretical and experimental sides. Although a definitive conclusion has not been reached yet, most authors opted for an unconventional mechanism of superconductivity, in which the magnetic fluctuations originated in the adjacent magnetic ordered phase (x~0.5) would be intense enough to drive the system SC.

However, from our point of view, other basic points have not been still elucidated, and could play a role in the ocurrence of superconductivity in Na_xCoO_2. Mainly, we can list the following open questions:

1. What is the role of intercalated water in the achievement of superconductivity in this system?

2. It is really important the charge ordered phase at x=0.5, very close in composition to the superconducting host?

3. Can Na_xCoO_2 still be considered as a 2D system after water intercalation? Does it behave like a 2D system from the electronic point of view?

Obviously, intercalated water into the galleries between CoO_6 sheets leads to a substantial increase of the interlayer distance, increasing the 2D character of the system (at least structurally), which is believed to play an important role in inducting superconductivity. The superconductive hydrated phase corresponds to that one with an amount of water of y=1.3 molecules per unit formula H_2O molecules coordinate to the Na^+ ions and form two water layers in the gallery sandwiching the Na^+ plane, transforming the parent oxide into a bilayer-hydrate (BLH). On the other hand, the most common partially hydrated phases contain around y=0.6 water molecules

---

[170] M. Roger, D. J. P. Morris, D. A. Tennant, M. J. Gutmann, J. P. Goff, J.-U. Hoffmann, R. Feyerherm, E. Dudzik, D. Prabhakaran, A. T. Boothroyd, N. Shannon, B. Lake and P. P. Deen. *Nature* **445**, 631 (**2007**).

[171] N. D. Mathur, F. M. Grosche, S. R. Julian, I. R. Walker, D. M. Freye, R. K. W. Haselwimmer and G. G. Lonzarich. *Nature* **394**, 39 (**1998**).

[172] P. Monthoux, D. Pines and G. G. Lonzarich. *Nature* **450**, 1177 (**2007**).

per unit formula, in which H_2O molecules occupy positions in the same layer of Na^+ ions, forming a monolayer-hydrate (MLH)[173].

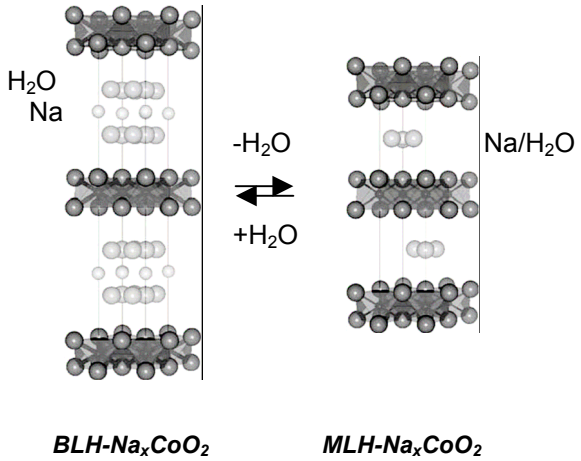

Figure 4.2: *Structural drawings of (left) BLH-Na_xCoO_2 and (right) MLH-Na_xCoO_2. (From Ref. 6).*

Also other partially hydrated and no superconductive phases with smaller water content, such as y=0.3 and y=0.1, have been reported[174,175,176,177]. Although direct water content is very difficult to be measured, it is translated in different interlayer distances[178,179,180,181]. It

[173] K. Takada, H. Sakurai, E. Takayama-Muromachi, F. Izumi, R. A. Dilanian and T. Sasaki. *J.Solid State Chem.* **177**, 372 (**2004**).
[174] D. P. Chen, H. C. Chen, A. Maljuk, A. Kulakov, H. Zhang, P. Lemmens and C. T. Lin. *Phys. Rev. B* **70**, 024506 (**2004**).
[175] M. L. Foo, R. E. Schaak, V. L. Miller, T. Klimczuk, N. S. Rogado, Y. Wang, G. C. Lau,C. Craley, H. W. Zandbergen, N. P. Org and R. J. Cava. *Solid State Commun*. **127**, 33 (**2003**).
[176] J. Cmaidalka, A. Baikalov, Y. Y. Xue, R. L. Meng and C. W. Chu. *Physica C* **403**, 125 (**2004**).
[177] C. T. Lin, D. P. Chen, P. Lemmens, X. N. Zhang, A. Maljuk and P. X. Zhang. *Journal of Crystal Growth* **275**, 606 (**2005**).
[178] K. Takada, H. Sakurai, E. Takayama-Muromachi, F. Izumi, R. A. Dilanian, and T. Sasaki, *Phys. C* **14**, 412 (**2004**).

suggests that the separation between CoO_2 layers appears to be critical in obtaining superconductivity, since it is only achieved for a hydrated phase with *c*~19.8 Å, while intermediate hydrated phases with *c*~12 Å and anhydrous phases with even smaller CoO_2-CoO_2 interlayer spacing are not superconducting[173,175]. The importance of a reduced interlayer coupling for stabilizing the superconducting ground state in this compound is evidenced by the hydrostatic pressure dependence of T_c, where a suppression of the superconducting state takes place at high pressure as a consequence of a significant reduction of the *c*- axis[182] (Figure 4.3). In fact, synchrotron measurements with pressure in $Na_{\sim 0.8}CoO_2$ evidenced that the compressibility in the *c*-direction is much higher than in the *a*-direction (see Chapter 2).

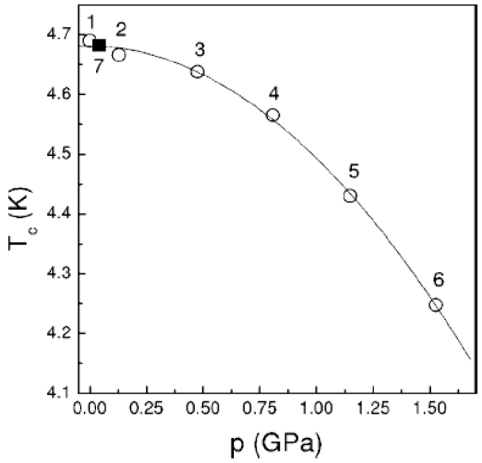

Figure 4.3: *Superconducting transition temperature (Tc) dependence of the applied hydrostatic pressure (p). T_c was estimated from the onset of the diamagnetic signal. Fill square represents the recovery of the initial superconducting properties as highest pressure is released. (From Ref. 15).*

---

[179] K. Ishida, Y. Ihara, H. Takeya, C. Michioca, K. Yoshimura, K. Takada, T. Sasaki, H. Sakurai and E. Takayama-Muromachi. *Phys. C* **460-462**, 192 (**2007**).
[180] H. Sakurai, K. Takada, F. Izumi, R. A. Dilanian, T. Sasaki and E. Takayama-Muromachi. *Phys. C* **412-414**, 182 (**2004**).
[181] C. J. Milne, D. N. Argyriou, A. Chemseddine, N. Aliouane, J. Veira, S. Landsgesell and D. Alber. *Phys. Rev. Lett.* **93**, 247007 (**2004**).
[182] B. Lorenz, J. Cmaidalka, R. L. Meng and C. W. Chu. *Phys. Rev. B* **68**, 132504 (**2003**).

Although the interlayer distance increases as sodium content decreases and still more after water intercalation, does it behave like a 2D system also from an electronic point of view? Electrical resistance measurements in single crystals from *Wang et al*[183] show a dimensional crossover from 2D to 3D with decreasing concentration of Na^+, opposite to what we expected for an increase of the interlayer distance between the CoO_6 sheets because of a lower sodium content. In this sense, the behaviour is very similar to what happens in intercalated graphite[184], in which 2D to 3D transition has been obtained after intercalation. Recovery of the 2D character takes place as water is intercalated into the structrue after hydration process. So, the fact that the carrier density in the CoO_6 is kept unchanged in both BLH and MLH phases strongly suggests that only an optimum level of carrier doping into the CoO_6 layers is not enough for inducing the superconductivity, and also that an optimum interlayer separation between the CoO_6 layers is indispensable for the superconductivity.

But the most important and maybe the most controversial question is the dependence of T_c with Na^+ doping. It is well know the existence of a certain range of Na^+ composition where the superconductivity occurs in this material ($0.3 \leq x \leq 0.45$), but the dependence of T_c as a function of Na^+ doping inside this interval remains still unclear. The first superconducting phase diagram for the hydrated superconductor $Na_{0.3}CoO_2 \cdot 1.3H_2O$ has been proposed by *Schaak et al*[185] (Figure 4.4).

[183] C. H. Wang, X. H. Chen, J. L. Luo, G. T. Liu, X. X. Lu, H. T. Zhang, G. Y. Wang, X. G. Luo and N. L. Wang. *Phys. Rev. B* **71**, 224515 (**2005**).
[184] T. E. Weller, M. Ellerby, S. S. Saxena, R. P. Smith and N. T. Skipper. *Nature Physics* **1**, 39 (**2005**).
[185] R. E. Schaak, T. Klimczuk, M. L. Foo and R. J. Cava. *Nature* **424**, 527 (**2003**).

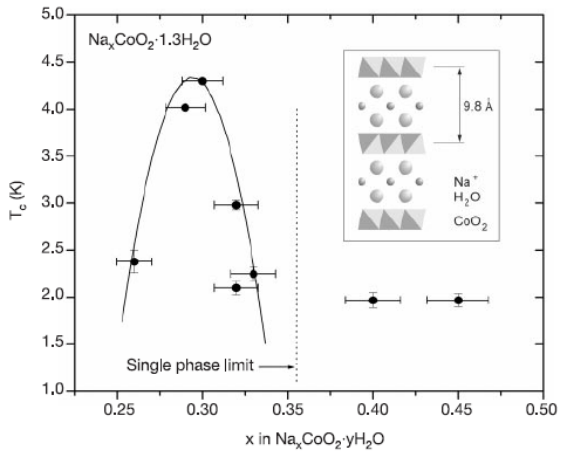

Figure 4.4: *Superconducting phase diagram for $Na_xCoO_2{\cdot}1.3H_2O$. Main panel: T_c as a function of x as determined from the AC susceptibility measurements. (From Ref. 18).*

These experimental results show a strong correlation between T_c and the Na^+ content of the samples. Bulk superconductivity with T_c>2 K has been reported to exist over a very narrow range of Na^+ compositions, approximately $1/4 \leq x \leq 1/3$, where it is established an optimal chemical doping level for superconductivity with $Tc \approx 4.5$ K around x=0.3. And T_c decreases for both underdoped and overdoped materials. This "dome-like" dependence of superconducting transition temperature with doping shows the same trend as in cuprate superconductors. For this reason, it has been thought that the origin of SC in this material could have some points in common with the superconductivity in cuprates.

To explain this dependence *Baskaran et al*[186] presented a theory based on the idea that this compound would give different ordered phases at the Na^+ compositions of x=1/4 and x=1/3 respectively. They argued that charge ordering at these doping levels in the CoO_2 layers would be a competitor to superconductivity leading to a strong decrease in T_c. Therefore, the highest T_c would be achieved between these specific compositions.

However, experimental results from *Chen et al*[174] disagree with the superconducting "dome" of $T_c(x)$ by *Shaak et al*[185]:

[186] G. Baskaran. *Phys. Rev. Lett.* **91**, 097003 (**2003**).

1. No variation in T_c as a function of sodium content in the range $0.22<x<0.47$ is found (Figure 4.5). Out of this doping level interval no superconducting transition has been detected.

2. The superconducting phase approaches to the phase line where the non-hydrated $Na_{0.5}CoO_2$ shows a metal-insulator transition[187]. We will see from our results in the next chapter that this fact could be more important than previously thought.

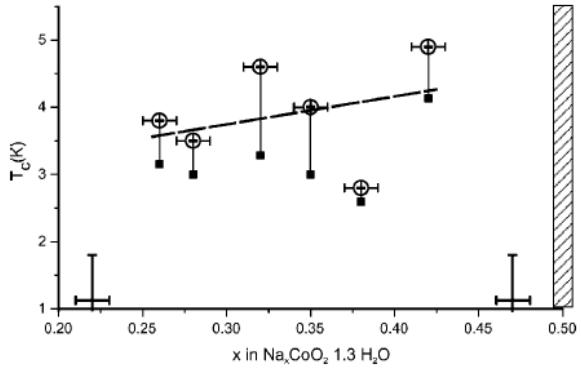

Figure 4.5: *Superconducting transition temperature, T_c, as a function of sodium doping, x, in Na_xCoO_2•1.3 H_2O. The dashed line is a guide to the eye. The dashed bar marks the metal-insulator transition observed in non-hydrated $Na_{0.5}CoO_2$. (From Ref. 20)*

Also *Milne et al*[181] have found that T_c does not change significantly with *x* over the region $0.28<x<0.37$. In the superconducting phase diagram determined from their measurements, Figure 4.6 (a), T_c differs from 4.3 K to 4.8 K in that Na^+ composition range, which is very close to the optimum value reported by *Shaak et al* for this material[185].

All papers that have appeared after the report of *Schaak et al*[185] on physical properties and theoretical calculations have been based on the Co oxidation state of ca. 3.7+, which is deduced directly from the Na^+ content

[187] Q. Huang, M. L. Foo, J. W. Lynn, H. W. Zandbergen, G Lawes, YayuWang, B. H. Toby, A. P. Ramirez, N. P. Ong and R J Cava. *J. Phys.: Condens. Matter* **16**, 5803 (**2004**).

(*x*~0.3). But, as we have already shown in Chapter 1 and also from other works, the Co valence state does not vary notably in the sodium composition range where SC is obtained, the electronic band filling is the result of a complex Co(t_{2g}):O(2p) hibridization plus the t_{2g} splitting. That makes that representation of T_c as a function of the sodium content not totally correct, since the oxidation state of Co is lower that the expected only from Na^+ content[174,181,188,189] (see Figure 1.9 in Chapter 1).

On the other hand, *Milne et al*[181] reported a significant discrepancy between the expected valence of Co based on Na^+ content and the values obtained from redox titration, drawing a more correct representation where T_c is plotted against Co formal valence and not as a function of Na^+ content. Figure 4.6 (b) shows this representation in comparison with that one obtained from the data of *Schaak et al*[185].

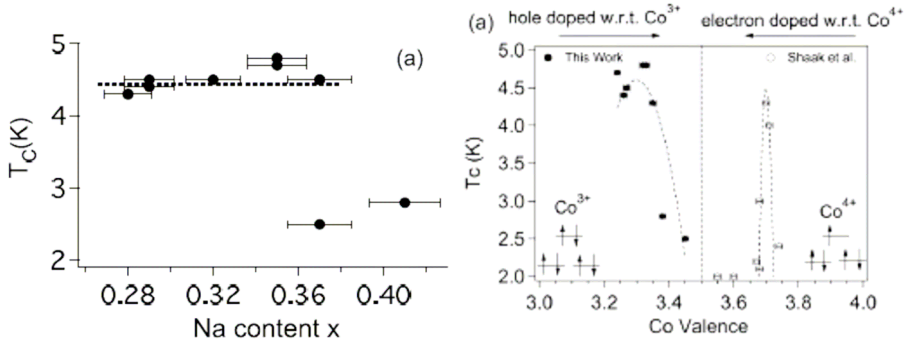

Figure 4.6: *(a) T_c as a function of Na^+ content, x, in Na_xCoO_2•1.3 H_2O. (b) T_c as a function of the Co valence state (right) obtained from redox titration in comparison with (left) plot derived from Shaak's data[185]. (From Ref. 14).*

In this superconducting phase diagram they find that optimal T_c is reached over the region of cobalt valence 3.24-3.35 (that will correspond to an *x*~0.6), while T_c decreases to values of <3 K for Co valence states >3.35+. They also demonstrated that the occurrence of superconductivity is strongly linked to the dimensionality of the structure. They observed that the c/a ratio increases as Co oxidation state is tuned into the optimal T_c region.

---

[188] M. Karppinen, I. Asako, T. Motohashi and I. Yamauchi. *Phys. Rev. B* **71**, 092105 (**2005**).
[189] H. Sakurai, S. Takenouchi, N. Tsujii and E. Takayama-Muromachi. *J. Phys. Soc. Jpn.* **73**, 2081 (**2004**).

Structural characterization of the hydrated superconducting cobalt oxide phase has been carried out by several groups[169,190,191,192]. But most of them considered just the Na^+ ions and H_2O molecules as the guest species. That means that the formation process of the superconducting phase was though to involve just the oxidative extraction of Na^+ ions and the topotactic insertion of H_2O molecules. However, the actual achivement of superconductivity in this system is more complicated and other chemical species and more complex reactions take place. In fact, the stochiometry of this superconductor has been again revised by *Takada et al*[190] and more recently *Sakurai et al*[193]. They concluded that H_3O^+ ions are necessarily inserted substituting partially the Na^+ ions between two CoO_2 layers to compensate the charge, in addition to water molecules. This topotactic ion-exchange of Na^+ ions by H_3O^+ mechanism maintains a constant Co valence and is strongly supported by their structural studies based on Raman spectroscopy and X-ray powder diffraction, which also suggested that the oxonium ions occupy the same crystallographic sites as Na^+ ions. That means that guest species in the new structure model are not only Na^+ ions and H_2O molecules but also H_3O^+ ions, giving a composition of the superconducting phase of $Na_{0.337}(H_3O)_{0.234}CoO_2 \bullet yH_2O$ instead of the previous $Na_{0.3}CoO_2 \bullet yH_2O$. Afterwards, that was also confirmed by *Milne et al*[181], indicating that Na^+ substoichiometry alone does not control the electronic doping of these materials, H_3O^+ playing an important role also.

However, none of these recent works considered the possibility of a presence of oxygen vacancies in the chemical composition of the superconducting phase (already propposed by *Molenda et al* [194] in 1989). Previously, *Rivadulla et al*[195] discussed that possibility in the superconducting hydrated phase and they propossed a model where, if existing, they would be refilled by the O^{2-} heads of the intercalated water molecules, leading to a creation of H^+ protons into the structure. Later, our results and those ones from other authors[196,197,198] confirmed the presence of

[190] K. Takada, K. Fukuda, M. Osada, I. Nakai, F. Izumi, R. A. Dilanian, K. Kato, M. Takata, H. Sakurai, E. Takayama-Muromachi and T. Sasaki. *J. Mater. Chem*. **14**, 1448 (**2004**).
[191] J. W. Lynn, Q. Huang, C. M. Brown, V. L. Miller, M. L. Foo, R. E. Schaak, C. Y. Jones, E. A. Mackey and R. J. Cava. *Phys. Rev. B* **68**, 214516 (**2003**).
[192] J. D. Jorgensen, M. Avdeev, D. G. Hinks, J. C. Burley and S. Short. *Phys. Rev. B* **68**, 214517 (**2003**).
[193] H. Sakurai, M. Osada and E. Takayama-Muromachi. *Chem. Mater.* **19**, 6073 (**2007**).
[194] J. Molenda, C. Delmas, P. Dordor and A. Stoklosa. *Solid State Ionics* **12**, 473 (**1989**).
[195] F. Rivadulla, J.-S. Zhou and J. B. Goodenough. *Phys. Rev. B* **68**, 75108 (**2003**).
[196] M. Karppinen, I. Asako, T. Motohashi and H. Yamauchi. *Chem. Mater.* **16**, 1693 (**2004**).
[197] Morita et al. *J. Solid State Chem*. **177**, 3150 (**2004**).

oxygen vacancies in the system below x<0.7, which increase as Na^+ content decreases. But, even though a lower than expected Co valence state was also found by other authors in both non-superconducting and superconducting phases, in the case of the superconducting phase they could not distinguish which effect took place to raise the charge balance: if oxygen vacancies or formation of extra H_3O^+.

Figure 4.7 shows the X-ray diffraction patterns for the unhydrated Na^+ deintercalated precursor and the superconducting phase after hydration. Both of them were single phase without the presence of any impurity. However, the pattern corresponding to the hydrated sample shows a complex mixture constituted by both unhydrated and hydrated phases with different amounts of H_2O per formule unit, as reported by other authors[174]. This fact leads to an overlapping of the reflexions from different phases and made difficult their indexing. For this reason the refinment of the structure could not be carried out in the hydrated and superconductive phase. On the other hand, it can be observed, looking at the reflexion indexed as (002), that the CoO_2 interlayer distance increases as water is introduced into the structure.

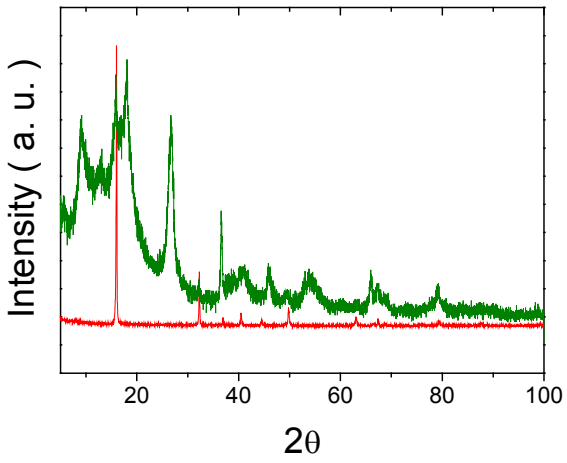

Figure 4.7: *X-ray diffraction patterns for (red) $Na_{0.36}CoO_2$ and (green) $Na_{0.36}CoO_2 \bullet yH_2O$.*

[198] F. C. Chou, E. T. Abel, J. H. Cho and Y. S. Lee. *J. Phys. Chem. Solids* **66**, 155 (**2005**).

The determination of the actual content of water of different hydrated samples by a direct method is highly inaccurate. Thermogravimetric analysis of superconducting phases can be found in the literature.[175,177] However, the continuous and fast decrease of the mass in the whole temperature range makes difficult a certain determination of the water content for each stable hydrated phase. Therefore, it is important to take into account that the stochiometry of the water content of the fully and partially hydrated phases appearing in the literature could be affected by similar inaccuracies.

Figure 4.8 shows the ZFC-FC of the sample before hydration. Once the sample has been hydrated by stirring in destilled water for two days, a diamagnetic response, characteristic of the superconducting state, shows up at T<4 K.

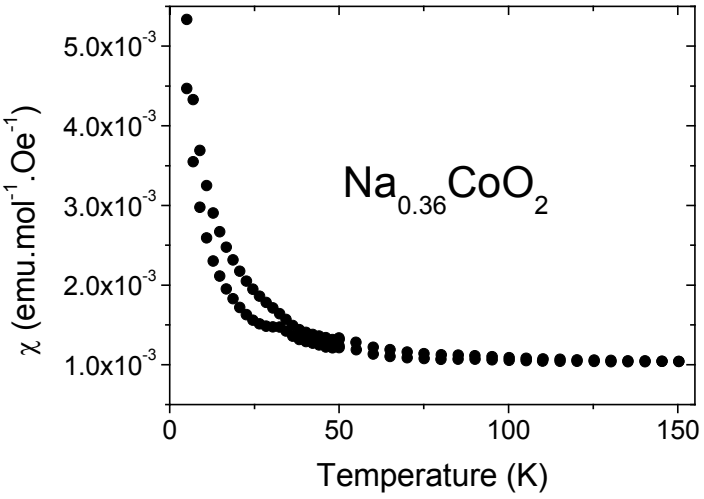

Figure 4.8: *χ(T) curves for $Na_{0.36}CoO_2$ in ZFC-FC conditions at a magnetic applied field of H=100 Oe.*

Figure 4.9 shows the superconducting behaviour of $Na_{0.36}CoO_2 \cdot 1.3H_2O$ at different magnetic applied fields. It is important to remark that the magnetic transition at T~30 K in the ZFC curve of the non-hydrated sample dissapears completely once the sample became superconductive. That reinforces our theory about its intrinsic magnetic character, not due to impurities.

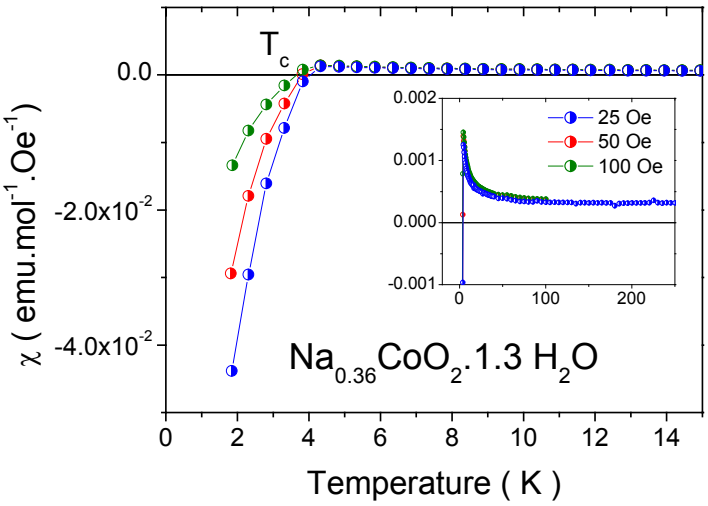

Figure 4.9: *Magnetic susceptibility as a function of the temperature in ZFC conditions for $Na_{0.36}CoO_2$•$1.3H_2O$ under several magnetic applied fields: 25 Oe, 50 Oe and 100 Oe. The superconducting transition temperature is T_c=3.5 K.*

The magnetization loop in an applied magnetic field up to 0.1 T is also showed in Figure 4.10 at a temperature below T_c. It follows the typical diamagnetic behavior of a superconducting material at low fields and the transition to the normal state at high field.

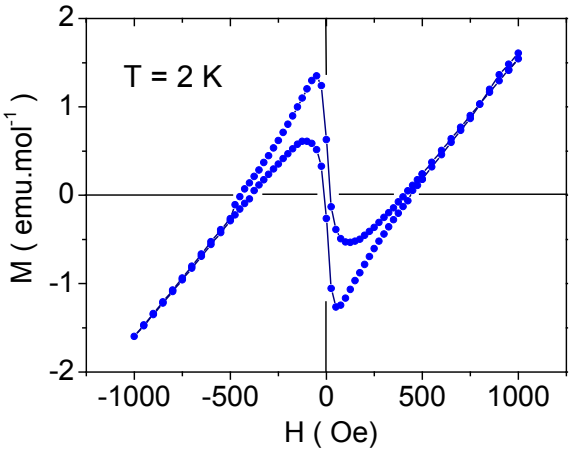

Figure 4.10: *Magnetization loop as a function of the magnetic applied field up to 1000 Oe. The measurement has been carried out at temperature below T_c (T=2 K).*

In Figure 4.11 we have monitored the evolution of the thermopower as the unhydrated precursor is hydrated to render the superconductive phase. Thermoelectric power in the powder is dominated by the *ab*-plane[199] due to its higher conductivity; the influence of the dimensionality is low, so we are testing the variations in the number of charge carriers available for scattering in the electronically active CoO_2 planes[200] (provided that the material remains metallic). For this reason, any amount of water that is not introduced between the layers or the intergrain scattering contribution is not a source of error for this experiment. In Figure 4.11 an appreciable increase is obtained for the superconducting sample with respect to the non-hydrated precursor. We have also monitored the thermoelectric behavior of this superconducting sample after a heating treatment at 360 ºC for 48 hours, with the aim of eliminating a significant amount of water. A partial recovery of the thermoelectric behavior of the superconducting precursor before hydration is observed as sample is dried. The initial behavior is not totally recovered, since probably at the end of the heating process the intercalated water is not eliminated completely and some of it still remains. Moreover, at

[199] I. Terasaki, Y. Sasago and K. Uchinokura. *Phys. Rev. B* **56**, 12685 (**1997**).
[200] M. L. Foo, Y. Wang, S. Watauchi, H. W. Zandbergen, T. He, R. J. Cava and N. P. Ong. *Phys. Rev. Lett*. **92**, 247001 (**2004**).

this temperature there could be an appreciable reordering of the Na^+ ions in the structure.

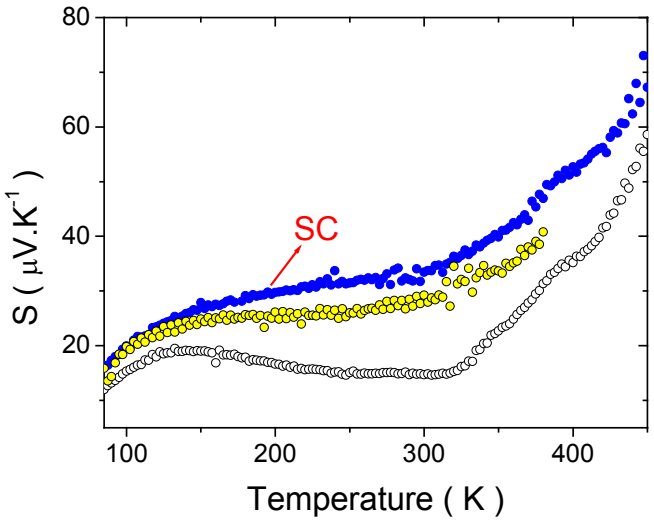

Figure 4.11: *Thermoelectric power of polycrystalline $Na_xCoO_2 \bullet yH_2O$ samples as a function of the temperature: (open circles) $Na_{0.36}CoO_2$; (blue) $Na_{0.36}CoO_2 \bullet 1.3H_2O$; (yellow) $Na_{0.36}CoO_2 \bullet 1.3H_2O$ partially dried.*

This is consistent with a substantial change in the oxidation of the CoO_2 planes due to H_2O intercalation. Alternatively, the anisotropic expansion of the structure was suggested to introduce the possibility of a change in the density of states at the Fermi energy, $N(E_F)$, due to the overlapping of the e^T and a_1^T bands at E_F[195,201], which could also contribute to the thermopower. To distinguish between these two possibilities, we have synthesized K_xCoO_2 (with identical structure to Na_xCoO_2 except for the interlayer space which is larger in the K^+ sample) and compared the thermopower for two samples with almost identical composition (Figure 4.12). The thermopower presents identical behavior in both materials irrespective of whether the interlayer spacer is Na^+ or K^+. It is true that the increase in the *c*-axis parameter in the K^+ samples with respect to the Na^+ phase is much lower than in the hydrated superconductors, but the

[201] D. J. Singh. *Phys. Rev. B* **61**, 13397 (**2000**).

thermopower remains practically insensitive to the lattice spacer. This result makes us believe that a change in the oxidation state of the CoO_2 planes and the elimination of oxygen vacancies that perturb the periodic potential gives H_2O an active chemical role in stabilizing the superconducting state.

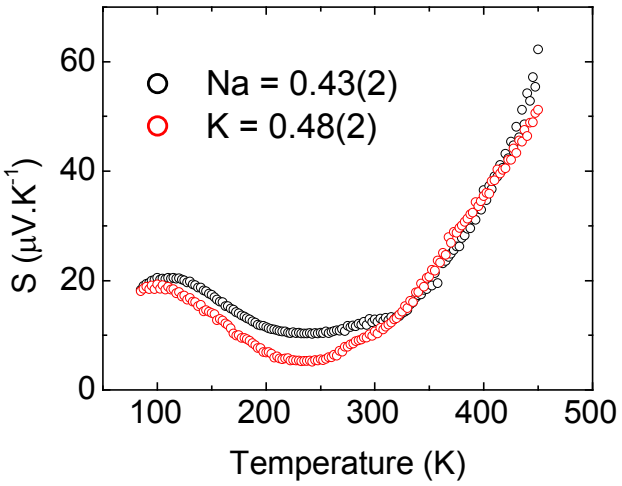

Figure 4.12: *Temperature dependence of the thermopower of $Na_{0.43(2)}CoO_{2-\delta}$ and $K_{0.48(2)}CoO_{2-\delta}$.*

The increase in the thermopower after water insertion could in principle be interpreted as a signature of reduction, that is, of an increase of the effective valence of Co or in the e^--doping. However, a conclusion like that could be erroneous, in a system where the population of more than one band crossing the Fermi energy is changing continuously.

However, after the heat treatment in order to eliminate as amount of intercalated water as possible (and although it has not been completely removed), it is important to remark that the material looses its superconducting properties (Figure 4.13). The new magnetic behaviour also shows an interesting peak in ZFC curve around T~40 K similar to that one appearing in the magnetic measurements of Na^+ deintercalated samples at $x \approx 0.5$, where a possible sodium ordering is thought to induce new magnetic phases in the material.

Below the magnetic transition temperature, ZFC and FC curves are separated sharing a strong temperature dependence. The character of the

magnetic phase has not still determined, but it looks like an inhomogeneous AFM. Once the superconducting sample has lost its superconducting properties by heating treatment, these ones can not be recovered after a new hydration process. We think that a competition between a superconducting and a magnetic phase occurs to develop and the balance is biased towards one or the other during the water intercalation and drying processes. This point will be discussed in the next chapter.

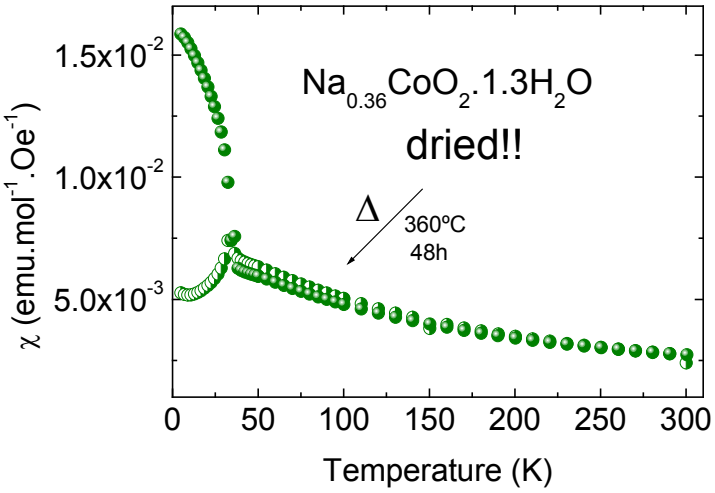

Figure 4.13: *Temperature dependence of the molar susceptibility (χ) in a superconductive sample after a heating treatment at 360 ºC for 48 hours. It is important to remark that the superconducting properties are not recovered as the sample is immersed in water again for a long time.*

Therefore, and as a conclusion, we think water also plays an active role in the doping of the CoO_2 planes.

If the oxygen of the intercalated H_2O enters the oxygen vacancies of the CoO_2 planes (as occurs for bound H_2O on the surface of an oxide particle), it gives its proton to the free interstitial water to create (H_3O^+)-ions, which reduce the CoO_2 sheets like the Na^+ ions. On the other hand, the bound O^{2-} ions from the water decrease the strong perturbations of the periodic potential created by the vacancies, oxidizing at the same time the CoO_2 sheets.

These conclusions are supported by the work by *Karppinen et al* [196] who reported a net increase in the oxidation state of Co as the hydrated

superconducting phase is obtained from the corresponding nonhydrated one. If we assume that the water molecules intercalated between CoO_2 layers are electrically neutral and that the (H_3O^+) ions are counterbalanced by the O^{2-} ions, a reduction of the oxygen vacancies and an increase of the oxidation state of Co would explain the continuous increase in the *c*-axis lattice parameter that it is observed in the hydrated samples as *x* is reduced, despite the constant amount of water introduced.

This will be further discussed in the next chapter.

5. The especial case of half doping: $Na_{0.5}CoO_2$

After our systematic exploration of the magnetic and thermoelectric properties of Na_xCoO_2, we considered interesting to focus on the half-doped sample (x=0.5) because of its particular/original physical properties, i.e. it is the only member of the series at $x \leq 0.7$that shows some kind of magnetic ordering, it undergoes a metal-to-semiconductor transition associated to a CO transition and it displays a crossover to a negative Seebeck coeficient with temperature. Therefore, after a brief introduction about this specific phase, we will show a more detailed study about the characteristic physical properties of the $Na_{0.5}CoO_2$ phase and the decisive role that we think this phase plays in the appearance of superconductivity in $Na_xCoO_2 \cdot yH_2O$.

The superconducting phase in hydrated Na_xCoO_2 is considered to condense from a Fermi liquid (FL) with AFM correlations at low values of *x*, typically around *x*~0.35[202]. At high doping, *x*~0.7, the coupling of itinerant carriers to localized S=1/2 spins is normally considered as the origin of the non-FL behaviour, establishing a candidate quantum spin-liquid state at low temperature[203]. These two thermodynamically distinguishable metals are separated at zero Kelvin by an AFM charge ordered state at half doping, *x*=0.5[204]. The origin of this state is not absolutely clarified, although it has been tentatively related to the influence of an ordered pattern of Na^+ ions between the CoO_2 layers, which disturbs the potential over the $Co^{3+/4+}$ sheets and forces the system to a certain type of charge ordering[205,206,207]. Several superestructures have been observed experimentally from electron diffraction studies in a wide composition range[205] and it was suggested that the low temperature CO is a spin density wave (SDW) state driven by a nesting of the Fermi surface characteristic of the ordered Na^+ pattern at *x*=0.5 [208,209]. In an alternative possibility, the SDW could result from the strong nesting tendencies of a hexagonal Fermi surface in which six small hole pockets derived from the $e_{g'}$ bands are symmetrically placed around the Γ point[210].

Polycrystalline γ-$Na_{0.7}CoO_2$ was obtained by conventional solid state reaction with a final firing at 900 ºC as described previously in Chapter 1. The XRD pattern shows a single phase consistent with a hexagonal unit cell,

[202] G. Lang, J. Bofroff, H. Alloul, G. Collin and N. Blanchard. *Phys. Rev. B* **78**, 155116 (**2008**).
[203] L. Balicas, Y. J. Jo, G. J. Shu, F. C. Chou and P. A. Lee. *Phys. Rev. Lett.* **100**, 126405 (**2008**).
[204] M. L. Foo, Y. Wang, S. Watauchi, H. W. Zandbergen, T. He, R. J. Cava and N. P. Ong. *Phys. Rev. Lett.* **92**, 247001 (**2004**).
[205] H. W. Zandbergen, M. Foo, Q. Xu, V. Kumar, and R. J. Cava. *Phys. Rev. B* **70**, 024101 (**2004**).
[206] D. N. Argyriou, O. Prokhnenko, K. Kiefer and C. J. Milne. *Phys. Rev. B* **76**, 134506 (**2007**).
[207] T. P. Choy, D. Galanakis and P. Phillips. *Phys. Rev. B* **75**, 073103 (**2007**).
[208] J. Bobroff, G. Lang, H. Alloul, N. Blanchard and G. Collin. *Phys. Rev. Lett.* **96**, 107201 (**2006**).
[209] N. L. Wang, Dong Wu, G. Li, X. H. Chen, C. H. Wang and X. G. Luo *Phys. Rev. Lett.* **93**, 147403 (**2004**).
[210] M. D. Johannes, I. I. Mazin, D. J. Singh and D. A. Papaconstantopoulos. *Phys. Rev. Lett.* **93**, 097005 (**2004)**.

space group *P63/mmc*, and lattice parameters a=2.8328(1) Å and c=10.8511(6) Å. To obtain $Na_{0.5}CoO_2$, Na^+ was removed with Br_2/acetonitrile The Na/Co ratio was confirmed by ICP-OES to be 0.51(1). Reflexions from Co_3O_4 or other minority phases are completely absent (see Figure 5.1).

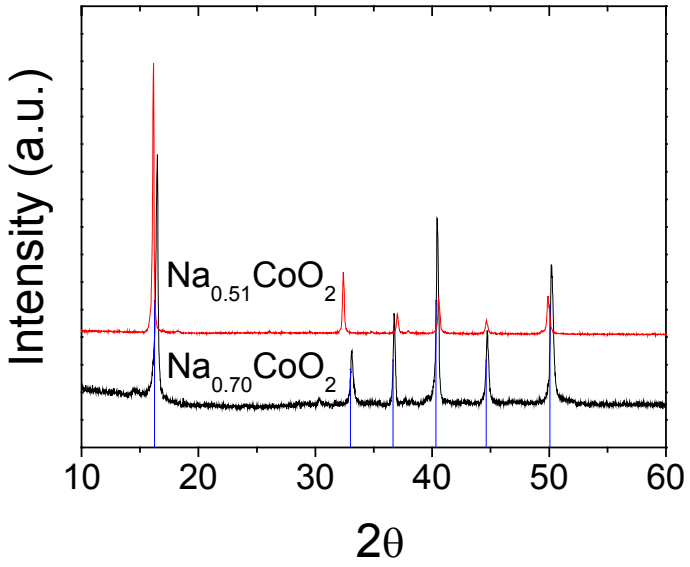

Figure 5.1: *X-ray diffraction pattern of Na_xCoO_2 (x=0.70 and x=0.51). The vertical blue lines show the expected reflections for the space group P63/mmc. The Na/Co ratio was measured by ICP-OES.*

Figure 5.2 shows the temperature dependence of the absolute electrical resistance and the ZFC-FC magnetization curves in $Na_{0.51}CoO_2$. The results are similar to those reported by *Shu et al*[211] for electrochemically deintercalated crystals. We want to emphasize that we have not performed any additional annealing to the samples after Na^+ extraction and before the transport/magnetic experiments. This was done so in order to prevent any possible rearrangement of Na^+, oxygen loss, etc. after the synthesis, and to

[211] G. J. Shu, A. Prodi, S. Y. Chu, Y. S. Lee, H. S. Sheu and F. C. Chou. *Phys. Rev. B* **76**, 184115 (**2007**).

make the results as much comparable to the process followed in single crystals as we can. Then, only the relative changes in the resistance should be considered and not its absolute value.

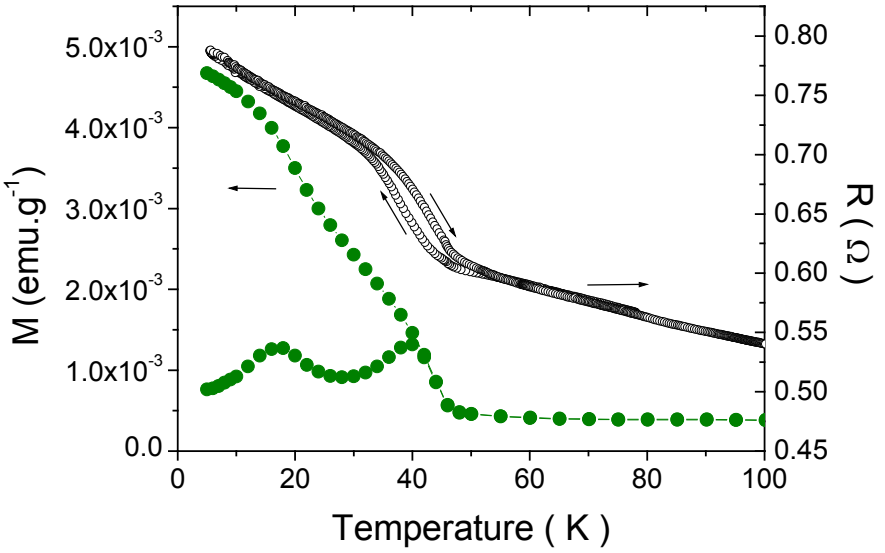

Figure 5.2: *ZFC-FC magnetization curves at H=100 Oe, and electric resistance of $Na_{0.51}CoO_2$. The arrows indicate the direction followed during the measurement.*

We have found an increase in the resistance reminiscent of a CO effect below ~45 K, similar to the reported in single crystals[204], although it is very modest compared with that in single crystals. This effect is related to the formation of a SDW[212] and hence does not result in such an effective localization as it does the CO state in manganites or nickelates for example[213], in which the step in resistance involves several orders of magnitude.

[212] J. Bobroff, G. Lang, H. Alloul, N. Blanchard and G. Collin. *Phys. Rev. Lett.* **96**, 107201 (**2006**).
[213] "Colossal Magnetoresistance, Charge Ordering and Related Properties of Manganese Oxides", C. N. R. Rao, B. Raveau, Eds. World Scientific, Singapore (**1998**).

On the other hand, intrinsic transport properties can be proved through the Seebeck coefficient, a magnitude that is not sensitive to intergrain scattering as now current flows through the sample. Figure 5.3 shows the temperature dependence of the thermopower for two representative Na^+ compositions. As it was discussed in the previous chapter, *S(T)* shows a crossover towards negative values in the *x*=0.5 phase which is absent at larger and lower concentrations of Na^+. This is consistent with a local change in the curvature of the $N(\varepsilon_F)$ close to *x*=0.5, due to a partial gaping of the density of states, that develops gradually as temperature is reduced (not like a conventional phase transition).

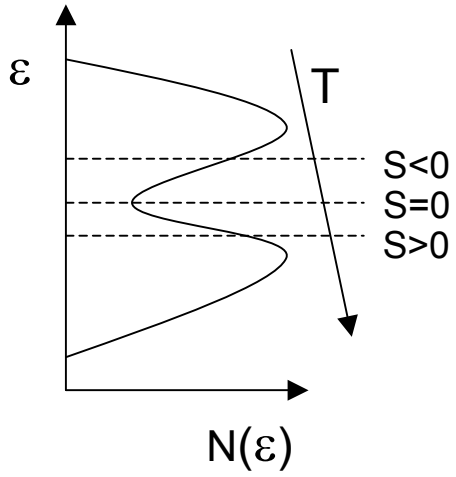

Scheme 5.1: *Representation of the density of states proposed for $Na_{0.5}CoO_2$. The sign of S depends on the position of the Fermi level (dot lines) at a specific temperature, which develops as indicated with temperature (arrow).*

Recent ^{23}Na NMR results found a crossover at T*~200 K that changes the nature of the spin correlation in *x*=0.5 from AFM at low temperatures to FM at high temperatures[202]. On the other hand, evidences for a pseudogap at low doping were obtained from photoemission

spectroscopy[214]. All these results are consistent with a partial gaping of the Fermi surface by a SDW instability occurring below ~200 K, where we have observed the change of sign of *S(T)* in $x \approx 0.5$.

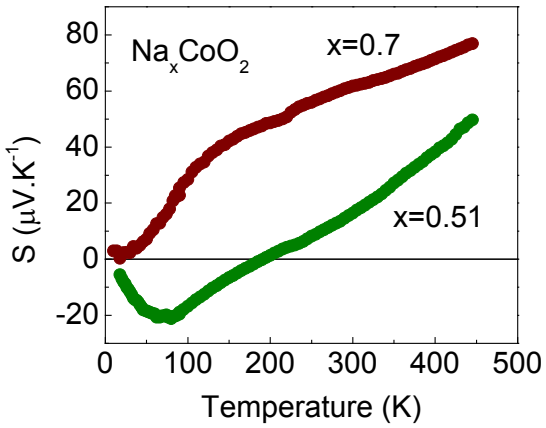

Figure 5.3: *Temperature dependence of the Seebeck coefficient at different x. At $x \approx 0.5$ thermopower goes negative below T~200 K.*

The increase in the electronic resistance is accompanied by a magnetic transition, indicating a partial spin polarization. Two additional magnetic transitions are observed at ≈18 K and ≈86 K (the latter not visible on the scale of Figure 5.2 but in Figure 5.4), consistent with previous reports, which reported up to three magnetic transitions for the half-doped phase at ~20 K, ~50 K and ~90 K[215,216,217]. The magnetic transition at ~90 K has been associated to a long range AFM ordering.[202] The small temperature

[214] T. Shimojima, T. Yokoya, T. Kiss, A. Chainani, S. Shin, T. Togashi, S. Watanabe, C. Zhang, C. T. Chen, K. Takada, T. Sasaki, H. Sakurai and E. Takayama-Muromachi. *Phys. Rev. B* **71**, 020505(R) (**2005**).
[215] Q. Huang, M. L. Foo, J. W. Lynn, H. W. Zandbergen, G. Lawes, Y. Wang, B. H. Toby, A. P. R. N. P. Ong, and R. J. Cava. *J. Phys.: Condens. Matter* **16**, 5803 (**2004**).
[216] G. Gasparovic, R. A. Ott, J.-H. Cho, F. C. Chou, Y. Chu, J. W. Lynn and Y. S. Lee. *Phys. Rev. Lett.* **96**, 046403 (**2006**).
[217] C. H. Wang, X. H. Chen T. Wu, X. G. Luo, G. Y. Wang and J. L. Luo. *Phys. Rev. Lett.* **96**, 216401 (**2006**).

differences with respect to our data could be due to small differences in the composition of Na^+ between the samples.

Also, as mentioned in Chapter 2, we have observed (as many authors reported before)[202,204] the existence of a thermally activated term in $\chi(T)$ for x≤0.5, indicative of some kind of spin gap. Figure 5.4 shows a more detailed scale for the magnetization data of several representative Na^+ compositions, where a decrease of the magnetic susceptibility with temperature in the range above the magnetic phase transition and up to room temperature is observed. In fact, the slope of the curves changes from negative to positive at around *x*=0.5 (see Figure 5.5), further supporting the singular nature of this point.

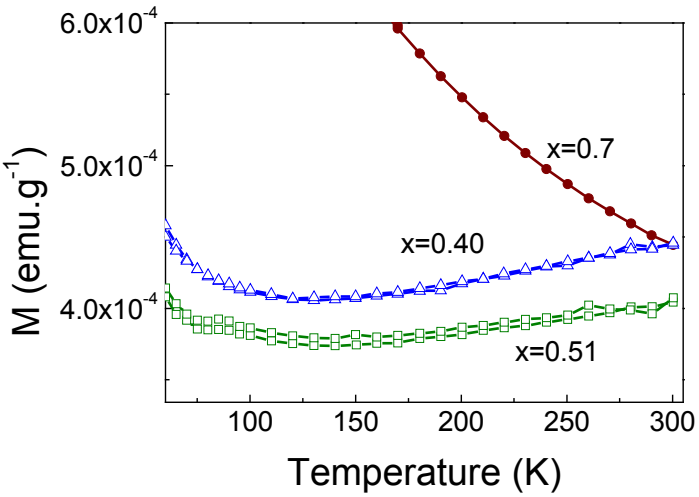

Figure 5.4: *Temperature dependence of the magnetization for different x.*

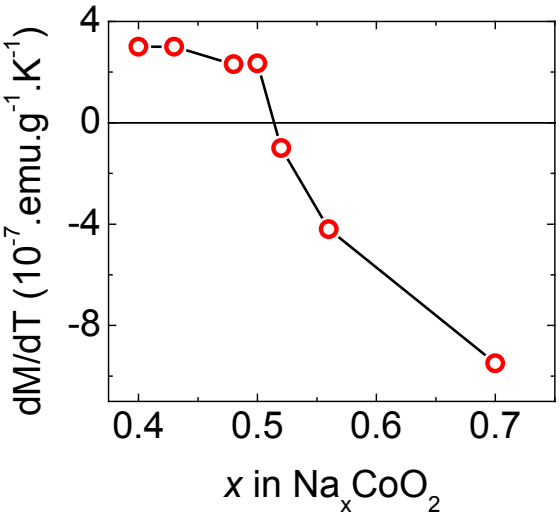

Figure 5.5: *Change of slope from positive (x≤0.5) to negative (x>0.5). The values are calculated from the fitting of the high temperature data to a straight line, and hence are only indicative of the general behavior.*

For a more detailed characterization of the magnetic properties of the half doped phase, the stability of the magnetic phases with the applied magnetic field was also studied. Figure 5.6 shows the magnetic curves at different applied magnetic fields between 2.5×10^{-3} T and 1 T. Their position at 17 K and 40 K remains unchanged until H=0.1 T, but they are slightly shifted at H=1 T. However, the irreversivility between the ZFC-FC curves is reduced as the applied magnetic field increases above 10^{-2} T. In order to carry out a complete magnetic characterization and determine which is the magnetic nature of the magnetic phases emerging at *x*=0.50, the hysterisis magnetic loops were performed at different representative temperatures below and above the magnetic transitions in ZFC conditions. Figure 5.7 shows the hysterisis cycles at T=5 K, 28 K and 80 K.

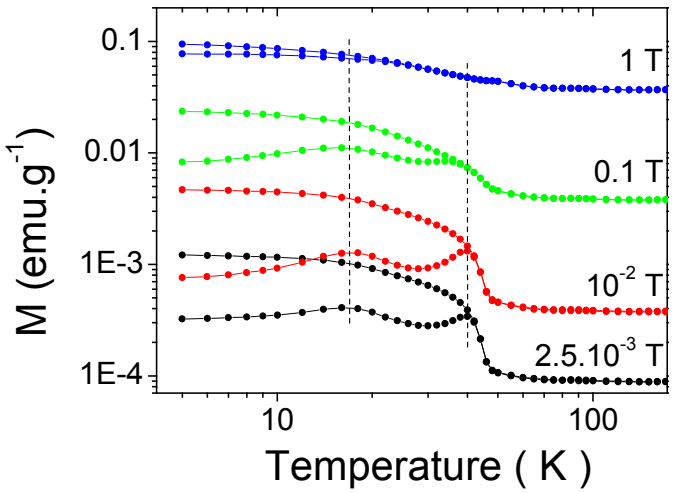

Figure 5.6: *Magnetization curves as a function of the applied magnetic field ($H=2.5\times10^{-3}$, 10^{-2}, 0.1, 1 T) in a log-log scale.*

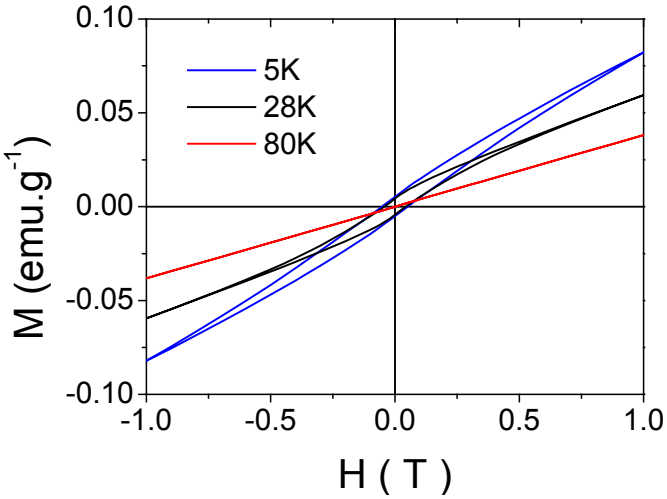

Figure 5.7: *ZFC magnetization loops at several temperatures (T=5 K, 28 K and 80 K) for the x=0.50 phase, up to an applied magnetic field of 1 T.*

At T=80 K the magnetization is in the almost temperature independent regime (Pauli PM-like), what is also evidenced by the linear contribution of the magnetization with the applied magnetic field and the no presence of cohercitive field (H_c). As the temperature decreases, T=28 K, an important FM contribution with $Hc \approx 4.2 \times 10^{-2}$ T and higher absolut values of the magnetization are observed, although it is not saturated at the maximum applied magnetic field (H=1 T). The same effect is even more pronunced at T=5 K, where the Hc from the FM contribution is of ~0.052 T. So, from these results we think that an inhomogeneous AFM state (with a resulting net FM moment) develops at low temperature from a PM state at high temperature.

So, in order to confirm the stability of the magnetic phases and its relationship with a particular Na^+ arrangement, we have studied their evolution with time, doping, fast quenching to low temperatures, hydration and topotactic exchange with divalent-cations. First of all we have observed that all the magnetic and electronic transitions discussed in this paper are robust against both relatively long time aging (Figure 5.8) and fast quenching of the sample from room temperature to liquid He. The cooling rate does not affect to their appeareance, and hence it seems to be of electronic instead of ionic ordering origin. This most probably discards any link between them and a particular Na^+ arrangement, as it was discussed for other magnetic transitions at high doping[218]. However, it also true that if any Na^+ arrangement is particularly stable at x=0.5 already at room temperature, fast quenching is not expected to have any influence on it.

[218] T. F. Schulze, P. S. Häfliger, Ch. Niedermayer, K. Mattenberger, S. Bubenhofer and B. Batlogg. *Phys. Rev. Lett.* **100**, 026407 (**2008**).

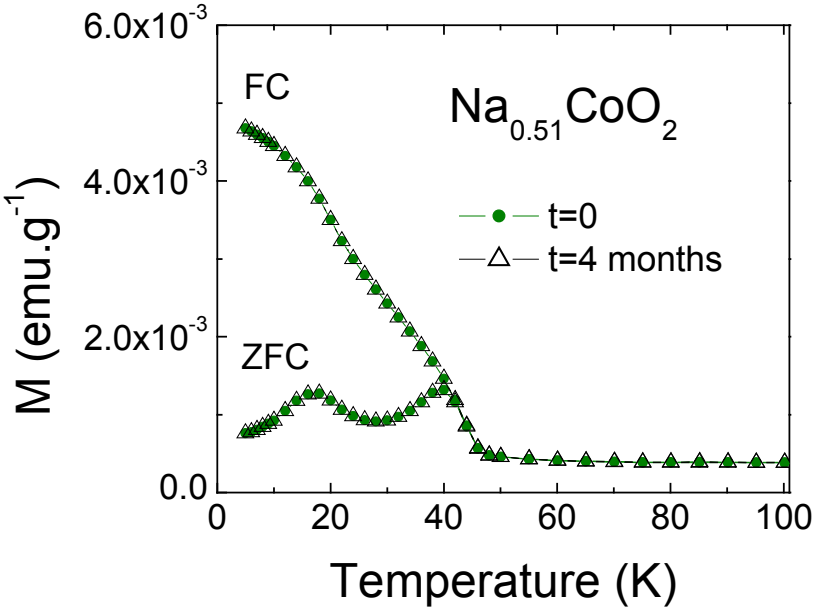

Figure 5.8: *Evolution of the magnetic properties of $Na_{0.51}CoO_2$ with time.*

On the other hand, we have performed a topotactic cation exchange reaction in which all Na^+ is replaced by Sr^{2+}, resulting in $Sr_{0.25}CoO_2$. The results shown in the inset to Figure 5.9 demonstrates that the magnetic transition is still present, although weakened with respect to the Na^+ phase. Although the Co valence remains more or less unchanged, introducing Sr^{2+} increases considerably the *c*-axis parameter and reduces interlayer coupling, at the time that changes the ordering pattern at the interlayer.

In contrast, room temperature Na^+ deintercalation/intercalation processes from the x=0.5 precursor has a clear effect on the magnetic phase transitions: the peak at ~45 K is partially lost and that at ~17 K decreases progressively (compare Figure 5.9 and Figure 5.2). Both transitions are completely erased for $0.40>x>0.60$.

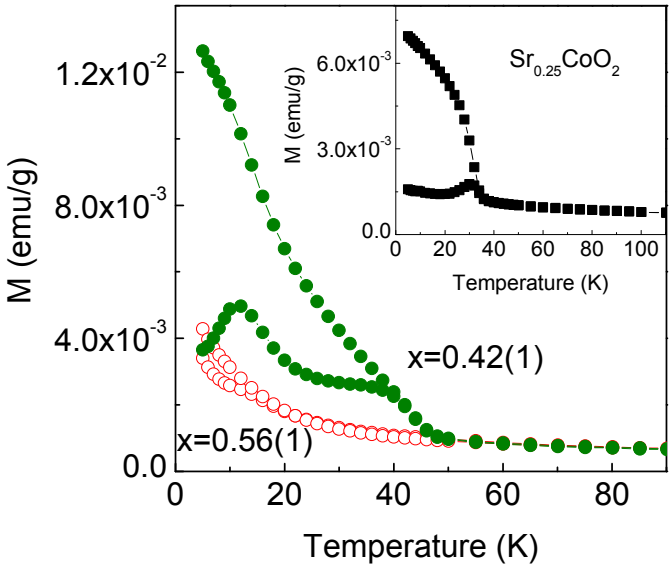

Figure 5.9: *ZFC-FC magnetization curves at H=100 Oe after subsequent Na^+ deintercalation (close circles) and intercalation (open circles) from $Na_{0.51}CoO_2$. The inset shows the ZFC-FC curves (H=100 Oe) of $Sr_{0.25}CoO_2$.*

So, the combination of these results probes that the magnetic/electronic transitions observed at half-doping are intrinsic to the ratio $Co^{3+}/Co^{4+}\approx1$, and most probably independent of the particular Na^+ arrangement. In this sense, the half doped state can be thought as a singular point in the phase diagram of Na_xCoO_2, in which two different metals are separated at 0 K by a magnetically ordered phase.

In Chapter 2, we demonstrated that the oxidation state is more or less constant below x~0.4, and in Chapter 4 we showed the intercalated water could reduce the $Co^{4+/3+}$ redox couple in $Na_{0.3}CoO_2$ to make it similar to the filling in $Na_{0.5}CoO_2$. This, together with the claims of a SC state induced by magnetic fluctuations make it natural to think about the posibility of the magnetic phase at x=0.5 being competing with the SC phase to develop. Given the relevance of the x=0.5 phase for a global understanding of the phase diagram of the system it could be very important to verify whether a superconducting phase can condense directly from the

suppression of the magnetic phase at *x*~0.5, without changing the oxidation state. This could establish an important correlation with the superconducting Fe-oxypinictides, in which superconductivity shows up after a SDW is suppressed, either by dopping or pressure[219].

So, we attempted a direct replacement of H_3O^+ by Na^+ in the *x*=0.5 phase.

Takada *et al*[220] proposed that apart from intercalation of water molecules, the process of hydration involves the following chemical reaction:

$$Na_xCoO_2 + y\,H_2O \rightarrow Na_{\frac{x-y}{2}}\left(H_3O^+\right)_{\frac{y}{2}}CoO_2 + \frac{y}{2}NaOH$$

If we keep the medium slightly acidified, this will result in an ionic exchange of Na^+ by H_3O^+. Given that the oxonium ions occupy the same position as Na^+ between the layers[220,221], the substitution occurs topotactically. *Milne et al*[219] already considered this possibility and suggested that the correct formula to express the superconducting phase would be $Na_x(H_3O^+)_{x'}CoO_2 \bullet yH_2O$. They proposed that optimal doping for superconductivity occurs at a Co valence in the range 3.24-3.35, i.e. at hole instead of electron doping. Similarly, *Sakurai et al*[221,222] demonstrated that is possible to go from a superconducting to a non-superconducting phase, just changing the H_3O^+/Na^+ ratio, without modifying the Co valence.

In view of these results, we should, in principle, be able to force the topotactic replacement of Na^+ by H_3O^+ in $Na_{0.51}CoO_2$, and to study the effect on the magnetic phase and its relationship with superconductivity.

In a first attempt, one sample of $Na_{0.51}CoO_2$ was stirred in water for four days at room temperature. After this process the magnetic transitions are weakened and displaced towards lower temperatures (Figure 5.10).

---

[219] C. J. Milne, D. N. Argyriou, A. Chemseddine, N. Aliouane, J. Veira, S. Landsgesell and D. Alber. *Phys. Rev. Lett.* **93**, 247007 (**2004**).

[220] K. Takada, K. Fukuda, M. Osada, I. Nakai, F. Izumi, R. A. Dilanian, K. Kato, M. Takata, H. Sakurai, E. Takayama-Muromachi and T. Sasaki. *J. Mater. Chem.* **14**, 1448 (**2004**).

[221] H. Sakurai, K. Takada, T. Sasaki and E. Takayama-Muromachi. *J. Phys. Soc. Jpn.* **74**, 2909 (**2005**).

[222] H. Sakurai, N. Tsujii, O. Suzuki, H. Kitazawa, G. Kido, K. Takada, T. Sasaki, E. Takayama-Muromachi. *Phys. Rev. B* **74**, 092502 (**2006**).

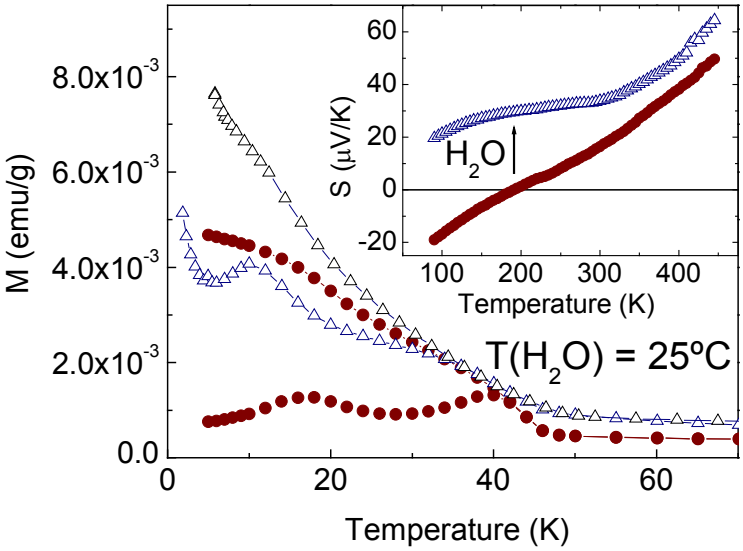

Figure 5.10: *Temperature dependence of the ZFC-FC magnetization (H=25 Oe) of dry $Na_{0.51}CoO_2$ (closed circles) and after hydration at 25 ºC (open triangles). The inset shows the thermoelectric power for dry $Na_{0.51}CoO_2$ (closed squares) and hydrated $Na_{0.42}(H_3O^+)_{0.1}CoO_2 \cdot yH_2O$ (open squares).*

Increasing the time of hydration did not result in a complete suppression of the magnetic transition. Then, in order to increase the amount of water introduced between the CoO_2 layers, the sample of $Na_{0.51}CoO_2$ was kept in water at 70°C for 4 days. The slight increase in temperature should increase the Na^+ diffusion appreciably, favoring the exchange reaction. Consistent with that hypothesis, in some cases the magnetic transitions were completely erased after reaching a partially hydrated composition, but in other cases, the material underwent a superconducting transition at ~2.4 K (Figure 5.11). We have also verified that superconductivity is robust against fast/slow cooling speeds.

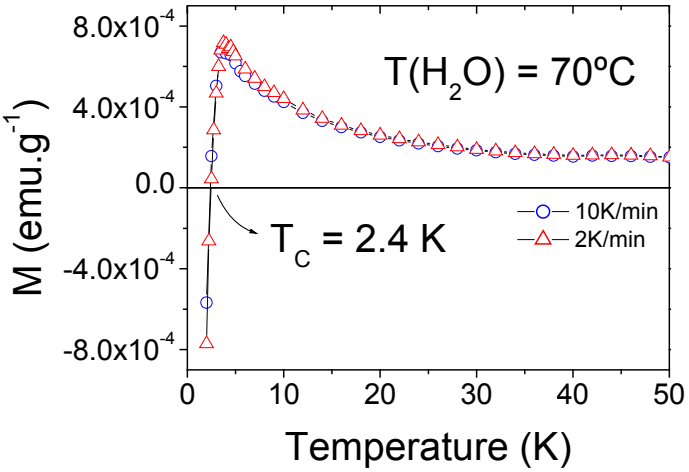

Figure 5.11: *Magnetic susceptibility of the $Na_{0.51}CoO_2$ sample after water insertion at 70 ºC. The thermoelectric response is practically identical to that of the sample hydrated at 25 ºC.*

The Na^+, H_3O^+ and total H_2O content were determined by combined ICP-OES and TGA analysis. These data, along with the dependence of the *c*-axis on *y*, were used to determine a chemical composition (assuming the electrical neutrality of the samples) of the hydrated samples.

Acording to the chemical formula $Na_x(H_3O^+)_{x'}CoO_2 \bullet yH_2O$, we have estimated the value of x' from the values of Na^+ and considering that the valence of Co does not change so much during the process of Na^+ removal, as suggested by *Sakurai et al*.[¡Error! Marcador no definido.,222]

The determination of the actual content of H_2O only by a direct thermogravimetric analysis (TGA) is highly inaccurate. There is a continuous loss of water that it is difficult to assign with a certain amount of adsorbed or intercalated molecules. Even the final plateau of the a priori "water free" sample is not always reached, and the weight continues decreasing until it reaches the point where Na starts evaporating (around 700 ºC). This inaccuracy of the TGA analysis is common in the literature. In fact, previous reports[223] showed that the deintercalated samples are chemically unstable under ambient conditions. Even if the sample is touched during its handling,

[223] M. L. Foo, R. E. Schaak, V. L. Miller, T. Kliimczuk, N. S. Rogado, Y. Wang, G. C. Lau, C. Craley, H. W. Zandbergen, N. P. Ong and R. J. Cava. *Solid State Commun.* **127**, 33 (**2003**).

this will result in an alteration of the hydration. This makes the determination of the actual amount of water intercalated, especially in a system with such a fast kinetics of hydration/dehydration at mild conditions, highly inaccurate.

The same inaccuracy results if we try to estimate the amount of water simply from the elongation of the *c*-axis parameter. A phase with a 19.6 Å *c*-axis does not guarantee bulk superconductivity, as already noted by other authors. Even samples synthesized under the same conditions can result in completely different physical properties[223]. The X-ray patterns vary very much from one to another, and show the presence of intermediate phases (or mixtures of phases) which cannot be identified. The coexistence of many phases with different degrees of hydration was also noted by *Lin et al* [224], which complicates the analysis of the diffraction patterns. Therefore, we cannot establish a direct correlation between the variation of the *c*-axis of hydrated samples and the physical properties of the samples.

That is why we decided to carry out an exhaustive characterization of the water content of our samples based on our combined ICP-OES, TGA and X-ray. In this way, it is important to remark that the TGA and X-ray analysis of newly synthetized and hydrated samples were carried out immediately after being removed from water.

In Figure 5.12 we show the TGA of two samples, hydrated at room temperature and at 70 ^{o}C, respectively. The continuous loss of water slightly above room temperature was only observed in the samples hydrated at 70^{o}C. *Foo et al*[223] already observed that effect in the TGA, and attributed it to the transition from y=1.4 to y=0.6. This marks the transition from the superconducting to the non-superconducting compositions, and it is, actually, very important to understand our results.

[224] C.T. Lin, D.P. Chen, P. Lemmens, X.N. Zhang, A. Maljuk and P.X. Zhang. *J. Crystal Growth.* **275**, 606 (**2005**).

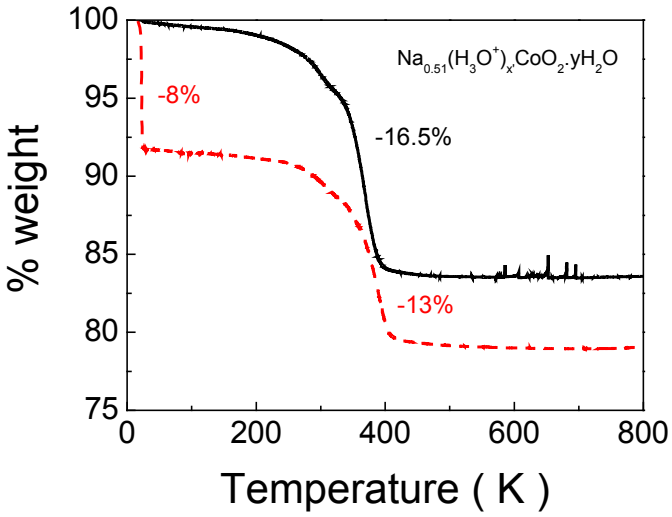

Figure 5.12: *TGA analysis of a sample hydrated at room temperature (solid line) and at 70 °C (dashed line).*

From the analysis of the X-ray diffraction patterns we have extracted the *c*-axis value, which was compared with our previous results for dry Na^+ deintercalated samples (see Figure 1.7 in Chapter 1) and also with hydrated samples from the literature (mainly from *Foo et al*[223], *Lin et al*[224] and *Chen et al*[225]).

Figure 5.13 shows the X-ray diffraction pattern of the superconducting sample obtained after hydration of $Na_{0.51}CoO_2$ at 70 ºC for 4 days (top red line). Peaks characteristic of different phases are identified. The peaks corresponding to the y=1.2 are the characteristic of the superconducting phase (see for example Ref. 223). For the sample hydrated at room temperature (not superconducting), the peak characteristic of the dry sample is still visible (bottom black line). We also noticed that the broad peak closer to 20 (2θ) is actually the combination of two different reflexions corresponding to different hydrated phases, which change their relative intensity after hydration at 70 ºC. It indicates that certain reflexions corresponding to a higher hydrated phases grow to the expense of others

[225] D. P. Chen, H. C. Chen, A. Maljuk, A. Kulakov, H. Zhang, P. Lemmens and C. T. Lin. *Phys. Rev. B* **70**, *024506* (**2004**).

that belong to lower hydration ones. It also shows that full hydration is only reached after the high temperature treatment.

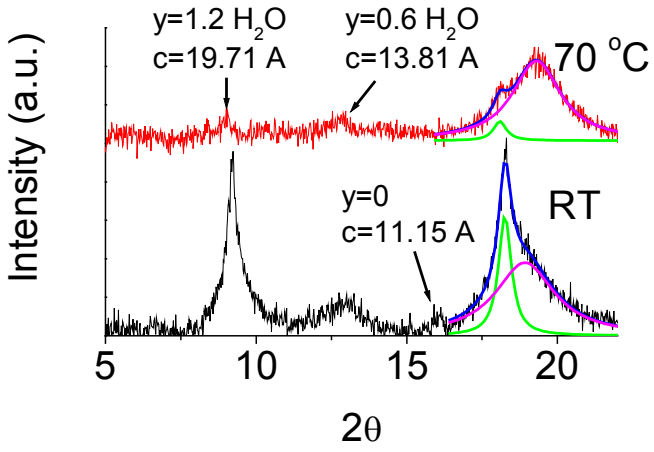

Figure 5.13: *X-ray patterns of the hydrated samples at room temperature (red) and at 70 ºC (black). At room temperature (RT), the peaks of the dry sample are still visible. After immersion at 70 ºC for four days, these peaks disappear, although a mixture of phases with different degree of hydration is still visible.*

Therefore, assuming the electrical neutrality of the samples, we should be able to give an estimation of the approximate chemical composition of the superconducting samples (to get a number for x, x' and y), based on the combined analysis of ICP, TGA and X-ray data.

In this way, the chemical formula for the hydrated sample at room temperature resulted to be $Na_{0.41}(H_3O^+)_{0.1}CoO_2.0.8H_2O$. The fact that the magnetic response was very similar to that of dry $Na_{0.42}CoO_2$ (Figure 5.9) and that the Seebeck coefficient recovered positive values (Figure 5.10 inset) supports this composition. Both results demonstrate that topotactic exchange of Na^+ by H_3O^+ produces an electronic reconstruction (keeps the valence of the $Co^{4+/3+}$ redox pair unchanged) but weakens the SDW phase, probably through decreasing the interlayer coupling. The samples hydrated at 70 ºC and non-superconductive resulted to be $Na_{0.38}(H_3O^+)_{0.13}CoO_2 \cdot 1.0H_2O$, while those ones which underwent a superconducting transition showed an approximate chemical composition of $Na_{0.38}(H_3O^+)_{0.13}CoO_2 \cdot 1.2H_2O$ (the characteristic double layer), although the amount of H_3O^+ could

be a little bit larger (x'~0.16 and y~1.6). The existence of other phases complicates the analysis and makes impossible to be more accurate. Other phases identified have a composition $\approx Na_{0.38}(H_3O^+)_{0.13}CoO_2 \cdot (0.6)H_2O$ (not superconducting) and $\approx Na_{0.38}(H_3O^+)_{0.13}CoO_2 \cdot (1.0)H_2O$ (not superconducting). Many variables of the hydration process are still not known at the moment (exchange rate dependence on *x*, temperature, time, etc.), and hence to reproduce the same exact compositions is a trial and error process.

In any case, we have observed a mixture of phases with different degrees of hydration (y= 0.6, 1.2; Figure 5.13), which makes difficult a more reliable determination of the amount of intercalated/substituted water in the superconducting phase. This was previously observed also in hydrated samples with lower Na^+ content.[225] In view of our results, we demonstrate that SC can be induced at $x \approx 0.5$, after suppression of the magnetic phase by topotactic replacement of H_3O^+ by Na^+ at moderate temperatures.

The phase diagram for this system should probably consider a magnetically ordered phase at an [electron]/[hole] ratio of ≈1, that is progressively suppressed by a decrease of dimensionality (we never observed coexistence of the magnetic and superconducting phases), see Figure 5.14. It also follows from our results that the right place to look for superconductivity through the introduction of neutral, nonaqueous spacers (e.g., supercritical CO_2, etc) is probably $Na_{0.5}CoO_2$ rather than $Na_{0.3}CoO_2$.

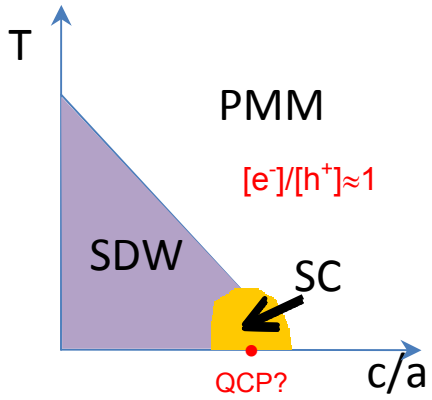

Figure 5.14: *Schematic qualitative phase diagram proposed for the system $Na_{0.5-x}(H_3O^+)_xCoO_2 \cdot yH_2O$. SDW, SC and PMM stand for spin-density wave, superconductor and paramagnetic metal.*

6. Topotactic Cation exchange in Na_xCoO_2: Li^+, Ca^{2+}, Sr^{2+}

Other layered oxides M_xCoO_2 (M= Li^+, Ca^{2+}, Sr^{2+}) have been also synthesized during the course of this thesis. Li_xCoO_2 has been obtained directly by solid state reaction while the others (M= Ca^{2+}, Sr^{2+}) have been synthesized from the corresponding layered Na_xCoO_2 precursor through the low temperature ion exchange (topotactic) reaction. The main purpose of this part was to explore the electronic/magnetic phase diagram of other isostructural compounds with Li^+ and 2^+-ions at the Na^+ site. In this chapter, the structural, magnetic and transport properties of the resulting M_xCoO_2 layered compounds will be described and compared with Na_xCoO_2.

Low-temperature ion-exchange reactions provide an important and simple route to synthesize metastable materials. In this chapter we will focus specifically on topotactic cation exchange reactions, although some of the compounds described below were obtained from direct solid state reactions.

A topotactic reaction is characterized by some internal atomic similarity between the initial and fianal structures. This technique is the only option to obtain an interesting group of isostructural and metastable materials which would be not accessible by standard high temperature routes or direct synthesis. Although the monovalent-for-monovalent exchange reactions are much more common than multivalent-for-monovalent ones, there are several examples that demonstrate the usefulness of such reactions: like $H_2Ti_3O_7$[226], HNb_3O_8,[227] β''-alumina[228], ferrites[229], niobates[230] or double-layered perovskites[231]. In many cases, these exchange reactions have led to new compounds or new structural phases of already existing compositions.

In particular, the Na_xCoO_2 compounds present a high mobility of the Na^+ ions between the CoO_6 layers, so it is well suited for ion exchange. Some examples of monovalent-for-monovalent ion exchange reactions in the Na_xCoO_2 system were carried out with Li^+ and Ag^+, resulting in $LiCoO_2$ with a metastable *O2*-type structure and Ag_xCoO_2 delafossite-type oxides[232,233], respectively. However, divalent-for-monovalent ion exchange reactions in M_xCoO_2 materials are far less usual. One example found in the literature is the ion exchange of α-$NaFeO_2$ with Mg^{2+} and Ni^{2+}, yielding spinel-like magnesium and nickel ferrites[229]. Specifically, in the Na_xCoO_2 system, we were interested in exchanging Na^+ for other divalent cations as Ca^{2+} and Sr^{2+} and check the effect of an increase of the cation charge in the physical properties of the new resulting compounds.

---

[226] H. Izawa, S. Kikkawa and M. Koizumi. *J. Solid State Chem.* **69**, 336 (**1987**)

[227] R. Nedjar, M. M. Borel and B. Raveau. *Mater. Res. Bull.* **20**, 1291 (**1985**)

[228] S. Sattar, B. Ghosal, M. L. Underwood, H. Mertwoy, M. A. Saltzberg, W. S. Grydrych, G. S. Rohrer and G. C. Farrington. *J. Solid State Chem.* **65**, 231 (**1986)**.

[229] O. Kalogirou. *J. Solid State Chem.* 102, 318 (1993).

[230] R. Nedjar, M. M. Borel, A. Leclaire and B. Raveau. *Mater. Res. Bull.* **23**, 497 (**1988**).

[231] K. G. S. Ranmohotti , E. Josepha , J. Choi , J. Zhang and J. B. Wiley. *Adv.Mater.* **23**, 442 (**2011**).

[232] C. Delmas, J. Braconnier and P. Hagenmuller. *Mater. Res. Bull.* **17**, 117 (**1971**).

[233] Y.-J. Shin, J.-H. Kwak and S. Yoon. *Bull. Korean Chem. Soc.* **18**, 775 (**1997**).

6.1. Monovalent cation exchange

6.1.1. Li_xCoO_2

$LiMO_2$ oxides exhibit easy lithium intercalation/deintercalation properties and have been used as cathodes for lithium ion cells[234]. It has the *O3*-type structure with three CoO_2 sheets per unit cell with an *ABCABC* stacking, in which the Li^+ ions occupy octahedral sites. On the other hand, $Na_{0.7}CoO_2$ has the P2-type structure with two CoO_2 sheets per unit cell, in which the Na^+ ions occupy trigonal prismatic sites. This is one of the reasons why $LiCoO_2$ material presents better electrochemical properties that allows it to be used in lithium ion cells. The lower energy cost needed to move the Li^+ ions through the structure and its lower size/mass provides it a higher ionic movility in comparison to $Na_{0.7}CoO_2$.

In this case, we attempted the synthesis of $LiCoO_2$ by direct solid state reaction, from Li_2CO_3 and Co_3O_4 at 900 ºC for 24 h in air. The reactants were mixed and grinded in an excess of 2% of Li with respect to the stochiometric molar amounts, to compensate for the evaporation of lithium that may ocurr during the high temperature firing.

The extraction of lithium at ambient temperature provides a convenient route to access Li_xMO_2 phases that are otherwise inaccessible by direct high-temperature synthetic procedures. Chemical extraction of lithium from $LiCoO_2$ was achieved by stirring $LiCoO_2$ powder in 25mL of an oxidizer Br_2/acetonitrile solution under air for 2 days (see Chapter 1 for a similar procedure in $Na_{0.7}CoO_2$), following:

$$Li_xCoO_2(s) + \left(\frac{y}{2}\right)Br_2(l) \leftrightarrow Li_{x-y}CoO_2(s) + y\,Li^+ + y\,Br^-$$

Products with different Li^+ contents can be achieved by controlling the ratio of $LiCoO_2$ to Br_2 in the reaction medium. In this way, different excesses of Br_2 with respect to the stoichiometric amounts needed to deintercalate all the lithium present in $LiCoO_2$ were used to achieve different Li_xCoO_2 samples. The Br_2 excesses used were $\times$0.5, $\times$1 and $\times$10 (being $\times$1 the stochiometric amount of Br_2 needed to extract all the lithium in the

[234] K. Kizushima, P. C. Jones, P. J. Wiseman and J. B. Goodenough. *Mater. Res. Bull.* **15**, 783 (**1980**).

$LiCoO_2$ precursor). After that, the products were filtered, washed several times with acetonitrile to remove the Li^+ and Br^- ions and finally dried in a vacuum desicator, where they were stored.

In order to obtain a Li_xCoO_2 sample with the lowest Li^+ content as possible, Li^+ extraction was carried out by stirring $LiCoO_2$ powder in 25mL of an acetonitrile solution with a stronger oxidizer, NO_2BF_4, under an Ar atmosphere for 2 days. Strong oxidizers as NO_2PF_6 or NO_2BF_4 have been used to deintercalate Li^+ from $LiCoO_2$. For instance, *Chebaim et al* [235,236] showed that bulk samples of CoO_2 free from carbon and binder can be synthesized successfully by chemically extracting lithium from $LiCoO_2$ at ambient temperatures with NO_2PF_6 in acetonitrile. In this way, a Li:NO_2BF_4 molar ratio of 1:1 was used following the reaction below,

$$LiCoO_2\,(s) + y\,NO_2BF_4(l) \leftrightarrow Li_{1-y}CoO_2\,(s) + y\,NO_2 + y\,LiBF_4$$

Due to the high reactivity of NO_2BF_4 and the possibility of its decomposition prior to use and other parallel reactions, the experiments invariably required higher amounts of the oxidizer than would be expected on the basis of the stochiometry of the reaction to achieve a specific value of lithium content in $Li_{1-x}CoO_2$. For this reason, in order to finally obtain the lowest Li^+ content as possible, we used a high excess of NO_2BF_4. The Li_xCoO_2 products formed were filtered, washed repeatedly with acetonitrile under an argon atmosphere to remove $LiBF_4$, and dried under vacuum at room temperature in a desicator. After drying, the reaction flasks were opened in an argon-filled glovebox to avoid any reaction of the samples with ambient air.

The excesses of the oxidazing agent used in the Li^+ extraction process and the approximate Li^+ content of the resulting samples are summarized in the Table 6.1.

[235] R. V. Chebaim, F. Prado and A. Manthiram. *Chem. Mater.* **13**, 2951 (**2001)**.
[236] R. V. Chebaim, F. Prado and A. Manthiram *J. Solid State Chem.* **163**, 5 (**2002)**.

Table 6.1: *Li^+ content of the samples in the Li_xCoO_2 serie.*

Sample	Oxidazer	Excess of oxidazer	Li^+ content (x)
A	-	-	1
B	Br_2	×0.5	0.74≤x≤0.94
C	Br_2	×1	0.5≤x≤0.74
D	Br_2	×10	<0.50
E	NO_2BF_4	×1	0.45
F	NO_2BF_4	×2	<0.50

The lithium content in our Li_xCoO_2 samples was determined by comparison of the corresponding XRD patterns to those ones reported by *Venkatram et al*[237], where they associated to each difractogram a specific Li^+ content determined by atomic absorption spectroscopy analysis. Figure 6.1 shows the X-ray diffraction patterns of Li_xCoO_2 samples obtained after chemical treatment with different oxidizers. The $LiCoO_2$ precursor obtained directly from the synthesis is a single phase belonging to a rombohedral symmetry space group *R-3m* (nº160), with the lattice parameters *a=2.8174(1) Å* and *c=14.0635(2) Å*, in good agreement with those previously reported[238,239,240]. According to the structural results from *Venkatram et al*[237], the initial *O3*-type structure and the rombohedral symmetry (R-3m) of the precursor, *x*=1 (pattern *A*), is maintained over the whole range of Li_xCoO_2 compositions within the range 0.5≤x≤1 (patterns *B*, *C*), as well as the narrowness of the lines and the crystallinity. In patterns *D*, *E* and *F*, the original *(006)* reflexion dissapears completely, indicating a lithium content x≤0.5. Specifically, pattern *E* reproduces exactly the XRD pattern from *Venkatram et al*[237] in which the presence of a small shoulder on the right side of the strong *(003)* reflexion (marked as an asterisk in the Figure 6.1) was suggested to correspond to a lithium composition around *x*=0.45. According to these authors, it indicates the formation of another phase that

[237] S. Venkatram and A. Manthiram. *Chem. Mater*. **14**, 3907 (**2002**).
[238] T. Motohashi, Y. Katsumata, T. Ono, R. Kanno, M. Karppinen and H. Yamauchi. *Chem. Mater*. **19**, 5063 (**2007**).
[239] M. Ménétrier, I. Saadoune, S. Levasseur and C. Delmas. *J. Mater. Chem*. **9**, 1135 (**1999**).
[240] S. Levasseur, M. Ménétrier, E. Suard and C. Delmas. *Solid State Ionics*, **128**, 11 (**2000**).

growths with further Li^+ extraction below x<0.45, where a mixture of both *O3-* and *P3-type* phases were considered. In pattern *F* this reflexion is totally absent, in agreement with a phase with a lithium composition very close to *x*=0.5. However, the position of the *(003)* reflexion at the lowest angles indicates that sample F has the lowest Li^+ content in the series.

A closer inspection of the evolution of the (003) reflexion during Li^+ deintercalation is shown in Figure 6.2. We can clearly observe how it is displaced to lower angles with decreasing Li^+ content, confirming our assumptions derived from the XRD results about the progressive decrease of the lithium content with the excess and strenght of the used oxidazer. It is important to remark that in pattern *B* this *(003)* reflexion is actually the contribution of two different peaks. The gradual dissapearance of the original peak (2θ = 18.84º) and the appearance of a new one at lower angle (2θ = 18.61º) during further lithium extraction indicate the existence of a two-phase domain for $0.75 \leq x \leq 0.94$, in very good agreement with the X-ray studies previoulsy reported[239,241] (although at slightly different values of 2θ).

The existence of a two phase region has been also observed in the electrochemical Li^+ deintercalation/intercalation in Li_xCoO_2.[242] The voltage-composition curve decreases continuously as Li^+ is intercalated and shows a plateau at $0.75<x<0.95$, indicative of a phase transition along these Li^+ compositions.

The nature of this structural phase transition was deeply discussed and it was suggested to be associated to an electronic delocalization ocurring at that Li^+ composition[239].

However, it is important to note that some of the XRD patterns from our deintercalated samples do not follow the gradual displacement (D and E) probably due to mixtures of different phases. This is mainly due to the inhomogeniety of the chemically deintercalated samples. Similar to Na_xCoO_2 the interlayer spacing increases as the Li^+ content decreases due to higher electrostatic repulsion forces between charged CoO_2 layers.

[241] J. N. Reimers and J. R. Dahn. *J. Electrochemical Soc.* **139**, 2091 (**1992**).

[242] S. S. Prasad. *Handbook of solid state batteries and capacitors.* Ed. by M. Z. A. Munshi. World Scientific Publishing. Co. Pte. Ltd. Singapure (1999).

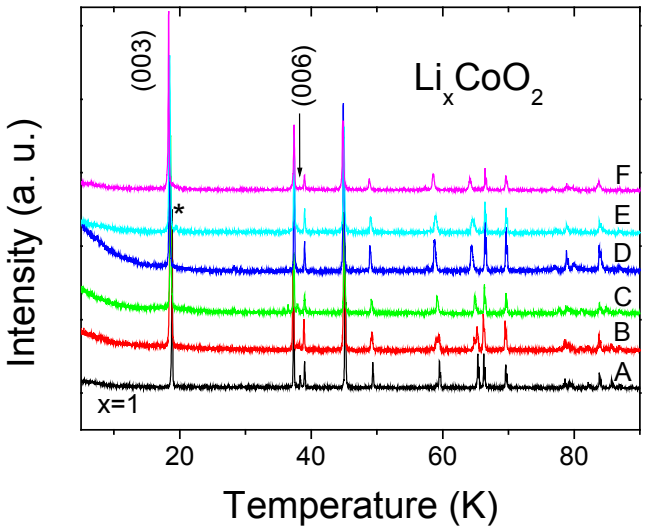

Figure 6.1: *X-ray diffraction patterns of Li_xCoO_2 samples.* The asterisc (∗) indicates the new reflexion corresponding to a *P3* phase.

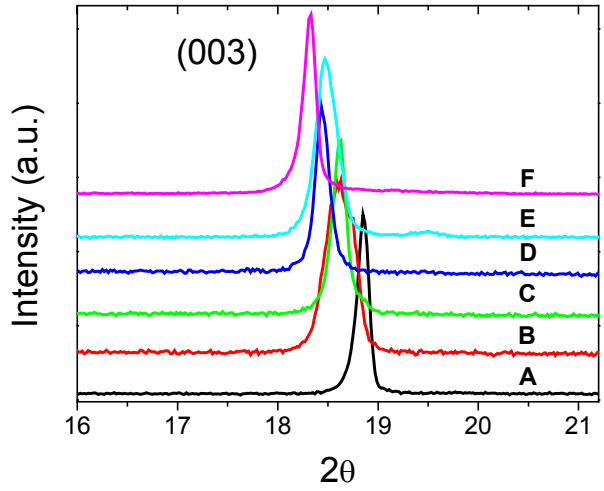

Figure 6.2: *Evolution of the (003) reflexion to lower angles as Li^+ content decreases.*

The lattice parameters for all the samples were determined by Lebail refinements with Rietica considering the rombohedral simmetry group *R-3m* (Table 6.2), and their evolution as a function of the Li^+ content is shown in Figure 6.3.

Table 6.2: *Lattice parameters of Li_xCoO_2 after refinements with Rietica.*

Sample	Li^+ content, x	a=b	c
A	1	2.8174(1)	14.0635(2)
B	0.75≤x≤0.95	2.8132(1)	14.0553(1)
C	0.5≤x≤0.75	2.8130(1)	14.2090(3)
D	<0.50	2.8111(1)	14.3828(3)
E	0.45	2.8165(1)	14.330(1)
F	<0.45	2.8093(1)	14.4657(3)

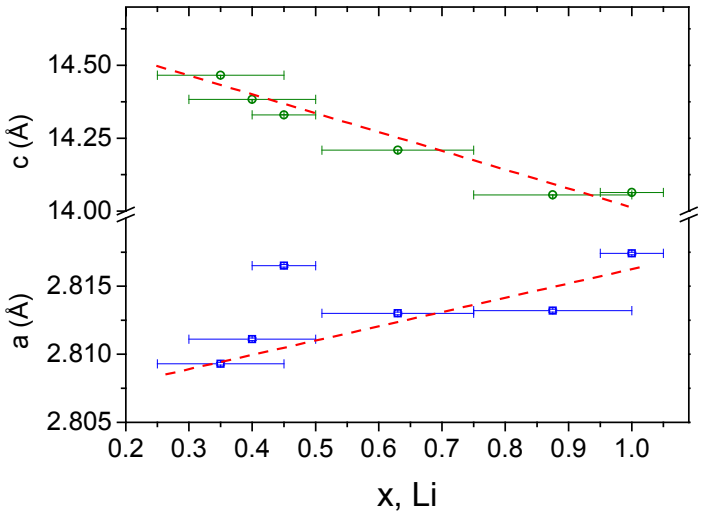

Figure 6.3: *Evolution of the lattice parameters of Li_xCoO_2 determined by lebail refinements of the x-ray powder patterns. Dashed lines are a guide for the eye (sample E showed an a-lattice parameter anomoulsy higher than expected and it was not considered in order to show the general trend).*

We observed a strong increase of the unit cell in the *c*-direction (about 3% of the original distance) as Li^+ content decreases. At the same time, the *a*-lattice parameter decreases, although the reduction is one order of magnitud lower than in the case of the *c*-lattice parameter, about 0.3%. If we compare the evolution of the lattice parameters from Li_xCoO_2 to that one in Na_xCoO_2 (see Figure 1.7 in Chapter 1), we can observe a similar increase in the *c*-direction, although the compression of the unit cell in the *a*-direction is about ~3.4 times smaller, $\Delta a / a_0 = 9.87\text{x}10^{-3}$ *(Na)* and $2.87\text{x}10^{-3}$ *(Li),* within the maximum and minimum compositional range in each case (0.7<x<0.3 and ~0.35<x<1 for Na and Li cobaltates, respectively).

However, the *c/a* ratio in Li_xCoO_2 showed in Figure 6.4 does not reach a plateau below x~0.55 indicating that the extraction is more effective in this system and does not produce oxygen losses.

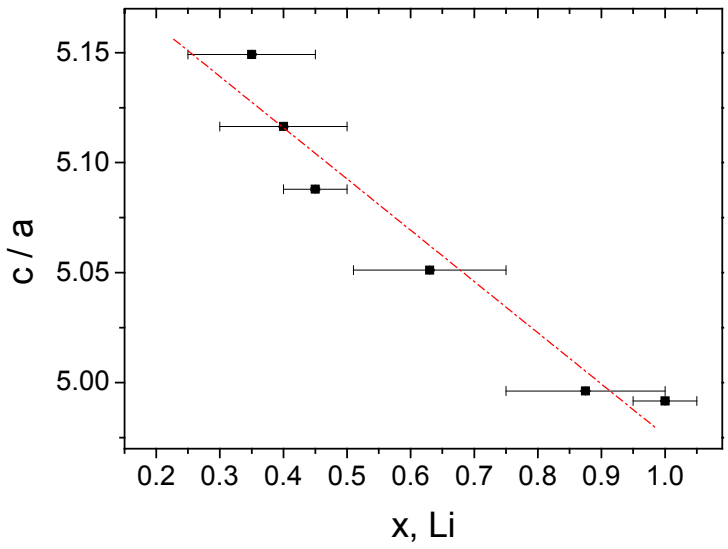

Figure 6.4: *Evolution of the c/a ratio in Li_xCoO_2. Line is a guide for the eye.*

The results of the magnetic susceptibility measurements on representative Li_xCoO_2 samples are displayed in Figure 6.5. The magnetic properties of Li_xCoO_2 were studied for samples A, C and E (x=1, 0.5<x<0.75 and x=0.45, respectively) in the temperature range 5K<T<270K.

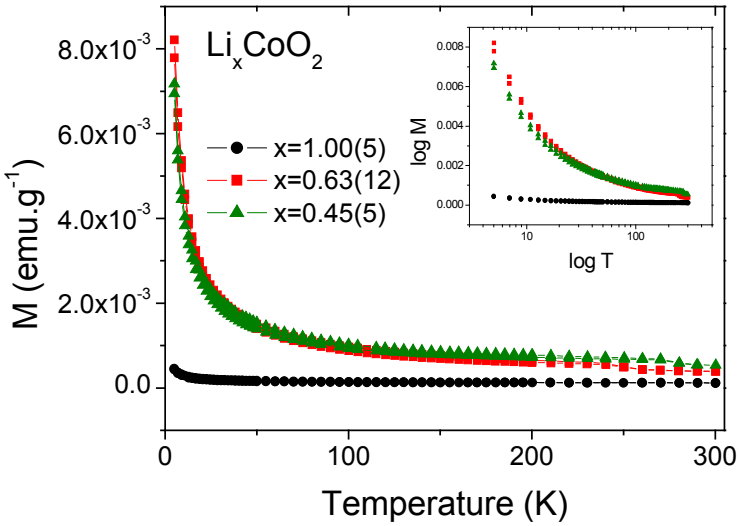

Figure 6.5: *ZFC-FC magnetic curves for representative Li_xCoO_2 samples under an applied magnetic field of 100Oe (x=1, 0.5≤x≤0.75, x=0.45).*

No magnetic ordering is observed in any of the samples down to the lowest temperature measured (T=5 K). Magnetic anomalies at T=175 K previously reported by other authors[243] were not observed in our samples. Similary to the low Na^+ content samples, the magnetic susceptibility of $LiCoO_2$ is low and practically temperature independent in the range 50K<T<270K. This temperature independent magnetic contribution to the susceptibility decreases as the Li^+ content decreases. Figure 6.5 shows a significant CW-like character in the susceptibilities of Li_xCoO_2 at low temperatures, even in the case of x=1, which is formed by non-magnetic Co^{3+} ions. This divergency in the *M(T)* curve at low temperatures is much more evident as the Li^+ content decreases, reaching a value of

[243] J. T. Hertz, Q. Huang, T. McQueen, T. Klimezuk, J. W. G. Bos, L. Viciu and R. J. Cava. *Phys. Rev. B* **77**, 075119 (**2008**).

magnetization four times higher than that observed in $LiCoO_2$. These results are in good agreement with the magnetic results from *Levasseur et al*[244].

Figure 6.6 shows Curie-Weiss fits performed using the equation [3.4] in chapter 2. The fitted values of χ_0, C, θ and μ_{eff} are shown in Table 6.3 and the value of χ_0 calculated was used to plot the temperature dependence of $1/(\chi-\chi_0)$ for each sample in Figure 6.7. In order to calculate the effective magnetic moments in each case, the molecular weights of the unit formulas were determined by assuming a Li^+ content x=1±0.05 for sample A, x=0.63±0.12 for sample C and x=0.45±0.05 for sample E. The data behave as expected for a Curie-Weiss behaviour for x=0.63±0.12 and x=0.45±0.05 (the fits are linear), whereas slight deviations from the linearity are noticed at high temperature for x=1±0.05.

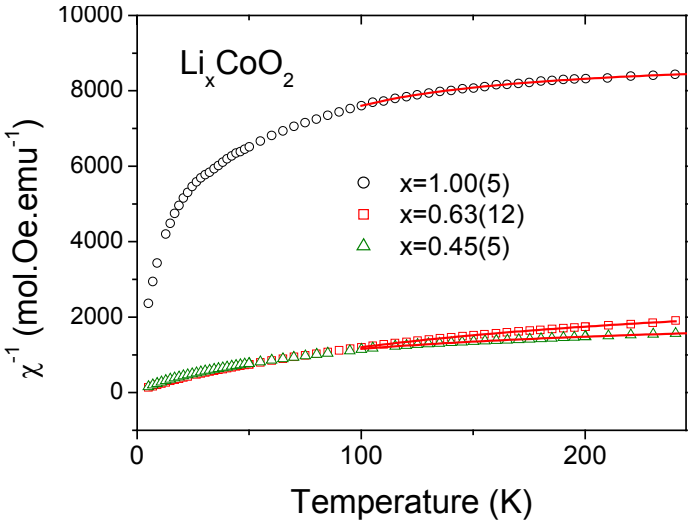

Figure 6.6: *Temperature dependence of the inverse of the susceptibility for three representative samples of Li_xCoO_2.*

[244] S. Levasseur, M. Ménétrier, Y. Shao-Horn, L. Gautier, A. Audemer, G. Demazeau, A. Largeteau and C. Delmas. *Chem. Mater.* **15**, 348 (**2003**).

Table 6.3: *Magnetic characterization of Li_xCoO_2.*

x, Li	χ_0 ($emu.mol^{-1}.Oe^{-1}$)	C ($emu.K.mol^{-1}.Oe^{-1}$)	Θ_{CW} (K)	μ_{eff} (μ_B)	T_range (K)
1.00(5)	$1.1(2)\times10^{-4}$	$16(1)\times10^{-4}$	21(3)	0.11(6)	100-270
0.63(12)	$3.1(6)\times10^{-4}$	0.05(8)	2(5)	0.6(1)	100-240
0.45(5)	$4.5(3)\times10^{-4}$	0.05(1)	−18(9)	0.63(8)	100-270

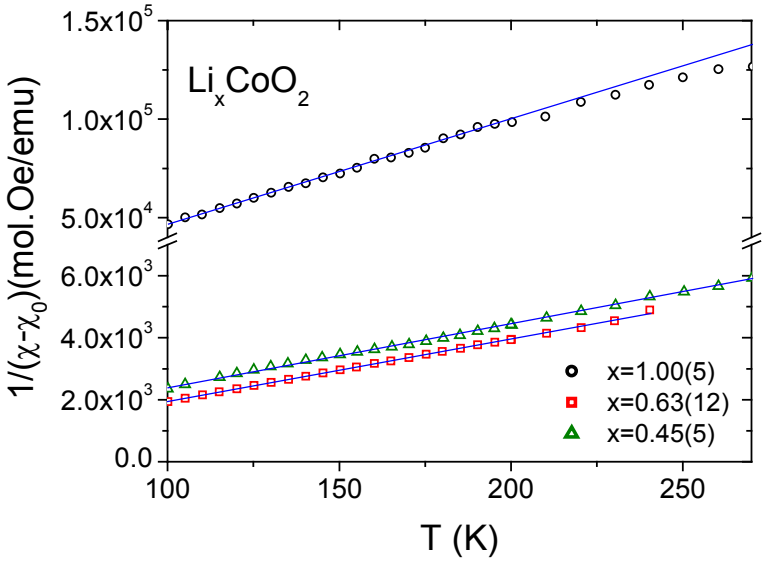

Figure 6.7: *The temperature dependence of $1/(\chi-\chi_0)$ for three representative Li_xCoO_2 samples above and below the two-phase domain over the range $100K \leq T \leq 270K$.*

Figure 6.8 shows the variation of the effective magnetic moment per Co as a function of the Li^+ content in Li_xCoO_2. The effective magnetic moment depends on the average oxidation state of cobalt, which is strongly related to the amount of Li^+ in the compound. However, it has been reported that this relationship is not direct in the whole range of *x* for Li_xCoO_2[237].

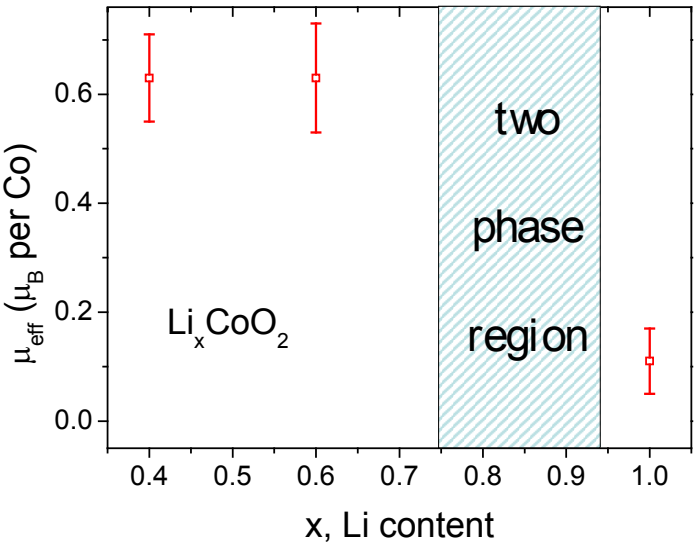

Figure 6.8: *Variation of μ_{eff} per Co atom with x for Li_xCoO_2.*

Lithium deintercalation is accompained by the formal oxidization of a cobalt atom from the non-magnetic Co^{3+} (t_{2g}^6 e_g^0, S=0) to the magnetic Co^{4+} (t_{2g}^5 e_g^0, S=1/2). Taking this into acount, and assuming a spin localized scenario, the μ_{eff} due to the unpaired spins present in Co^{4+} is expected to increase with decreasing lithium. In fact, our results show a significant increase of the μ_{eff} from x~1 to x~0.63, lithium compositions at both sides of the two-domain phase region. The fact that the values for x~0.63 and x~0.45 are coincident agrees with previous results from *Hertz et al*[243] and *Venkatram et al*[237], although our values are slightly higher (μ_{eff}~0.6 μ_B). The latter showed an evolution of the oxidation state of the Co ion as a function of the Li^+ content, which remains unchangeable below *x*=0.6 at around +3.45.

We can also observe that the nominally stoichiometric $LiCoO_2$ sample also exhibits a small magnetic moment, which is not justified if all the Co atoms are in the oxidation state +3. It suggests the existence of a few Co^{4+} ions in the starting oxide, which could be due to a small departure from the stoichiometry. This interpretation was also assumed previously by other authors in order to explain the electronic[245] and magnetic properties[243] of $LiCoO_2$.

The more stable spin configuration of the $Co^{3+/4+}$ ions in Li_xCoO_2 ($x \leq 1$, otherwise the possible presence of Co^{2+} should be considered), has been a matter highly discussed. Although the spin state of Co^{3+} and Co^{4+} ions in both Na_xCoO_2 and Li_xCoO_2 compounds are generally found to be in their low-spin d^6 and d^5 configurations[246,247], other authors as *Molenda et al*[248], and more recently *Hertz et al*[243], explained their results under the hypothesis of trivalent and tetravalent cobalt in the high spin configuration, respectively, in spite of the strong stabilization of the t_{2g}^6 configuration[232,249] due to Co-*3d*:O-*2p* hybridization.

We analized our calculated effective magnetic moments shown in Table 6.3 considering the low spin configuration for the Co^{4+} ion (S=1/2, 1.73 μ_B) and the oxygen vacancies determined at those Li^+ compositions by S. Venkatram *et al*[237]. According to this, we deduce an actual stoichiometry for nominal $Li_{\sim 1}CoO_2$ that corresponds to $Li_{0.93}CoO_2$. However, assuming the hypothesis of a high spin state at this composition in which the Co^{4+} ion has 5 unpaired electrons and exhibits an effective magnetic moment of $5.92\mu_B$, the new stoichiometry corresponds to $Li_{0.98}CoO_2$, which is closer to the nominal composition. This Li^+ composition would explain the presence of magnetism in the Li parent compound. Similarly, for $Li_{\sim 0.63}CoO_2$ exhibing the observed effective moment of 0.632 μ_B, the fraction of Co^{4+} present would lead to a stoichiometry of $Li_{0.63}CoO_2$ if we assume a low-spin configuration, which agrees quite well with that one expected $x \sim 0.63$. These results support the hypothesis of a spin state transition of Co^{4+} in Li_xCoO_2 from high spin at compositions above the two domain region to low spin at compositions below the two phase region.

Regarding the electronic properties, *Menetrier et al*[239] and *Molenda et al*[248] showed a very strong increase in conductivity upon Li^+

[245] A. Honders, J. M. der Kinderen, A. H. Van Heeren, J. H. W. de Witt and G. H. J. Broers. *Solid state ionics* **14**, 205 (**1984**).
[246] I. Terasaki, Y. Sasago and K. Uchinokura. *Phys. Rev. B* **56**, R12685 (**1997**).
[247] M. H. Whangbo, D. Dai and R. K. Kremer. *Inorg. Chem.* **45**, 5989 (**2006**).
[248] J. Molenda, A. Stoklosa and T. Bak. *Solid State Ionics* **36**, 53 (**1989**).
[249] Saadoune and C. Delmas. *J. Solid State Chem.* **136**, 8 (**1998**).

deintercalation. They observed semiconductor behaviour for the lithium-rich phases and metallic for those more deintercalated, implying a semiconductor-metallic transition at intermediate Li^+ concentrations ($x<0.75$).

Co-*3d* bands in $LiCoO_2$ split into the Co-t_{2g} valence band and the Co-e_g conduction band as a consequence of the ligand field around the Co atoms in CoO_6; this is strong enough to stabilize a Co^{3+} low spin state[250, 251]. The semiconductor behaviour of $LiCoO_2$ could be explained by the departure from the ideal lithium stoichiometry and the presence of a few Co^{4+} ions in the starting Co^{3+} lattice, in agreement with our magnetic results. This hypothesis is consistent with ^{7}Li NMR of Li_xCoO_2 in the solid solution $0.94<x\leq1.0$[239].

Extraction of Li^+ from $LiCoO_2$ introduces holes through oxidation of the Co^{4+}/Co^{3+} redox pair in the way of Co^{4+} ions. Due to the strong covalency of the O-*2p* and Co-*3d* states, the new holes have a strong *2p* character, as observed by X-ray photoemision spectroscopy[252,253].

Thermoelectric power for Li_xCoO_2 was measured as a function of temperature in the range $15K\leq T\leq450K$ (Figure 6.9). The positive values of the Seebeck coefficient in the whole temperature range evidence the hole-like character of the charge carriers. However, differences were found between different Li_xCoO_2 compositions. For x=1, *S(T)* saturates below ~100 K due to the small conductivity of the sample. These results are in good agreement with the electronic conductivity and transport measurements previously reported[239]. Above 300K, the thermoelectric power is temperature independent, around 250 $\mu V.K^{-1}$. For x~1 the generalized Heikes approximation predicts a TEP of 335 μV/K, higher than the experimental value found of 250 μV/K. However, if we take into acount the term introduced by *Koshibae et al*[254], that includes the different possible spin configurations of the Co^{3+} and Co^{4+} ions, in a situation where the LS and HS states of Co^{3+} are very close in energy and the HS state of Co^{4+} site is stable, g_3/g_4=16/6, the TEP predicted is 251 μV/K, in perfect agreement with both experiment and assumption of high spin state for Co^{4+} at high x, as deduced from our magnetic results.

---

[250] M. K. Aydinol, A. F. Kohan, G. Ceder, K. Cho and J. Joannopoulos. *Phys. Rev. B* **56**, 1354 (**1997**).
[251] C. Wolverton and A. Zunger. *Phys. Rev. Lett.* **81**, 606 (**1998**).
[252] K. Kushida and K. Kuriyama. *Solid State Comm.* **129**, 525 (**2004**).
[253] V. R. Galakhov, N. A. Ovechkina, A. S. Shkvarin, S. N. Shamin, E. Z. Kurmaev, K. Kuepper, A. F. Takács, M. Raekers, S. Robin, M. Neumann, G.-N. Gavrilă, A. S. Semenova D. G. Kellerman, T. Käämbre and J. Nordgren. *Phys. Rev. B* **74**, 045120 (**2006**).
[254] W. Koshibae, K. Tsutsui and S. Maekawa. *Phys. Rev. B* **62**, 6869 (**2000**).

For Li^+ deintercalated samples the values of the Seebeck coefficient are much lower, as a consequence of the oxidation of the Co^{3+} ions to Co^{4+} and the consequent increase in the number of charge carriers. Similar to Na_xCoO_2 at high *x*, these samples show a linear temperature dependence below 100 K, and a slow tendency towards saturation as temperature increases. A more detailed study is needed in order to explain the thermoelectric behavior in Li_xCoO_2 below the two phase domain region.

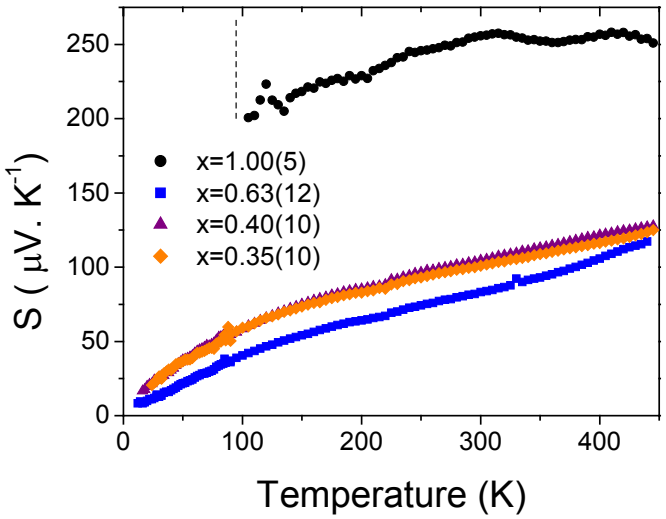

Figure 6.9: *Temperature dependence of the thermopower with temperature for Li_xCoO_2. Dashed line indicates the temperature which S(T) for $Li_{1\pm0.05}CoO_2$ is saturated.*

6.2. Divalent cation exchange

6.2.1. Sr_xCoO_2

B. Cushing et al[255] developed a new method of replacing monovalent ions with divalent ones using a low-temperature ion exchange technique. *R. Ishikawa et al*[256] adopted this experimental procedure for strontium substitution and they succeeded in synthesizing a new cobaltite, Sr_xCoO_2, from a Na_xCoO_2 precursor with x=0.7. Here, we itend take advantage of this ion exhange technique and replace Sr^{2+} for Na^+ in our Na_xCoO_2 precursors.

The low-temperature ion exchange reaction that takes place is the following:

$$Na_xCoO_2 + \left(\frac{x}{2}\right)Sr(NO_3)_2 \rightarrow Sr_{x/2}CoO_2 + x\,NaNO_3$$

Powder of $Na_{0.7}CoO_2$ precursor was mixed thoroughly with 10% molar excess anhydrous $Sr(NO_3)_2$ and pressed into 12 mm pellets. The pellets were placed in an alumina and heated at 310 ºC for 24 h under O_2 gas flow. The $NaNO_3$ byproduct or any excess of $Sr(NO_3)_2$ were removed by repeating grinding the products under distilled water. After that, the filtered powder was dried at 120 ºC in air for 1h and stored in an argon-filled glove box.

The chemical composition of the sample was determined by ICP-OES spectroscopy and confirmed by EDAX analysis of individual crystallites, resulting to be Sr/Co=0.35(1). It is important to point out that the divalent character of the strontium cations results in the insertion of an amount of Sr^{2+} ions exactly equal to half the original amount of Na^+ in the precursor, to keep the charge neutrality of the compound. In addition, the XRD pattern coincides exactly with that one reported by *Ishikawa et al*[256], which shows that $Sr_{0.35}CoO_2$ is isomorphic to $Na_{0.7}CoO_2$, with the hexagonal space group *P63/mmc* (Nº194), Figure 6.10.

---

[255] B. L. Cushing, A. U. Falster, W. B Simmons and J. B. Wiley. *Chem. Comm.* **23**, 2635 (**1996**).
[256] R. Ishikawa, Y. Ono, Y. Miyazaki and T. Kajitani. *Jpn. J. Appl. Phys.* **41**, 337 (**2002**).

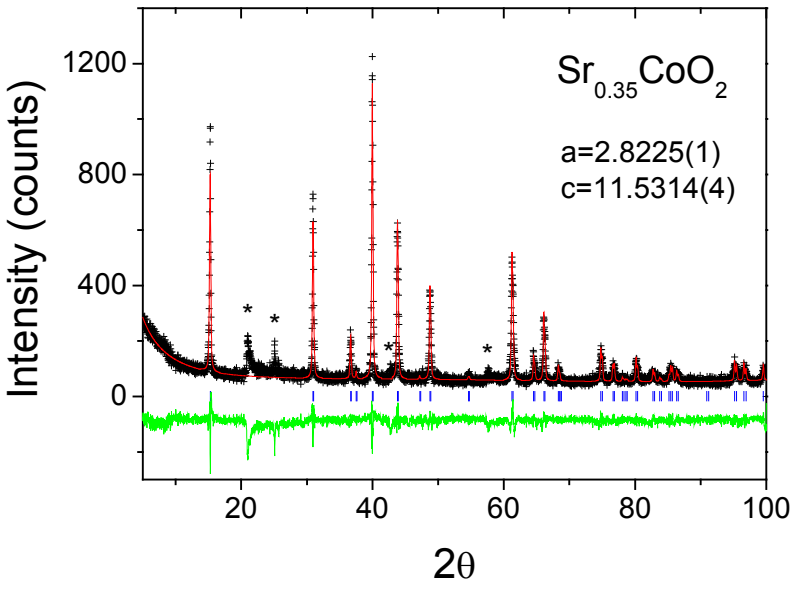

Figure 6.10: *X-ray diffraction pattern (+) and lebail fitting (red line) of $Sr_{0.35}CoO_2$ sample considering the P63/mmc symmetry group. Vertical blue lines mark the expected position of the reflexions of the space group P63/mmc. Green line is the difference between the experimental and calculated intensities. Asterisks mark reflexion that we were unable to identify. The lattice parameters are also shown.*

The attemps to synthesize Sr_xCoO_2 with x<0.35 by Sr^{2+} deintercalation with Br_2 from $Sr_{0.35}CoO_2$ was not succesful. Different excesses of Br_2 with respect the needed amount to deintercalate all the Sr^{2+} present in the Sr^{2+} precursor, ×0.5 (sample A) and ×10 (sample B), were checked in order to evaluate the efficiency of the deintercalation method for divalent cations. However, we have observed that the extraction of divalent cations is not possible through these oxidative reactions.

However, we were able to obtain different Sr/Co ratios by starting with different precursors Na_xCoO_2 0.3<x<0.7. Figure 6.11 shows the XRD patterns of two Sr_xCoO_2 samples (x=0.35, x=0.22) obtained through topotactic ion exchange reaction from the corresponding Na^+ precursors (x=0.7 and x=0.44, respectively) (lower pannel), and also those corresponding to $Sr_{0.35}CoO_2$ after different oxidative treatments in order to adress the strontium deintercalation (upper pannel).

The symmetry of the structure keeps unvariable in all the samples and can be indexed considering the *P63/mmc* space group. This confirms that $Sr_{0.35}CoO_2$ and $Na_{0.7}CoO_2$ are isomorphic.

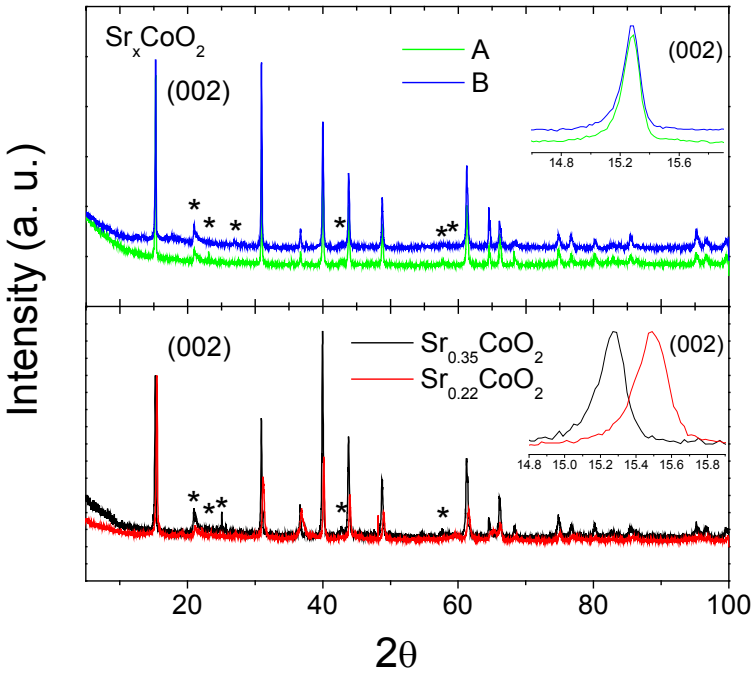

Figure 6.11: *X-ray diffraction patterns of Sr_xCoO_2: (Upper) A and B samples corresponding to attempts of Sr^{2+} deintercalation from $Sr_{0.35}CoO_2$ at different Br_2* excesses (x0.5 and x10, respectively). *(Lower) x=0.35 and x=0.22. The asterisks mark the reflexion peaks not identified. Insets show the position of the (002) reflexion peak indicating the inefficiency of the method to obtain different $Sr_{x<0.35}CoO_2$ samples.*

XRD analysis indicates the inefficiency of the chemical Sr^{2+} deintercalation process, as it is shown by the (002) reflexion that remains invariant after the oxidazing treatments (Figure 6.11, upper inset). In order to obtain a different Sr_xCoO_2 sample with x<0.35, the ion-exchange reaction has been carried out using a Na_xCoO_2 precursor with x<0.70. In this way, $Sr_{0.22}CoO_2$ has been obtained from the $Na_{0.44}CoO_2$ precursor. The structural

analysis of the XRD patterns showed a shift of the (002) reflexion to higher angles as Sr^{2+} content decreases (Figure 6.11, lower inset). It is very important to remark that this shift ocurrs to higher angles, in opossite to what happens in the case of Na_xCoO_2, where the displacement of the (002) reflexion with decreasing Na^+ content is toward lower angles (Figure 6.12). That means that while in the case of Na_xCoO_2 a reduction of the Na^+ content leads to an increase of the CoO_2-CoO_2 distance, in the Sr_xCoO_2 system this distance decreases as Sr^{2+} content does.

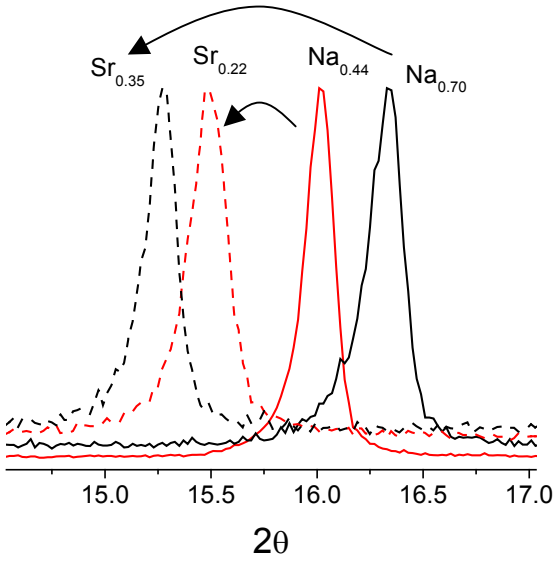

Figure 6.12: *(002) peak for Sr_xCoO_2 (x=0.35 and x=0.22) and Na^+ precursors (x=0.7 and x=0.44).*

The lattice parameters of the Sr_xCoO_2 samples were determined by lebail refinements with Rietica considering the hexagonal simmetry group *P63/mmc* (Table 6.4).

Table 6.4: *Lattice parameters of Sr_xCoO_2 samples after refinement of the XRD patterns with Rietica.*

Sample	Br_2 excess	Sr^{2+} content, x	a=b	c
$Sr_{0.35}CoO_2$	-	0.35	2.8225(1)	11.5314(4)
$Sr_{0.22}CoO_2$	-	0.22	2.8232(1)	11.4776(6)
A	×0.5	0.35	2.8225(1)	11.5348(2)
B	×10	0.35	2.8235(1)	11.5365(2)

The determination of the lattice parameters shows an almost imperceptible variation in the *ab*-plane, while a contraction in the *c*-direction is clearly observed from *x*=0.35 to *x*=0.22. If we focus on the Sr^{2+} deintercalated samples from $Sr_{0.35}CoO_2$ (samples A and B), it is confirmed again the inefficiency of the oxidative deintercalation method, since the *a* and *c*-lattice parameters are hardly modified with respect to those in the Sr^{2+} precursor, *x*=0.35.

From the thermopower measurements, Figure 6.13 shows that no significant changes are observed between the polycrystalline Sr^{2+} precursor and the lower Sr^{2+} content sample. Practically the same trend is observed for both Sr^{2+} compositions, what indicates that the Seebeck effect does not depend too much on the Sr^{2+} content in that compositional range. The temperature dependence of *S* is similar to that of $Na_{0.7}CoO_2$, suggesting the similarity of their elecronic states in the vicinity of the Fermi level. However, whereas no significant differences are observed in the thermopower between $Sr_{0.35}CoO_2$ and $Na_{0.7}CoO_2$, the *S(T)* curve for $Sr_{0.22}CoO_2$ shows higher values in comparison to its $Na_{0.44}CoO_2$ precursor. Such a difference could lie in the different variation of the enegy of $N(E_F)$ with x for both systems (it will be discussed deeper later).

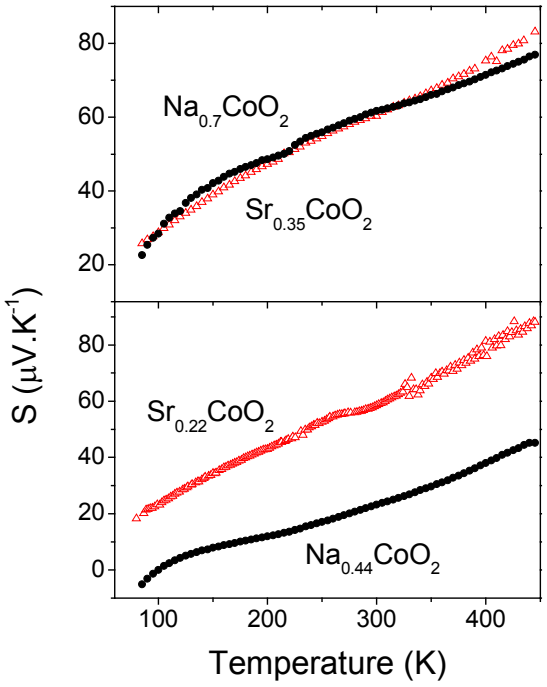

Figure 6.13: *S(T) for $Sr_{0.35}CoO_2$ and $Sr_{0.22}CoO_2$* precursors in comparison with the Na_xCoO_2 precursors *x*=0.7 and *x*=0.44, respectively.

Figure 6.14 shows the electrical resistivity for polycrystalline $Sr_{0.35}CoO_2$. It is important to remark that the electrical measurement was carried out in a *cold-pressed* powder sample obtained directly from the low-temperature ion exchange reaction, without additional annealing at higher temperatures. $Sr_{0.35}CoO_2$ exhibits metallic behaviour over the whole range of temperature measured, although the values are clearly much lower than those ones of $Na_{0.7}CoO_2$ (notice that the values of the R(T) curve for $Sr_{0.35}CoO_2$ are multiplied by a factor 10). It is important to remark that $Na_{0.7}CoO_2$ sample was additionality sinterized at 800 ºC for 12h before measuring. Otherwise, its porous morfology and hygroscopic character made impossible the electrical measurament. These results agree with

reported data in the literature both experimentally[256,257,258] and theoretically from band structure calculations[259].

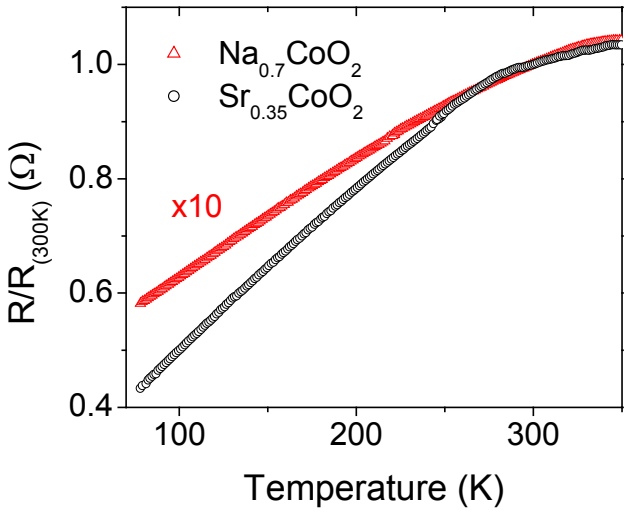

Figure 6.14: *Normalized R(T) curves for $Sr_{0.35}CoO_2$ (non-sinterized) and its corresponding $Na_{0.7}CoO_2$ precursor (sinterized). Note the R(T) curve from $Na_{0.7}CoO_2$ is multiplied x10 for a better comparison between them.*

Other authors claimed that R(T) is sensitive to the Sr^{2+} content[257], where a crossover from insulating to metallic behavior is observed with increasing x. From our results we cannot support this conclussion. At this time we only can assure that the replacement of the monovalent by divalent cation modifies the electrical properties. In order to establish a more coherent study and comparison with Na_xCoO_2, the synthesis of several Sr_xCoO_2 samples with slightly different Sr^{2+} contents with x<0.35 is needed.

[257] Y. Q. Guo, J. L. Luo, G. T. Liu, H. X. Yang, J. Q. Li, N. L. Wang, D. Jin and T. Xiang. *Phys. Rev. B* **74**, 155129 (**2006**).
[258] Y. Q. Guo, J. L. Luo, D. Wu, Z. Li, N. L. Wang, D. Jin, H. Y. Zhang and Y. G. Zhao. *Phys. Rev. B* **75**, 214432 (**2007**).
[259] R. J. Xiao, H. X. Yang, L. F. Xu, H. R. Zhang, Y. G. Shi and J. Q. Li. *Solid State Commun.* **135**, 687 (**2005**).

Figure 6.15 shows the magnetic measurements for $Sr_{0.35}CoO_2$ at different applied magnetic fields between 50 to 1000 Oe. The upper pannel shows the magnetization curve in ZFC-FC conditions just at two applied magnetic fields (50 and 1000 Oe) for a better clarity.

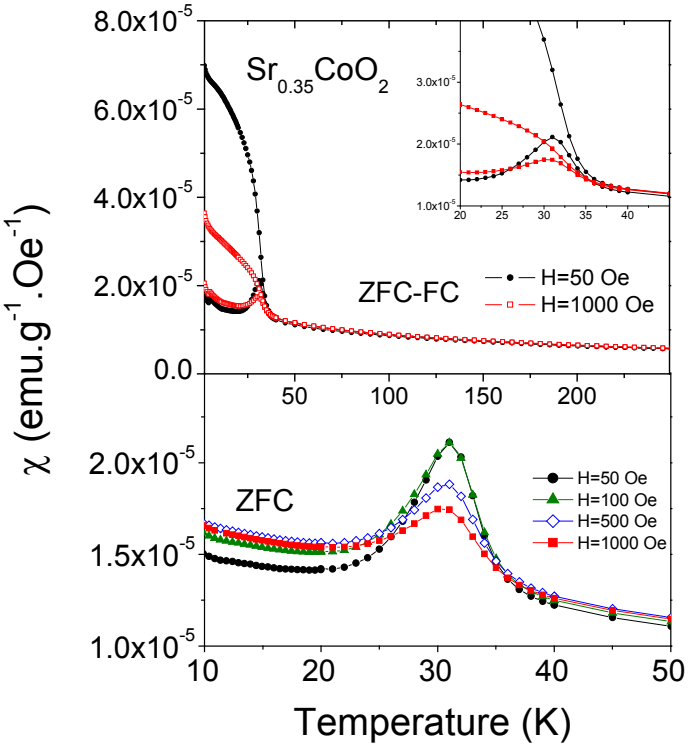

Figure 6.15: *$\chi(T)$ susceptivility curves in (upper) ZFC-FC conditions under applied magnetic fields of H=50 Oe and H=1000 Oe and (lower) ZFC conditions at H=50, 100, 500 and 1000 Oe. Inset of the upper pannel shows the ZFC-FC splitting temperature for clarity.*

Two magnetic transitions are clearly observed at T_1=5K and T_2=31K. Below T_2, a strong splitting between the ZFC and FC magnetic curves is observed. And below T_1, the magnetization increases dramatically to the lowest temperature reached. This splitting between the ZFC and FC magnetic curves does not coincide exactly at the temperature at which the magnetic transition shows up, T_2, and even slight temperature shifts to

higher values are observed as the applied magnetic fields are increased (inset Figure 6.15, upper part). However, the strenght of the magnetic transition at T_2 is confirmed by the fact that it reamains invariable at the same temperature for different values of applied magnetic field (Figure 6.15, lower part).

Assuming a localized magnetic system, Figure 6.16 shows the fitting of the magnetic data above 100K to a modified Curie-Weiss equation (eq.[3.4]) in order to calculate the effective magnetic moment, which resulted to be μ_{eff}=1.1 μ_B. It is very similar to that one in the precursor $Na_{0.7}CoO_2$ ($\mu_{eff}\approx$1 μ_B), so we can deduce that Na^+ by Sr^{2+} substitution hardly changes the magnetic state of the Co ions in the paramagnetic range.

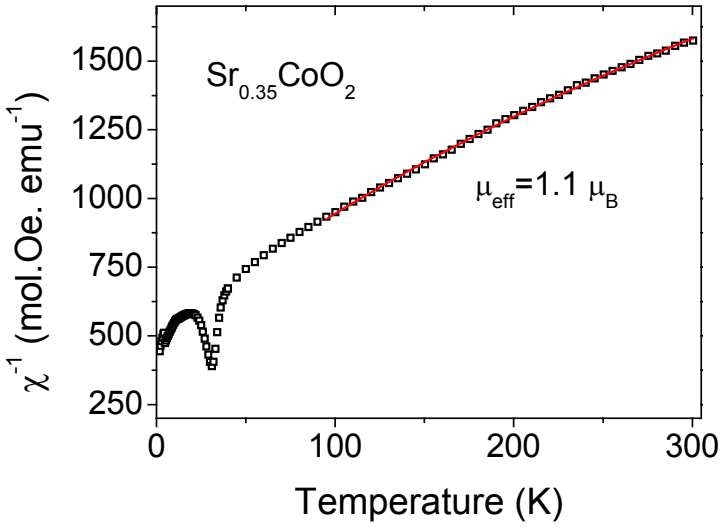

Figure 6.16: *χ^{-1}(T) curve of $Sr_{0.35}CoO_2$. Red line is the fitting of the magnetic data to a modified Curie-Weiss equation. The magnetic effective moment, $\mu_{eff,}$ is also shown.*

The possible presence or trace impurities of Co_3O_4 origined during the exchange reaction, which could be affecting the magnetic properties of $Sr_{0.35}CoO_2$, has been ruled out at the sight of the magnetic properties of both commercial and synthetized Co_3O_4 particles shown in the Appendix B. The departure of the magnetic transition observed in the magnetic

measurements of Co_3O_4 particles does not coincide with $Sr_{0.35}CoO_2$, neither the magnetic behaviour below this magnetic transition does.

The origin of this manetic behaviour in $Sr_{0.35}CoO_2$, clearly different from that of the $Na_{0.7}CoO_2$ precursor, could have its origin in an ion rearrangement between the CoO_2 layers as a consequence of the thermal treatment performed: the Na^+ by Sr^{2+} substitution implies a thermal treatment of the Na^+ precursor at 360 ºC for 48 h under O_2 gas flow. That means that the specific Na^+ ion distribution in the lattice could go through an ion rearrangement, being responsible for the observed magnetic behaviour in $Sr_{0.35}CoO_2$.

6.2.2. Ca_xCoO_2

$Ca_{0.35}CoO_2$ and $Ca_{0.20}CoO_2$ compounds were synthesized by low temperature ion exchange reaction from the $Na_{0.7}CoO_2$ precursor and the Na^+ deintercalated sample, $Na_{0.40}CoO_2$, respectively. The ion exchange tecnique has been previously used by *Cushing et al* to obtain calcium oxides[260]. A certain amount of Na_xCoO_2 was mixed thororughly with 10% molar excess of anhydrous $Ca(NO_3)_2$ powder and then heated at 310 ºC for 48 h in air, following the reaction below:

$$Na_xCoO_2 + \left(\frac{x}{2}\right)Ca(NO_3)_2 \rightarrow Ca_{x/2}CoO_2 + x\,NaNO_3$$

The final products were ground under destilled water to remove the $Ca(NO_3)_2$ in excess and the $NaNO_3$ byproduct, filtered and dried at 120 ºC

[260] B. L. Cushing and J. B. Wiley. J. Solid State Chem. **141**, 385-391 (**1998**).

for several hours. Finally, they were stored in an argon-filled glove box. The final Ca composition was determined by ICP-OES and confirmed by EDAX analysis and resulted to be x=0.35.

Commercial hydrated $Ca(NO_3)_2.4H_2O$ must be dried to avoid the formation of possible hydrated Ca_xCoO_2 phases during the synthesis.

Therefore, before using, the comercial tetrahydrated calcium salt was heated at 400 ºC for 4 h in order to be dehydrated and transformed into anhydrous $Ca(NO_3)_2$.

In order to prepare Ca_xCoO_2 samples with x<0.35 we checked the suitability of an oxidant mixture formed by Br_2/acetonitrile. The excess of Br_2 used in the reaction was $\times$10 times the stochiometric amount needed to deintercalate all the Ca^{2+} present in the $Ca_{0.35}CoO_2$ precursor. However, the results indicated the inefficience of the method to deintercalate divalent ions from the structure, as it had been evidenced in the case of Sr^{2+}. For this reason, the synthesis of a Ca_xCoO_2 sample with x<0.35 was addressed by ion exchange of a low Na^+ content precursor. In this way, $Ca_{0.20}CoO_2$ was obtained from $Na_{0.40}CoO_2$ precursor following the synthesis conditions described above. The Ca^{2+} content of the new sample was also determined by ICP-OES and confirmed by EDAX analysis.

Figure 6.17 shows the X-ray patterns for $Ca_{0.35}CoO_2$ and $Ca_{0.20}CoO_2$ in comparison to their Na^+ precursors. Both of them were isostructural and well indexed considering the hexagonal group of symmetry *P63/mmc*. If we focus on the *(002)* reflexion, we observe that its position coincide exactly in both $Na_{0.7}CoO_2$ and $Ca_{0.35}CoO_2$ patterns (Figure 6.18), indicating a similar CoO_2-CoO_2 interlayer distance. It could be due to the similar ionic radius: r[Na^+]=0.95 Å and r[Ca^{2+}]=0.99 Å. However, the (002) reflexion in $Ca_{0.20}CoO_2$ appears at higher angles than in the case of its $Na_{0.40}CoO_2$ precursor, which could not be understable if we attend only to the size of the ions.

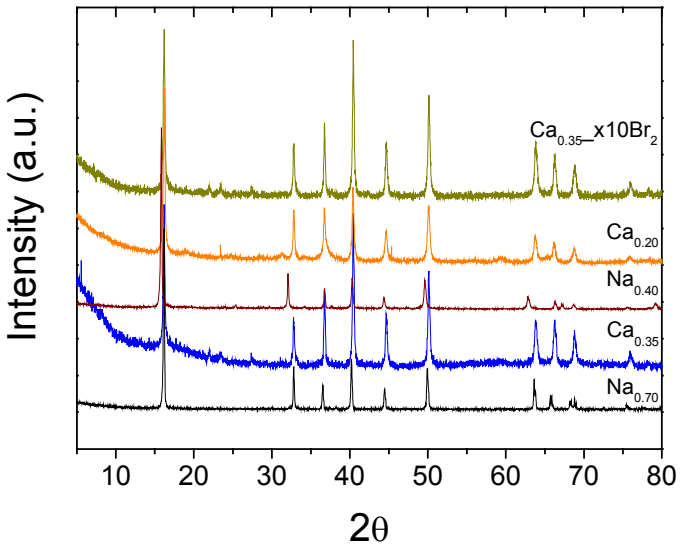

Figure 6.17: *X-ray diffraction patterns for $Ca_{0.35}CoO_2$, $Ca_{0.20}CoO_2$ and their corresponding Na^+ precursors: $Na_{0.7}CoO_2$ and $Na_{0.40}CoO_2$, respectively. The pattern for $Ca_{0.35}CoO_2$ after treatment with Br_2/acetonitrile is also shown.*

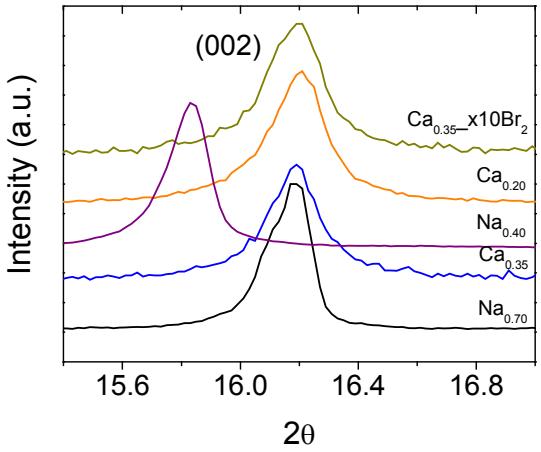

Figure 6.18: *Detail of the position of the (002) reflexion peak in the Ca^{2+} substitued and Na^+ precursors diffraction patterns.*

The lattice parameters calculated by fitting the X-ray diffraction patterns with Rietica are summarized in the Table 6.5. From these results, we confirm that the lattice dimensions in $Ca_{0.35}CoO_2$ and $Ca_{0.20}CoO_2$ are very similar to those in Na_xCoO_2. Specifically, the *c*-lattice parameter is practically identical to that in $Na_{0.7}CoO_2$, and considerably lower than in $Sr_{0.35}CoO_2$. This is justified by the similar ionic radius for both Na^+ and Ca^{2+} cations, both of them smaller than Sr^{2+}.

Table 6.5: *Lattice parameters of Ca_xCoO_2 samples after refinement of the XRD patterns with Rietica.*

Sample	Br_2 excess	Ca,x	a=b	c
$Ca_{0.35}CoO_2$	-	0.35	2.8191(1)	10.9043(1)
$Ca_{0.20}CoO_2$	-	0.20	2.8232(1)	10.9036(1)

In order to check the influence of high temperatures in the physical properties of $Ca_{0.35}CoO_2$, a thermal treatment at 800 ºC for 12 h was performed. Figure 6.19 shows the X-ray diffraction patterns for the $Ca_{0.35}CoO_2$ precursor before and after annealing, where significant structural differences are observed. In order to identify the nature of this new phase at high temperature we carried out a deeper structural analysis, which pointed out an evidence of a structural phase transition into the misfit layered cobaltite $Ca_3Co_4O_9$. In order to check this out, we synthetized $Ca_3Co_4O_9$ by firing well mixed stochiometric amounts of $CaCO_3$ and Co_3O_4 at 800 ºC for 12 h, twice. The sample was well characterized and its structural, magnetic, electrical and thermoelectric properties were in good agreement with previous published data for $Ca_3Co_4O_9$ data[261,262]. The corresponding diffraction pattern was included in red in the Figure 6.19. In fact, several coincident reflexions (marked with arrows) were detected by comparison of the annealed $Ca_{0.35}CoO_2$ and $Ca_3Co_4O_9$ patterns. However, it should be noticed that the X-ray diffractograms show in both cases other reflexions which have not been identified.

[261] A. C. Masset, C. Michel, A. Maignan, M. Hervieu, O. Toulemonde, F. Studer, B. Raveau and J. Hejtmanek. *Phys. Rev. B* **62**, 166 (**2000**).
[262] P.Limelette, V. Hardy, P. Auban-Senzier, D. Jérome, D. Flahaut, S. Hébert, R. Frésard, Ch. Simon, J. Noudem and A. Maignan. *Phys. Rev. B* **71**, 233108 (**2005**).

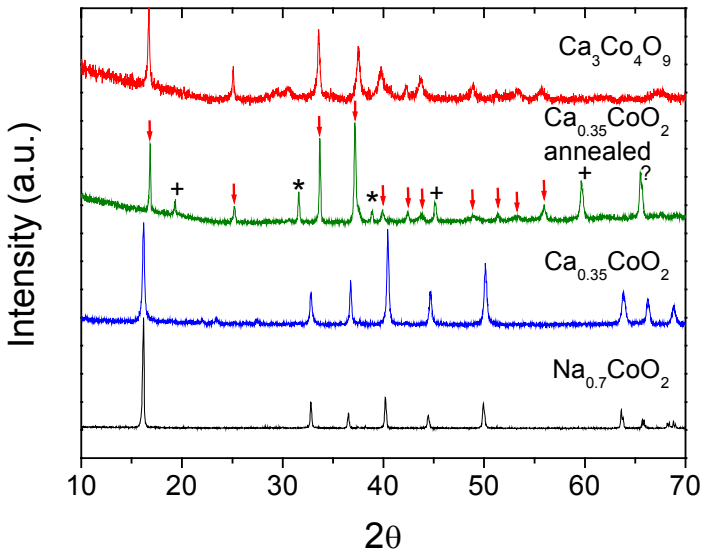

Figure 6.19: *XRD patterns of $Na_{0.7}CoO_2$, $Ca_{0.35}CoO_2$, $Ca_{0.35}CoO_2$ annealed and $Ca_3Co_4O_9$. Arrows indicate the reflexions in the annealed $Ca_{0.35}CoO_2$ pattern which are also present in the $Ca_3Co_4O_9$ one, while the (+) and (*) show the Co_3O_4 and $CaCO_3$ impurities, respectively. (?) shows the non identified reflexions.*

The complicated structural model propossed by *Masset et al*[261] for the misfit layered oxide $Ca_3Co_4O_9$ consists in the coexistence of two monoclinic subsystems which exhibit common ***a***, ***c*** and β parameters and only differ by the *b*-axis. The crystal structure consists of an alterante stack of a distorted three-layered rock salt Ca_2CoO_3 block layer and a CdI_2-type CoO_2 conducting sheet, as it is shown in the Figure 6.20.

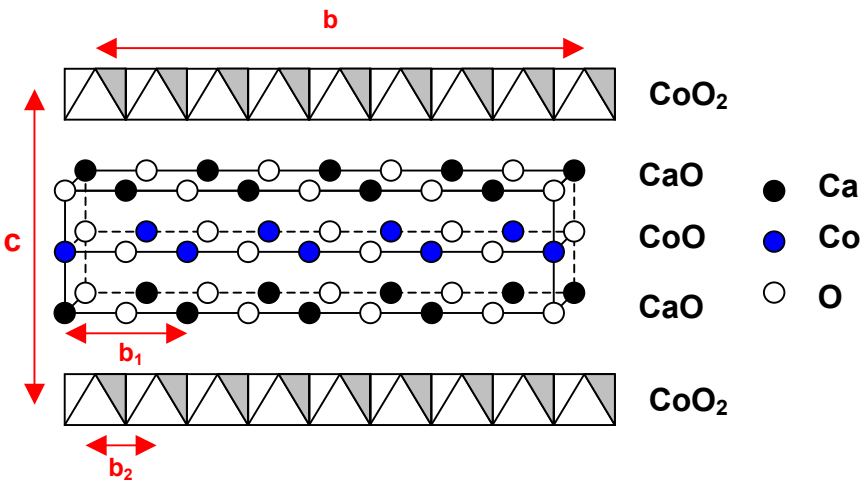

Figure 6.20: *Structural model of the misfit layered oxide $Ca_3Co_4O_9$.*

The $Ca_3Co_4O_9$ compound shows an incommensurable periodicity along the *b-axis* and such anisotropic structure is believed to be favorable for the achievement of large thermoelectric power and low thermal conductivity simultaneously, necessary for good thermoelectric materials. Figure 6.21 shows the thermoelectric curves with temperature for several layered calcium oxides. In fact, the annealed $Ca_{0.35}CoO_2$ sample shows a substancial TEP increase of more than 3 times the value measured in others Ca_xCoO_2 samples at the lowest temperature. Even in the whole temperature independent range from 200 K to 350 K the thermopower overcomes the 110 μV/K. The thermoelectric behaviour of Ca_xCoO_2 is qualitatively quite similar to that in Na_xCoO_2, although quantitatively higher: $Ca_{0.35}CoO_2$ showed values of 100 μV/K at 450 K, whereas $Ca_{0.20}CoO_2$ reached 120 μV/K.

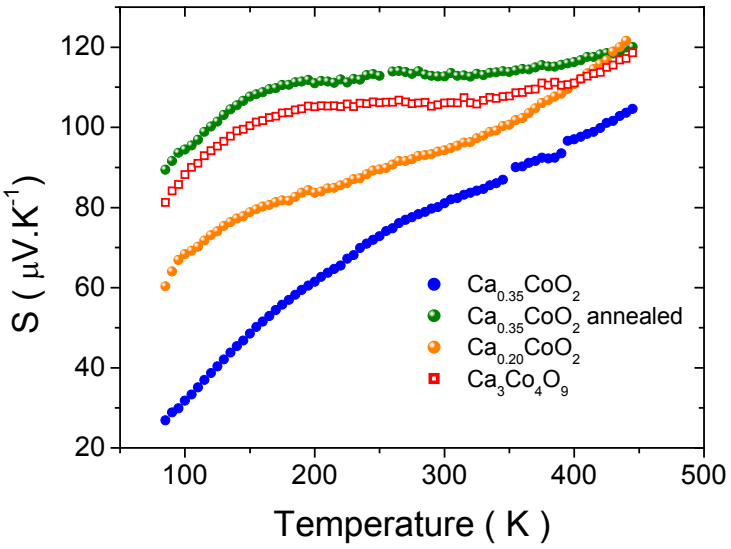

Figure 6.21: *S(T) curves for several Ca_xCoO_2 samples.*

The effect of the annealing and the phase transition into the misfit cobaltite $Ca_3Co_4O_9$ was also evidenced in the electric transport and magnetic measuraments. Figure 6.22 shows the electrical resistivity vs. temperature for $Ca_{0.35}CoO_2$ before and after annealing at I=0.1mA in comparison to that of $Ca_3Co_4O_9$. Silver wires were pasted on a piece of a sinterized bar of material following the four-probe method. The electronic behaviour of $Ca_{0.35}CoO_2$ resulted to be tipically semiconductor. Surprisingly, the conductivity decreased for the sinterized analogue and its ρ(T) curve went through a temperature independent tram in the range between 125 K and 225 K. The $\rho(T)$ curve of the annelaled $Ca_{0.35}CoO_2$ sample reminds that of $Ca_3Co_4O_9$, although the conductivity is lower and the measured temperature range is shorter. A plausible reason could be that in the annealed $Ca_{0.35}CoO_2$ sample a second heat treatment to sinterize the grains was not performed, while it was done in the case of $Ca_3Co_4O_9$.

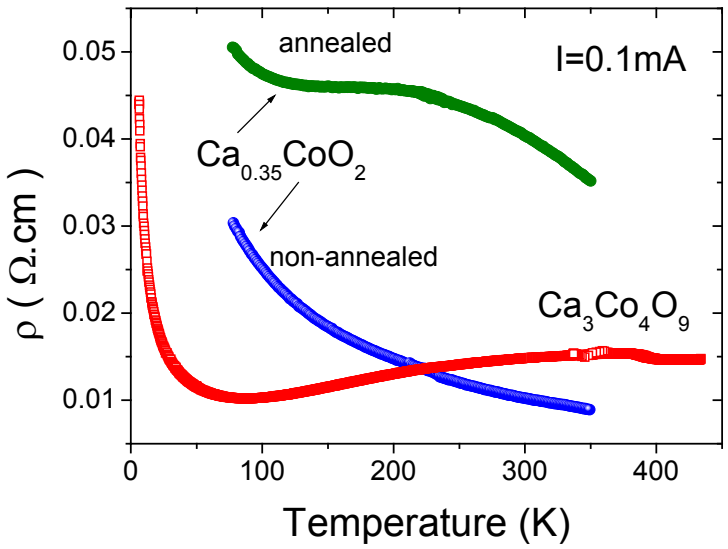

Figure 6.22: *ρ(T) curves for non-annealed and annealed $Ca_{0.35}CoO_2$ and $Ca_3Co_4O_9$ samples.*

On other hand, Figure 6.23 shows the magnetic susceptibility curves for both annealed and non-annealed $Ca_{0.35}CoO_2$ and $Ca_3Co_4O_9$ samples. The magnetic measuraments were performed at an applied magnetic field of H=100 Oe. In the non-annealed $Ca_{0.35}CoO_2$ sample a very weak magnetic transition at ~30 K can be noticed in the ZFC curve. However, in the annealed sample, this magnetic transition is imperceptible, while a new and more pronounced one shows up at ~12 K. Below this temperature, a dramatic increase of the magnetic susceptibility is observed. This magnetic transition is also observed in the susceptibility curves of $Ca_3Co_4O_9$, below which a strong splitting between the ZFC and FC curves takes place. An increase of the magnetic signal with annealing is also noticed, such a way that the susceptibility is higher for the annealed $Ca_{0.35}CoO_2$ than for the non-annealed $Ca_{0.35}CoO_2$ precursor, and it is higher for $Ca_3Co_4O_9$ in comparison to the annealed $Ca_{0.35}CoO_2$. This is other evidence that confirms that $Ca_{0.35}CoO_2$ is going through a structural phase transition into $Ca_3Co_4O_9$ with annealing.

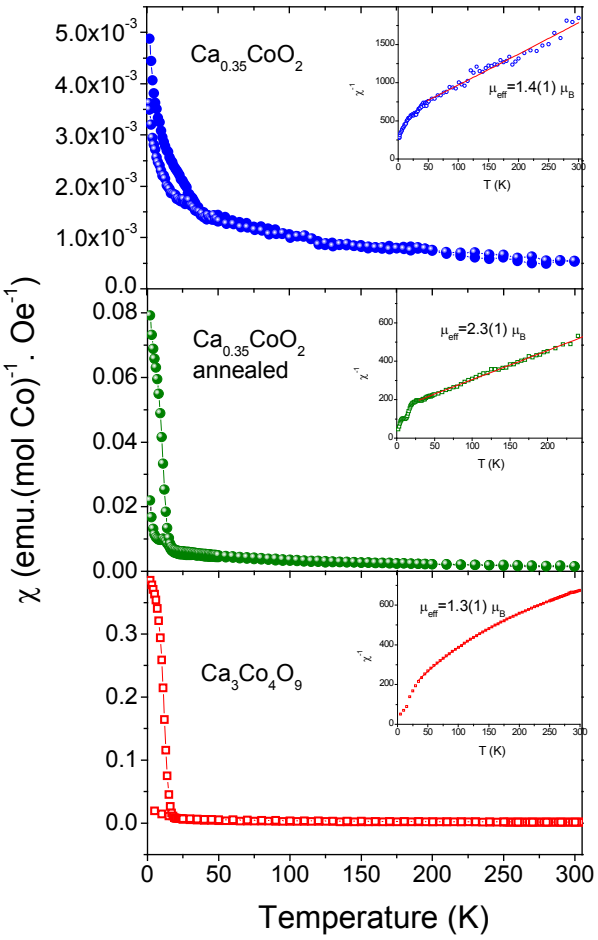

Figure 6.23: *$\chi(T)$ for (upper) non-annealed and (center) annealed $Ca_{0.35}CoO_2$ and (lower) $Ca_3Co_4O_9$ samples. Insets show the fitting of the high temperature magnetic data to a Curie-Weiss equation.*

The χ^{-1} was plotted versus temperature in order to fit the magnetic data at high temperatures to a Curie-Weiss law and calculate the effective magnetic moment in each case assuming a localized magnetic system (Figure 6.23, insets). No significant differences were found in the effective magnetic moment for the non-annealed $Ca_{0.35}CoO_2$ and $Ca_3Co_4O_9$ samples, obtaining values of μ_{eff}=1.4(1) μ_B and μ_{eff}=1.3(1) μ_B per Co atom,

respectively. A Curie-Weiss behaviour is not able to explain the magnetic behaviour of these layered cobaltites, since the calculated effective moment makes no sense even assuming that all the cobalt ions were in the formal charge state +4 and LS configuration. Therefore, a fundamental revision of the theory is highly needed in order to understand the dependence of the susceptibility with temperature for Ca_xCoO_2 and $Ca_3Co_4O_9$, as in the case of other cobaltites previously studied in this thesis.

In order to provide to the reader a general overview about the more outstanding differences found in the structural and transport properties of several $M^+/M^{2+}CoO_2$ systems, I would like to compare the main results obtained in both X-ray diffraction and thermooelectric power for different layered oxides. Figure 6.24 shows the displacement of the (002) reflexion peak from each other of a series of M_xCoO_2 compounds. The position of the (002) reflexion indicates the interlayer distance in the system, being higher as it is shiftted to lower angles. In this way, Li_xCoO_2 shows the lower separation between the CoO_2 layers while Sr_xCoO_2 present the higher interlayer distance. The balance between the cation size and the corresponding screening of the Co layers constitue the reason of such structural differences.

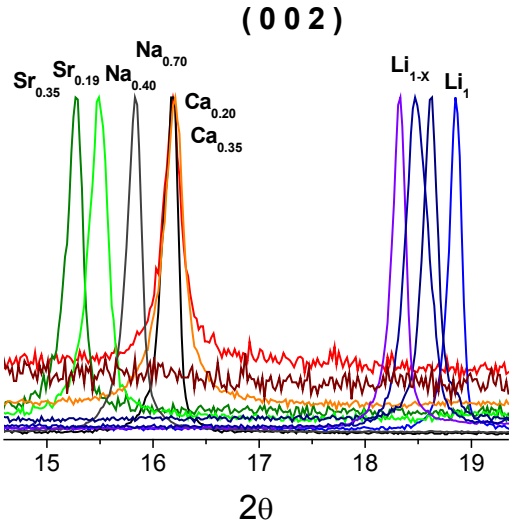

Figure 6.24: *Position of the (002) reflexion for different M_xCoO_2 ($M=Li^+$, Na^+, Sr^{2+}, Ca^{2+}) systems.*

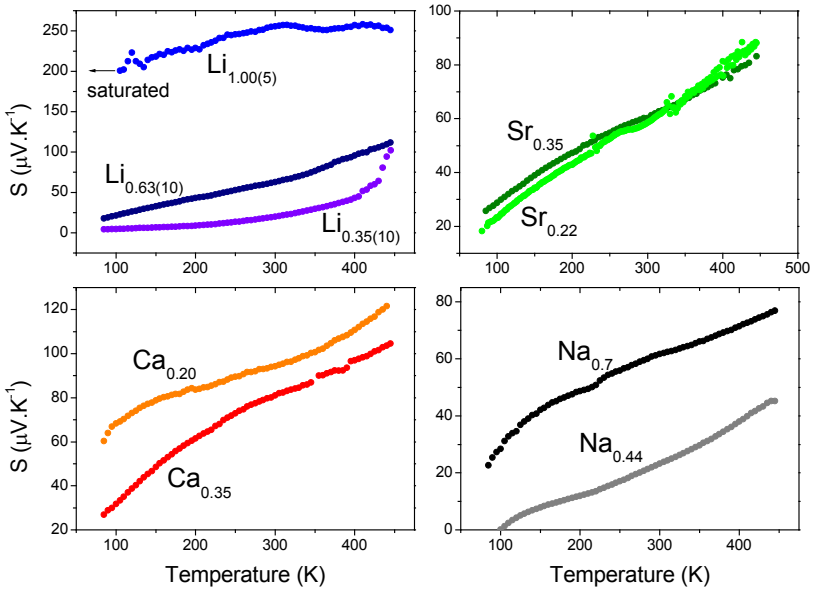

Figure 6.25: *Comparison of the thermoelectric power for representative compositions of M_xCoO_2 ($M=Li^+$, Na^+, Sr^{2+}, Ca^{2+}).*

Figure 6.25 shows the thermoelectric power for representative compostions of several M_xCoO_2 systems. The highest values were obtained for $LiCoO_2$, reaching the 250 μV/K at 450 K. As the Li^+ content decreases, $Li_{1-x}CoO_2$, *S(T)* also decreases drastically. For the rest of M_xCoO_2 systems, the difference between the non-deintercalated and M^+/M^{2+}-deintercalated samples, such as $Ca_{0.35}CoO_2$ and $Ca_{0.20}CoO_2$, or $Na_{0.7}CoO_2$ and $Na_{0.36}CoO_2$, or $Sr_{0.35}CoO_2$ and $Sr_{0.22}CoO_2$, is not so marked. However, there is an interesting point that should be remarked: whereas for the M_xCoO_2 ($M=Li^+$, Na^+) systems the Seebeck effect decreases as Na^+ and Li^+ contents decrease, it hardly varies for Sr_xCoO_2 and even increases for Ca_xCoO_2 with decreasing Sr^{2+} and Ca^{2+} content, respectively.

For a clearer comparison of the thermoelectric power of several M_xCoO_2 systems, Figure 6.26 shows the thermopower results for a) $Na_{0.7}CoO_2$, $Li_{0.63(10)}CoO_2$, $Sr_{0.35}CoO_2$, $Ca_{0.35}CoO_2$ and b) $Na_{0.44}CoO_2$, $Li_{0.35(10)}CoO_2$, $Sr_{0.22}CoO_2$, $Ca_{0.20}CoO_2$. Although the effective doping in the members of each group is similar, the relative position of their Co^{3+}/Co^{4+}

electronic bands induces differences in their electronic states at the vecinity of the Fermi level.

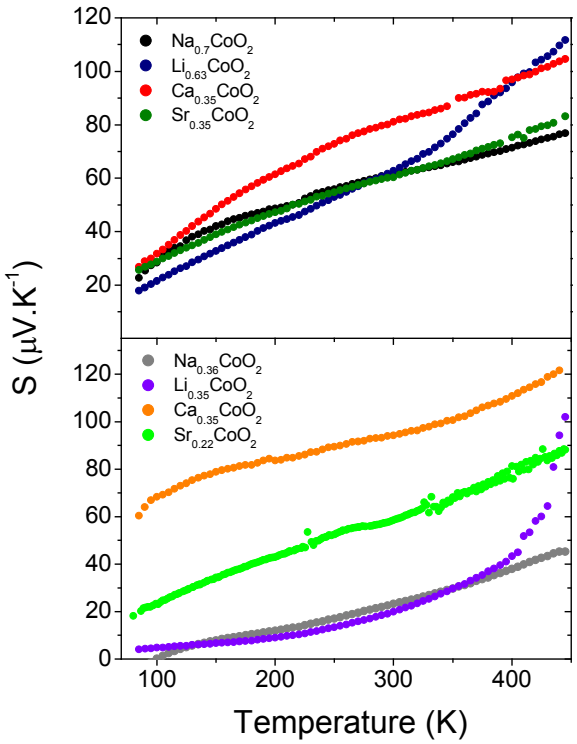

Figure 6.26: *Comparison of the thermoelectric power for representiative compositions of M_xCoO_2 ($M=Li^+$, Na^+, Sr^{2+}, Ca^{2+}).*

The structural characteristics of the CoO_2 layers of M_xCoO_2 systems directly impact their electronic properties. Therefore, they could explain the differences found in the thermoelectric power between different compositions of a M_xCoO_2 system. Related to this, *Viciu et al* proposed that the distorsion of the CoO_6 octahedron is an important indicator of the electronic state in Na_xCoO_2[263], and it would be later applied to Li_xCoO_2.[243]

[263] L. Viciu, J. W. Bos, H. W. Zandbergen, Q. Huang, M. L. Foo, S. Ishiwata, A. P. Ramirez, M. Lee, N. P. Ong and R. J. Cava. *Phys. Rev. B* **73**, 174104 (**2006**).

The shape of the CoO_6 octahedra is expected to influence the energies of Co t_{2g} and e_g orbitals. To quantify this effect, the in-plane Co-Co distance can be used to calculate the CoO_2 layer thickness that would be expected if the CoO_6 octahedra were ideal in shape. The relationship between thickness of a layer of ideal edge sharing CoO_6 octahedra and the in-plane Co-Co distance is equal to $\left(\sqrt{6}/3\right)\times d\left(Co-Co\right)$.

Figure 6.27 shows the evolution of the CoO_2 thickness with x for Na_xCoO_2 in comparison to Li_xCoO_2, Ca_xCoO_2 and Sr_xCoO_2. The continuous expansion of the CoO_2 layer observed in the c-direction for Na_xCoO_2 at 0.3<x<0.7 suggest that gradual and significant changes in electronic band occupancy occur at that composition, whereas the much smaller change in size observed for LixCoO2 indicates that the electronic system does not undergo qualitative changes in that case. These results agree with those reported by *Q. Huang et al*[264] and *Hertz et al* [243] for Na_xCoO_2 (x<0.7)and Li_xCoO_2.

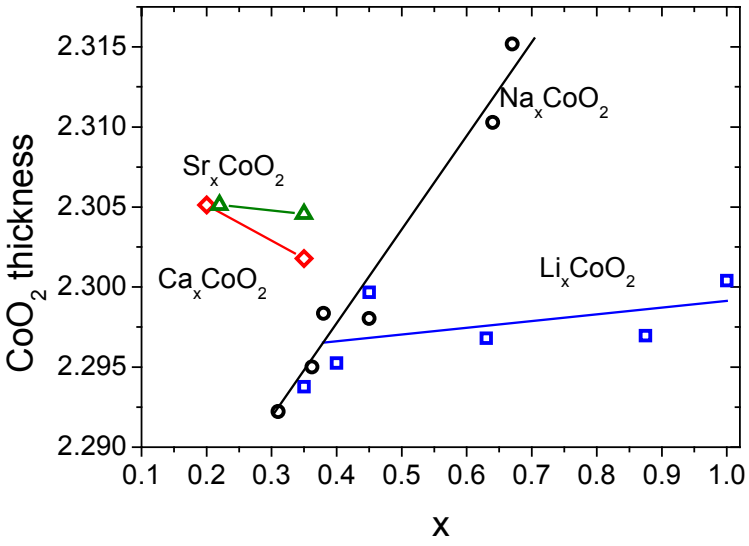

Figure 6.27: Variation of the CoO_2 thickness for several M_xCoO_2 systems ($M=Li^+$, Na^+, Ca^{2+}, Sr^{2+}).

[264] Q. Huang, M. L. Foo, R. A. Pascal, Jr., J. W. Lynn, B. H. Toby, T. He, H. W. Zandbergen and R. J. Cava. *Phys. Rev. B* **70**, 184110 (**2004**).

These results would explain the significant differences found in the thermoelectric power for Na_xCoO_2 and Li_xCoO_2 with *x*. Although more data are needed to extract some reliable conclusion about Ca_xCoO_2 and Sr_xCoO_2, our data suggest that the slight variation of their CoO_2 layer thickness in comparison to Na_xCoO_2 and Li_xCoO_2 could be the cause of not so qualitative differences in the thermopower observed for different x.

Finally, I would like to remark some other aspects that have been also studied in this thesis regarding the use of the low temperature topotactic reaction in order to exchange monovalent by divalent ions in cobaltites (results are not shown for clarity). I really believe that they can be helpful for future research about it. They are the following:

1. In the synthesis of Sr_xCoO_2 and Ca_xCoO_2 we have checked different amounts in excess of the starting salts with respect to the stochometric amounts in order to force the $(Ca, Sr)^{2+}$ ions to go into the structure. However, the amount of divalent cations capable of entering in the structure does not depend on the excess of salt used, but only on the Na^+ content of the precursor.

2. Other experiments were driven in order to produce a second ion exchange reaction in these systems, where the divalent cations $(Ca, Sr)^{2+}$ would be substitued again for monovalent ones $(Na, K)^+$. However, XRD and EDAX data analysis indicated the inefficiency of the method.

3. Sr_xCoO_2 and Ca_xCoO_2 were also tried to be synthetized by conventional solid state reaction from $SrCO_3$, $CaCO_3$ and Co_3O_4 as reactants, respectively. The synthesis procedure was carried out in the same way that Na_xCoO_2. However, the final products were not the expected and many non identified impurity phases were found. This point confirms that topotactic ion exchange reaction constitutes a suitable method in order to obtain $M_x^{2+}CoO_2$ materials from the proper precursors.

It is also very important to mention that the low Na^+ precursor used in the ion exchange (topotactic) reactions previously described, both monovalent for monovalent and divalent for monovalent, become superconductor after hydration below T_c=5 K. All the substitued M_xCoO_2 compounds synthetized from it were hydrated for several days in destilled water and checked for superconductivity. In any case superconductivity was not found.

7. Conclusions

As conclusion, I will summarize below the more remarkable goals achieved in this thesis:

1. We have demonstrated that below $x \approx 0.4$ in Na_xCoO_2, the formal oxidation state of Co remains constant around 3.45+, which indicates oxygen loss from the CoO_2 layers.

2. The role of lattice dimensionality is probably important in the occurrence of superconductivity in the hydrated samples by a modification of $N(E_F)$, but our experiments point to H_2O molecules playing a role other than a passive lattice spacer, with a direct implication in the control of the effective doping at the CoO_2 planes.

3. We have shown that metallic Na_xCoO_2 is a Fermi-liquid at high doping levels of Na, with the quasiparticle mass m* becoming heavily renormalized and field dependent at low temperature. When the Na^+ content is around the optimum values for superconductivity, a phase with spin-glass and non-FL characteristics develops at low temperature.

Our experimental evidence suggests that this behavior is a consequence of the proximity to a second-order magnetic QPT, although measurements at lower temperature would be desirable.

4. We have shown that the temperature dependence of the magnetic susceptibility in triangular lattice Co-oxides cannot be interpreted by a localized magnetic model. We suggest that it is dominated by the temperature dependence of the local amplitude spin fluctuations.

5. The unusually large thermopower in Na_xCoO_2 is related to a band-structure effect in an itinerant-electron system, not to a spin-entropy contribution. The conventional Heikes formula predicts correctly the sign and magnitude of the thermopower in these systems, given the correct number of charge carriers. The continuous increase in S observed above room temperature in some members of the family could be reflecting a change in the statistics due to a continuous spin-state transitions or Na^+ rearrangements.

6. We were able to force a topotactic replacement of Na^+ by H_3O^+ in the half-doped $Na_{0.5}CoO_2$. Superconductivity was achieved in the resulting $Na_{0.38}(H_3O^+)_{0.13}CoO_2 \bullet 1.2H_2O$. In view of our results, the phase diagram for this system should probably consider an SDW phase at an [electron]/[hole] ratio of ≈1 that is progressively suppressed by a decrease of dimensionality (we never observed coexistence of the magnetic and superconducting phases). It also follows from our results that the right place to look for superconductivity through the introduction of neutral, nonaqueous spacers (e.g., supercritical CO_2) is probably $Na_{0.5}CoO_2$ rather than $Na_{0.3}CoO_2$.

7. Different M_xCoO_2 were succesfully obtained both solid state and topotactic exchange reactions from Na_xCoO_2 precursors. Our data agree with a LS to HS spin transition for Li_xCoO_2 above the two phase domain for $0.75 \leq x \leq 0.94$. We have also observed that the differences found in the thermoelectric power between different compositions of M_xCoO_2 systems ($M=Li^+$, Na^+, Ca^{2+}, Sr^{2+}) could be related to the thickness of the CoO_2 layers, which is strongly related to the energy at the Fermi level.

Appendix A

Synthesis and Magnetic properties of Co_3O_4

Soon after the appearance of the reports of magnetic phase transition at ~40 K many authors suggested the possibility of these results to be extrinsic, due to Co_3O_4 impurities, not detected by X-ray. In order to demonstrate the intrinsic character of the magnetic properties of the M_xCoO_2 (M=Li, Na, Ag, Ca, Sr) systems, shown in this thesis, we have performed a careful study of the magnetic properties of cobalt oxide, Co_3O_4. First of all, we have magnetically characterized commercial Co_3O_4, directly from Sigma-Aldrich. Secondly, we have synthesized Co_3O_4 nanoparticles in order to mimic the size of the impurities that could be formed during the thermal treatments to synthesize M_xCoO_2 compounds. In the following, I will describe the chemical synthesis and the structural characterization of Co_3O_4 nanoparticles, and subsequently, I will show the magnetic properties of both commercial and synthesized Co_3O_4 powders.

A.1. Synthesis of Co_3O_4 nanoparticles

The synthesis of Co_3O_4 particles was carried in two steps:

1.1. Synthesis of the $Co(OH)_2$ precursor.

The cobalt hidroxide, $Co(OH)_2$, was obtained by basic precipitation of a $CoCl_2.6H_2O$ aqueous solution with NaOH. In this process, 100mL of a basic solution 0.2M of NaOH was slowly added into 100mL 0.1M of an aqueous solution of $CoCl_2.6H_2O$ under magnetic stirring in air. The apparation of a dark brown precipitate was inmediate. Then, it was filtered and washed several times with destiled water. Finally, it was dried in a heater at 70ºC for 1h.

1.2. Oxidation of $Co(OH)_2$ into Co_3O_4.

In order to oxidized the $Co(OH)_2$ precursor to Co_3O_4, the hydroxide was annealed in an oven at 450ºC for 6h in air. The success of the oxidation was confirmed by X-ray diffraction. Figure A1 shows both $Co(OH)_2$ and Co_3O_4 diffraction patterns and their identification by comparison to the ICSD data base.

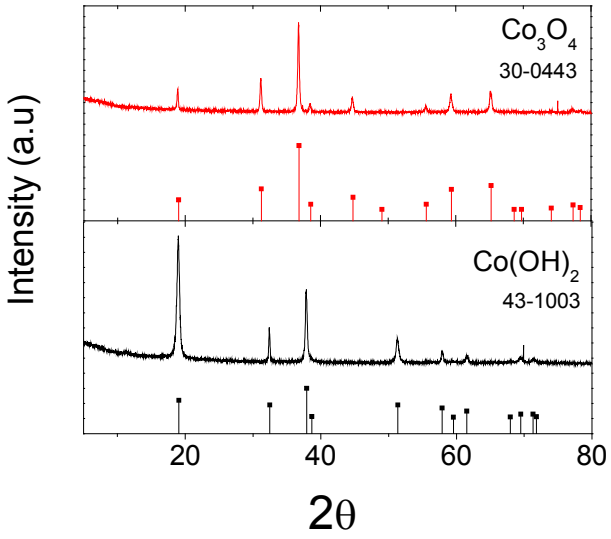

Figure A1: *X-ray diffraction patterns for the $Co(OH)_2$ precursor (bottom) and the final Co_3O_4 compound (upper). Vertical lines show in each case the the concordance of the reflexion peaks with the corresponding diffraction patterns from the ICSD data base.*

Co_3O_4 has a normal cubic spinel structure described by a formula unit AB_2O_4, where the Co^{2+} and Co^{3+} ions occupy the tetrahedral (A) and the octahedral (B) sites, respectively. The bulk Co_3O_4 compound is antiferromagnetic (AF) with a Néel temperature about 40 K. Deviations of the Néel temperature from the bulk have been observed in nanoparticles, which can be well described by the theory of finite-size scaling[265,266,267,268]. The Co_3O_4 unit cell contains 8 Co^{2+} tetrahedral ions ordered antiferromagnetically and 16 Co^{3+} octahedral ions exhibiting diamagnetism, as a consequence of the splitting of 3d levels by the octahedral crystal field and complete filling of

[265] E. L. Salabas, A. Rumplecker, F. Kleitz, F. Radu and F. Schüth. *Nano Lett*. **6**, 2977 (**2006**).
[266] D. A. Resnick, K. Gilmore, Y. U. Idzerda, M. T. Klem, M. Allen, T. Douglas, E. Arenholz and M. Young. *J. Appl. Phys*. **99**, 08Q501 (**2006**).
[267] S. A. Makholouf. *J. Magn. Magn. Mater*. **246**, 184 (**2002**).
[268] H. T. Zhu, J. Luo, J. K. Liang, G. H. Rao, J. B. Li, J. Y. Zhang and Z. M. Du. *Physica B* **403**, 3141 (**2008**).

t_{2g} levels (low-spin Co^{3+}). The effetive magnetic moment per ion in the paramagnetic state reported for Co_3O_4 is $\mu_{eff} \approx 4.4\mu_B$ [267,269,270]. It arises due to the spin of Co^{2+} ions mainly, but it has a small adittional contribution from spin-orbit coupling.

A.2. Magnetic properties of Co_3O_4 powder

The magnetic susceptibility, χ, versus temperature for both commercial and synthesized Co_3O_4 powder has been measured in order to compare its magnetic behaviour with that one of M_xCoO_2 systems, checking in this way its possible presence as an impurity in these systems.

Figure A2 shows the $\chi(T)$ curves in ZFC and FC conditions for both samples at a magnetic applied field of 100Oe. For both commercial and synthetized samples, their magnetic behaviour is practically identical. The antiferromagnetic transition temperature, T_N, shows up around 37 K. However, the ZFC and FC curves were bifurcated at slightly lower temperature, T≈27 K. Above 60 K, the χ^{-1} versus T is linear, indicating that the magnetization obeys a Curie-Weiss law. From the linear fit of the magnetic data, the effective magnetic moment, μ_{eff}, resulted to be 4.9BM and 4.7BM for the commercial and synthesized samples, respectively.

[269] P. Dutta, M. S. Seehra, S. Thota and J. Kumar. *J. Phys.:Condens. Matter* **20**, 015218 (**2008**).
[270] Y. Ichiyanagi and S. Yamada. *Polyhedron* **24**, 2813 (**2008**).

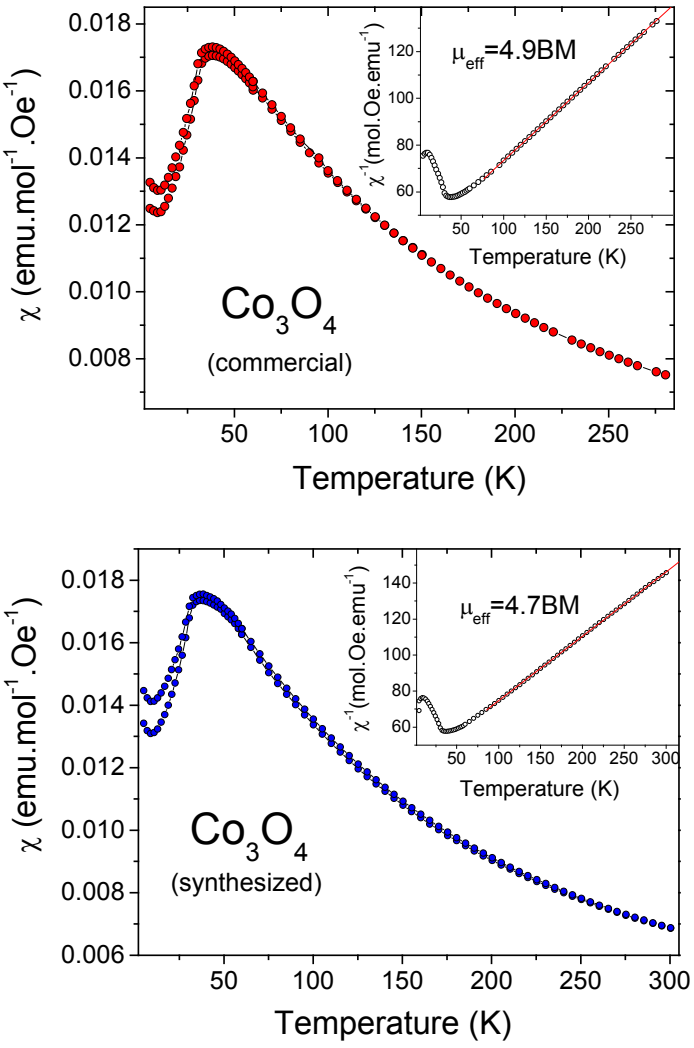

Figure A2: *Magnetic susceptibility curves for both commercial (upper) and synthesized (bottom) Co_3O_4 polycrystals under an applied magnetic field of 100Oe. Inset shows the inverse of the susceptibility vs temperature. Red line is the linear fitting of the data above 100 K to the Curie-Weiss law in order to calculate the effective moment, μ_{eff}, of the material.*

In the log-plot shown in Figure A3 the difference between T_N and the point of irreversibility between the ZFC-FC curves can be better appreciated.

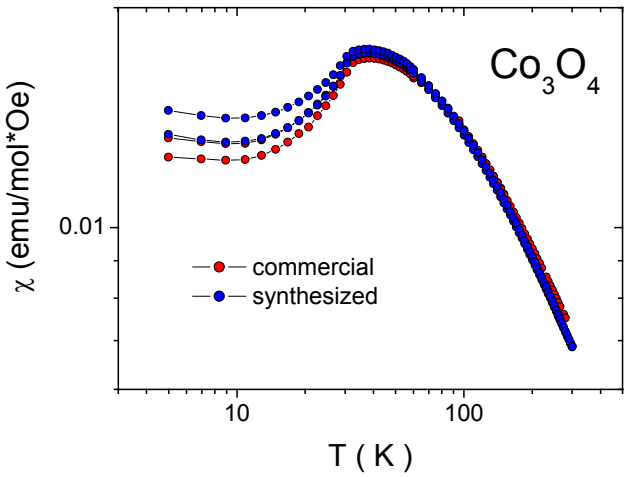

Figure A3: *Log-plot of the χ(T) curves for both commercial and synthesized Co_3O_4 samples.*

From the magnetic behaviour of Co_3O_4 particles, we deduce that the magnetic properties of all the M_xCoO_2 materials observed along this thesis are not affected by the presence of impurities of Co_3O_4. Taking into account the μ_{eff} calculated from high temperature magnetic data for the different compounds, the amount of Co_3O_4 needed to justify those values would be anomalously high. Even in the specific case of Sr_xCoO_2, where the XRD patterns showed the presence the impurities of Co_3O_4 after the exchange topotactic reaction, the amount that would be needed to explain the magnetic properties would be completely irrealistic.

This study evidences the intrinsic character of the magnetic properties of the M_xCoO_2 systems analysed in this thesis.

Post-graduate Publications

1. **M. Bañobre López**, C.Vázquez Vázquez, M. A. López Quintela, J. Rivas. *Nanotechnology* 14, 318 (**2003**)

2. **M. Bañobre López**, C.Vázquez Vázquez, M. A. López Quintela, J. Rivas. Coloides e Interfases, Ed.: Luis M. Liz Marzán et al. D. L. C. 1369-2003 - ISBN 84-8158-242-5. Universidad de Vigo, pp. 237-240. Vigo (**2003**).

3. C.Vázquez Vázquez, **M. Bañobre López**, M. A. López Quintela, Luis E. Hueso, J. Rivas. *Journal of Magnetism and Magnetic Materials* 272-276, 1547 (**2004**).

4. **M. Bañobre López**, F. Rivadulla, M. A. López Quintela, J. Rivas, J. B. Goodenough. *Chemistry of Materials* 17, 1965 (**2005**).

5. F. Rivadulla, **M. Bañobre López**, M. A. López Quintela, J. Rivas. *Physical Review B* 73, 054503 (**2006**).

6. Miguel A. Correa-Duarte, Verónica Salgueirino-Maceira, **M. Bañobre-López**, Marek Grzelczak, José Rivas, Luis M. Liz-Marzán. *Advanced Functional Materials* 18, 616 (**2008**).

7. C. Vázquez Vázquez1, **M. Bañobre-López**, A. Mitra, M. A. López-Quintela and J. Rivas. *Langmuir* 25(14), 8208 (**2009**).

8. **M. Bañobre-López**, F. Rivadulla, M. A. López-Quintela and J. Rivas. *Journal of American Chemical Society* 131 (28), 9632 (**2009**).

9. F. Rivadulla, **M. Bañobre-López**, C. X. Quintela, A. Piñeiro, V. Pardo, D. Baldomir, M. A. López-Quintela, J. Rivas, C. A. Ramos, H. Salva, J.-S. Zhou and J. B. Goodenough. *Nature Materials* 8, 947 (**2009**).

10. M. Sanles-Sobrido, **M. Bañobre-López**, V. Salgueiriño, M. A. Correa-Duarte, B. Rodríguez-González, J. Rivas and L. M. Liz-Marzán. *Journal of Materials Chemistry* 20, 7360 (**2010**).

11. **M. Bañobre-López**, Y. Piñeiro-Redondo, R. De Santis, A. Gloria, L. Ambrosio, A.Tampieri, V. Dediu and J. Rivas. *Journal of Applied Physics* 109, 07B313 (**2011**).

12. **M. Bañobre-López**, Y. Piñeiro-Redondo, R. De Santis, A. Gloria, L. Ambrosio, A.Tampieri, V. Dediu and J. Rivas. *Virtual Journal of Nanoscale Science and Nanotechnology* 23 (15) (**2011**).

13. Y. Piñeiro-Redondo, **M. Bañobre-López**, I. Pardiñas-Blanco, G. Goya, M. A. López-Quintela and J. Rivas. *Nanoscale Research Letters* (**in press**).

14. A. Tampieri, T. D'Alessandro, M. Sandri, E. Landi, L. Bertinetti, S. Panseri, **M. Bañobre-López**, J. Rivas. Submitted to *Chemistry of Materials.*